

Jieying Zhou

---

# Improved Sorptive Removal of Polar Organic Micropollutants from Water Using Surface Modified and Polarized Activated Carbons

**Improved Sorptive Removal of Polar Organic Micropollutants from  
Water Using Surface Modified and Polarized Activated Carbons**

Der Fakultät für Chemie und Mineralogie  
der Universität Leipzig  
vorgelegte

DISSERTATION

zur Erlangung des akademischen Grades  
DOCTOR RERUM NATURALIUM  
(Dr. rer. nat.)

von M.Sc. Jieying Zhou

geboren am 05.01.1991 in Shanghai, China

Leipzig, den 26.08.2021



The present thesis was conducted in the period from May 2018 to August 2021 at the Department of Environmental Engineering, Helmholtz Centre for Environmental Research – UFZ under the supervision of Dr. Anett Georgi and Prof. Dr. Frank-Dieter Kopinke.



Bibliographic description

Jieying Zhou

**Improved Sorptive Removal of Polar Organic Micropollutants from Water Using Surface Modified and Polarized Activated Carbons**

Leipzig University, Doctoral Thesis

178 Pages, 59 Figures, 23 Tables, 393 References

**Abstract**

Emerging organic persistent and mobile (PM) micropollutants can survive the conventional water treatment barriers and end up as hazards in drinking water. Activated carbon (AC) adsorption is one of the prevailing strategies in modern wastewater treatment facilities, which shows satisfying removal ability for non-polar organic compounds, yet not for many highly hydrophilic PM substances. Knowledge in the adsorption drivers for traditional non-polar organic micropollutants urgently needs to be updated for polar neutral, ionizable and ionic compounds taking into account the additional adsorbent/adsorbate interactions. In the scale of this dissertation, we investigated the effect of surface chemical modification (i.e. surface defunctionalization and surface oxidation) and electric polarization of AC felts on the adsorption behaviors of seven environmentally relevant PM contaminants representing polar neutral, cationic and anionic compounds. Surface defunctionalization was found to provide a universal strategy to improve the AC adsorption efficiency for all probed PM types while additional electric polarization can further broaden the flexibility in regulating the uptake and release of charged PM compounds. The electro-assisted ad-/desorption of PM molecules with promising enrichment effects estimated from the batch and flow experiments as well as long-term stability (>20 days, 5 cycles) was proven, which proposes a facile, green, *in-situ* AC regeneration compared to the state-of-the-art off-site high-temperature regeneration approach. Moreover, we showcased a membrane-free, single-channel flow unit using two AC electrodes carrying different surface chemistries for an effective removal of highly polar trifluoroacetate from tap water. Our findings shall inspire the next-generation design of adsorbent materials and (electro-)sorptive processes to treat water contaminated by emerging PM substances.

Bibliographische Beschreibung

Jieying Zhou

**Verbesserung der sorptiven Entfernung von polaren organischen Mikroverunreinigungen aus Wasser durch oberflächenmodifizierte und polarisierte Aktivkohlen**

Universität Leipzig, Dissertation

178 Seiten, 59 Abbildungen, 23 Tabellen, 393 Referenzen

**Kurzreferat**

Neu auftretende organische, persistente und mobile (PM) Mikroverunreinigungen können die Schadstoffbarrieren in konventionellen Wasserbehandlungsanlagen leicht überwinden und sogar die Qualität des Trinkwassers beschädigen. Adsorption an Aktivkohle (AK) ist eine der etablierten Technologien in modernen Wasseraufbereitungsanlagen. Damit können unpolare organische Verbindungen weitgehend entfernt werden, jedoch bleiben dabei hydrophile PM-Substanzen unberührt. Die Kenntnisse über die Treiber zur Adsorption unpolarer Verbindungen müssen für die Klasse der polaren Verbindungen - neutrale, ionisierbare und ionische Verbindungen - erweitert werden, wobei zusätzliche Adsorbens-Adsorbat-Wechselwirkungen zu berücksichtigen sind. Im Rahmen dieser Dissertation untersuchten wir die Auswirkungen von chemischen Modifizierungen der AK-Oberfläche (Defunktionalisierung und Oxidation) und der elektrischen Polarisierung von AK-Filzen auf das Adsorptionsverhalten von sieben relevanten PM-Schadstoffen, die neutrale, kationische und anionische Verbindungen repräsentieren. Wir haben herausgefunden, dass die Oberflächendefunktionalisierung eine universelle Strategie zur Verbesserung der AK-Adsorptionseigenschaften für alle untersuchten PM-Verbindungen darstellt. Eine zusätzliche elektrische Polarisierung ermöglicht eine größere Flexibilität bei der Steuerung der Adsorption und Desorption ionischer Verbindungen. Die potenzialunterstützte Ad- und Desorption ermöglicht die Aufkonzentrierung von PM-Schadstoffen in vielfach kleineren Wasservolumina. In Batch- und Durchflussexperimenten wurde die Stabilität (>20 Tage, 5 Zyklen) der Elektrosorptionsfilter gezeigt. Die Methode ermöglicht eine einfache und umweltfreundliche *In-situ*-Regenerierung der AK-Filter. Darüber hinaus stellen wir eine membranfreie Ein-Kanal-Durchflusseinheit mit zwei verschiedenen oberflächenmodifizierten

AK-Elektroden zur effektiven Entfernung von schweren eliminierbaren PM-Schadstoff Trifluoracetat (TFA) vor. Zusammenfassend sollen unsere Ergebnisse die nächste Generation von kohlenstoffbasierten Adsorptionsmaterialien und die Entwicklung von Elektrosorptionsprozessen zur Wasserreinigung, insbesondere mit Blick auf neue PM-Substanzen, voranbringen.



## Contents

1. Introduction .....	1
2. Research background.....	4
2.1. Polar organic micropollutants .....	4
2.1.1. Definition and classification .....	4
2.1.2 Sources, emission and detection .....	5
2.1.3 Environmental concern .....	7
2.2 Water treatment strategies for PM substances .....	8
2.2.1 AC adsorption .....	8
2.2.2 Reverse osmosis .....	12
2.2.3 Oxidative degradation strategies .....	14
2.3 Electro-assisted sorption processes for PM removal .....	16
2.3.1 Inspiration from capacitive deionization (CDI).....	16
2.3.2 Development of electro-assisted sorption for PM removal .....	20
2.3.3 Unknowns of state-of-the-art PM electrosorption .....	24
References .....	27
3. Research questions and manuscripts' overview .....	38
3.1 Adsorption of polar and ionic organic compounds on activated carbon: Surface chemistry matters.....	41
3.2 Electro-assisted removal of polar and ionic organic compounds from water using activated carbon felts .....	87
3.3 Efficient removal of trifluoroacetic acid from water using surface-modified activated carbon and electro-assisted desorption.....	130
4. Summary .....	171
Declaration of authorship contribution .....	175
Acknowledgement.....	176
Curriculum vitae .....	177



## 1. Introduction

The quality of water resources is being threatened by diverse organic micropollutants. With the vast development in analytical devices, a large number of organic micropollutants carrying polar, ionizable or ionic structures become increasingly identifiable in different water sources worldwide [1, 2]. Contrary to the traditional organic micropollutants of non-polar structures, these newly emerging contaminants are highly mobile in aquatic systems, which can pose a particular hazard to drinking water. Although present in low concentration ranges of ng/L – µg/L, they may accumulate after recirculating in short water cycles [1, 3], and raise significant toxicological concerns after long-term exposure [1, 2, 4-9]. Since 2006, actions are taken by the German Environment Agency (UBA) to regulate these compounds as persistent and mobile (PM) substances [10]. *Mobility* (M) is now a new criteria to assess the environmental impact of related organic water contaminants in contrast to *Bioaccumulative ability* (B) used in the classification of persistent, bioaccumulative and toxic (PBT) substances, such as polychlorinated biphenyls (PCBs), identified 50 years ago [11].

Activated-carbon (AC) based adsorption is one of the prevailing strategies extensively used in water treatment due to its low investment costs, operational flexibility and simplicity as well as low environmental impact [9, 12, 13]. With typically large specific surface areas of  $\sim 10^3 \text{ m}^2/\text{g}$ , AC materials show reliable adsorption performance in the removal of many non-polar organic micropollutants, yet often not able to sufficiently purify water contaminated by highly polar PM substances [2, 7, 14, 15]. A significant treatment gap in the state-of-the-art water treatment processes exists for PM substances where techniques to enhance the adsorption capability of AC-based adsorbents are urgently required [11]. Many current knowledge based on the interactions between carbonaceous adsorbents and non-polar organic compounds need to be updated in order to tackle the unknowns in the adsorption of PM substances where additional drivers such as electrostatic interactions, ion exchange, ion bridging, electron donor-acceptor (EDA) interactions and charge-assisted H-bonds come into play [16]. Recent developed prediction models for PM adsorption on carbon-based adsorbents reveal the lack in high-quality materials characterization and adsorption experimental data on a diverse selection of PM candidates in the literature pool. They need to be improved by identifying the key properties of both the adsorbent and PM adsorbates [17-19].

Previous studies demonstrated improved adsorption efficiency of AC adsorbents to specific types of PM substances via tailored surface functional groups [20-22] or electrically polarized surfaces [23-25]. The latter approach for PM removal is based on the concept of electrosorption, for which porous materials can be directly utilized as electrodes due to their adequate conductivity and high capacitance [26]. Electrosorption was being intensively investigated and applied for capacitive deionization (CDI) where vast advances in materials and processes design achieved during the past two decades were seen [27, 28]. With the growing awareness of PM pollution, e.g. the first appearance of PMT (T for toxic) substances on the EU watch list 2007/2008 [29], electrosorption started to be used in treating many environmentally relevant PM substances including pesticides [30, 31], herbicides [32-34], pharmaceuticals [35-38], endocrine disruptors [38] and poly-and perfluoroalkyl substances (PFASs) [23, 39-42]. By reversible tuning the AC surface polarization, enhanced adsorption and *in-situ* regeneration of the exhausted adsorbents can take place subsequently [23-25, 31, 43]. This proposes a facile and green alternative much more favored today in the context of global warming compared to the common off-site high-temperature regeneration. This applies in particular when early adsorber breakthroughs and thereby short regeneration intervals are expected for the highly mobile organic compounds. Nonetheless, very limited work has been so far performed covering all three PM types with nonionic, cationic, and/or anionic structures [36, 44, 45], or conducted to investigate the effect of surface chemical properties of AC on its performance in the PM electrosorptive removal processes.

In the scope of this dissertation, three AC felts carrying distinct surface chemistries, i.e. the surface defunctionalized, surface oxidized and the pristine materials, were applied. Seven environmentally relevant PM substances were selected as target compounds, including three permanently positively charged substances (tetrapropylammonium (TPA<sup>+</sup>), benzyl-triethylammonium (BTEA<sup>+</sup>), benzyl-trimethylammonium (BTMA<sup>+</sup>)), two organic anions (*p*-toluenesulfonate (*p*-TsO<sup>-</sup>) and trifluoroacetate (TFA, with  $pK_a < -1$  [46, 47] and 0.23 [48], respectively) and two neutral compounds at pH 7 (*p*-toluenesulfonamide (*p*-TSA,  $pK_a = 10.5$  [49], methyl-*tert*-butyl ether (MTBE)). Based on the results of comprehensive AC characterizations and adsorption experiments, we first aimed at providing insights to the role of AC surface chemistry in PM adsorption and suggesting surface modification strategies to facilitate the adsorption of individual PM type in the absence of additional electric fields. By comparing our results with the values predicted by the most recently developed model

[17], we aimed to identify the key adsorbent properties for the mechanistic understanding of PM adsorption behaviors on carbonaceous materials.

Then, we explored the applicability of electrosorption in removal of various types of PM substances using AC felts carrying different surface chemistries being the electrodes/adsorbents. The effect of electrode polarization on the adsorption behaviors of PM substances as well as the long-term stability (>20 days) of electro-assisted PM removal was investigated in batch systems. Derived from Freundlich parameters of adsorption isotherms obtained in batch electrosorption cells, we estimated the enrichment factors achievable for each PM/AC pair under different operation conditions. In the end, we transferred the knowledge gained from the adsorption study of PM molecules on surface modified AC materials with and without externally applied potentials to the design of a flow-unit for electro-assisted removal of TFA from tap water in the presence of inorganic anions. Overall, the present dissertation shall provide useful guidance in future design of materials and operation conditions for facilitated sorptive and electro-sorptive removal of various PM substances from water.

## 2. Research background

### 2.1. Polar organic micropollutants

#### 2.1.1. Definition and classification

Organic micropollutants in the aquatic environment are hazards existing in trace level concentration ranging from ng/L to µg/L [50]. These compounds can be further classified according to their *mobility (M)*, *persistence (P)*, and *toxicity (T)*. Unlike the conventional non-polar micropollutants, such as the notorious initial 12 Persistent Organic Pollutants (POP)s from “Stockholm Convention” [51], the polar organic micropollutants are generally more mobile in the aquatic phase. One suggested parameter to quantify the mobility of the *neutral* organic compounds by the German Environment Agency (UBA) [52] is  $K_{oc}$ , that is, the soil organic carbon-water partition coefficient.  $K_{oc}$  (L/kg) is defined as the ratio of a compound adsorbed onto soil organic matter (µg/kg) versus its dissolved concentration (µg/L) in the surrounding water at equilibrium. If not available experimentally,  $K_{oc}$  can be estimated from the octanol-water partition coefficient  $K_{ow}$  according to the following empirical equation discovered by Karickhoff *et al.* (1979) based on a series of hydrophobic organic compounds (i.e., chlorinated hydrocarbons and polycyclic aromatics) [53].

$$\log K_{oc} = \log K_{ow} - 0.21 \quad (1)$$

By 2019, nearly a half of the European chemicals regulation (REACH) registered organic compounds exhibit highly polar, ionic or ionizable structures [1, 10]. For ionic and ionizable substances, their mobility can be estimated using the pH-dependent soil organic carbon-water partition coefficient  $D_{oc}$  instead, as the total amount of ionic and neutral form (for the non-permanent ionic compounds) should be considered in the adsorbed and dissolved status. . For monoprotic acids and bases,  $D_{oc}$  is related to substances'  $K_{oc}$  and  $pK_a$  as shown in **Eqs. 2 and 3**, respectively [1].

$$D_{oc} = \frac{K_{oc}}{1 + 10^{pH - pK_a}} \quad (2)$$

$$D_{oc} = K_{oc} - \frac{K_{oc}}{1 + 10^{pH - pK_a}} \quad (3)$$

According to the text 126/2019 from the German Federal Environment Agency [10], organic compounds with a  $\log K_{oc}$  or  $\log D_{oc} < 4.0$  over the pH range 4–9 are defined as mobile (M) while assessed as very mobile (vM) with values below a cut-off at 3.0.

Persistence (P) of the organic micropollutants is regulated according to Annex XIII of REACH based on the substance's freshwater half-life [54]. Compounds are referred as persistent (P) with freshwater half-lives >40 days, and very persistent (vP) with longer half-lives >60 days. Arp *et al.* (2017) [1] defined in addition organic micropollutants as “potentially persistent” with half-lives >20 days. In their study, 5155 REACH-registered identifiable organic compounds (by December 2014) were ranked according to a scoring system involving categories of persistence (P) and mobility (M) as shown in **Fig. 1**, which pinpointed 44% of the substances reaching the score of 3 out of 5.

P4 >60 days	Immobile POC	4	4	4.5	5	
P3 >40 days		3	4	4.5	5	
P2 >20 days	Transient		1	2	3	
P1					Unstable MOC	
Min log $K_{oc}$ or log $D_{oc}$ :		M1 ≥ 4.5	M2 3 – 4.5	M3 2 – 3	M4 1 – 2	M5 <1

**Fig. 1.** Modified illustration of the scoring system for persistent (P) and mobile (M) organic micropollutants. Adapted from Arp *et al.* (2017) [1]. Note: in this study, a pH range 4–10 is considered; parameters are determined at a temperature of 12°C or closest temperature possible. The threshold for mobile compounds is defined with a minimal log  $K_{oc}$  or log  $D_{oc}$  at 4.5.

A PM or vPvM substance can be defined as a PMT substance when it fulfills additionally the criteria of toxicity (T) according to Annex XIII of REACH [54] or meets additional toxicity (T) standards, e.g. as being an endocrine disruptor, is carcinogenic or germ cell mutagenic or has effects on or via lactation [55].

### 2.1.2 Sources, emission and detection

Since 2008, PMT substances including insecticides, antibiotics, endocrine disruptors and UV filters are involved on the EU watch list [29, 56]. The types of PM substances, however, go far beyond those. A broad variety of chemicals originated from industrial raw materials and

products [57, 58], pharmaceuticals [59-61], pesticides and herbicides [32, 43, 62] and daily care products [2, 14] fall into the category of PM substances. **Fig. 2** illustrates how PM substances are directly discharged into the surface and ground water from different sources [11, 63]. Unlike non-polar organic micropollutants that can to a large extent be effectively removed by conventional wastewater treatment plants (WWTP), PM substances can readily slip through different barriers in the water treatment facilities and enter the drinking water [11]. Some are even generated within WWTP [2, 63] upon degradation steps [64] or accumulated in the reverse osmosis concentrates [11, 15]. Sjerps *et al.* (2016) [65] screened 174 organic contaminants in 151 Dutch water samples, and found that the most polar organic micropollutants passed WWTP and remained in drinking water. Scheurer *et al.* (2017) [64] reported the high detected concentration of trifluoroacetic acid (TFA), a vPvM with potential toxicity [10], over 20 µg/L in the bank filtration (tap water) from the river Neckar in Germany which contained >100 µg/L TFA resulted from an industrial discharge located 300 km away. These studies evidently demonstrated the high mobility of PM substances in aquatic cycles despite various state-of-the-art barriers.

**Fig. 2.** Emission sources of PM substances in aquatic systems with different barriers in a semi-closed water cycle. Adapted from Reemtsma *et al.* (2016) [66].



including methyl-*tert*-butyl ether (MTBE, ranked 3/936), TFA (ranked 218/936), benzyltrimethylammonium (BTMA) chloride (ranked 313/936).

Although emerging PM substances are increasingly detected in various aquatic environments ever since the invention of the liquid chromatography coupled with mass spectroscopy (LC-MS), it remains a challenge to detect the vM substances with extremely low log  $D_{ow}$  ( $\leq -1$ ) in many analytical labs [11]. Special columns, e.g. mixed-mode LC (MMLC) or hydrophilic interaction LC (HILIC) separation columns [15], need to be employed instead of the most commonly installed reverse phase (RP)–LC column to allow an adequate retardation of vM substances. To complement, ion chromatography (IC) could be utilized to detect ionic vM compounds, such as TFA [64, 69]. Alternatively, some PM substances, such as glyphosate, can be detectable using RPLC-MS after additional derivatization approaches [70]. Considering these required upgrades to a modern analytical lab, it is no wonder that emerging vPvM substances, such as benzyltrimethylammonium (BTMA<sup>+</sup>) and trifluoromethanesulfonic acid, are only detected since 2016 despite their frequent presence in water bodies according to a screen test of 14 European water samples performed in 2019 [15]. Schulze *et al.* (2019) [15] concluded that hundreds of PM substances are likely still undiscovered to date due to this analytical gap [11].

### **2.1.3 Environmental concern**

With the increasing number of emerging organic micropollutants, more work is required to be done for the assessment of the environmental concerns of each PM substance. So far, ecotoxicity studies on PM compounds mainly focused on pharmaceuticals [5, 7, 8, 71] and pesticides [4, 7], while often missing for frequently detected industrial products such as *p*-toluenesulfonic acid [15], except for a few reports on chemicals including benzotriazoles [7] and perfluoroalkyl acids (PFAAs) [7, 72]. Studies on fate of PM substances in water bodies are rather limited as well [56].

Reemtsma *et al.* (2016) [11] posed the question in their feature article: “Is M (Mobility) the new B (Bioaccumulation)?” by comparing PMT with persistent, bioaccumulative toxic (PBT) substances. Unlike the PBT compounds first identified in 1960s, PMT substances are not as prone to accumulate in living organisms. Instead, they are recognized as common hazards to our drinking water today as they effortlessly survive the modern WWTP, posing a special

threat to human and wildlife upon long-term exposure. Particularly, the ionic PM compounds are reported to accumulate in terminal water bodies that are easily evaporated [73, 74]. In the next sections, up-to-date strategies in WWTP are discussed in terms of removal efficiency for PM substances.

## **2.2 Water treatment strategies for PM substances**

A long list of PM substances is resistant to the biodegradation step in the sewage treatment plants [1, 43]. Hence, in this section, we will mainly discuss about the following removal methods for PM substances: activated carbon (AC) adsorption, reverse osmosis and ion exchange, and some oxidative degradation processes such as ozonation. Up to date, these are the most applied techniques in treating PM-contaminated water.

### **2.2.1 AC adsorption**

AC adsorption technique is a quite mature and one of the prevailing water treatment strategies extensively used for removal of pharmaceuticals [13-15, 62], industrial chemicals [75, 76] and pesticides [62]. AC adsorbents typically possess large specific surface area around 1000 m<sup>2</sup>/g and heterogeneous, often micropore ( $\varnothing \leq 2$  nm) -dominant morphology [77, 78]. They exhibit high performance especially for removal of less polar organic micropollutants with  $\log D_{ow} \geq 1$  including various PBTs [11, 79, 80]. Nevertheless, the removal efficiency for very polar organic contaminants, e.g. short-chain PFAAs [64, 69] and MTBE [22, 81], is much less satisfactory on as-received commercially available AC products. One means to improve the adsorption efficiency towards ionic and ionizable PM substances is to equip the AC surface with desired functional groups which allows additional driving forces, such as electrostatic interactions, ion exchange, ion bridging, electron donor-acceptor (EDA) interactions and charge-assisted H-bonds [16].

#### **2.2.1.1 Surface chemistry of pristine AC and its characterization methods**

The as-received AC adsorbents carry a variety of acidic and basic O-containing groups as illustrated in **Fig. 3**. The  $pK_a$  of carboxylic, phenolic, lactone and pyrone groups at the edges of the basal planes in carbonaceous adsorbents are in the range of 3–6 [82], 8–10 [83], 7–9 [78] and 4–13 [84], respectively. The delocalized  $\pi$ -electron regions ( $C\pi$  in **Fig. 3**) appear basic as they can adsorb protons from the aqueous surrounding (the exact  $pK_a$  is yet

unknown [78]) [20, 85]. The mixture of functional groups on the pristine AC surfaces indicates the co-existence of negatively and positively charged sites over an environmentally relevant pH range, and often leads to slightly charged surfaces (negative or positive) at neutral pH values [20, 22, 86].

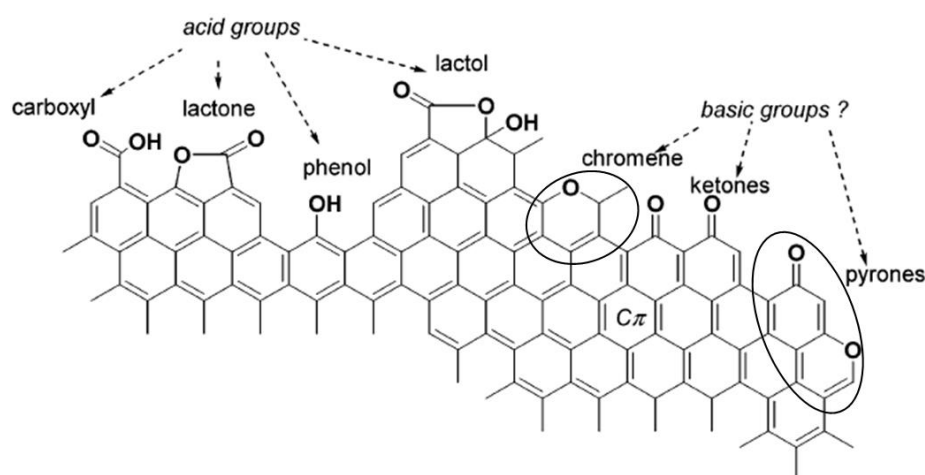


**Fig. 3.** Commonly existing oxygen-containing functional groups on pristine AC surfaces. Adapted from and modified after Fuente *et al.* (2003) [84].

Many parameters are reported in literatures to assess the surface charge status of AC materials, yet in fact providing different insights into the AC chemical properties. The most frequently reported related characteristics are O/C ratio and point of zero charge ( $\text{pH}_{\text{pzc}}$ ), while sometimes total acidity, zeta potential ( $\zeta$ ) and ion exchange capacities are also determined.

The O/C ratio, often derived from the elemental analysis, is more an indicator for AC surface hydrophobicity [17] than a direct statement in surface charge status due to the ambiguous basic and acidic properties of each O-containing moiety (see **Fig. 3**).

Although zeta potential is regularly measured for nanomaterial [87], membranes [88] and metallic oxides [89], etc., it is less suitable to address the charge status right at the surface of the AC pores. The reason is that zeta potential characterizes the external surface of a particle whereas porous adsorbents are dominated by their intraparticle surface. Both surfaces may possess different properties. **Fig. 4** illustrates the electrical double layer (EDL) formation on a carbonaceous surface once it encounters an electrolyte solution. Due to the comparable Debye radius  $\lambda_D$  (i.e. the length within which the electrostatic effect persists) to the micropore diameters, an EDL overlap is expected in the AC micropores, which can be better

described by the modified Donnan model (**Fig. 4b**) than the traditional Gouy-Chapman-Stern model (**Fig. 4a**). The zeta potential is defined as the potential at the beginning of the diffuse layer [6], which is clearly distinct from the potential at the carbon surface [90] as shown in **Fig. 4**.

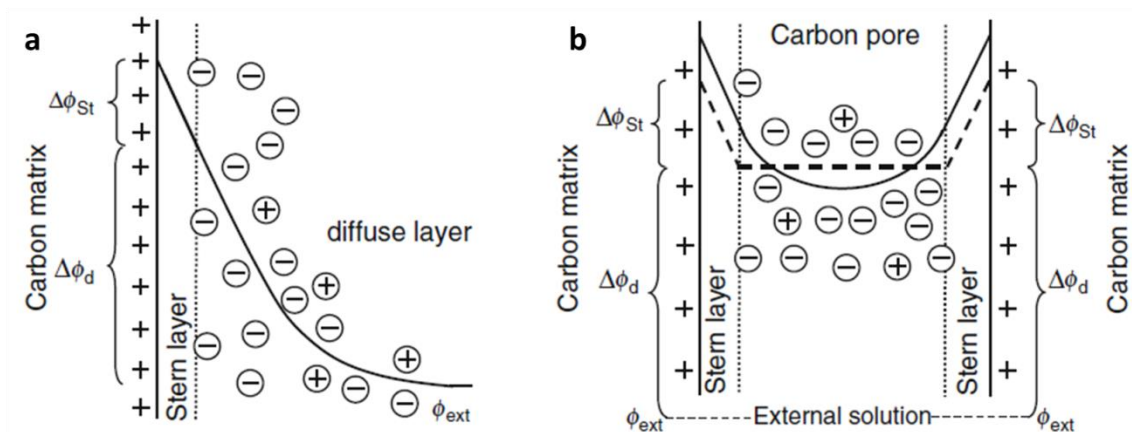


**Fig. 4.** Schematic illustrations of electrical double layer (EDA) models for one carbonaceous material. (a) Gouy-Chapman-Stern model without EDL overlap. (b) modified Donnan model with EDL overlap in micropores. The curves are the course of the electrical potential. Adapted from Biesheuvel *et al.* (2014) [91].

$pH_{pzc}$  (or more precisely, the point of zero net proton charge =  $pH_{PZNPC}$ ) is the pH value at which the net surface charge of adsorbent is equal to zero [92]. Both  $pH_{pzc}$  and total acidity (or more precisely, the titratable acidity [93]) can, however, only reflect AC surface changes associated with the exchange sites for protons. In comparison, although less often reported, ion exchange capacity can provide quantitative information of adsorbent surface charges at specified pH values [81]. Sigmund *et al.* (2020) [17] and our recent studies [20, 81] pointed out that the ion exchange capacity is “a frequently underestimated key property” for assessing AC adsorbents targeting at PM adsorption which shall be regularly determined in the future studies to contribute for an in-depth understanding of PM adsorption on carbonaceous materials.

Besides the above mentioned (semi-)quantitative parameters, a spectrum of materials characterization techniques can shed light on the exact types of heteroatom-containing functional groups which an AC adsorbent contains originally or upon surface modification (see **Section 2.2.1.2**). Frequently applied techniques include infrared spectroscopy (IR) [77] and high-resolution X-ray photoelectron spectroscopy (XPS) [81], both can specify O=C=O,

C=O, C–O, C–C/C–H moieties and beyond. Raman spectroscopy was reported to measure the graphitized grade of AC materials [94-96]. By thermally treating the AC materials in different atmospheres following a heating program one can gain information of the functional groups of AC from the analysis of the released gas molecules. Two examples of this technique are temperature-programmed desorption (TPD, AC detaches or desorbs functional groups upon heating in an inert atmosphere) [81] and temperature-programmed reaction spectroscopy (TPRS, AC undergoes reaction with the gas flow) [97]. An understanding of the exact AC surface chemistry is essential to evaluate various interactions between PM substances and carbon surface during the adsorption process [16].

### **2.2.1.2 Effect of AC surface chemistry on PM adsorption**

Two strategies are commonly used to introduce anion exchange sites on AC surface and thereby promote anionic PM uptake: 1) defunctionalization and 2) functionalization with N-containing groups.

Through annealing in inert ( $N_2$  or Ar) or reducing atmosphere ( $H_2$  or  $N_2/H_2$  mixture) at elevated temperatures  $\geq 900$  °C, AC surfaces become rich in  $\pi$ -systems and poor in O-content [21, 22, 98, 99]. Not only anion exchange sites are generated in forms of protonated  $\pi$ -systems, the AC surface turns more hydrophobic as well. This allows electrostatic attraction and enhanced non-Coulombic interaction between anionic PM substances and AC surfaces and resulted in improved adsorption efficiencies for 2,4-dichlorophenoxy acetic acid ( $pK_a = 2.73$  [100]) and benazolin ( $pK_a = 3.04$  [101]) [99], perfluorooctanoic acid (PFOA,  $pK_a = 0-1$  [102]), perfluorooctanesulfonic acid (PFOS,  $pK_a = -3.27$  [103]) and perfluorobutanoic acid (PFBA) ( $pK_a = 0.4-0.7$  [102]) [21, 98] as well as TFA [69] ( $pK_a = 0.23$  [48]). Also, better adsorption performance was found for nonionic polar organic compounds such as MTBE [22, 81] and *p*-toluenesulfonamide [81] on defunctionalized AC adsorbents due to enhanced hydrophobic effects. Alternatively, AC surfaces modified with N-containing group are positively charged and thus can electrostatically interact with anionic PM substances to facilitate the adsorption. Zhi *et al.* (2016) [86] modified AC surfaces by treating the adsorbent in ammonia gas at 700 °C to improve its PFOA and PFOS uptake [86]. Sun *et al.* (2019) designed quaternary nitrogen-grafted [104] and polypyrrole-grafted [105] AC surfaces, which significantly enhance the adsorption of TFA.

Water PM contaminants are not limited to neutral and anionic ones. Quite a few compounds including surfactants (e.g. BTMA<sup>+</sup>), herbicides (e.g. triazine), pharmaceuticals (e.g. sulfamethazine and adamantan-1-amine) and industrial chemicals (e.g. 2-(piperazin-1-yl)ethan-1-amine) are permanently or predominantly positively charged within a certain pH range [15]. Yet no straightforward surface modification strategy can serve as a universal solution to improve AC adsorption towards cationic PM substances. That is because the introduction of cation exchange sites on AC by surface oxidation comes at a price of reduced surface hydrophobicity. The final trade-off between the enhanced electrostatic attraction and the weakened hydrophobic effects does not necessarily lead to an improved adsorption performance. Duman *et al.* (2010) [106] pointed out a minor contribution of electrostatic interactions and a major driving force from hydrophobic effects for the adsorption of eight aromatic cationic surfactants on a single type of AC cloth [106]. However, our recent study [81] indicates a more significant contribution of the electrostatic interactions for the adsorption of the smaller, more polar cationic compounds, as the oxidized AC shows the best adsorption efficiency for BTMA<sup>+</sup> (calculated  $\log D$  (or  $\log D_{ow}$ ) = -2.25 [107]) whereas not for benzyltriethylammonium (BTEA<sup>+</sup>,  $\log D$  = -1.18 [107]) and tetrapropylammonium (TPA<sup>+</sup>,  $\log D$  = -0.45 [107]). Compared to the adsorption studies on anionic and nonionic PM substances, much less research has been conducted for cationic compounds. Sigmund *et al.* (2020)[17] described the available data from the currently existing AC adsorption studies on cationic organic compounds as a “small and noisy data set” when developing the latest prediction tool for PM adsorption on carbonaceous materials using a deep learning neural network approach. A more detailed discussion on the advantages and limitations of the recent prediction models for PM adsorption on AC is given in the publication in **Section 3.1**.

### 2.2.2 Reverse osmosis

Just like AC adsorption, reverse osmosis and ion exchange are in most cases pure separation processes (unless the AC or membrane surfaces are modified with reactive sites) that generate no problematic transformation products.

**Reverse osmosis** is the water treatment technique which works as a universal strategy for PM removal of various kinds and presents one of the best efficiencies [11, 64, 108]. Albergamo *et al.* (2019) [108] showed high rejection  $\geq 75\%$  for 30 PM substances containing in a riverbank filtrate from a Dutch province using reverse osmosis. Among them,

outstanding rejection of  $\geq 92\%$  were found for all 8 neutral and moderate hydrophobic PM substances (calculated  $\log D \geq 2$  at pH 7 using Chemaxon [107]) regardless of their structural features. For 10 non-charged and hydrophilic PM substances ( $\log D < 2$  at pH 7), a clear correlation between size and rejection was observed, i.e. the larger the molecule, the better the removal efficiency. A less satisfactory rejection of around 75% was found for the smallest PM, 1H-benzotriazole ( $M = 119$  g/mol), in this category. In addition to the non-charged PM substances, 9 anionic and 3 cationic PM substances were also included in this study. The additional electrostatic repulsion between the negatively charged polyamide-based ESPA2 membrane and the anionic PM substances are claimed to account for nearly no passage found for anionic PM substances. On the contrary, lower rejection of cationic PM substances with comparable sizes was seen.

A monitoring study from Appleman *et al.* (2014) [75] on the treatment of PFAS in 15 full-scale water treatment systems in the U.S. shows generally comparable or higher removal efficiencies by means of reverse osmosis than AC adsorption. In particular, reverse osmosis maintained its good removal efficiency for short-chain PFAAs (down to C4, i.e. PFBA) whereas declined adsorption efficiency was found on AC. However, according to Saeidi *et al.* (2020) [21], the adsorption affinity and capacity towards PFBA, PFOA and PFOS were drastically improved after AC surface defunctionalization by >20-folds and >60-folds, respectively, indicating the potential of applying AC adsorption to treat PFAA-contaminated water.

Despite the superior removal effectiveness of reverse osmosis in general, it remains by far one of the most costly and energy-demanding water treatment techniques [75]. Besides, a considerable amount of brine produced during the reverse osmosis needs to be further treated [11], e.g. by means of capacitive deionization (CDI).

**Anion exchange (AIX)** is a technique getting increasing attention in the field of water treatment due to many emerging anionic PM substances at neutral pH, such as PFASs [64, 75, 76, 109]. Appleman *et al.* (2014) [75] reported an adequate removal efficiency of  $\geq 75\%$  for PFOA by AIX and a high removal efficiency of  $\geq 90\%$  for PFOS in comparison to only around 80% for perfluorobutanesulfonic acid (PFBS) and almost no removal for PFBA. McCleaf *et al.* (2017) [76] also confirmed the generally higher removal effectiveness of AIX for perfluoroalkyl sulfonic acids (PFSAs) than for perfluoroalkyl carboxylic acids (PFCAs) and a

declining removal efficiency for short-chain PFAAs by ca. 10% “per perfluorocarbon chain length”. Desorption of PFAA (C4-C8) were observed, with the longer-chain ones found at higher bed volumes, presumably due to the considerable competition of the present longer-chain PFAS (C9-C12, C14) and/or dissolved organic carbon (DOC). Franke *et al.* (2021) [109] concluded a superior efficiency for PFAS removal as well as a better cost-effectiveness by means of AIX over granular AC adsorption [109]. However, as mentioned above, enhanced adsorption performance achievable by AC surface defunctionalization was again not considered in their cost estimation. On top of that, our recent work on adsorption of TFA in a rapid small scale flow unit using a defunctionalized AC felt (see Manuscript in **Section 3.3**) demonstrates an effective, favored removal of TFA over co-existing inorganic anions including  $\text{Cl}^-$ ,  $\text{SO}_4^{2-}$  and  $\text{NO}_3^-$ , which was not the case (i.e. strong interfered TFA removal by the present anions) in the reported AIX process [64].

### 2.2.3 Oxidative degradation strategies

After being separated from water and enriched in concentration, PM micropollutants need to be degraded to non-toxic species by means of different degradation strategies. The degradation efficiency depends on the types of PM molecules and the degradation mechanism. Oxidative degradation processes are commonly applied strategies in water treatment. A huge amount of literature exists on this topic [110-113]. Here, we chose a few examples of typical oxidative processes on degrading PM substances in this section for discussion.

Ozonation is widely applied for water disinfection. Modern ozonation processes often combine  $\text{O}_3$  with another oxidant, e.g.  $\text{H}_2\text{O}_2$ , or activation energy source, e.g. UV, or catalysts, e.g. metal oxides, to produce a higher yield of reactive  $\bullet\text{OH}$  radicals and thereby improve the mineralization degree [11, 110]. Rekhate *et al.* (2020) [110] recently published a comprehensive review on ozone-based approaches for the degradation of various PM substances. Excellent removal efficiencies ( $\geq 90\%$ ) of advanced ozone-based degradation were shown for 4-nitrophenol, ciprofloxacin, 4-chlorophenol, bisphenol-A, phenacetin, oxalic acid as well as a variety of dye compounds. A complete removal of ibuprofen was reported via  $\text{O}_3/\text{WO}_3$  treatment under visible light irradiation [114]. Nevertheless, only partial mineralization (40-70%) was achievable for diclofenac [115], sulfamethoxazole [116] and sulfamethazine [117]. Other advanced oxidation processes (AOPs) in organic contaminant



degradation using the oxidizing power of highly reactive  $\bullet\text{OH}$  radicals generated chemically, sonochemically, photochemically or electrochemically are comprehensively reviewed in [111, 112].

Oxidative degradation approaches based on  $\text{Cl}\bullet$  or  $\text{SO}_4^{\bullet-}$  radicals are also applied in wastewater treatment. Sichel *et al.* (2011) [118] compared the performance and energy efficiency of a UV/chlorine approach to the state-of-the-art UV/ $\text{H}_2\text{O}_2$  process on the degradation of 8 model emerging organic contaminants including benzotriazole, desethylatrazine, sulfamethoxazole, diclofenac, iopamidole, carbamazepine, tolyltriazole and 17 $\alpha$ -ethinylestradiol. Except for desethyl-atrazine, the UV/chlorine approach presented comparable or superior degradation efficiencies and considerable reductions (30-75%) in the estimated energy consumption. The excess chlorine can be eliminated by adding thiosulfate to the system after the degradation process.

Being less reactive than  $\bullet\text{OH}$  radicals,  $\text{SO}_4^{\bullet-}$  radicals with lower scavenger rates can selectively target certain organic moieties. While  $\bullet\text{OH}$  and  $\text{Cl}\bullet$  radicals are ineffective against PFAS,  $\text{SO}_4^{\bullet-}$  radicals generated for example by photolysis of sodium persulfate can oxidize PFCAs and lead to full mineralization of this subgroup of “forever chemicals” [75, 119]. Total mineralization of PFOA towards  $\text{CO}_2$  and  $\text{F}^-$  was also reported by direct electrochemical oxidation on boron-doped diamond (BDD) anodes [120]. PFOS carrying the sulfonic group is more reluctant to oxidation processes than PFOA. It was reported to be partially degraded only by electrochemical oxidation on mixed metal oxide [121] or BDD anodes [122], or via photocatalytic degradation [123].

One drawback of oxidative degradation approaches in wastewater treatment is the potential formation of toxic by-products [124, 125], making themselves an additional source of even more mobile organic contaminants (e.g. the shorter-chain PFSA formed after the partial degradation of PFOS) in water. During the electrochemical oxidation processes, undesired  $\text{ClO}_4^-$  and halogenated organic compounds can be easily generated since  $\text{Cl}^-$  is almost inevitable in water sources [125]. The formation of such unwanted by-products can be limited by adjusting the applied current density, background pH value and/or charging duration [126]. Alternatively, one can apply a CDI step in advance to remove chloride and then replace the background solution by a Cl-free electrolyte, such as sodium sulfate. Overall, modern WWTP efficient in PM removal shall involve combined separation and degradation

techniques in subsequent steps to target emerging PM substances with diverse properties [109].

## **2.3 Electro-assisted sorption processes for PM removal**

### **2.3.1 Inspiration from capacitive deionization (CDI)**

Electro-assisted ad-/desorption approach for the removal of organic contaminants from water was developing along with capacitive deionization (CDI) for water desalination. CDI is a promising, ambient alternative to reverse osmosis and ion exchange for the removal of inorganic ions from water via electro-controllable sorption-based processes. The adsorbents, which also function as the electrodes in CDI, can be regenerated *in-situ* as the ions are desorbed when short-circuited or upon reversed polarization (and energy thereby recovered like in a capacitor) [27]. The concept was first used in Blair and Murphy's pioneering work in 1960 [127]. About 10 years later, Strohl and Dunlap presented the first electrosorption study on organic compounds to separate nonionic quinones from quinone sulfonic salts [128]. After the initial slow progress of CDI, the past two decades have seen vast development in terms of theory [129, 130], designs of electrode [131, 132] and cell configuration [133, 134], etc., which finally inspired applications in water desalination worldwide [133, 135, 136]. In contrast, the development of organic micropollutant removal via electrosorption is delayed until recently as the emerging organic contaminants bearing features closer to inorganic ions, i.e. ionic PM substances, are just started to become increasingly detected and regulated [15]. In this section, we will discuss 1) which options on electrode materials, operation modes and cell configurations are offered by the advanced CDI technique, and 2) which options have been or can be applied for electro-assisted removal of PM substances by identifying the differences between electrosorption of ions and polar organic compounds.

Porous materials as for electrosorption of organic compounds are intensively used in CDI to allow the capacitive uptake of inorganic ions from the water media. Carbonaceous or carbon-based hybrid materials, conductive and easy to equip with porous morphologies, are the most frequently applied electrode materials in CDI [26]. In addition to the carbon-based porous electrodes, classic battery electrodes also find their applications in CDI (see configuration E and F in Fig. 5) [132, 137, 138]. For instance, Lee *et al.* (2014) [132] developed a "hybrid capacitive deionization (HCDI)" system which includes a  $\text{Na}_4\text{Mn}_9\text{O}_{18}$  electrode for the selective capture of sodium ions and a porous carbon electrode covered by

an anion exchange membrane for the uptake of chloride ions from the inflow NaCl stream. The system showed a doubled capacity of ion removal compared to a typical CDI reactor equipped with symmetric activated carbon electrodes. Moreover, the selective adsorption of sodium manganese oxide towards cations eliminates the usage of cation exchange membrane otherwise needed in the traditional membrane CDI (MCDI, configuration **C** in **Fig. 5**). However, a concern rises accordingly on the performance of such battery electrodes for desalination in real water matrix where many various kinds of ions co-exist, as these electrodes are currently only designed for the adsorption of single ion species [27]. In comparison, MCDI based on the use of symmetric porous carbon electrodes are expected to provide a universal salt removal solution for the water sources of various kinds.

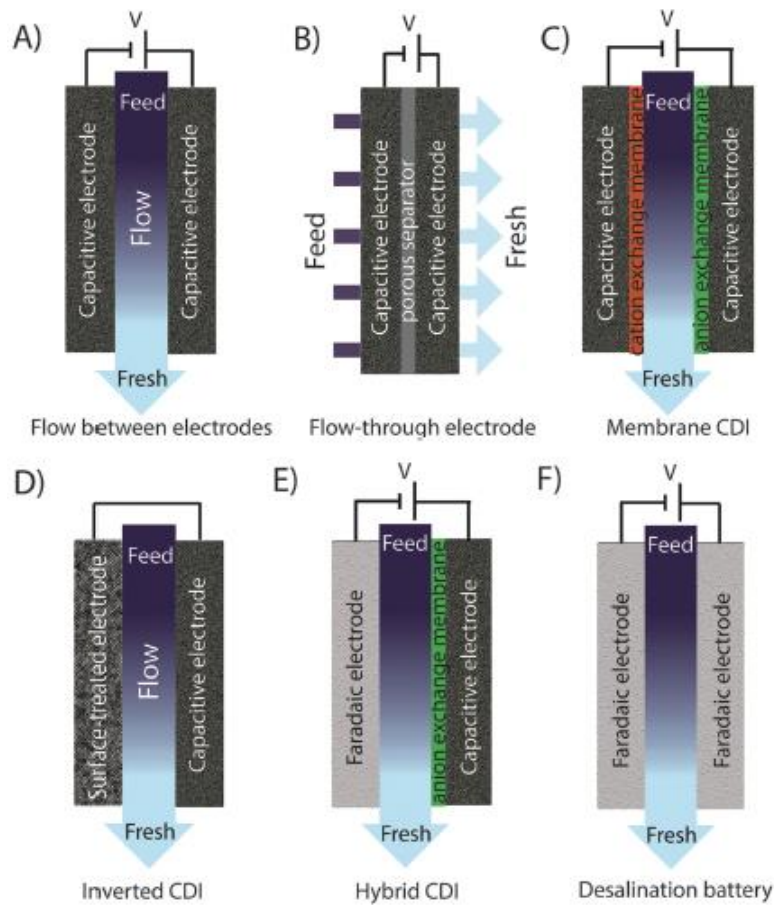


**Fig. 5.** Schematic illustrations of different CDI configurations. Adapted from Suss *et al.* (2015) [27].

Carbon surface chemical modification opens up the possibility to use inverted CDI (i-CDI) system (configuration **D** in **Fig. 5**) for water desalination [139, 140]. The idea of i-CDI is to achieve cation and anion adsorption onto surface modified porous carbon electrodes

carrying respectively net negative and positive charges at no external charging (adsorption during discharging), and desorb the ions by applying an adverse potential to the electrodes (desorption during charging). Gao *et al.* (2015) [140] pointed out that the system stability of an i-CDI cell is much better compared to a CDI cell operated in the normal way, as the surface oxidized porous carbon electrode which takes up the cations at no external potential can hardly lose its adsorption efficiency due to a further oxidation during the desorptive charging. The working voltage window of an i-CDI cell is dependent on the carbon surface modification and defined by the difference of the potential of zero charge ( $E_{pzc}$ ) of the anode and the cathode [139].  $E_{pzc}$  is the applied potential at which the carbon surface carries zero net charge and shows the minimal capacitance. It relates adversely to the  $pH_{pzc}$  of the carbon material, meaning a higher  $pH_{pzc}$  is found to correlate with a lower  $E_{pzc}$  value [140]. Both cyclic voltammetry (CV) and electrochemical impedance spectroscopy (EIS) can be used to evaluate the capacitive electrode's  $E_{pzc}$  [140-142].

Other CDI configurations, such as the flow-through CDI cell (configuration **B** in Fig. 5), are as well reported. Avraham *et al.* (2009) [134] observed a faster cell charging in a flow-through cell over a flow-between (also called flow-by) cell. However, Cohen *et al.* (2015) [143] reported a better system stability of the flow-between cell. The recently published review paper by Wang *et al.* (2021) [28] further summarized the second to third generations of CDI cell designs involving novel electrode materials and mechanisms, and/or multi-channel structures.

The rapid progress in CDI provides many valuable references for the development of novel approaches for electro-assisted PM removal (see further discussion in **Section 2.3.3**). Yet, not every experience is directly transferable, since a few fundamental differences as listed below exist for ion electrosorption and PM electrosorption, which lead to distinct key factors in the design of these two approaches.

**1) Different adsorption drivers.** Unlike for inorganic ions, drivers for PM adsorption on carbonaceous materials are not limited to electrostatic attraction, ion bridging and/or ion- $\pi$  interactions. In many cases, hydrophobic effects and  $\pi$ - $\pi$  interactions are identified to have a significant impact on the adsorption of PM compounds [81, 96, 106]. Therefore, porous carbon electrodes are likely to be more suitable than metal oxide battery electrodes in terms of PM adsorption upon electrode polarization. Due to the difference in driving factors in

adsorption, a fast charging velocity is probably not as important for PM electrosorption as for ion electrosorption.

2) **Different desired adsorbent pore size.** Micropores ( $\varnothing \leq 2$  nm) of porous carbon electrodes contribute the most to the desalination capacity in CDI cells [130, 144, 145], whereas mesopores ( $\varnothing = 2$ -50 nm) can be important for the uptake of the bulkier organic compounds [146-148]. Carbon-based materials with significant portions of mesopores, such as carbon aerogels after thermal activation in CO<sub>2</sub> and N<sub>2</sub> [97], could allow the electro-assisted uptake of a wider range of PM substances than materials with micropores alone.

3) **Different required potential windows.** Cations that are regularly targeted in CDI such as alkali and alkaline earth metals are chemically inert, whereas common inorganic anions such as chloride and nitrate can undergo electro-redox reactions upon electrode charging [149, 150]. A relative small cell voltage ( $\approx 1$  V) should be applied in CDI to reduce water splitting and other unwanted redox reactions [27]. It is more complicated to determine the potential window for electrosorptive PM removal as the functional groups of PM molecules exhibit highly diverse electrochemical redox properties: for example, anilines can be easily oxidized even at mild charging conditions (oxidation potentials around 0.6-1.2 V vs. standard hydrogen electrode (SHE) according to [151]), whereas PFAS can only be oxidized at very high anodic potential (with cell voltage  $> 5$  V in [122]). Dependent on the target PM types, different potential windows should be set to avoid complex Faradaic processes, unless the PM electrochemical degradation is well-understood and also desired. Three- or four-electrode cell is recommended to be applied instead of two-electrode systems where only a certain cell voltage can be set, so that the electrode processes can be better controlled and investigated [140, 152]. Ion exchange membranes can be applied to block the access of redox-reactive ionic PM towards anode or cathode and thereby exclude undesired redox reactions.

4) **Different contaminant initial concentration.** Contrary to the typically  $> 10^5$ -fold higher ion concentrations in water to be treated with CDI, PM substances are usually present in ng/L -  $\mu$ g/L range in the aquatic systems. As a result, high adsorption *capacity* of the electrode is a key for CDI application whereas high adsorption *affinity* is more essential for treatment of water contaminated by PM substances. Due to the generally stronger interactions between PM substances and porous carbon compared to ions and the much lower initial

concentration of PM substances, much extended operation time needed for full uptake can be expected for PM substances. In this sense, the system stability could be an even more crucial factor in the design of PM electrosorptive removal approaches.

### 2.3.2 Development of electro-assisted sorption for PM removal

The development timeline of the electrosorption of organic compounds in 1985-2010 is demonstrated in **Fig. 6** indicated with a few milestones. After the first work from Strohl and Dunlap on the organic substance electrosorption was published in 1972 [128], it is a big step forward in terms of adsorption capacity when AC started to be used instead of graphite-like carbon in the investigation of organic compounds electrosorption 13 years later [153]. In 1986, Woodard *et al.* [44] made the first attempt to improve the ad-/desorption of positively charged Rhodamine B at 0.04 V and 0.84 V vs. SHE and showcased the selective removal of tyrosine cations and benzene sulfonate anions from a mixture via electrosorption. The pioneering electro-assisted “Get&Dump” concept mentioned back then was the first inspiration for later case studies where an enhanced PM removal and *in-situ* adsorbent regeneration were achieved via swings of electrode polarization [23-25, 31, 36, 42, 96, 154-157].

As Woodard *et al.*'s work [44] already enlightened that the surface functionalization of the adsorbent is an influencing factor on electrosorption, Bán *et al.* (1998) [154] introduced the key parameter, i.e., the adsorbent's potential of zero charge ( $E_{pzc}$ ), in the study of electrosorption behaviors of differently charged organic compounds on AC materials. By plotting the loading (represents adsorption capacity) and Freundlich parameter  $K_F$  (represents adsorption affinity) vs. the applied bias potential  $E$  on carbon related to its  $E_{pzc}$ , the impact of the carbon surface charges on the electrosorption was “normalized” so that the distinct electrosorption behaviors of neutral (benzyl alcohol), cationic (methyl-quinolinium cation) and anionic (naphthalenesulfonate and naphthoate) organic compounds resulted from their charge statuses became visible. A bell-shape profile of the electrosorption of neutral benzyl alcohol was observed: the best adsorption performance was seen at  $E = E_{pzc}$  where the carbon surface was neutralized, and desorption took place at more positive and more negative bias potentials upon the intensified competition of the water adsorption on AC. On the contrary, only a half bell-shape profile (i.e. a rising or falling curve) was observed for ionic organic compounds in the investigated potential range (-0.4 V to +0.8

V vs. SHE). The adsorption of the cationic methylquinolinium was enhanced as a more negative bias potential was applied whereas the adsorption of anionic naphthalenesulfonate and naphthoate was improved by applying a more positive bias potential.

Bán *et al.* [154] has provided a powerful model for a systematic investigation of the effects of 1) adsorbent surface chemistry and 2) adsorbate (charge) properties on electrosorption, which was however surprisingly rarely considered in later studies, except for in Fischer's dissertation (2001) [23] and in the recent works [23, 96]. Fischer (2001) [23] proposed the full bell-shape profiles to ionic organic solutes in a wider potential range where the maximum adsorption capacity and affinity should be shifted to  $E > E_{pzc}$  for anionic compounds and  $E < E_{pzc}$  for cationic ones, and desorption should then occur at extended bias potentials as seen for the neutral compounds. Saeidi *et al.*'s (2021) findings [23] on the electrosorption of PFOA and PFBA confirmed Fisher's hypothesis. However, complicated redox reactions of water and AC expected at the boundary conditions (e.g. -0.8 V and 1.2 V vs. SHE) [149, 152] could have had an additional effect on the "electro-sorption" profiles. In addition, our most recent study followed the inspiration from Bán *et al.* and broadened the picture by involving two AC felts carrying distinct surface chemistries and a selection of neutral, cationic and anionic PM targets [96].

An increasing number of studies came out on the electrosorption of more environmentally relevant PM substances since 2007/2008 when PMT substances first appeared on the EU watch list [29]. The targeted PM pollutants for electrosorption cover the surfactants (sodium dodecyl-benzene sulfonate (-) [158]), pesticides (bentazone [30, 31]), herbicides (metribuzin [32], 8-quinolinecarboxylate (-) [33], 2,4-Dichlorofenoxyacetate (-) [34]), PFAS ((-) at pH 7) [23, 39-42], antibiotics and other pharmaceuticals (tetracycline [35], sulfadimethoxine (predominantly (-) at pH 7) [36], ciprofloxacin (predominantly (+) at pH 7) [36], clarithromycin (predominantly (+) at pH 7) [36], norfloxacin ((-) at pH 7) [37], carbamazepine [38], pentoxifylline [38]), and hormone and endocrine disruptors (estrone [38], bisphenol A [38]) in the past decade.

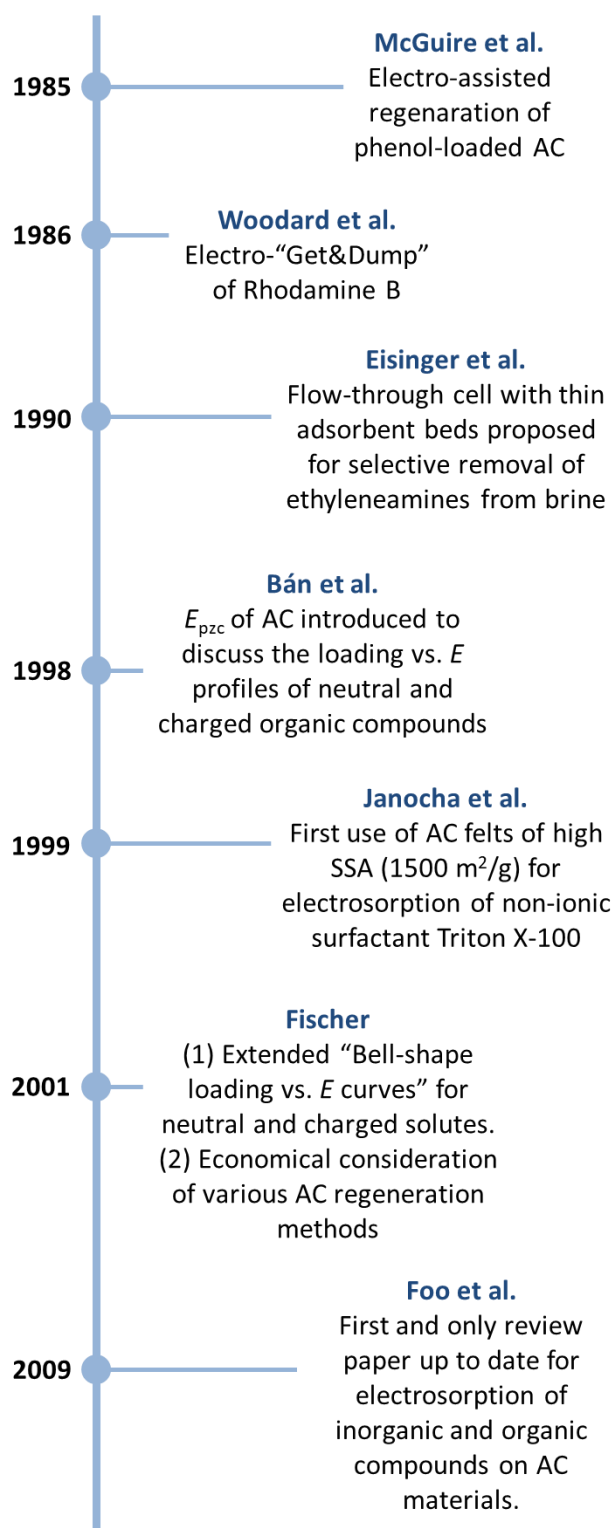


**Fig. 6.** Milestones of the development of electrosorption of organic compounds on AC-based materials (1985-2010). The cited papers are McGuire *et al.* (1985) [153], Woodard *et al.* (1986) [44], Eisinger *et al.* (1990) [159], Bán *et al.* (1998) [154], Janocha *et al.* (1999) [160], Fischer (2001) [161] and Foo *et al.* (2009) [162].



Wang *et al.* (2018) [36] investigated the electrosorption of sulfadimethoxine, ciprofloxacin and clarithromycin in a batch and flow mode using AC felts being the anode and cathode asymmetrically (i.e. triple the amount of AC used for anode than for cathode). A significant enhancement in the removal efficiency indicated by a 5-fold higher adsorption capacity was achieved when external potentials were added. *In-situ* generation of sulfadimethoxine-loaded AC felt was proven feasible by pumping the system with clean electrolyte solution at a high flow rate (20-fold higher than the flow rate in the adsorption step) when a polarization condition adverse to that needed for the enhanced adsorption was applied. An adequate system stability over four electro-assisted ad-/desorption cycles of sulfadimethoxine was shown (i.e., still 84% adsorption capacity at the fifth cycle and maintained desorption efficiency of 96% during the first four cycles). Although the adsorption capacity towards the target PM substances was harmed in the presence of dissolved organic carbon (DOC) in real water matrix, applied potential still showed a remarkable enhancing effect on the removal of PM substances as well as DOC. In spite of the certainly useful scientific outcomes for the future design of electrosorption cells from this article, its value in application is limited by using a two-electrode system in the experiments as the effect of a certain cell voltage provided by a two-electrode system is often not directly transferable when the cell configuration/construction is slightly changed. At least a three-electrode setup will be needed to monitor the bias potential and/or current on the anode and/or cathode so that a comparable electrosorption effect on a certain target PM can be expected when the same polarization conditions are applied in another electrochemical cell [140].

Some most recent research demonstrated the successful combination of electrosorption with advanced techniques, such as renewable energy generation and electrooxidative degradation, for upgraded treatment of water contaminated by PM substances. For instance, Yang *et al.* (2015) [35] designed a flow-mode electrosorption cell powered by microbial fuel cells for the removal of tetracycline. Chen *et al.* (2018) [163] developed an energy-efficient pulsed “electrosorption-electrooxidation-electrosorption” circuit on porous TiO<sub>2</sub>-nanotubes/3D-SnO<sub>2</sub>-Sb electrode for the effective removal of benzoic acid from water. The electrosorption step was identified to have a great contribution to the degradation efficiency. Kim *et al.* (2020) [42] also integrated electrosorption (capture&release) with *in-situ* electrooxidative degradation on BDD electrode for the removal of PFAS. Novel conductive

redox-copolymers carrying amine (N-H) functional groups were used as the adsorbent and electrode during the electrosorption step. The amine groups can be oxidized to nitroxyl radicals (N-O•), which are redox-active and can become positively charged (+N=O) upon anodic polarization. As shown in **Fig. 7**, the ratio of amine groups and nitroxyl radicals can be optimized in a controllable manner, which can then regulate the adsorbent hydrophobicity as well as anion exchange capacity for the best electrosorption performance. Nevertheless, as pointed out by Suss *et al.* (2015) [27], there must be a trade-off in Kim *et al.*'s approach between the sacrificed energy efficiency in capacitive uptake of target anionic PM substances and the advances using electrochemically controllable trap and release, which need to consume the electric energy that could otherwise be used fully for the capacitive adsorption.

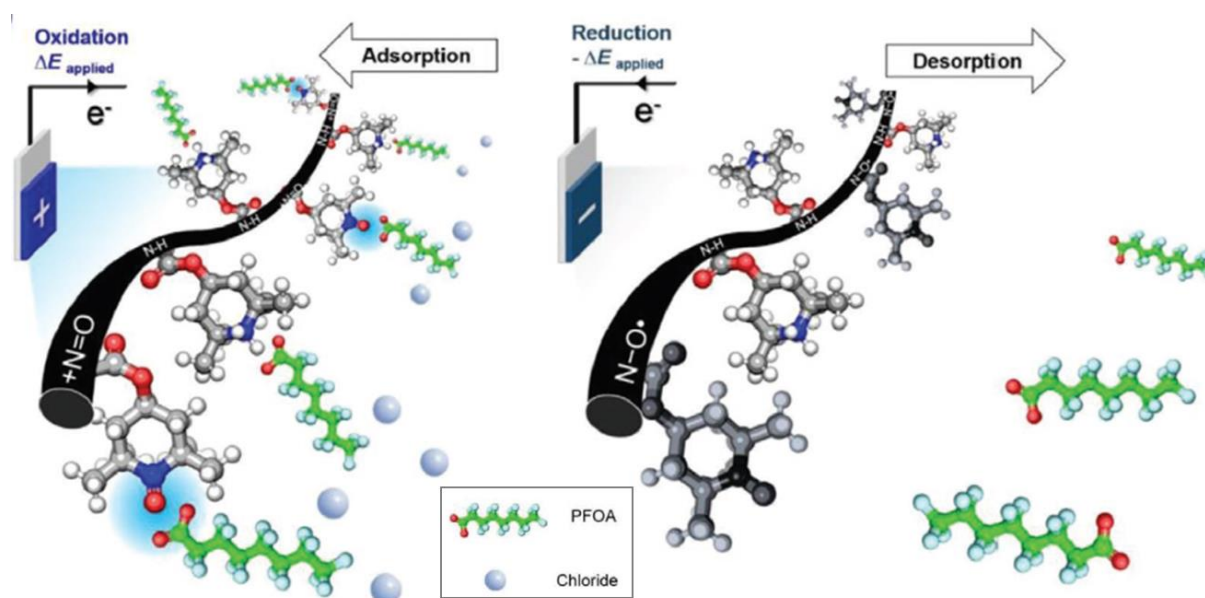


**Fig. 7.** Schematic illustrations of electrochemically controllable PFOA ad- and desorption in the system with N-containing redox-copolymers being the electrode. Adapted from Kim *et al.* (2020) [42].

### 2.3.3 Unknowns of state-of-the-art PM electrosorption

To realize the electro-assisted PM removal technique in real water treatment applications, one needs to tackle the following unknowns of state-of-the-art research.

- Unknown 1: *Can electrosorption provide a universal removal strategy for all PM types?*

Very limited work on PM electrosorption has covered a variety of nonionic, cationic and anionic compounds [36, 44, 45], leaving the question rather unsorted.

- Unknown 2: *How do AC physiochemical properties affect PM electrosorption?*

The effect of surface chemistry or morphology was hardly considered in the previous studies except in refs. [43, 44], leaving it rather unclear how AC surface chemistry can be modified to facilitate its electrosorption efficiency towards PM compounds.

- Unknown 3: *How is the system stability of an effective PM electrosorption approach (1) using ACs of different physiochemical properties and (2) under different operation conditions? And how can it be improved?*

Porous carbon anodes are prone to electrooxidation both in CDI cells and electrosorption cells for PM removal over ad-/desorption cycles, which significantly diminished the system performance [140, 143, 164]. Not only has the carbon surface chemistry altered, Ania and Béguin (2008) [31] also reported a 20% shrinkage in specific surface area and total pore volume of AC cloth after being used for bentazone adsorption and electro-assisted regeneration at ca. -1 V vs. SHE over 6 cycles. Still, investigation on the adsorbent stability during the electro-assisted PM removal processes was missing in general even in studies where ad-/desorption cycles were conducted, except for in a few cases [31, 43, 164].

Suggestions which could allow an improved system stability inspired by the existing research (mostly in the field of CDI) includes applying milder anodic conditions [23], performing electrosorption under inert atmosphere [143, 152], intermittent reversal of the polarization conditions on the electrodes [143, 165], and using a i-CDI-like operation mode where the electro-assisted desorption conditions should only have a weak effect on both cathode and anode [140]. We have recently applied a rapid small-scale flow system similar to a flow i-CDI for the electro-assisted removal of TFA [69] which shows an adequate system stability over 5 adsorption and eletro-desorption cycles (67% maintained adsorption capacity from 2<sup>nd</sup>-5<sup>th</sup> cycle + high recovery degree >88%). Further improvement could be made by considering other advices provided by the CDI community and/or optimizing the electrode materials.

- Unknown 4: *Can the electrosorption cell be applied for a mixture of PM substances? Would there be a matrix effect?*

It is quite clear that a selective removal of adversely charged organic compounds is feasible in an electrosorption cell equipped with only one porous carbon electrode and a non-adsorption-active counter electrode [44, 45]. However, advanced PM removal strategies based on electrosorption may ask for indiscriminate or specific adsorption and desorption depending on the situations. Especially, modern electrosorption approaches should not only focus on an improved adsorption performance for PM substances, but also allow an easy *in-situ* adsorbent regeneration (unless a degradation step happened to the pollutants in an adsorbed status is desired). The latter has been a challenge in traditional symmetric electrosorption cells without the employment of ion-exchange membranes. Novel CDI cells designed with two channels separated by a cation- or anion-exchange membrane [138] enables the system to capture (and release upon clean inflow water) only anions or cations from the inflow brine stream. This could open up new options for designing electro-assisted removal strategies for a mixture of co-existing PM substances.

Regarding the matrix effect on the system stability for ion electrosorption, controversial results were found in previous CDI studies [136, 166, 167]. For PM removal, Wang *et al.* (2018) [36] reported declined adsorption capacity of AC towards antibiotics in the presence of DOC due to competitive uptake, but still a remarkable enhanced adsorption performance under electrosorption conditions. We recently investigated the adsorption of TFA from tap water on defunctionalized AC felt followed by an electro-assisted adsorbent recovery [69]. A significant uptake of TFA was observed in spite of the competition of inorganic anions ( $\text{Cl}^-$ ,  $\text{SO}_4^{2-}$  and  $\text{NO}_3^-$ ) adsorption. In the step of desorption, a flexible choice of clean, electrochemically inert inflow electrolyte solution was possible to avoid unwanted processes and by-products, such as the formation of toxic chlorinated organic compounds in the presence of chlorides. Overall, more research is needed to address the complex matrix effect on PM removal from real water.

- Unknown 5: *Is electro-assisted PM removal an energy-efficient solution? Does it provide a cost-effective alternative to traditional adsorbent regeneration means?*

Techniques such as reverse osmosis for water treatment remains quite energy-demanding [75]. Zhao *et al.* (2013) [168] compared the energy consumption of a MCDI process with reverse osmosis for desalinating brackish water. They concluded that the MCDI can be a more energy-efficient option. Wang *et al.* (2018) [36] pointed out that the electric assistance for the ad-/desorption of antibiotics *per se* only costs very little additional energy while the majority of energy (ca. 99%) was consumed to operate the continuous flow process. Nonetheless, more comparison studies of electrosorption-based PM removal to present water treatment techniques need to be performed by considering the upgrade possibilities in current electro-assisted removal procedures.

Twenty years ago, Fischer [161] concluded in his dissertation that electro-assisted recovery of AC is not as cost-effective as steam regeneration due to an inadequate regeneration efficiency. We wonder if the situation has changed today with several recent cases [25, 30, 36, 69] showing considerable regeneration efficiencies, although the issue regarding long-term system stability still needs to be addressed. With the much-increased concern on global warming in recent years and a rapid rise in transportation costs, an effective, green approach for on-site adsorbent regeneration provided by electrosorption would be favored by our society more than ever compared to the state-of-the-art off-site high-temperature treatments which cause a significant loss in carbon and release in global-warming gases.

## References

- [1] H.P.H. Arp, T.N. Brown, U. Berger, S.E. Hale, Ranking REACH registered neutral, ionizable and ionic organic chemicals based on their aquatic persistency and mobility, *Environ. Sci.: Process. Impacts*. 19 (2017) 939-955. <https://doi.org/10.1039/C7EM00158D>.
- [2] R. Loos, R. Carvalho, D.C. António, S. Comero, G. Locoro, S. Tavazzi, B. Paracchini, M. Ghiani, T. Lettieri, L. Blaha, B. Jarosova, S. Voorspoels, K. Servaes, P. Haglund, J. Fick, R.H. Lindberg, D. Schwesig, B.M. Gawlik, EU-wide monitoring survey on emerging polar organic contaminants in wastewater treatment plant effluents, *Water Res.* 47 (2013) 6475-6487. <https://doi.org/10.1016/j.watres.2013.08.024>.
- [3] B. Teychene, F. Chi, J. Chokki, G. Darracq, J. Baron, M. Joyeux, H. Gallard, Investigation of polar mobile organic compounds (PMOC) removal by reverse osmosis and nanofiltration: rejection mechanism modelling using decision tree, *Water Supply* 20 (2020) 975-983. <http://doi.org/10.2166/ws.2020.020>.
- [4] C.J. Sinclair, A.B.A. Boxall, Assessing the ecotoxicity of pesticide transformation products, *Environ. Sci. Technol.* 37 (2003) 4617-4625. <http://doi.org/10.1021/es030038m>.
- [5] K. Fent, A.A. Weston, D. Caminada, Ecotoxicology of human pharmaceuticals, *Aquat. Toxicol.* 76 (2006) 122-159. <https://doi.org/10.1016/j.aquatox.2005.09.009>.
- [6] V.S. Thomaidi, A.S. Stasinakis, V.L. Borova, N.S. Thomaidis, Is there a risk for the aquatic environment due to the existence of emerging organic contaminants in treated domestic wastewater?

- Greece as a case-study, *J. Hazard. Mater.* 283 (2015) 740-747.  
<https://doi.org/10.1016/j.jhazmat.2014.10.023>.
- [7] M.I. Farré, S. Pérez, L. Kantiani, D. Barceló, Fate and toxicity of emerging pollutants, their metabolites and transformation products in the aquatic environment, *TrAC Trends Anal. Chem.* 27 (2008) 991-1007. <https://doi.org/10.1016/j.trac.2008.09.010>.
- [8] B.t. Ferrari, N. Paxéus, R.L. Giudice, A. Pollio, J. Garric, Ecotoxicological impact of pharmaceuticals found in treated wastewaters: study of carbamazepine, clofibric acid, and diclofenac, *Ecotoxicol. Environ. Saf.* 55 (2003) 359-370. [https://doi.org/10.1016/S0147-6513\(02\)00082-9](https://doi.org/10.1016/S0147-6513(02)00082-9).
- [9] C. Sophia A, E.C. Lima, Removal of emerging contaminants from the environment by adsorption, *Ecotoxicol. Environ. Saf.* 150 (2018) 1-17. <https://doi.org/10.1016/j.ecoenv.2017.12.026>.
- [10] H.P.H. Arp, S.E. Hale, REACH: Improvement of guidance and methods for the identification and assessment of PMT/vPvM substances, Umweltbundesamt  
<https://www.umweltbundesamt.de/publikationen/reach-improvement-of-guidance-methods-for-the>, 2019 (accessed 1 June 2021).
- [11] T. Reemtsma, U. Berger, H.P.H. Arp, H. Gallard, T.P. Knepper, M. Neumann, J.B. Quintana, P.d. Voogt, Mind the gap: persistent and mobile organic compounds—water contaminants that slip through, *Environ. Sci. Technol.* 50 (2016) 10308-10315. <https://doi.org/10.1021/acs.est.6b03338>.
- [12] EPA, United States Environmental Protection Agency: drinking water treatment technology unit cost models and overview of technologies <https://www.epa.gov/sdwa/drinking-water-treatment-technology-unit-cost-models-and-overview-technologies> <https://www.epa.gov/sdwa/drinking-water-treatment-technology-unit-cost-models-and-overview-technologies>, 2020 (accessed 16 April 2021).
- [13] J. Watson, Separation methods for waste and environmental applications, Marcel Dekker, New York, 1999.
- [14] T. Reemtsma, S. Weiss, J. Mueller, M. Petrovic, S. González, D. Barcelo, F. Ventura, T.P. Knepper, Polar pollutants entry into the water cycle by municipal wastewater: a european perspective, *Environ. Sci. Technol.* 40 (2006) 5451-5458. <https://doi.org/10.1021/es060908a>.
- [15] S. Schulze, D. Zahn, R. Montes, R. Rodil, J.B. Quintana, T.P. Knepper, T. Reemtsma, U. Berger, Occurrence of emerging persistent and mobile organic contaminants in European water samples, *Water Res.* 153 (2019) 80-90. <https://doi.org/10.1016/j.watres.2019.01.008>.
- [16] M. Kah, G. Sigmund, F. Xiao, T. Hofmann, Sorption of ionizable and ionic organic compounds to biochar, activated carbon and other carbonaceous materials, *Water Res.* 124 (2017) 673-692. <https://doi.org/10.1016/j.watres.2017.07.070>.
- [17] G. Sigmund, M. Gharasoo, T. Hüffer, T. Hofmann, Deep learning neural network approach for predicting the sorption of ionizable and polar organic pollutants to a wide range of carbonaceous materials, *Environ. Sci. Technol.* 54 (2020) 4583-4591. <http://doi.org/10.1021/acs.est.9b06287>.
- [18] Y. Zhao, S. Lin, J.-W. Choi, J.K. Bediako, M.-H. Song, J.-A. Kim, C.-W. Cho, Y.-S. Yun, Prediction of adsorption properties for ionic and neutral pharmaceuticals and pharmaceutical intermediates on activated charcoal from aqueous solution via LFER model, *Chem. Eng. J.* 362 (2019) 199-206. <https://doi.org/10.1016/j.cej.2019.01.031>.
- [19] K. Zhang, S. Zhong, H. Zhang, Predicting aqueous adsorption of organic compounds onto biochars, carbon nanotubes, granular activated carbons and resins with machine Learning, *Environ. Sci. Technol.* 54 (2020) 7008-7018. <https://doi.org/10.1021/acs.est.0c02526>.
- [20] N. Saeidi, F.-D. Kopinke, A. Georgi, Understanding the effect of carbon surface chemistry on adsorption of perfluorinated alkyl substances, *Chem. Eng. J.* 381 (2020) 122689. <https://doi.org/10.1016/j.cej.2019.122689>.
- [21] N. Saeidi, F.-D. Kopinke, A. Georgi, What is specific in adsorption of perfluoroalkyl acids on carbon materials?, *Chemosphere* (2020) 128520. <https://doi.org/10.1016/j.chemosphere.2020.128520>.
- [22] L. Li, P.A. Quinlivan, D.R.U. Knappe, Effects of activated carbon surface chemistry and pore structure on the adsorption of organic contaminants from aqueous solution, *Carbon* 40 (2002) 2085-2100. [https://doi.org/10.1016/S0008-6223\(02\)00069-6](https://doi.org/10.1016/S0008-6223(02)00069-6).

- [23] N. Saeidi, F.-D. Kopinke, A. Georgi, Controlling adsorption of perfluoroalkyl acids on activated carbon felt by means of electrical potentials, *Chem. Eng. J.* 416 (2021) 129070. <https://doi.org/10.1016/j.cej.2021.129070>.
- [24] E. Bayram, E. Ayranci, Electrochemically enhanced removal of polycyclic aromatic basic dyes from dilute aqueous solutions by activated carbon cloth electrodes, *Environ. Sci. Technol.* 44 (2010) 6331-6336. <https://doi.org/10.1021/es101177k>.
- [25] E. Bayram, E. Ayranci, Structural effects on electrosorptive behavior of aromatic organic acids from aqueous solutions onto activated carbon cloth electrode of a flow-through electrolytic cell, *J. Electroanal. Chem.* 683 (2012) 14-20. <https://doi.org/10.1016/j.jelechem.2012.07.028>.
- [26] Y. Liu, C. Nie, X. Liu, X. Xu, Z. Sun, L. Pan, Review on carbon-based composite materials for capacitive deionization, *RSC Adv.* 5 (2015) 15205-15225. <https://doi.org/10.1039/C4RA14447C>.
- [27] M.E. Suss, S. Porada, X. Sun, P.M. Biesheuvel, J. Yoon, V. Presser, Water desalination via capacitive deionization: what is it and what can we expect from it?, *Energy Environ. Sci.* 8 (2015) 2296-2319. <https://doi.org/10.1039/C5EE00519A>.
- [28] L. Wang, Y. Zhang, K. Moh, V. Presser, From capacitive deionization to desalination batteries and desalination fuel cells, *Curr. Opin. Electrochem.* (2021) 100758. <https://doi.org/10.1016/j.coelec.2021.100758>.
- [29] European commission, European commission implementation decision 2018/840 establishing a watch list of substances for union-wide monitoring in the field of water policy pursuant to directive 2008/105/EC of the European parliament and of the council and repealing commission implementing decision (EU) 2015/495. *Off. J. Eur. Union* 61, 9–12 (5 June 2018, L141/9). 2018.
- [30] C.O. Ania, F. Béguin, Mechanism of adsorption and electrosorption of bentazone on activated carbon cloth in aqueous solutions, *Water Res.* 41 (2007) 3372-3380. <https://doi.org/10.1016/j.watres.2007.03.031>.
- [31] C.O. Ania, F. Béguin, Electrochemical regeneration of activated carbon cloth exhausted with bentazone, *Environ. Sci. Technol.* 42 (2008) 4500-4506. <https://doi.org/10.1021/es703192x>.
- [32] O. Kitous, A. Cheikh, H. Lounici, H. Grib, A. Pauss, N. Mameri, Application of the electrosorption technique to remove Metribuzin pesticide, *J. Hazard. Mater.* 161 (2009) 1035-1039. <https://doi.org/10.1016/j.jhazmat.2008.04.091>.
- [33] S. López-Bernabeu, R. Ruiz-Rosas, C. Quijada, F. Montilla, E. Morallón, Enhanced removal of 8-quinolinecarboxylic acid in an activated carbon cloth by electroadsorption in aqueous solution, *Chemosphere* 144 (2016) 982-988. <https://doi.org/10.1016/j.chemosphere.2015.09.071>.
- [34] E. Bayram, Ç. Kızıl, E. Ayranci, Flow-through electrosorption process for removal of 2,4-D pesticide from aqueous solutions onto activated carbon cloth fixed-bed electrodes, *Water Sci. Technol.* 77 (2018) 848-854. <https://doi.org/10.2166/wst.2017.598>.
- [35] W. Yang, H. Han, M. Zhou, J. Yang, Simultaneous electricity generation and tetracycline removal in continuous flow electrosorption driven by microbial fuel cells, *RSC Adv.* 5 (2015) 49513-49520. <https://doi.org/10.1039/C5RA05545H>.
- [36] S. Wang, X. Li, H. Zhao, X. Quan, S. Chen, H. Yu, Enhanced adsorption of ionizable antibiotics on activated carbon fiber under electrochemical assistance in continuous-flow modes, *Water Res.* 134 (2018) 162-169. <https://doi.org/10.1016/j.watres.2018.01.068>.
- [37] X. Li, Y. Hu, D. She, W.-B. Shen, Modified activated carbon fiber felt for the electrosorption of norfloxacin in aqueous solution, *Sustainability* 12 (2020). <https://doi.org/10.3390/su12103986>.
- [38] Y. Lester, E. Shaulsky, R. Epsztein, I. Zucker, Capacitive deionization for simultaneous removal of salt and uncharged organic contaminants from water, *Sep. Purif. Technol.* 237 (2020) 116388. <https://doi.org/10.1016/j.seppur.2019.116388>.
- [39] X. Li, S. Chen, X. Quan, Y. Zhang, Enhanced adsorption of PFOA and PFOS on multiwalled carbon nanotubes under electrochemical assistance, *Environ. Sci. Technol.* 45 (2011) 8498-8505. <https://doi.org/10.1021/es202026v>.
- [40] S. Wang, X. Li, Y. Zhang, X. Quan, S. Chen, H. Yu, H. Zhao, Electrochemically enhanced adsorption of PFOA and PFOS on multiwalled carbon nanotubes in continuous flow mode, *Chin. Sci. Bull.* 59 (2014) 2890-2897. <https://doi.org/10.1007/s11434-014-0322-6>.

- [41] Z. Niu, Y. Wang, H. Lin, F. Jin, Y. Li, J. Niu, Electrochemically enhanced removal of perfluorinated compounds (PFCs) from aqueous solution by CNTs-graphene composite electrode, *Chem. Eng. J.* 328 (2017) 228-235. <https://doi.org/10.1016/j.cej.2017.07.033>.
- [42] K. Kim, P. Baldaguez Medina, J. Elbert, E. Kayiwa, R.D. Cusick, Y. Men, X. Su, Molecular tuning of redox-copolymers for selective electrochemical remediation, *Adv. Funct. Mater.* 30 (2020) 2004635. <https://doi.org/10.1002/adfm.202004635>.
- [43] S. Delpeux-Ouldriane, M. Gineys, N. Cohaut, F. Béguin, The role played by local pH and pore size distribution in the electrochemical regeneration of carbon fabrics loaded with bentazon, *Carbon* 94 (2015) 816-825. <https://doi.org/10.1016/j.carbon.2015.07.010>.
- [44] F.E. Woodard, D.E. McMackins, R.E.W. Jansson, Electrosorption of organics on three dimensional carbon fiber electrodes, *J. Electroanal. Chem. Interf. Electrochem.* 214 (1986) 303-330. [https://doi.org/10.1016/0022-0728\(86\)80105-X](https://doi.org/10.1016/0022-0728(86)80105-X).
- [45] J.M. Serrano, A.U. Khan, T. Liu, Z. Xu, A.R. Esker, G. Liu, Capacitive organic dye removal by block copolymer based porous carbon fibers, *Adv. Mater. Interfaces* 7 (2020) 2000507. <https://doi.org/10.1002/admi.202000507>.
- [46] J.P. Guthrie, Hydrolysis of esters of oxy acids: pKa values for strong acids; Brønsted relationship for attack of water at methyl; free energies of hydrolysis of esters of oxy acids; and a linear relationship between free energy of hydrolysis and pKa holding over a range of 20 pK units, *Can. J. Chem.* 56 (1978) 2342-2354. <https://doi.org/10.1139/v78-385>.
- [47] E.P. Sergeant, B. Dempsey, Ionisation constants of organic acids in aqueous solution. IUPAC chemical data series No. 23, Pergamon Press, New York, 1979.
- [48] J.C. Boutonnet, P. Bingham, D. Calamari, C.d. Rooij, J. Franklin, T. Kawano, J.-M. Libre, A. McCulloch, G. Malinverno, J.M. Odom, G.M. Rusch, K. Smythe, I. Sobolev, R. Thompson, J.M. Tiedje, Environmental risk assessment of trifluoroacetic acid, *Hum. Ecol. Risk Assess.* 5 (1999) 59-124. <http://doi.org/10.1080/10807039991289644>.
- [49] J.L. Atwood, J.W. Steed, *Encyclopedia of supramolecular chemistry* CRC Press, New York, 2004. <https://doi.org/10.1201/9780429075728>
- [50] M. Ahting, F. Brauer, A. Duffek, I. Ebert, A. Eckhardt, E. Hassold, M. Helmecke, I. Kirst, B. Krause, P. Lepom, S. Leuthold, C. Mathan, V. Mohaupt, J.F. Moltmann, A. Müller, I. Nöh, C. Pickl, U. Pirntke, K. Pohl, J. Rechenberg, M. Suhr, C. Thierbach, L. Tietjen, P. Von der Ohe, Recommendations for reducing micropollutants in waters, background report, German Federal Environmental Agency, 2018.
- [51] All POPs listed in the Stockholm Convention, <http://chm.pops.int/TheConvention/ThePOPs/AllPOPs/tabid/2509/Default.aspx>, (accessed 31 May 2021).
- [52] F. Kalberlah, J. Oltmanns, M. Schwarz, J. Baumeister, A. Striffler, Guidance for the precautionary protection of raw water destined for drinking water extraction from contaminants regulated under REACH, UFOPLAN Project FKZ 371265416, German Federal Environmental Agency, 2015.
- [53] S.W. Karickhoff, D.S. Brown, T.A. Scott, Sorption of hydrophobic pollutants on natural sediments, *Water Res.* 13 (1979) 241-248. [https://doi.org/10.1016/0043-1354\(79\)90201-X](https://doi.org/10.1016/0043-1354(79)90201-X).
- [54] European Parliament and Council (2006) Regulation (EC) No 1907/2006 of the European Parliament and of the Council of 18 December 2006 concerning the Registration, Evaluation, Authorisation and Restriction of Chemicals (REACH), establishing a European Chemicals Agency, amending Directive 1999/45/EC and repealing Council Regulation (EEC) No 793/93 and Commission Regulation (EC) No 1488/94 as well as Council Directive 76/769/EEC and Commission Directives 91/155/EEC, 93/67/EEC, 93/105/EC and 2000/21/EC. *Official Journal L* 396,30.12.2006, pp 1–849.
- [55] H. Rüdél, W. Körner, T. Letzel, M. Neumann, K. Nödler, T. Reemtsma, Persistent, mobile and toxic substances in the environment: a spotlight on current research and regulatory activities, *Environ. Sci. Eur.* 32 (2020) 5. <https://doi.org/10.1186/s12302-019-0286-x>.
- [56] A. Jurado, M. Walther, M.S. Díaz-Cruz, Occurrence, fate and environmental risk assessment of the organic microcontaminants included in the Watch Lists set by EU Decisions 2015/495 and 2018/840 in the groundwater of Spain, *Sci. Total Environ.* 663 (2019) 285-296. <https://doi.org/10.1016/j.scitotenv.2019.01.270>.



- [57] L. Li, P.A. Quinlivan, D.R.U. Knappe, Predicting adsorption isotherms for aqueous organic micropollutants from activated carbon and pollutant properties, *Environ. Sci. Technol.* 39 (2005) 3393-3400. <http://doi.org/10.1021/es048816d>.
- [58] A.B. Lindstrom, M.J. Strynar, E.L. Libelo, Polyfluorinated compounds: past, present, and future, *Environ. Sci. Technol.* 45 (2011) 7954-7961. <http://doi.org/10.1021/es2011622>.
- [59] L. Kovalova, D.R.U. Knappe, K. Lehnberg, C. Kazner, J. Hollender, Removal of highly polar micropollutants from wastewater by powdered activated carbon, *Environ. Sci. Pollut. Res.* 20 (2013) 3607-3615. <http://doi.org/10.1007/s11356-012-1432-9>.
- [60] R. Mailler, J. Gasperi, Y. Coquet, C. Derome, A. Buleté, E. Vulliet, A. Bressy, G. Varrault, G. Chebbo, V. Rocher, Removal of emerging micropollutants from wastewater by activated carbon adsorption: experimental study of different activated carbons and factors influencing the adsorption of micropollutants in wastewater, *J. Environ. Chem. Eng.* 4 (2016) 1102-1109. <https://doi.org/10.1016/j.jece.2016.01.018>.
- [61] R. Mailler, J. Gasperi, Y. Coquet, S. Deshayes, S. Zedek, C. Cren-Olivé, N. Cartiser, V. Eudes, A. Bressy, E. Caupos, R. Moilleron, G. Chebbo, V. Rocher, Study of a large scale powdered activated carbon pilot: removals of a wide range of emerging and priority micropollutants from wastewater treatment plant effluents, *Water Res.* 72 (2015) 315-330. <https://doi.org/10.1016/j.watres.2014.10.047>.
- [62] M. Shirmardi, N. Alavi, E.C. Lima, A. Takdastan, A.H. Mahvi, A.A. Babaei, Removal of atrazine as an organic micro-pollutant from aqueous solutions: a comparative study, *Process Saf. Environ. Prot.* 103 (2016) 23-35. <https://doi.org/10.1016/j.psep.2016.06.014>.
- [63] K. Nödler, M. Scheurer, Substances from Multiple Sources (SMS): the presence of multiple primary and secondary sources of persistent and mobile organic contaminants is an upcoming challenge for the drinking water sector and regulatory frameworks, *Environ. Sci. Technol.* 53 (2019) 11061-11062. <https://doi.org/10.1021/acs.est.9b05168>.
- [64] M. Scheurer, K. Nödler, F. Freeling, J. Janda, O. Happel, M. Riegel, U. Müller, F.R. Storck, M. Fleig, F.T. Lange, A. Brunsch, H.-J. Brauch, Small, mobile, persistent: trifluoroacetate in the water cycle – overlooked sources, pathways, and consequences for drinking water supply, *Water Res.* 126 (2017) 460-471. <https://doi.org/10.1016/j.watres.2017.09.045>.
- [65] R.M.A. Sjerps, D. Vughs, J.A. van Leerdam, T.L. ter Laak, A.P. van Wezel, Data-driven prioritization of chemicals for various water types using suspect screening LC-HRMS, *Water Res.* 93 (2016) 254-264. <https://doi.org/10.1016/j.watres.2016.02.034>.
- [66] T. Reemtsma, M. Jekel, Eds.; *Organic Pollutants in the Water Cycle*, Wiley-VCH, Weinheim, Germany, 2006. <https://doi.org/10.1002/352760877X>.
- [67] S. Schulze, D. Sättler, M. Neumann, H.P.H. Arp, T. Reemtsma, U. Berger, Using REACH registration data to rank the environmental emission potential of persistent and mobile organic chemicals, *Sci. Total Environ.* 625 (2018) 1122-1128. <https://doi.org/10.1016/j.scitotenv.2017.12.305>.
- [68] Candidate List of substances of very high concern for Authorisation, European Chemicals Agency, ECHA, <https://echa.europa.eu/candidate-list-table>, (accessed 21 July 2021).
- [69] J. Zhou, N. Saeidi, L.Y. Wick, Y. Xie, F.-D. Kopinke, A. Georgi, Efficient removal of trifluoroacetic acid from water using surface-modified activated carbon and electro-assisted desorption, *J. Hazard. Mater.* (2021) ready to submit.
- [70] M. Ibáñez, O.J. Pozo, J.V. Sancho, F.J. López, F. Hernández, Re-evaluation of glyphosate determination in water by liquid chromatography coupled to electrospray tandem mass spectrometry, *J. Chromatogr. A* 1134 (2006) 51-55. <https://doi.org/10.1016/j.chroma.2006.07.093>.
- [71] G.L. Brun, M. Bernier, R. Losier, K. Doe, P. Jackman, H.-B. Lee, Pharmaceutically active compounds in Atlantic Canadian sewage treatment plant effluents and receiving waters, and potential for environmental effects as measured by acute and chronic Aquatic Toxicity, *Environ. Toxicol. Chem.* 25 (2006) 2163-2176. <https://doi.org/10.1897/05-426R.1>.
- [72] K. Sznajder-Katarzyńska, M. Surma, I. Cieřlik, A review of perfluoroalkyl acids (PFAAs) in terms of sources, applications, human exposure, dietary intake, toxicity, legal regulation, and methods of determination, *J. Chem.* 2019 (2019) 2717528. <https://doi.org/10.1155/2019/2717528>.

- [73] T.M. Cahill, C.M. Thomas, S.E. Schwarzbach, J.N. Seiber, Accumulation of trifluoroacetate in seasonal wetlands in California, *Environ. Sci. Technol.* 35 (2001) 820-825. <https://doi.org/10.1021/es0013982>.
- [74] M.H. Russell, G. Hoogeweg, E.M. Webster, D.A. Ellis, R.L. Waterland, R.A. Hoke, TFA from HFO-1234yf: accumulation and aquatic risk in terminal water bodies, *Environ. Toxicol. Chem.* 31 (2012) 1957-1965. <https://doi.org/10.1002/etc.1925>.
- [75] T.D. Appleman, C.P. Higgins, O. Quiñones, B.J. Vanderford, C. Kolstad, J.C. Zeigler-Holady, E.R.V. Dickenson, Treatment of poly- and perfluoroalkyl substances in U.S. full-scale water treatment systems, *Water Res.* 51 (2014) 246-255. <https://doi.org/10.1016/j.watres.2013.10.067>.
- [76] P. McCleaf, S. Englund, A. Östlund, K. Lindegren, K. Wiberg, L. Ahrens, Removal efficiency of multiple poly- and perfluoroalkyl substances (PFASs) in drinking water using granular activated carbon (GAC) and anion exchange (AE) column tests, *Water Res.* 120 (2017) 77-87. <https://doi.org/10.1016/j.watres.2017.04.057>.
- [77] X. Zhang, B. Gao, A.E. Creamer, C. Cao, Y. Li, Adsorption of VOCs onto engineered carbon materials: A review, *J. Hazard. Mater.* 338 (2017) 102-123. <https://doi.org/10.1016/j.jhazmat.2017.05.013>.
- [78] D.R.U. Knappe, Chapter 9 - Surface chemistry effects in activated carbon adsorption of industrial pollutants, in: G. Newcombe, D. Dixon (Eds.) *Interface Science and Technology*, Elsevier 2006, pp. 155-177. [https://doi.org/10.1016/S1573-4285\(06\)80078-5](https://doi.org/10.1016/S1573-4285(06)80078-5).
- [79] D. Kupryianchyk, M.I. Rakowska, I. Roessink, E.P. Reichman, J.T.C. Grotenhuis, A.A. Koelmans, In situ treatment with activated carbon reduces bioaccumulation in aquatic food chains, *Environ. Sci. Technol.* 47 (2013) 4563-4571. <https://doi.org/10.1021/es305265x>.
- [80] E. Patmont, M. Jalalizadeh, M. Bokare, T. Needham, J. Vance, R. Greene, J. Cargill, U. Ghosh, Full-scale application of activated carbon to reduce pollutant bioavailability in a 5-Acre Lake, *J. Environ. Eng.* 146 (2020) 04020024. [https://doi.org/10.1061/\(ASCE\)EE.1943-7870.0001667](https://doi.org/10.1061/(ASCE)EE.1943-7870.0001667).
- [81] J. Zhou, N. Saeidi, L.Y. Wick, F.-D. Kopinke, A. Georgi, Adsorption of polar and ionic organic compounds on activated carbon: surface chemistry matters, *Sci. Total Environ.* (2021) 148508. <https://doi.org/10.1016/j.scitotenv.2021.148508>.
- [82] V. Strelko, D.J. Malik, M. Streat, Characterisation of the surface of oxidised carbon adsorbents, *Carbon* 40 (2002) 95-104. [https://doi.org/10.1016/S0008-6223\(01\)00082-3](https://doi.org/10.1016/S0008-6223(01)00082-3).
- [83] F. Xiao, J.J. Pignatello, Effects of post-pyrolysis air oxidation of biomass chars on adsorption of neutral and ionizable compounds, *Environ. Sci. Technol.* 50 (2016) 6276-6283. <http://doi.org/10.1021/acs.est.6b00362>.
- [84] E. Fuente, J.A. Menéndez, D. Suárez, M.A. Montes-Morán, Basic surface oxides on carbon materials: a global view, *Langmuir* 19 (2003) 3505-3511. <http://doi.org/10.1021/la026778a>.
- [85] G.V. Nunell, M.E. Fernandez, P.R. Bonelli, A.L. Cukierman, Nitrate uptake improvement by modified activated carbons developed from two species of pine cones, *J. Colloid Interface Sci.* 440 (2015) 102-108. <https://doi.org/10.1016/j.jcis.2014.10.058>.
- [86] Y. Zhi, J. Liu, Adsorption of perfluoroalkyl acids by carbonaceous adsorbents: Effect of carbon surface chemistry, *Environ. Pollut.* 202 (2015) 168-176. <https://doi.org/10.1016/j.envpol.2015.03.019>.
- [87] L.C. Cheng, H.M. Chen, T.C. Lai, Y.C. Chan, R.S. Liu, J.C. Sung, M. Hsiao, C.H. Chen, L.J. Her, D.P. Tsai, Targeting polymeric fluorescent nanodiamond-gold/silver multi-functional nanoparticles as a light-transforming hyperthermia reagent for cancer cells, *Nanoscale* 5 (2013) 3931-3940. <https://doi.org/10.1039/c3nr34091k>.
- [88] A. Schulze, M. Went, A. Prager, Membrane Functionalization with Hyperbranched Polymers, *Materials* 9 (2016) 706. <https://doi.org/10.3390/Ma9080706>.
- [89] X. Fan, H. Zhao, Y. Liu, X. Quan, H. Yu, S. Chen, Enhanced permeability, selectivity, and antifouling ability of CNTs/Al<sub>2</sub>O<sub>3</sub> membrane under electrochemical assistance, *Environ. Sci. Technol.* 49 (2015) 2293-2300. <https://doi.org/10.1021/es5039479>.
- [90] P. Chingombe, B. Saha, R.J. Wakeman, Surface modification and characterisation of a coal-based activated carbon, *Carbon* 43 (2005) 3132-3143. <https://doi.org/10.1016/j.carbon.2005.06.021>.

- [91] P.M. Biesheuvel, S. Porada, M. Levi, M.Z. Bazant, Attractive forces in microporous carbon electrodes for capacitive deionization, *J. Solid State Electrochem.* 18 (2014) 1365-1376. <https://doi.org/10.1007/s10008-014-2383-5>.
- [92] W. Hao, S.L. Flynn, D.S. Alessi, K.O. Konhauser, Change of the point of zero net proton charge (pHPZNPC) of clay minerals with ionic strength, *Chem. Geol.* 493 (2018) 458-467. <https://doi.org/10.1016/j.chemgeo.2018.06.023>.
- [93] R. Boulton, The relationships between total acidity, titratable acidity and pH in grape tissue, *Vitis* 19 (1980) 113-120. <https://doi.org/10.5073/vitis.1980.19.113-120>
- [94] H. Zhao, L. Qian, Y. Chen, Q. Wang, G. Zhao, Selective catalytic two-electron O<sub>2</sub> reduction for onsite efficient oxidation reaction in heterogeneous electro-Fenton process, *Chem. Eng. J.* 332 (2018) 486-498. <https://doi.org/10.1016/j.cej.2017.09.093>.
- [95] W. Chen, X. Zhou, S. Shi, N. Thiphuong, M. Chen, Synergistical enhancement of the electrochemical properties of lignin-based activated carbon using NH<sub>3</sub>-H<sub>2</sub>O dielectric barrier discharge plasma, *RSC Adv.* 7 (2017) 7392-7400. <http://doi.org/10.1039/C6RA26010A>.
- [96] J. Zhou, Y. Zhang, M. Balda, V. Presser, F.-D. Kopinke, A. Georgi, Electro-assisted removal of polar and ionic organic compounds from water using activated carbon felts, *Chem. Eng. J.* (2021) in revision.
- [97] H. Zhao, L. Qian, X. Guan, D. Wu, G. Zhao, Continuous bulk FeCuC aerogel with ultradispersed metal nanoparticles: an efficient 3D heterogeneous electro-Fenton cathode over a wide range of pH 3–9, *Environ. Sci. Technol.* 50 (2016) 5225-5233. <https://doi.org/10.1021/acs.est.6b00265>.
- [98] Y. Zhi, J. Liu, Surface modification of activated carbon for enhanced adsorption of perfluoroalkyl acids from aqueous solutions, *Chemosphere* 144 (2016) 1224-1232. <https://doi.org/10.1016/j.chemosphere.2015.09.097>.
- [99] P. Chingombe, B. Saha, R.J. Wakeman, Effect of surface modification of an engineered activated carbon on the sorption of 2,4-dichlorophenoxy acetic acid and benazolin from water, *J. Colloid Interface Sci.* 297 (2006) 434-442. <https://doi.org/10.1016/j.jcis.2005.10.054>.
- [100] G. Sigmund, H. Sun, T. Hofmann, M. Kah, Predicting the Sorption of Aromatic Acids to Noncarbonized and Carbonized Sorbents, *Environ. Sci. Technol.* 50 (2016) 3641-3648. <https://doi.org/10.1021/acs.est.5b06033>.
- [101] K.A. Lewis, J. Tzilivakis, D.J. Warner, A. Green, An international database for pesticide risk assessments and management, *Hum. Ecol. Risk Assess.* 22 (2016) 1050-1064. <https://doi.org/10.1080/10807039.2015.1133242>.
- [102] K.-U. Goss, The pK<sub>a</sub> values of PFOA and other highly fluorinated carboxylic acids, *Environ. Sci. Technol.* 42 (2008) 456-458. <https://doi.org/10.1021/es702192c>.
- [103] D. Brooke, A. Footitt, T.A. Nwaogu, Environmental risk evaluation report: Perfluorooctanesulphonate (PFOS) [https://www.gov.uk/government/uploads/system/uploads/attachment\\_data/file/290857/scho1009brbl-e-e.pdf](https://www.gov.uk/government/uploads/system/uploads/attachment_data/file/290857/scho1009brbl-e-e.pdf), 2004 (accessed 1 June 2021).
- [104] H. Sun, F.S. Cannon, X. He, Enhanced trifluoroacetate removal from groundwater by quaternary nitrogen-grafted granular activated carbon, *Sci. Total Environ.* 660 (2019) 577-585. <https://doi.org/10.1016/j.scitotenv.2019.01.057>.
- [105] H. Sun, F.S. Cannon, X. He, Polypyrrole-tailored activated carbon for trifluoroacetate removal from groundwater, *Environ. Eng. Sci.* 36 (2019) 1379-1387. <https://doi.org/10.1089/ees.2018.0453>.
- [106] O. Duman, E. Ayranci, Adsorptive removal of cationic surfactants from aqueous solutions onto high-area activated carbon cloth monitored by in situ UV spectroscopy, *J. Hazard. Mater.* 174 (2010) 359-367. <https://doi.org/10.1016/j.jhazmat.2009.09.058>.
- [107] ChemAxon online platform, <https://chemicalize.com>, (accessed 11 June 2021).
- [108] V. Albergamo, B. Blankert, E.R. Cornelissen, B. Hofs, W.-J. Knibbe, W. van der Meer, P. de Voogt, Removal of polar organic micropollutants by pilot-scale reverse osmosis drinking water treatment, *Water Res.* 148 (2019) 535-545. <https://doi.org/10.1016/j.watres.2018.09.029>.
- [109] V. Franke, M. Ullberg, P. McCleaf, M. Wålinder, S.J. Köhler, L. Ahrens, The price of really clean water: combining nanofiltration with granular activated carbon and anion exchange resins for the

removal of per- and polyfluoralkyl substances (PFASs) in drinking water production, *ACS ES&T Water* 1 (2021) 782-795. <https://doi.org/10.1021/acsestwater.0c00141>.

[110] C.V. Rekhate, J.K. Srivastava, Recent advances in ozone-based advanced oxidation processes for treatment of wastewater- A review, *Chem. Eng. J. Adv.* 3 (2020) 100031. <https://doi.org/10.1016/j.cej.2020.100031>.

[111] M.A. Oturan, J.-J. Aaron, Advanced oxidation processes in water/wastewater treatment: principles and applications. A review, *Crit. Rev. Environ. Sci. Technol.* 44 (2014) 2577-2641. <https://doi.org/10.1080/10643389.2013.829765>.

[112] Y. Deng, R. Zhao, Advanced oxidation processes (AOPs) in wastewater treatment, *Curr. Pollut. Rep.* 1 (2015) 167-176. <https://doi.org/10.1007/s40726-015-0015-z>.

[113] C.A. Martínez-Huitle, M. Panizza, Electrochemical oxidation of organic pollutants for wastewater treatment, *Curr. Opin. Electrochem.* 11 (2018) 62-71. <https://doi.org/10.1016/j.coelec.2018.07.010>.

[114] A. Rey, E. Mena, A.M. Chávez, F.J. Beltrán, F. Medina, Influence of structural properties on the activity of WO<sub>3</sub> catalysts for visible light photocatalytic ozonation, *Chem. Eng. Sci.* 126 (2015) 80-90. <https://doi.org/10.1016/j.ces.2014.12.016>.

[115] G. Gao, J. Shen, W. Chu, Z. Chen, L. Yuan, Mechanism of enhanced diclofenac mineralization by catalytic ozonation over iron silicate-loaded pumice, *Sep. Purif. Technol.* 173 (2017) 55-62. <https://doi.org/10.1016/j.seppur.2016.09.016>.

[116] R.C. Martins, M. Cardoso, R.F. Dantas, C. Sans, S. Esplugas, R.M. Quinta-Ferreira, Catalytic studies for the abatement of emerging contaminants by ozonation, *J. Chem. Technol. Biotechnol.* 90 (2015) 1611-1618. <https://doi.org/10.1002/jctb.4711>.

[117] Z. Bai, Q. Yang, J. Wang, Catalytic ozonation of sulfamethazine using Ce<sub>0.1</sub>Fe<sub>0.9</sub>OOH as catalyst: Mineralization and catalytic mechanisms, *Chem. Eng. J.* 300 (2016) 169-176. <https://doi.org/10.1016/j.cej.2016.04.129>.

[118] C. Sichel, C. Garcia, K. Andre, Feasibility studies: UV/chlorine advanced oxidation treatment for the removal of emerging contaminants, *Water Res.* 45 (2011) 6371-6380. <https://doi.org/10.1016/j.watres.2011.09.025>.

[119] H.V. Lutze, J. Brekenfeld, S. Naumov, C. von Sonntag, T.C. Schmidt, Degradation of perfluorinated compounds by sulfate radicals – new mechanistic aspects and economical considerations, *Water Res.* 129 (2018) 509-519. <https://doi.org/10.1016/j.watres.2017.10.067>.

[120] T. Ochiai, Y. Iizuka, K. Nakata, T. Murakami, D.A. Tryk, A. Fujishima, Y. Koide, Y. Morito, Efficient electrochemical decomposition of perfluorocarboxylic acids by the use of a boron-doped diamond electrode, *Diam. Relat. Mater.* 20 (2011) 64-67. <https://doi.org/10.1016/j.diamond.2010.12.008>.

[121] Q. Zhuo, M. Luo, Q. Guo, G. Yu, S. Deng, Z. Xu, B. Yang, X. Liang, Electrochemical oxidation of environmentally persistent perfluorooctane sulfonate by a novel lead dioxide anode, *Electrochim. Acta* 213 (2016) 358-367. <https://doi.org/10.1016/j.electacta.2016.07.005>.

[122] J.N. Uwayezu, I. Carabante, T. Lejon, P. van Hees, P. Karlsson, P. Hollman, J. Kumpiene, Electrochemical degradation of per- and poly-fluoroalkyl substances using boron-doped diamond electrodes, *J. Environ. Manage.* 290 (2021) 112573. <https://doi.org/10.1016/j.jenvman.2021.112573>.

[123] L. Qian, F.-D. Kopinke, A. Georgi, Photodegradation of perfluorooctanesulfonic acid on Fe-zeolites in water, *Environ. Sci. Technol.* 55 (2021) 614-622. <https://doi.org/10.1021/acs.est.0c04558>.

[124] J. Margot, C. Kienle, A. Magnet, M. Weil, L. Rossi, L.F. de Alencastro, C. Abegglen, D. Thonney, N. Chèvre, M. Schärer, D.A. Barry, Treatment of micropollutants in municipal wastewater: ozone or powdered activated carbon?, *Sci. Total Environ.* 461-462 (2013) 480-498. <https://doi.org/10.1016/j.scitotenv.2013.05.034>.

[125] Y. Lan, C. Coetsier, C. Causserand, K. Groenen Serrano, On the role of salts for the treatment of wastewaters containing pharmaceuticals by electrochemical oxidation using a boron doped diamond anode, *Electrochim. Acta* 231 (2017) 309-318. <https://doi.org/10.1016/j.electacta.2017.01.160>.

[126] H. Li, Y. Long, X. Zhu, Y. Tian, J. Ye, Influencing factors and chlorinated byproducts in electrochemical oxidation of bisphenol A with boron-doped diamond anodes, *Electrochim. Acta* 246 (2017) 1121-1130. <https://doi.org/10.1016/j.electacta.2017.06.163>.

- [127] J.W. Blair, G.W. Murphy, *Electrochemical Demineralization of Water with Porous Electrodes of Large Surface Area*, Saline Water Conversion, American Chemical Society, Washington. DC, 1960, pp. 206-223. <https://doi.org/10.1021/ba-1960-0027.ch020>.
- [128] J.H. Strohl, K.L. Dunlap, Electrosorption and separation of quinones on a column of graphite particles, *Anal. Chem.* 44 (1972) 2166-2170. <http://doi.org/10.1021/ac60321a012>.
- [129] P.M. Biesheuvel, R. Zhao, S. Porada, A. van der Wal, Theory of membrane capacitive deionization including the effect of the electrode pore space, *J. Colloid Interface Sci.* 360 (2011) 239-248. <https://doi.org/10.1016/j.jcis.2011.04.049>.
- [130] S. Porada, L. Borchardt, M. Oschatz, M. Bryjak, J.S. Atchison, K.J. Keesman, S. Kaskel, P.M. Biesheuvel, V. Presser, Direct prediction of the desalination performance of porous carbon electrodes for capacitive deionization, *Energy Environ. Sci.* 6 (2013) 3700-3712. <https://doi.org/10.1039/C3EE42209G>.
- [131] M.E. Suss, T.F. Baumann, W.L. Bourcier, C.M. Spadaccini, K.A. Rose, J.G. Santiago, M. Stadermann, Capacitive desalination with flow-through electrodes, *Energy Environ. Sci.* 5 (2012) 9511-9519. <https://doi.org/10.1039/C2EE21498A>.
- [132] J. Lee, S. Kim, C. Kim, J. Yoon, Hybrid capacitive deionization to enhance the desalination performance of capacitive techniques, *Energy Environ. Sci.* 7 (2014) 3683-3689. <https://doi.org/10.1039/C4EE02378A>.
- [133] J.-B. Lee, K.-K. Park, H.-M. Eum, C.-W. Lee, Desalination of a thermal power plant wastewater by membrane capacitive deionization, *Desalination* 196 (2006) 125-134. <https://doi.org/10.1016/j.desal.2006.01.011>.
- [134] E. Avraham, Y. Bouhadana, A. Soffer, D. Aurbach, Limitation of Charge Efficiency in Capacitive Deionization, *J. Electrochem. Soc.* 156 (2009) 95. <https://doi.org/10.1149/1.3115463>.
- [135] B. van Limpt, A. van der Wal, Water and chemical savings in cooling towers by using membrane capacitive deionization, *Desalination* 342 (2014) 148-155. <https://doi.org/10.1016/j.desal.2013.12.022>.
- [136] P. Xu, J.E. Drewes, D. Heil, G. Wang, Treatment of brackish produced water using carbon aerogel-based capacitive deionization technology, *Water Res.* 42 (2008) 2605-2617. <https://doi.org/10.1016/j.watres.2008.01.011>.
- [137] M. Pasta, C.D. Wessells, Y. Cui, F. La Mantia, A desalination battery, *Nano Letters* 12 (2012) 839-843. <https://doi.org/10.1021/nl203889e>.
- [138] P. Srimuk, X. Su, J. Yoon, D. Aurbach, V. Presser, Charge-transfer materials for electrochemical water desalination, ion separation and the recovery of elements, *Nat. Rev. Mater.* 5 (2020) 517-538. <https://doi.org/10.1038/s41578-020-0193-1>.
- [139] X. Gao, A. Omosebi, J. Landon, K. Liu, Enhanced salt removal in an inverted capacitive deionization cell using amine modified microporous carbon cathodes, *Environ. Sci. Technol.* 49 (2015) 10920-10926. <https://doi.org/10.1021/acs.est.5b02320>.
- [140] X. Gao, A. Omosebi, J. Landon, K. Liu, Surface charge enhanced carbon electrodes for stable and efficient capacitive deionization using inverted adsorption-desorption behavior, *Energy Environ. Sci.* 8 (2015) 897-909. <https://doi.org/10.1039/C4EE03172E>.
- [141] L.-H. Shao, J. Biener, D. Kramer, R.N. Viswanath, T.F. Baumann, A.V. Hamza, J. Weissmüller, Electrocapillary maximum and potential of zero charge of carbon aerogel, *Phys. Chem. Chem. Phys.* 12 (2010) 7580-7587. <https://doi.org/10.1039/B916331J>.
- [142] V. Lockett, R. Sedev, J. Ralston, M. Horne, T. Rodopoulos, Differential Capacitance of the Electrical Double Layer in Imidazolium-Based Ionic Liquids: Influence of Potential, Cation Size, and Temperature, *J. Phys. Chem. C* 112 (2008) 7486-7495. <https://doi.org/10.1021/jp7100732>.
- [143] I. Cohen, E. Avraham, Y. Bouhadana, A. Soffer, D. Aurbach, The effect of the flow-regime, reversal of polarization, and oxygen on the long term stability in capacitive de-ionization processes, *Electrochim. Acta* 153 (2015) 106-114. <https://doi.org/10.1016/j.electacta.2014.12.007>.
- [144] M.E. Suss, Size-based ion selectivity of micropore electric double layers in capacitive deionization electrodes, *J. Electrochem. Soc.* 164 (2017) E270-E275. <https://doi.org/10.1149/2.1201709jes>.

- [145] Y. Zhang, P. Srimuk, S. Husmann, M. Chen, G. Feng, V. Presser, Effect of pore size on the ion electrosorption and hydrogen/deuterium electrosorption using sodium chloride in H<sub>2</sub>O and D<sub>2</sub>O, *J. Electrochem. Soc.* 166 (2019) A4158-A4167. <https://doi.org/10.1149/2.0571916jes>.
- [146] W. Teng, Z. Wu, J. Fan, W.-x. Zhang, D. Zhao, Amino-functionalized ordered mesoporous carbon for the separation of toxic microcystin-LR, *J. Mater. Chem. A* 3 (2015) 19168-19176. <https://doi.org/10.1039/C5TA05320J>.
- [147] X. Zhuang, Y. Wan, C. Feng, Y. Shen, D. Zhao, Highly efficient adsorption of bulky dye molecules in wastewater on ordered mesoporous carbons, *Chem. Mater.* 21 (2009) 706-716. <https://doi.org/10.1021/cm8028577>.
- [148] A. Kuvayskaya, B. Lotsi, R. Mohseni, A. Vasiliev, Mesoporous adsorbents for perfluorinated compounds, *Microporous and Mesoporous Materials* 305 (2020) 110374. <https://doi.org/10.1016/j.micromeso.2020.110374>.
- [149] C. Zhang, D. He, J. Ma, W. Tang, T.D. Waite, Faradaic reactions in capacitive deionization (CDI) - problems and possibilities: A review, *Water Res.* 128 (2018) 314-330. <https://doi.org/10.1016/j.watres.2017.10.024>.
- [150] D. Reyter, Electrochemical Reduction of Nitrate, in: G. Kreysa, K.-i. Ota, R.F. Savinell (Eds.) *Encyclopedia of Applied Electrochemistry*, Springer New York, New York, NY, 2014, pp. 585-593. [https://doi.org/10.1007/978-1-4419-6996-5\\_135](https://doi.org/10.1007/978-1-4419-6996-5_135).
- [151] A.S. Pavitt, E.J. Bylaska, P.G. Tratnyek, Oxidation potentials of phenols and anilines: correlation analysis of electrochemical and theoretical values, *Environ. Sci.: Process. Impacts.* 19 (2017) 339-349. <https://doi.org/10.1039/C6EM00694A>.
- [152] N. Holubowitch, A. Omosebi, X. Gao, J. Landon, K. Liu, Quasi-steady-state polarization reveals the interplay of capacitive and Faradaic processes in capacitive deionization, *ChemElectroChem* 4 (2017) 2404-2413. <https://doi.org/10.1002/celec.201700082>.
- [153] J. McGuire, C.F. Duggins, P.S. Fedkiw, The electrosorption of phenol onto activated carbon, *J. Appl. Electrochem.* 15 (1985) 53. <https://doi.org/10.1007/BF00617740>.
- [154] A. Ban, A. Schafer, H. Wendt, Fundamentals of electrosorption on activated carbon for wastewater treatment of industrial effluents, *J. Appl. Electrochem.* 28 (1998) 227-236. <https://doi.org/10.1023/A:1003247229049>.
- [155] J. Niu, B.E. Conway, Adsorptive and electrosorptive removal of aniline and bipyridyls from waste-waters, *J. Electroanal. Chem.* 536 (2002) 83-92. [https://doi.org/10.1016/S0022-0728\(02\)01206-8](https://doi.org/10.1016/S0022-0728(02)01206-8).
- [156] J. Niu, B.E. Conway, Molecular structure factors in adsorptive removal of pyridinium cations, 1,4-pyrazine and 1-quinoline at high-area C-cloth electrodes for waste-water remediation, *J. Electroanal. Chem.* 529 (2002) 84-96. [https://doi.org/10.1016/S0022-0728\(02\)00910-5](https://doi.org/10.1016/S0022-0728(02)00910-5).
- [157] E. Bayram, N. Hoda, E. Ayrançi, Adsorption/electrosorption of catechol and resorcinol onto high area activated carbon cloth, *J. Hazard. Mater.* 168 (2009) 1459-1466. <https://doi.org/10.1016/j.jhazmat.2009.03.039>.
- [158] Y. Han, X. Quan, H. Zhao, S. Chen, Y. Zhao, Kinetics of enhanced adsorption by polarization for organic pollutants on activated carbon fiber, *Front. Environ. Sci. Eng. China* 1 (2007) 83-88. <https://doi.org/10.1007/s11783-007-0016-2>.
- [159] R.S. Eisinger, G.E. Keller, Electrosorption: A case study on removal of dilute organics from water, *Environ. Prog.* 9 (1990) 235-244. <https://doi.org/10.1002/ep.670090418>.
- [160] B. Janocha, H. Bauser, C. Oehr, H. Brunner, W. Göpel†, Electrosorption on activated carbon textile, *Chem. Eng. Technol.* 22 (1999) 750-752. [https://doi.org/10.1002/\(SICI\)1521-4125\(199909\)22:9<750::AID-CEAT750>3.0.CO;2-1](https://doi.org/10.1002/(SICI)1521-4125(199909)22:9<750::AID-CEAT750>3.0.CO;2-1).
- [161] V.M. Fischer, In Situ Electrochemical Regeneration of Activated Carbon, PhD Dissertation, University of Groningen, 2001.
- [162] K.Y. Foo, B.H. Hameed, A short review of activated carbon assisted electrosorption process: An overview, current stage and future prospects, *J. Hazard. Mater.* 170 (2009) 552-559. <https://doi.org/10.1016/j.jhazmat.2009.05.057>.

- [163] Y. Chen, Y. Tu, Y. Bai, J. Li, J. Lu, Electrosorption enhanced electrooxidation of a model organic pollutant at 3D SnO<sub>2</sub>-Sb electrode in superimposed pulse current mode, *Chemosphere* 195 (2018) 63-69. <https://doi.org/10.1016/j.chemosphere.2017.12.074>.
- [164] E. Bayram, E. Ayranci, Investigation of changes in properties of activated carbon cloth upon polarization and of electrosorption of the dye basic blue-7, *Carbon* 48 (2010) 1718-1730. <https://doi.org/10.1016/j.carbon.2010.01.013>.
- [165] X. Gao, A. Omosebi, N. Holubowitch, J. Landon, K. Liu, Capacitive deionization using alternating polarization: effect of surface charge on salt removal, *Electrochim. Acta* 233 (2017) 249-255. <https://doi.org/10.1016/j.electacta.2017.03.021>.
- [166] W. Zhang, M. Mossad, L. Zou, A study of the long-term operation of capacitive deionisation in inland brackish water desalination, *Desalination* 320 (2013) 80-85. <https://doi.org/10.1016/j.desal.2013.04.010>.
- [167] Y.-J. Kim, J. Hur, W. Bae, J.-H. Choi, Desalination of brackish water containing oil compound by capacitive deionization process, *Desalination* 253 (2010) 119-123. <https://doi.org/10.1016/j.desal.2009.11.022>.
- [168] R. Zhao, S. Porada, P.M. Biesheuvel, A. van der Wal, Energy consumption in membrane capacitive deionization for different water recoveries and flow rates, and comparison with reverse osmosis, *Desalination* 330 (2013) 35-41. <https://doi.org/10.1016/j.desal.2013.08.017>.

### 3. Research questions and manuscripts' overview

In this dissertation, we wish to enlighten the **Unknowns 1-3** mentioned in the **Section 2.3.3**.

The following research questions are aimed to be studied:

- 1) Which types of PM pollutants are amenable to electro-enhanced sorption processes on AC?
- 2) Which key features in surface chemistry should an AC electrode possess in order to deliver desired PM electrosorption performances, in terms of high adsorption capacity and affinity, desired selectivity, and adequate stability upon ad-/desorption cycles?
- 3) How should an electrosorption cell be designed and operated for selective PM removal?

To address the **research question 1)** and **2)**, it is reasonable to first discuss the following question:

- 0) How does the AC surface chemistry affect the adsorption behaviors of various PM types without externally applied potentials?

Three manuscripts were composed within the scale of this dissertation to shed light on the above-mentioned research questions. Note that in the manuscripts 3.1 and 3.2, PM substances are called PMOC (= persistent, mobile organic compounds) substances as suggested by Reemtsma *et al.* (2016) [11], Arp *et al.* (2017) [1] and Schulze *et al.* (2018) [67], *etc.*

Manuscript 3.1 on the adsorption of PM compounds on AC carrying different surface chemistries was aimed at providing the answers to **question 0)**. In this manuscript, we studied the effect of surface modifications of AC felts (pristine, defunctionalized and oxidized) on the adsorption of six selected PM molecules carrying polar or ionic groups, including benzyltrimethylammonium (BTMA<sup>+</sup>), benzyltriethylammonium (BTEA<sup>+</sup>), tetrapropylammonium (TPA<sup>+</sup>), *p*-toluenesulfonate (*p*-TsO<sup>-</sup>), methyl-tert-butyl ether (MTBE) and *p*-toluenesulfonamide (*p*-TSA). Comprehensive characterizations of the three types of AC felts were provided for discussion of the experimental findings. The defunctionalized AC felt (DeACF) carrying a more hydrophobic surface than the pristine AC felt as well as net positive surface charges at neutral pH shows the most promising adsorption capability for all PM types in probe, whereas the oxidized AC felt (OxACF) selectively improved the adsorption of the smallest and most mobile cationic BTMA<sup>+</sup>. Ion exchange capacity providing quantitative



information on adsorbent surface charges at a specified pH value is identified as a frequently underestimated key property of adsorbents targeting at PM adsorption. Except for adsorption isotherms (with Freundlich and Langmuir fittings) at ambient temperatures and neutral pH, additional adsorption experiments at various temperatures, pH values and electrolyte concentrations were performed to better understand the PM adsorption mechanisms. Moreover, we compared our experimental data to the prediction results of the recently published model for Freundlich parameters in PM adsorption on carbonaceous adsorbents, which was developed based on deep learning neural network by Sigmund *et al.* (2020) ([17] in the reference list of the **Section 2**). The comparison reveals the hitherto underestimated role of AC surface chemistry for PM adsorption.

Manuscript 3.2 on electro-assisted removal of PM compounds from water using ACFs discusses the research **question 1)** and **2)**. The same selection of PM substances except for BTEA<sup>+</sup> in manuscript 3.1 was involved in this manuscript, and their electrosorption behaviors on pristine AC felt and DeACF were investigated. While being not effective in regulating the ad-/desorption of neutral PM substances, significant promises in electro-assisted sorptive removal of ionic PM substances were demonstrated by large estimated enrichment factors ( $10^2$ – $10^3$ ) in flow systems applying mild polarization conditions for ad- and desorption (e.g. -0.1 V/+0.6 V vs. SHE on DeACF). DeACF equipped with lower O-content and more abundant surface  $\pi$ -systems was found more competent in the processes of electrosorption than the pristine AC felt regarding removal effectiveness for ionic PM substances (> 3-times better efficiency) and material stability (stable ad-/desorption performances over 5 electro-ad-/desorption cycles and 500 h operation time). Moreover, by plotting the single-point adsorption coefficient of the AC felts to different PM types vs. the applied bias potential related to the adsorbent's  $E_{pzc}$ , we compared the contribution of permanent AC chemical surface modification and reversible electric polarization to the improvement of adsorption performance.

Manuscript 3.3 on the removal of trifluoroacetic acid using surface-modified activated carbon and electro-assisted desorption offers additional insights to **question 2)** and showcases a lab-scale example to address **question 3)**. An effective, selective removal strategy designed for trifluoroacetic acid (TFA), a vPvM substance with potential toxicity as defined by German Federal Environment Agency, is urgently needed. Recognized as a

powerful adsorbent to anionic PM substances from our previous studies, DeACF was applied in this manuscript to treat TFA-contaminated water. DeACF presents an outstanding adsorption efficiency towards TFA in tap water (max. loading at 30.2 mg/g,  $K_d = (840 \pm 80)$  L/kg at  $c_e = 3.4$  mg/L). The time-lapse flow test results showed a clearly favored TFA adsorption over  $\text{Cl}^-$  and  $\text{SO}_4^{2-}$  in tap water on DeACF but a considerable co-uptake of  $\text{NO}_3^-$ , a known inorganic water pollutant. For an effective trap&release of TFA, we have applied an inverted-CDI (i-CDI)-like cell where TFA is strongly adsorbed on surface positively charged DeACF (and not at all on OxACF counter electrode carrying net negatively charged surface) at no externally applied potential, and released from DeACF upon cathodic polarization (while not attached to highly oxidized OxACF surface even at high anodic potentials, e.g. +0.8 V vs. Ag/AgCl). The electro-assisted desorption of TFA using clean 10 mM  $\text{Na}_2\text{SO}_4$  showed successful *in-situ* regeneration of the adsorbent with high recoveries of  $\geq 87\%$ . With the use of OxACF counter electrode, the required polarization conditions for an effective desorption of TFA can be achieved within a much declined cell voltage (<1.1 V) compared to the case where a bare Pt/Ti plate was used. Bias potential and flow rate for desorption were optimized for the best enrichment effect. In spite of an initial decline in TFA adsorption capacity after the first ad-/desorption cycle (by 33%) due to the surface oxidation of the DeACF, the system maintained its full removal capability over at least the next 4 successive cycles.

The findings in these three manuscripts can facilitate the design and targeted application of AC-based sorbents in treating water contaminated by emerging PM substances via sorptive and/or electro-assisted sorptive removal strategies.

### 3.1 Adsorption of polar and ionic organic compounds on activated carbon: Surface chemistry matters

Jieying Zhou<sup>a</sup>, Navid Saeidi<sup>a</sup>, Lukas Y. Wick<sup>b</sup>, Frank-Dieter Kopinke<sup>a</sup>, Anett Georgi<sup>a,\*</sup>

<sup>a</sup>*Helmholtz Centre for Environmental Research – UFZ, Department of Environmental Engineering, D-04318 Leipzig, Germany.*

<sup>b</sup>*Helmholtz Centre for Environmental Research – UFZ, Department of Environmental Microbiology, D-04318 Leipzig, Germany*

#### Abstract

Persistent and mobile organic compounds (PMOCs) are often detected micropollutants in the water cycle, thereby challenging the conventional wastewater and drinking water treatment techniques. Carbon-based adsorbents are often less effective or even unable to remove this class of pollutants. Understanding of PMOC adsorption mechanisms is urgently needed for advanced treatment of PMOC-contaminated water. Here, we investigated the effect of surface modifications of activated carbon felts (ACFs) on the adsorption of six selected PMOCs carrying polar or ionic groups. Among three ACFs, defunctionalized ACF bearing net positive surface charge at neutral pH provides the most versatile sorption efficiency for all studied PMOC types representing neutral, anionic and cationic compounds. Ion exchange capacity giving quantitative information of sorbent surface charges at specified pH is recognized as a frequently underestimated key property for evaluating adsorbents aiming at PMOC adsorption. A most recently developed prediction tool for Freundlich parameters in PMOC adsorption was applied and the prediction results are compared to the experimental data. The comparison demonstrates the so far underestimated importance of the sorbent surface chemistry for PMOC adsorption affinity and capacity. PMOC adsorption mechanisms were additionally investigated by adsorption experiments at various temperatures, pH values and electrolyte concentrations. Exothermic sorption was observed for all sorbate-sorbent pairs. Adsorption is improved for ionic PMOCs on AC carrying sites of the same charge (positive or negative) at increased electrolyte concentration, while not affected for neutral PMOCs unless strong electron donor-acceptor yet weak non-Coulombic interactions exist. Our findings will allow for better design and targeted application of activated carbon-based sorbents in water treatment facilities.

**Keywords:** AC, adsorption processes, surface modification, persistent and mobile organic compounds, water treatment

## 1. Introduction

Almost a half of the European chemicals regulation (REACH) registered organic substances with unique CAS numbers (including predicted hydrolysis products) exhibit highly polar, ionic or ionizable structures [1, 2]. Among them, the compounds with freshwater half-lives longer than 40 days and soil organic carbon–water distribution coefficients  $\log D_{oc} < 4.5$  (at pH = 4–10) are referred to persistent and mobile organic compounds (PMOCs) [1]. Many of these compounds readily pass the conventional water treatment processes and become increasingly detectable in aquatic environments [3-6]. Although detected in low concentrations (ng/L –  $\mu\text{g/L}$ ), they may recirculate and accumulate in short water cycles [1, 7], raising considerable toxicological concerns under long-term exposure [1, 4, 5, 8-12].

In wastewater and drinking water treatment plants, adsorption technology is widely used due to its advantages including flexibility in operation mode (batch or continuous processes), operational simplicity, low investment costs and low environmental impact [12-14]. Activated carbon (AC) materials with specific surface areas  $\sim 10^3 \text{ m}^2/\text{g}$  are frequently used as adsorbents. Besides ozonation, AC adsorption is presently the most broadly applied and recommended technique for upgrading wastewater treatment plants [15, 16].

The appearance of PMOCs in the aquatic environment points to a significant treatment gap in the current wastewater and drinking water purification processes where higher adsorption efficiency of AC adsorbents is urgently called for [15]. Being structurally different from the conventional nonpolar organic pollutants, PMOCs can interact with the sorbent surfaces additionally by means of electrostatic interactions, ion exchange, ion bridging, electron donor-acceptor (EDA) interactions and charge-assisted H-bonds [17]. Previous studies have shed light on the diverse effects of surface chemistry of AC materials on adsorption of PMOCs. For instance, it was discovered that defunctionalization of commercial activated carbon felts (ACFs) to remove oxygen-containing functional groups significantly fostered the adsorption of perfluorooctanoic acid (PFOA,  $pK_a$  between 0 and 1 [18]) and perfluorooctanesulfonic acid (PFOS,  $pK_a = -3.27$  [19]) yet less strongly for *n*-octanoic acid

( $pK_a = 4.9$  [20]). Nevertheless, an in-depth understanding of the links between AC properties and PMOCs adsorption is still missing to date [21, 22].

Given the large variety of chemical PMOC structures, generic mechanistic understanding and predictive modeling approaches of PMOC sorption on carbonaceous materials are needed for targeted sorbent design [6, 17]. Polyparameter linear free energy relationships (pp-LFERs) have long been successfully applied to predict partitioning and (under certain conditions) also adsorption processes of *non-ionic* organic compounds [23]. However, prediction tools for sorption of *polar and ionic* organic compounds onto activated carbon and related sorbents from aqueous systems were much less focused on and only started to emerge recently [24]. These model approaches are either based on LFERs [25], a combination of neural networks (NN) and pp-LFERs [26] or on NN solely [24]. All these models use Abraham descriptors of the sorbates as input parameters, i.e.  $E$  (excess molar refraction),  $S$  (effective dipolarity/polarizability),  $A$  (hydrogen bond acidity),  $B$  (hydrogen bond basicity) and  $V$  (characteristic McGowan volume,  $\text{cm}^3/\text{mol}/100$ ). The model only based on LFER by Zhao et al. (2019) [27] also included the specific ionic descriptors  $J^+$  and  $J^-$  for columbic interactions, yet neglected the influence of sorbent textural and chemical properties on PMOC adsorption. The model established by Zhang et al. (2020) [28] by contrast considers pore-filling and hydrophobic effects as adsorption drivers and, hence, includes total pore volume ( $V_t$ ) and BET-derived specific surface area ( $S_{\text{BET}}$ ) as sorbent-related input parameters. These two sorbent-parameters are, however, highly correlated [28]. This model is predominantly trained with sorption data on carbonaceous sorbents with  $S_{\text{BET}} \geq 400 \text{ m}^2/\text{g}$ . Another most recently developed model by Sigmund et al. (2020) [24] is based on the sorbent's  $S_{\text{BET}}$  and elemental composition (C wt%, H/C and O/C molar ratios) combined with the sorbates'  $\log D$ ,  $A^- \%$  or  $B^+ \%$  (pH-dependent percentage of anionic or cationic species, respectively). Although many data on the elemental composition of C-based adsorbents of moderate carbonization degree exist (e.g. for biochars), they are heavily missing for ACs applied in sorption studies. As a result, only 55 out of 330 items in the training-set for anionic and polar organic compounds used in [24] exhibit  $S_{\text{BET}} \geq 400 \text{ m}^2/\text{g}$ . While all three prediction tools deepen our understanding of PMOC sorption on carbon-based materials, they are all affected by limitations in appropriate experimental literature data for model training. Data shortages include (i) detailed characterization of AC sorbents and their ion exchange capacities [24], (ii)

high-quality adsorption isotherm data, and (iii) lack of adsorption studies on cationic organic compounds (“small and noisy data set” [24]).

In order to advance the presently limited knowledge on correlations between PMOC adsorption and AC properties, we here studied for the first time the adsorption of six environmentally relevant PMOCs on three types of ACFs of high specific surface area ( $S_{\text{BET}} = 1100\text{--}1500 \text{ m}^2/\text{g}$ ) and similar porous structures yet distinct surface functionalities. The PMOC adsorbates consist of three positively charged compounds (benzyltrimethylammonium (BTMA<sup>+</sup>), benzyltriethylammonium (BTEA<sup>+</sup>), tetrapropyl-ammonium (TPA<sup>+</sup>)), an organic anion (*p*-toluenesulfonate, *p*-TsO<sup>−</sup>, acid form with  $\text{p}K_{\text{a}} < -1$  [29, 30]), and two neutral molecules (at pH 7; methyl-*tert*-butyl ether (MTBE), *p*-toluenesulfonamide (*p*-TSA,  $\text{p}K_{\text{a}} = 10.5$  [31])). According to Schulze et al. (2018) [32], MTBE, *p*-TsO<sup>−</sup>, and BTMA<sup>+</sup> have a high environmental emission potential, i.e. were ranked 3<sup>rd</sup>, 50<sup>th</sup>, and 313<sup>th</sup> out of 936 REACH registered PMOCs. Additionally, MTBE, *p*-TsO<sup>−</sup>, and BTMA<sup>+</sup> are among the most persistent and mobile aquatic PMOCs with freshwater half-lives of >60 d,  $\log D_{\text{oc}}$  of <1 at pH = 4–10 and a water solubility >10 g/L [1]. Despite the high environmental relevance, very limited adsorption studies on such PMOCs were performed and yet, except for MTBE adsorption on 15 different AC materials reported by Li et al. (2002) [33], most previous studies did not focus on the impact of the sorbent surface chemistry [34–38]. Herein, to analyze effects of AC surface properties on the PMOCs’ sorption affinity and capacity, isotherms of individual sorbate-sorbent pairs were measured at different temperature, electrolyte concentration and pH conditions. To understand the role of AC surface chemistry for PMOC adsorption we further fitted our data with Freundlich and Langmuir equations and compared them to results predicted by the model suggested by Sigmund et al. (2020) [24].

## 2. Experimental section

### 2.1 Chemicals

*p*-TsO<sup>-</sup> (commercially available in form of C<sub>7</sub>H<sub>8</sub>O<sub>3</sub>S·H<sub>2</sub>O, > 98.5%) and BTMA hydroxide (C<sub>10</sub>H<sub>17</sub>NO, 20 w/w% aq.) were obtained from Alfa Aesar. *p*-TSA (C<sub>7</sub>H<sub>9</sub>NO<sub>2</sub>S, ≥99%) and TPA hydroxide (C<sub>12</sub>H<sub>29</sub>NO, 1.0 M aq.) were purchased from Sigma-Adrich. MTBE (C<sub>5</sub>H<sub>12</sub>O, >99%) and BTEA hydroxide (C<sub>13</sub>H<sub>23</sub>NO, 10 w/w% aq.) were acquired from Fluka Analytical and abcr GmbH, respectively. Selected sorbate properties are listed in **Table S1**. Ethanol (EtOH, ≥99.9%), HNO<sub>3</sub> (65%), HCl (37%), NaOH (99%), KCl (>99%), NaNO<sub>3</sub> (>99%), Na<sub>2</sub>SO<sub>4</sub> (99%), CuSO<sub>4</sub>·5H<sub>2</sub>O (>99%), citric acid monohydrate (C<sub>6</sub>H<sub>8</sub>O<sub>7</sub>·H<sub>2</sub>O, >99%) and the ammonia solution (25 w/w% aq.) were purchased from Merck. Methanol (>99.95%) and *i*-propanol (≥99.9%) were obtained from Th.Geyer. Oxalic acid bis(cyclohexylidene hydrazide) (Cuprizone, C<sub>14</sub>H<sub>22</sub>N<sub>4</sub>O<sub>2</sub>, > 98%) and ammonium acetate (C<sub>2</sub>H<sub>7</sub>NO<sub>2</sub>, ≥98.0%) were purchased from Bernd Kraft GmbH. Deionized water was used to prepare all solutions.

### 2.2 Materials

Actitex®-FC1001 (Jacobi CARBONS, ACF<sub>10</sub> in short, 30 cm<sup>2</sup>) was washed with *i*-propanol (60 mL) and five times with H<sub>2</sub>O (60 mL, shaking at 120 rpm, 30 min) followed by air-drying (80°C, overnight) before use or further treatment. The oxidized sample (OxACF<sub>10</sub>) was prepared by stirring ACF<sub>10</sub> (1.1 g) in HNO<sub>3</sub> (5 M, 130 mL) at 95°C for 6 h. The as-treated sample was then washed five times with H<sub>2</sub>O (shaking at 120 rpm, 30 min) until pH reached approx. 6 and then air-dried (50°C, overnight). The defunctionalized sample (DeACF<sub>10</sub>) was prepared by treating ACF<sub>10</sub> in a quartz tubular oven at 900°C under H<sub>2</sub> atmosphere for 2 h (heating rate: 150 K/min, starting from 20°C, gas flow rate: 40 mL/min). Before heating, the oven containing the sample was purged with N<sub>2</sub> for 30 min and then with H<sub>2</sub> for another 30 min. After heating, the oven was cooled automatically to 100°C in H<sub>2</sub>, then to 20°C in N<sub>2</sub>.

### 2.3 Material characterization

The specific surface area (*S*<sub>BET</sub>) of the sorbents was measured with the BET method (N<sub>2</sub> at 77 K) using BELSORP MINI (BEL Japan, Ltd.) with a sample pretreatment at 100°C. The mesopore size distribution ( $\varnothing > 2$  nm) was characterized by the BJH method. The size distribution of the micropores ( $\varnothing < 2$  nm) was determined using a magnetic suspension balance (Rubotherm GmbH) by means of CO<sub>2</sub> adsorption at 0°C and analysed by NLDFT fitting from the software

Pore analyser (Porotec GmbH). The point of zero net proton charge ( $\text{pH}_{\text{PZC}}$ ) of the ACF samples was determined as reported [39]. Cation and anion exchange capacities (CEC and AEC) were determined as described earlier [40, 41]. The detailed procedures for  $\text{pH}_{\text{PZC}}$  and CEC/AEC determination are given in SI. Elemental analysis was performed using a CHN analyser (LECO TruSpec CHN). The oxygen contents of the samples were calculated from the mass balance  $\text{O wt\%} = 100\% - \text{C wt\%} - \text{H wt\%} - \text{N wt\%} - \text{ash wt\%}$ . The ash content was determined gravimetrically as residue after burning the sample at  $750^\circ\text{C}$  in oxygen. Temperature-programmed desorption (TPD) results were recorded on a BELCAT-B chemisorption analyser (BEL Japan Ltd.) coupled with an Infralyt detector (SAXON Junkalor) for CO and  $\text{CO}_2$  detection. The ACFs were first pre-treated at  $150^\circ\text{C}$  for 30 min in an argon atmosphere (50 mL/min), then heated up from  $150^\circ\text{C}$  to  $1100^\circ\text{C}$  with a heating rate of 10 K/min. X-ray photoelectron spectroscopy (XPS) measurements were performed by an Axis Ultra photoelectron spectrometer (Kratos Analytical Ltd.) using monochromatized Al  $\text{K}\alpha$  radiation ( $h\nu = 1486.6 \text{ eV}$ ). For binding energy (BE) determination, the main component of the C1s signal at 284.8 eV was employed as reference. Peak deconvolution was performed with CasaXPS (<http://www.casaxps.com/>) by applying a Shirley background and sums of Gaussian and Lorentzian functions for the fitting. The attenuated total reflection (ATR)-FTIR was performed on a Nicolet iS50R FR-IR device (ThermoFischer). The morphology of ACFs was characterized using scanning electron microscopy (SEM) (Zeiss Merlin VP Compact).

## **2.4 Adsorption experiments**

0.1–4.0 g/L ACFs were shaken (120 rpm) for 24–48 h in aqueous  $\text{Na}_2\text{SO}_4$  solution (1–100 mM, 8–10 mL) followed by pH adjustment with 0.1 M NaOH and/or  $\text{H}_2\text{SO}_4$  solutions to desired values. Such pre-wetting step allows background solution to penetrate the inner pores, making them readily accessible for dissolved sorbates [38]. Then, stock solutions containing individual sorbate compounds (1–3 g/L) pre-neutralized to pH 7 were added to the ACF-containing batches to reach desired initial concentrations (2.5 – 80 mg/L). After shaking overnight at the selected temperatures ( $20^\circ\text{C}$ ,  $40^\circ\text{C}$ ,  $55^\circ\text{C}$ , and  $70^\circ\text{C}$ , 400 rpm with LLG-uniTHERMIX 2 pro), the pH values of the suspensions were adjusted back to desired values. Temperature dependence was measured for exploring the impact of entropy and enthalpy effects in the adsorption processes. For samples containing nonionic MTBE, the pH-adjustment during the adsorption process was abandoned. Also, gas-liquid volume ratios



<1:5 were set so that MTBE loss into the gas phase was negligible. After 48 h-adsorption at the selected temperature, samples were taken and filtered with Whatman® syringe filters (0.45 µm, PTFE), concentrated by evaporation of water under N<sub>2</sub> or diluted when necessary, and used for concentration measurement. The final pH values were detected in the range (± 0.5) close to the desired values.

The single-point adsorption coefficient  $K_d$  (L/m<sup>2</sup>) indicating the adsorption affinity of the sorbent towards the sorbate at a given condition was calculated as

$$K_d = \frac{q_e}{c_e} \quad (1)$$

where  $q_e$  (µmol/m<sup>2</sup>) related to sorbent's  $S_{BET}$  is the sorbent loading and  $c_e$  (µmol/L) the concentration of dissolved solute in the aqueous phase at the adsorption equilibrium.

The adsorption isotherms of sorbate-sorbent pairs were fitted with linearized forms of Freundlich (Eq. 2) and Langmuir equations (Eq. 3) expressed as follows,

$$\log q_e = n \cdot \log c_e + \log K_F \quad (2)$$

where  $n$  is the dimensionless Freundlich exponent and  $K_F$  ((µmol/m<sup>2</sup>)/(µmol/L) <sup>$n$</sup> ) is the Freundlich constant [42]. In addition,  $K_F$  in unit of (µg/kg)/(µg/L) <sup>$n$</sup>  is derived from fittings using  $q_e$  (µg/kg) related to adsorbent mass and  $c_e$  (µg/L) to compare with the model predictions in **Section 3.2.4**. Logarithms of parameters which carry units are to be understood as numbers after dividing by these units.

$$\frac{c_e}{q_e} = \frac{c_e}{q_{\max}} + \frac{1}{q_{\max} K_L} \quad (3)$$

where  $q_{\max}$  (µmol/m<sup>2</sup>) is the maximal (monolayer) sorbent loading and  $K_L$  (L/µmol) the Langmuir constant. Both  $K_F$  and  $K_L$  are related to the adsorption affinity of the sorbent towards the selected sorbate while  $q_{\max}$  represents the adsorption capacity.  $n \rightarrow 1$  indicates a more homogenous distribution of sorption sites on sorbent surface [33, 43].

## 2.5 Analytical methods

Aliquots of aqueous samples were taken using a syringes equipped with Whatman® (0.45 µm, PTFE) filters before being measured. The analysis of  $p$ -TsO<sup>-</sup> and TPA<sup>+</sup> was accomplished by a liquid chromatography equipment coupled with a photo diode array UV/VIS detector and

single-stage mass spectrometer (MS) with electrospray ionization (LC-MS2020, SHIMADZU Corporation). UV/VIS detection was applied for *p*-TsO<sup>-</sup> ( $\lambda$  = 220 nm) and the MS detector operated in selected ion monitoring (SIM) mode with  $m/z$  = 186 amu was used for TPA<sup>+</sup>. The concentrations of *p*-TSA were analysed by gas chromatography–mass spectrometry (SHIMADZU GC–MS 2010) in SIM mode ( $m/z$  = 171 amu) after solvent extraction (for details see SI part). MTBE concentrations were determined by Headspace-GC–MS analysis using a SHIMADZU AOC-5000 Plus autosampler coupled to the above mentioned GC–MS operated in SIM mode ( $m/z$  = 73 amu). The concentrations of dissolved BTMA<sup>+</sup> and BTEA<sup>+</sup> were both measured by UV/VIS spectrometry (SHIMADZU UVmini-1240) at  $\lambda$  = 207 nm. Corresponding blank samples without analytes were prepared for correcting the baseline. To measure the Cu<sup>2+</sup> concentrations, 1–6 mL aliquots were added to a combination of 1 mL cuprizone solution (0.5 wt% in EtOH:H<sub>2</sub>O = 1:1 v/v) and 1 mL triammonium citrate-ammonia buffer ((NH<sub>4</sub>)<sub>3</sub>C<sub>6</sub>H<sub>5</sub>O<sub>7</sub> –NH<sub>3</sub>, pH = 9) solution to form the copper-cuprizone complex absorbing intensively at 595 nm [44]. The mixture was shaken for 30 min (120 rpm) in darkness before diluted to the concentration range 0.1–2 mg/L and analysed by UV/VIS spectrometry. More detailed information of the measurements is given in the SI part.

### 3. Results and discussion

#### 3.1 Characterization of ACFs

Derived from a commercially available ACF<sub>10</sub>, two surface-modified ACFs were prepared to provide distinct sorbent properties for adsorption of selected polar organic compounds. All three ACFs were carefully characterized for their bulk chemical composition, surface functionalities and pore structures.

Elemental analyses were performed for all studied ACF types with results listed in **Table 1**. HNO<sub>3</sub> oxidation of ACF resulted a 1.8-fold increased O content (18.1 wt%) of OxACF<sub>10</sub> relative to untreated ACF<sub>10</sub> (9.9 wt%) while annealing of the original ACF<sub>10</sub> in H<sub>2</sub> flow at 900°C for 2 h resulted in a significant reduction in the O content (4.3 wt%) of DeACF<sub>10</sub>. TPD was performed to further characterize the O-containing functional groups (**Fig. S1**). Observed peaks at  $T \approx$  800 K, 1000 K and 1100–1200 K in the CO release profiles can be assigned to the destruction of aliphatic hydroxyl, phenolic hydroxyl and carbonyl groups, respectively [45]. In CO<sub>2</sub> release profiles, the peak around 500 K may refer to the decomposition of carboxylic or anhydride groups [45, 46] while CO<sub>2</sub> release at higher temperatures (700–1000 K) is likely to

be derived from lactone groups [46]. The ATR-FTIR spectra (**Fig. S2**) also confirm the origins of O-containing functional groups on OxACF<sub>10</sub>. XPS high resolution C1s spectra (**Fig. S3**) show an increased peak intensity relating to  $\pi \rightarrow \pi^*$  shake-up which implies higher contents of sp<sup>2</sup> C and, accordingly, more hydrophobic surfaces in the order of OxACF<sub>10</sub> < ACF<sub>10</sub> < DeACF<sub>10</sub>.

**Table 1:** Chemical properties of untreated ACF<sub>10</sub> and surface-modified OxACF<sub>10</sub> and DeACF<sub>10</sub>.

Sample	pH <sub>PZC</sub>	CEC (μmol/m <sup>2</sup> )	AEC (μmol/m <sup>2</sup> )	C wt%	H wt%	O wt% <sup>a</sup>	N wt%
OxACF <sub>10</sub>	2.4 ± 0.1	1.0	0.0087	78.5	0.3	18.1	2.7
ACF <sub>10</sub>	5.7 ± 0.2	0.040	0.025	87.7	0.3	9.9	1.8
DeACF <sub>10</sub>	10.2 ± 0.2	≤ 0.010	0.23	93.4	0.4	4.3	0.9

<sup>a</sup> Calculated from mass balance according to O wt% = 100% – C wt% – H wt% – N wt% – ash wt%.

To quantify charged sites on ACF surfaces, the ion exchange capacities towards inorganic cations and anions were characterized at circumneutral pH. Cation and anion exchange capacities (CEC and AEC, respectively) give quantitative information on surface charge densities of AC at a specified relevant pH. These are favoured compared to other parameters used for describing AC surface chemistry, such as O-content which does not contain information on the speciation of the O-containing groups or point-of-zero charge (pH<sub>PZC</sub>) which only gives qualitative information on the predominant charge at pH ≠ pH<sub>PZC</sub> for heterogeneous adsorbent surfaces. Distinct charge densities of the three ACF surfaces were found (**Table 1**). Differences in ion exchange capacities were mainly attributed to O contents of the samples due to the quasi absence of N in the ACFs [47]. Generally, higher CEC were found in ACFs carrying more O-containing functional groups and, hence, more negatively charged sites at circumneutral pH. In contrast, higher AEC was found for oxygen-poor DeACF<sub>10</sub>. As supported by the XPS spectra (**Fig. S11**), DeACF<sub>10</sub> surface is rather rich in aromatic regions free of O-containing functional groups, and possess highly delocalized  $\pi$ -electrons. Such structures are prone to adsorb protons and form positively charged sites [40]. The increase of the pH<sub>PZC</sub> of the ACFs was in the order of OxACF<sub>10</sub> < ACF<sub>10</sub> < DeACF<sub>10</sub> and relates to the order of the ACF ion exchange capacities. The CEC of the sorbents also reflects well their capacity to retain Cu<sup>2+</sup> (**Table S2**, **Fig. S4**).

Analysis of the textural properties (**Table 2**) revealed for all three ACF high specific surface areas ( $> 1000 \text{ m}^2/\text{g}$ ) as obtained from  $\text{N}_2$  BET analyses ( $S_{\text{BET}}$ ) suggesting high PMOC sorption capacities. 93% of  $S_{\text{BET}}$  is maintained for DeACF<sub>10</sub> after thermal treatment in  $\text{H}_2$  at  $900^\circ\text{C}$ , whereas a 27% loss in  $S_{\text{BET}}$  was found for OxACF<sub>10</sub> after oxidizing with hot  $\text{HNO}_3$  solution. The  $\text{N}_2$  adsorption-desorption isotherms of all ACFs (**Fig. S5a**) resemble the IUPAC Type I isotherm [48] typically observed for microporous AC materials. The narrow hysteresis loops further indicate a predominance of micropores in all ACFs [49-51]. Analysis of the pore volume distributions of the ACFs (**Fig. S5b**) reveals that oxidation of the ACF<sub>10</sub> led to a decrease in the fraction of micropores ( $\varnothing < 2 \text{ nm}$ ) likely due to pore blocking by O-containing surface functional groups [52, 53], and accordingly a reduced  $S_{\text{BET}}$ . The morphology of the three ACFs is shown in SEM images (**Fig. S6**).

**Table 2:** Textural properties of ACF<sub>10</sub>, OxACF<sub>10</sub>, and DeACF<sub>10</sub>.  $V_t$  = total pore volume;  $V_{\text{meso}}$  = mesopore volume;  $V_{\text{micro}, \varnothing < 1 \text{ nm}}$  and  $V_{\text{micro}, \varnothing = 1-2 \text{ nm}}$  = pore volume of micropores with  $\varnothing < 1 \text{ nm}$  and  $\varnothing = 1-2 \text{ nm}$ .

Sample	$S_{\text{BET}}$ ( $\text{m}^2/\text{g}$ ) <sup>a</sup>	$V_t$ ( $\text{cm}^3/\text{g}$ ) <sup>b</sup>	$V_{\text{micro}, \varnothing < 1 \text{ nm}}$ ( $\text{cm}^3/\text{g}$ ) <sup>b</sup>	$V_{\text{micro}, \varnothing = 1-2 \text{ nm}}$ ( $\text{cm}^3/\text{g}$ ) <sup>b</sup>	$V_{\text{meso}}$ ( $\text{cm}^3/\text{g}$ ) <sup>b</sup>
OxACF <sub>10</sub>	1100	0.51	0.16	0.31	0.04
ACF <sub>10</sub>	1500	0.57	0.14	0.39	0.04
DeACF <sub>10</sub>	1400	0.73	0.08	0.58	0.07

<sup>a</sup> Determined by  $\text{N}_2$  adsorption/desorption up to  $p/p_0 = 0.99$ . <sup>b</sup> Determined by  $\text{CO}_2$  adsorption.

### 3.2 PMOCs adsorption

#### 3.2.1 Adsorption affinities and capacities of ACFs towards PMOCs

Adsorption isotherms in 10 mM  $\text{Na}_2\text{SO}_4$  solution at pH 7 (**Fig. S7**) were determined to quantify PMOC adsorption affinities ( $K_d$ ) and capacities ( $q_{\text{max}}$ ) to the ACFs. All isotherms were fitted by both the Freundlich equation (**Eq. 2**) in the low  $c_e$  range (i.e. below saturation loading, **Fig. S8**) and by Langmuir equation (**Eq. 3**) in the whole data range (**Fig. S9**) as summarized in **Table 3**. Log  $K_d$  for all sorbate-sorbent pairs at  $c_e = 20 \mu\text{mol/L}$  (**Fig. 1**) were calculated from the Freundlich parameters by  $K_d = c_e^{n-1} \cdot K_F$  (cf. **Eqs. 1 & 2**).

As described in **Section 3.1**, all three ACF sorbents studied carry porous structures dominated by micropores. Based on the characterization results given in **Table 2**, the total

pore volumes on unit specific surface ( $(0.45 \pm 0.07) \text{ mm}^3/\text{m}^2$ ) are comparable for all three ACFs. Although the pore size distribution differs for the three ACF types, these differences should not result in large varieties in adsorption capacities towards target PMOCs (**Table 3**) due to the only minor to moderate pore filling extents as elucidated below. For instance,  $\text{TPA}^+$  exhibits the largest van der Waals molecular volume ( $\approx 139.8 \text{ cm}^3/\text{mol}$ ) and molecule size (0.63–0.97 nm [37]) of all tested PMOCs. However,  $\text{TPA}^+$  exhibited higher sorption to  $\text{OxACF}_{10}$  ( $q_{\text{max}} = 0.18 \text{ } \mu\text{mol}/\text{m}^2$ ) than to  $\text{DeACF}_{10}$  ( $q_{\text{max}} = 0.13 \text{ } \mu\text{mol}/\text{m}^2$ ) although the  $V_{\phi \geq 1 \text{ nm}}$  of  $\text{OxACF}_{10}$  was found to be about 50% lower than in  $\text{DeACF}_{10}$  (**Table 2**). With a simplified assumption that  $\text{TPA}^+$  molecules solely enter pores of  $\phi \geq 1 \text{ nm}$ , only about 7.9% of pores with  $\phi \geq 1 \text{ nm}$  of  $\text{OxACF}_{10}$  would be occupied (for calculation cf. SI). Similarly, we estimated the maximal pore filling extents of all sorbates in pores with  $\phi \geq 1 \text{ nm}$  of  $\text{OxACF}_{10}$ ,  $\text{ACF}_{10}$  and  $\text{DeACF}_{10}$  (**Table S3**). As-obtained data show that the pores were occupied between 0.7 and 32%, suggesting that the sorbent pore volumes may not be the limiting factor for PMOC sorption to the ACFs.

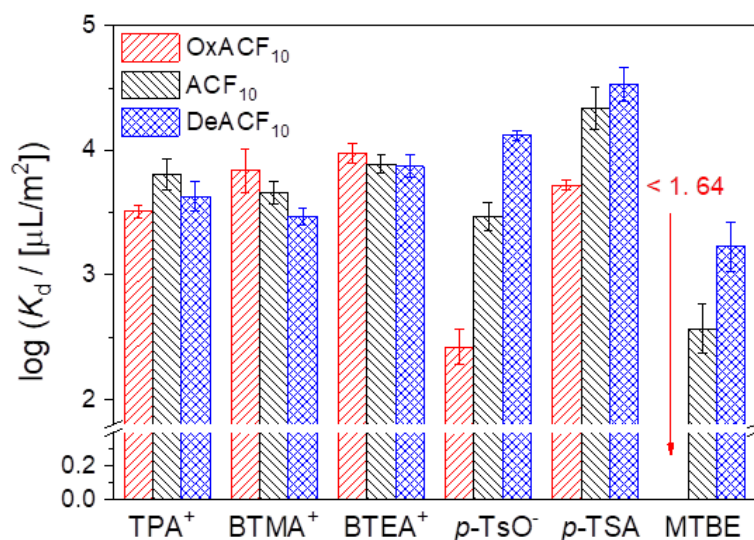


**Fig. 1:** Log  $K_d$  on ACFs for selected PMOCs at  $c_e = 20 \text{ } \mu\text{M}$  in 10 mM  $\text{Na}_2\text{SO}_4$  solution at pH 7 at 20 °C. These values were calculated from the corresponding Freundlich isotherm parameters. The error bars of log  $K_d$  are calculated from the errors in  $K_F$  and  $n$  obtained from the regression analyses of the Freundlich linear fittings.

**Table 3:** Freundlich and Langmuir isotherm parameters for adsorption of six PMOCs on three ACFs in 10 mM Na<sub>2</sub>SO<sub>4</sub> solution at pH 7, 20°C.

Sorbate	ACF sorbent	Freundlich			Langmuir		
		$K_F (10^{-3} (\mu\text{mol}/\text{m}^2)/(\mu\text{mol}/\text{L})^n)$	$n$	$R^2$	$q_{\text{max}} (\mu\text{mol}/\text{m}^2)$	$K_L (\text{L}/\mu\text{mol})$	$R^2$
TPA <sup>+</sup>	OxACF <sub>10</sub>	18	0.42	0.995	0.18	0.031	0.986
	ACF <sub>10</sub>	35	0.44	0.970	0.16	0.11	0.974
	DeACF <sub>10</sub>	28	0.37	0.958	0.13	0.11	0.996
BTMA <sup>+</sup>	OxACF <sub>10</sub>	19	0.67	0.998	0.53	0.018	0.969
	ACF <sub>10</sub>	34	0.33	0.974	0.23	0.035	0.941
	DeACF <sub>10</sub>	12	0.54	0.995	0.22	0.016	0.992
BTEA <sup>+</sup>	OxACF <sub>10</sub>	85	0.27	0.963	0.36	0.087	0.979
	ACF <sub>10</sub>	68	0.28	0.977	0.28	0.081	0.982
	DeACF <sub>10</sub>	68	0.26	0.934	0.30	0.060	0.976
<i>p</i> -TsO <sup>-</sup>	OxACF <sub>10</sub>	0.95	0.57	0.970	0.025	0.013	0.916
	ACF <sub>10</sub>	21	0.34	0.939	0.11	0.084	0.993
	DeACF <sub>10</sub>	100	0.31	0.994	0.38	0.14	1.000
<i>p</i> -TSA	OxACF <sub>10</sub>	13	0.69	0.999	0.36	0.024	0.944
	ACF <sub>10</sub>	75	0.59	0.947	1.0	0.037	0.997
	DeACF <sub>10</sub>	220	0.38	0.935	1.3	0.079	0.984
MTBE	OxACF <sub>10</sub>	n.d. <sup>a</sup>	n.d. <sup>a</sup>	n.d. <sup>a</sup>	n.d. <sup>a</sup>	n.d. <sup>a</sup>	n.d. <sup>a</sup>
	ACF <sub>10</sub>	0.77	0.76	0.980	0.098	0.0037	0.854
	DeACF <sub>10</sub>	3.6	0.75	0.977	0.16	0.014	0.974

<sup>a</sup> OxACF<sub>10</sub> has a very low adsorption to MTBE (no significant depletion up to ACF dosage of 5 g/L).

$K_d$  and  $q_{\text{max}}$  values propose distinct PMOC sorption to the ACFs; in particular for anionic *p*-TsO<sup>-</sup> and neutral *p*-TSA and MTBE. For instance, *p*-TSA and MTBE adsorption affinities (log  $K_d$ ; **Fig. 1**) and the maximum adsorption capacities ( $q_{\text{max}}$ ; **Table 3**) follow the order of DeACF<sub>10</sub> > ACF<sub>10</sub> > OxACF<sub>10</sub>. Two factors may explain these findings: (i) increasing polarity of the sorbent surfaces due to oxidation penalizes the organic sorbates in the competition with water molecules for adsorption. (ii) Additional EDA interactions between the lone electron

pairs of the *p*-TSA and MTBE heteroatoms and the protonated DeACF<sub>10</sub> surface as had been previously reported for MTBE [33]. *p*-TSA, however, was adsorbed with higher sorption affinities on all ACFs than MTBE despite its lower log *D* which shall indicate a weaker hydrophobic effect [17]. This is likely due to additional  $\pi$ - $\pi$  interactions [34] of *p*-TSA. Furthermore, charge-assisted hydrogen bonds (( $\pm$ ) CAHB, being relevant at  $\Delta pK_a < 5$  [54, 55]) between *p*-TSA ( $pK_a = 10.5$ ) and ACF surfaces (carboxyl groups with  $pK_a = 3-6$  [56] and phenolic groups with  $pK_a = 8-10$  [57]) might contribute as well. However, the strong increase in  $K_d$  and  $q_{max}$  of *p*-TSA upon defunctionalization of the carbon surface rather speaks for a minor contribution of ( $\pm$ ) CAHB to its overall sorption.

Adsorption of charged PMOCs requires charge compensation either by oppositely charged sites on adsorbent surface (ion exchange) or co-adsorption of charge-balancing counter ions from the electrolyte solution [17, 58]. As a measure of the surface charging state of AC surfaces, CEC and AEC values are highly relevant and recommended to be measured, yet largely missing in the literature pool [17, 24]. Different to the  $pH_{PZC}$  which only gives qualitative information on the net surface charge, CEC and AEC provide quantitative information on the content of negatively and positively charged surface sites, respectively, at a certain pH value. Since the CEC of the ACFs was OxACF<sub>10</sub> > ACF<sub>10</sub> >> DeACF<sub>10</sub> (**Table 1**), better sorption of the cationic PMOCs to OxACF<sub>10</sub> than to DeACF<sub>10</sub> could be expected. However, rather similar  $q_{max}$  and log  $K_d$  of TPA<sup>+</sup>, BTMA<sup>+</sup> and BTEA<sup>+</sup> were found for all ACFs (**Table 3, Fig. 1**) despite the low CEC of the defunctionalized and net positively charged DeACF<sub>10</sub> surface. Only for BTMA<sup>+</sup>, i.e., the smallest cationic PMOC under study, slightly higher log  $K_d$  and  $q_{max}$  were observed on OxACF<sub>10</sub>. This points at the relevance of hydrophobicity as a driving force for sorption and may also explain why adsorption capacities of TPA<sup>+</sup>, BTMA<sup>+</sup> and BTEA<sup>+</sup> ( $\geq 0.1 \mu\text{mol}/\text{m}^2$ ) were higher than the CECs of oxygen-poorer ACF<sub>10</sub> and DeACF<sub>10</sub>. Also, cation- $\pi$  EDA interactions might cause additional promoting effects in the adsorption of cationic PMOCs on AC surfaces containing a higher density of  $\pi$  systems [17]. On the contrary, the  $q_{max}$  of the cationic PMOCs was 50–80% lower than the CEC of OxACF<sub>10</sub> following the order of TPA<sup>+</sup> < BTEA<sup>+</sup> < BTMA<sup>+</sup> (<Cu<sup>2+</sup> that accounted for 87% of CEC, cf. **Fig. S4, Table S2**). The high  $q_{max}$  of cationic PMOCs beyond sorbents' CECs suggest a strong contribution of hydrophobic effects, i.e. the combination of van der Waals forces and solvophobic effects, to the overall sorption due to the relatively bulky non-polar parts in their molecule structure. Such interactions could even overcompensate the net negative

charge effects of ACF<sub>10</sub> surface, as has been described for sorption of alkyl ammonium cations of varying chain lengths to inorganic sorbents [58]. So far, however, systematic studies on similar effects on PMOC adsorption to AC materials are missing. Our results suggest that the reversal of sorbent surface net charge by adsorption of PMOCs depends on the AC surface chemistry: cationic PMOCs can be more easily accommodated beyond sorbents' CECs as found for hydrophobic ACF<sub>10</sub> and DeACF<sub>10</sub>, but not for hydrophilic OxACF<sub>10</sub>. One possible reason for the unexpectedly weak charge effects with cationic sorbates might be the shielding of the positive charge by four more or less bulky substituents, which may prevent a close approach of the N atom to negatively charged surface sites. Anionic sorbates such as *p*-TsO<sup>-</sup> are not affected in a similar way.

Contrary to the cationic PMOCs, the  $q_{\max}$  of negatively charged *p*-TsO<sup>-</sup> to all ACFs was larger than the sorbents' AECs (**Tables 1 & 3**) again indicating a superposition of non-Coulombic (hydrophobic) and anion exchange interactions between *p*-TsO<sup>-</sup> and ACF surfaces. The  $q_{\max}$  decreases in the order of DeACF<sub>10</sub> > ACF<sub>10</sub> >> OxACF<sub>10</sub> (**Table 3**) and reflects the simultaneous decrease in hydrophobicity and increased number of repulsive negatively charged sites (higher CEC) of OxACF<sub>10</sub> surface.  $K_d$  and  $q_{\max}$  of *p*-TsO<sup>-</sup>, however, were significantly lower than of its uncharged derivative *p*-TSA (**Fig. 1, Table 3**) and exhibited more pronounced differences for the differently treated ACFs. This suggests a minor contribution of negative (-) CAHB between *p*-TsO<sup>-</sup> ( $pK_a = -1.3$ ) and the carboxyl groups of OxACF<sub>10</sub> ( $pK_a = 3-6$ ) which should otherwise promote the adsorption, and emphasizes the combination of electrostatic and hydrophobic effects as drivers for the sorption of anionic PMOCs. Our findings support recent studies on the sorption trends of anionic per- and polyfluoroalkyl substances (PFAS) [40, 59].

### 3.2.2 Effect of temperature on adsorption of selected PMOCs

To separate enthalpic and entropic contributions of adsorption, adsorption experiments at different temperatures were performed for TPA<sup>+</sup>, BTMA<sup>+</sup>, *p*-TsO<sup>-</sup> and *p*-TSA and interpreted using a modified van't Hoff equation. The van't Hoff equation [60] links  $K_{ads}$  as adsorption equilibrium constant with  $\Delta H_{ads}$  and  $\Delta S_{ads}$  as adsorption enthalpy and entropy.

$$\ln K_{ads} = -\frac{\Delta H_{ads}}{RT} + \frac{\Delta S_{ads}}{R} \quad (4)$$



Note that there is an ongoing debate on the correct equilibrium constants to be applied in Eq. 4 for adsorption to solid surfaces (which in principle should be unit-free) [60, 61]. However, it becomes insignificant when aiming at values for adsorption *enthalpy* only. Thus, we apply a simplified approach, replacing  $K_{ads}$  by  $K_d$ , i.e., the single-point adsorption coefficient in the low sorbent loading range ( $q \ll q_{max}$ ) to give a modified van't Hoff equation. We consider the derived adsorption enthalpies ( $\Delta H_{ads} = -R \cdot d(\ln K_d)/d(1/T)$ ) as 'apparent' ones, being aware of the limited thermodynamic significance of these values. The calculated values are in the range from  $\Delta H_{ads} = 0$  for adsorption of TPA<sup>+</sup> on OxACF<sub>10</sub> to – 38 kJ/mol for adsorption of *p*-TsO<sup>–</sup> on DeACF<sub>10</sub>.

Exothermic sorption was observed for all sorbate-sorbent pairs, with less steep slopes (i.e. less exothermic adsorption) for adsorption to OxACF<sub>10</sub> than to DeACF<sub>10</sub> (**Fig. 2**). Especially, adsorption of cationic TPA<sup>+</sup> and BTMA<sup>+</sup> on OxACF<sub>10</sub> was found to be quasi thermoneutral. Although these sorbates should experience improved electrostatic attraction with the oxidized carbon surface, sacrificed non-Coulombic interactions on the more hydrophilic sorbent took over. Our findings are in accordance with previous results [38] which showed that adsorption of BTMA<sup>+</sup> and BTEA<sup>+</sup> onto microporous activated carbon cloth was dominated by hydrophobic effects. Entropy seems to be an important driving force for adsorption of the organic cations to the oxidized ACF surface, as most obvious for BTMA<sup>+</sup> where OxACF<sub>10</sub> shows the lowest slope (lowest  $\Delta H_{ads}$ ) but still highest  $K_d$ .

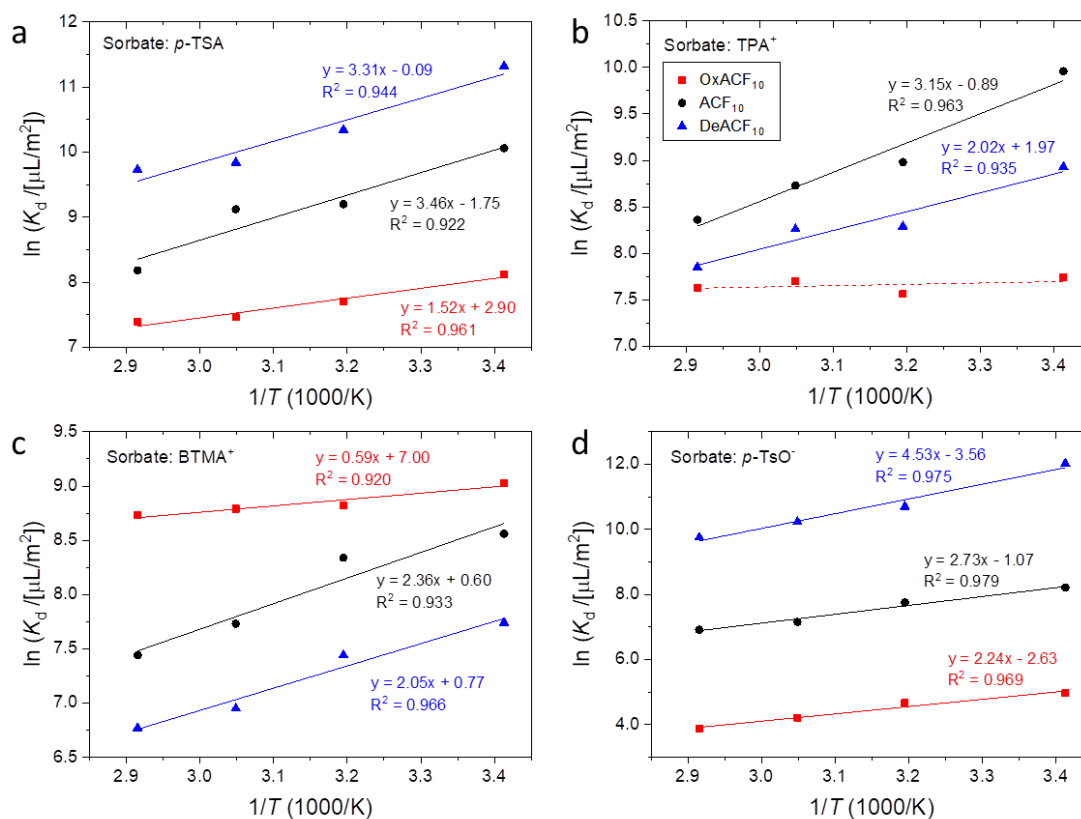


**Fig. 2:** Linear fittings of  $\ln K_d$  vs.  $(1/T)$  for (a)  $p$ -TSA, (b) TPA<sup>+</sup>, (c) BTMA<sup>+</sup> and (d)  $p$ -TsO<sup>-</sup> in 10 mM Na<sub>2</sub>SO<sub>4</sub> at pH 7. The initial concentration of dissolved sorbate was set at 20 mg/L. The experimental conditions (details given in SI) were selected giving  $q \leq \frac{1}{2} q_{\max}$ .

Defunctionalization of the ACF generally had minor impacts on the slopes of van't Hoff plots for neutral and cationic PMOCs, yet clearly enhanced the  $\Delta H_{\text{ads}}$  of  $p$ -TsO<sup>-</sup>. Here, the superposition of improved van der Waals forces,  $\pi$ - $\pi$  and  $n$ - $\pi$  EDA interactions and attractive Coulombic interactions (with protonated  $\pi$ -electron systems) leads to a more exothermic process.

### 3.2.3 Effect of the ionic strength and pH on adsorption

**Ionic strength (IS):** applying background electrolyte (Na<sub>2</sub>SO<sub>4</sub>) with increasing concentrations from 1 mM to 100 mM may influence adsorption of polar and ionic organic compounds by: (i) increased competition for sorption sites by inorganic ions [17, 40], (ii) higher shielding of the sorbent's ion exchange sites due to a compressed electric double layer (EDL) [62], and (iii) increased chemical activity of dissolved sorbates by possible salting-out effect [63]. As

salting-out effects were estimated to cause effects on  $\log K_d$  of  $< \pm 0.02$  [58], they are considered negligible for our interpretation and thus are not further considered.

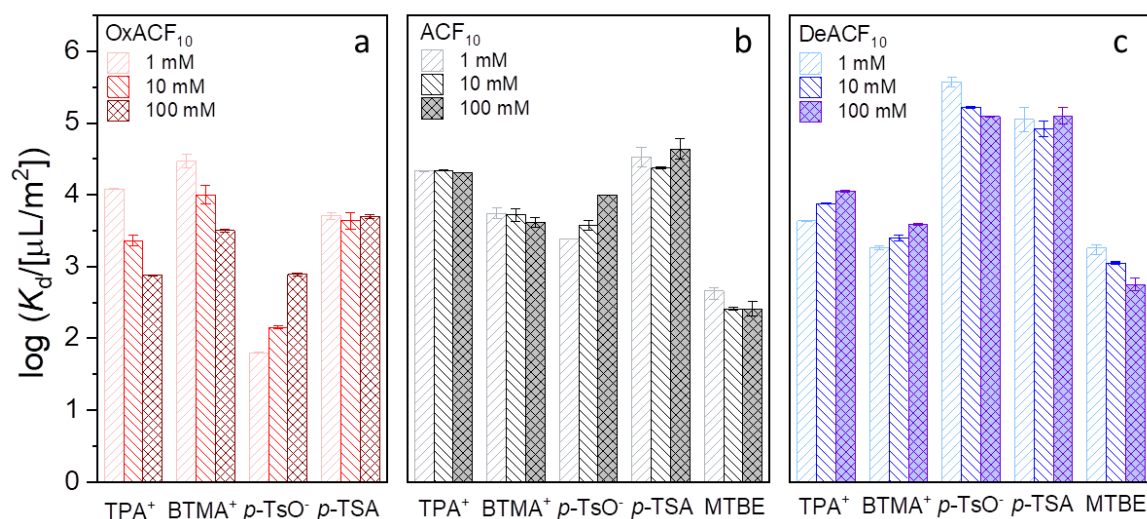


**Fig. 3:** The effect of electrolyte solution concentration on the adsorption of selected compounds on (a) OxACF<sub>10</sub>, (b) ACF<sub>10</sub> and (c) DeACF<sub>10</sub> in Na<sub>2</sub>SO<sub>4</sub> solution at pH 7. The experimental conditions (details given in SI) were selected to ensure  $q \leq 2/3 q_{\max}$ . The error bars are standard deviations of the single values from duplicate experiments with triplicate measurements each.

As shown in **Fig. 3**, poor influence of the salt concentration on  $\log K_d$  of *p*-TSA adsorption for any of the ACF was found. This indicates that the strong *p*-TSA adsorption to ACF is mainly driven by non-Coulumbic interactions. In contrast,  $K_d$  of MTBE on DeACF<sub>10</sub> decreased slightly at increasing ionic strengths. Contrary to likewise neutral *p*-TSA, MTBE has no  $\pi$ -electron system to interact with the ACF surface, and the EDA interactions may be hindered either by competitive sorption of SO<sub>4</sub><sup>2-</sup> or increased shielding of sorption sites. On OxACF<sub>10</sub>, increasing IS suppressed adsorption of cationic TPA<sup>+</sup> and BTMA<sup>+</sup>, whereas the anionic *p*-TsO<sup>-</sup> adsorbed more strongly. These opposite effects can be explained by the same mechanism: joint effect of EDL compression and competing Na<sup>+</sup> adsorption at the negatively charged OxACF<sub>10</sub> surface aroused a weakening of attractive or repulsive electrostatic interactions for cationic and anionic PMOCs, respectively. Similar reasons account for the changes in  $\log K_d$  on DeACF<sub>10</sub> for charged PMOCs upon IS change [40].

The effect of solution pH (at 4, 7 and 9) on the adsorption of selected PMOCs on OxACF<sub>10</sub> and DeACF<sub>10</sub> is shown in **Fig. S10**. Decreasing pH from 9 to 4 moderately reduced the

adsorption of TPA<sup>+</sup> and BTMA<sup>+</sup> on OxACF<sub>10</sub> (**Fig. S10a**). Since p<sub>H</sub>PZC of OxACF<sub>10</sub> is 2.4, the sorbent surface keeps a negative net charge at pH 4 while the density of negatively charged surface sites increases at higher pH, which clearly benefits the uptake of the cationic PMOCs. Accordingly, the adsorption affinity of *p*-TsO<sup>-</sup> on DeACF<sub>10</sub> (p<sub>H</sub>PZC = 10.2) increases when decreasing pH from 9 to 4 due to enhanced electrostatic interactions (**Fig. S10b**). In comparison, no change in log *K*<sub>d</sub> in the adsorption of neutral *p*-TSA on DeACF<sub>10</sub> was observed at different pH values as expected. The effect of a broader pH range on adsorption of especially weak organic acids and bases was reported to be studied using the bell-shape relationship [64].

In summary, increases in IS improved adsorption if solutes and net charges of the sorbent surface were of the same sign (positive or negative), while increased IS hindered adsorption if charges were of opposite signs. IS effects on neutral compounds were found only in case of strong EDA yet weak non-Coulombic interactions.

### 3.2.4 Comparison of experimental data with model predictions

Our experimental PMOC sorption data were compared to model predictions [24] adapted for the adsorption of polar organic compounds to carbonaceous materials. As Abraham parameters of ionic compounds are poorly accessible, the comparison was done for MTBE, *p*-TsO<sup>-</sup> and *p*-TSA with Abraham parameters (of their neutral forms) available from the UFZ LSER database [65] as also proposed by Sigmund et al. (2020) [24]. We further included previously published data on octanoic acid (OCA, p*K*<sub>a</sub> = 4.9 [20]) [66] and MTBE adsorption [33]. **Fig. 4** shows the comparison of Log *K*<sub>F</sub> and *n* as these two Freundlich parameters are separately predicted for each sorbate-sorbent pair by Sigmund et al. (2020) [65].

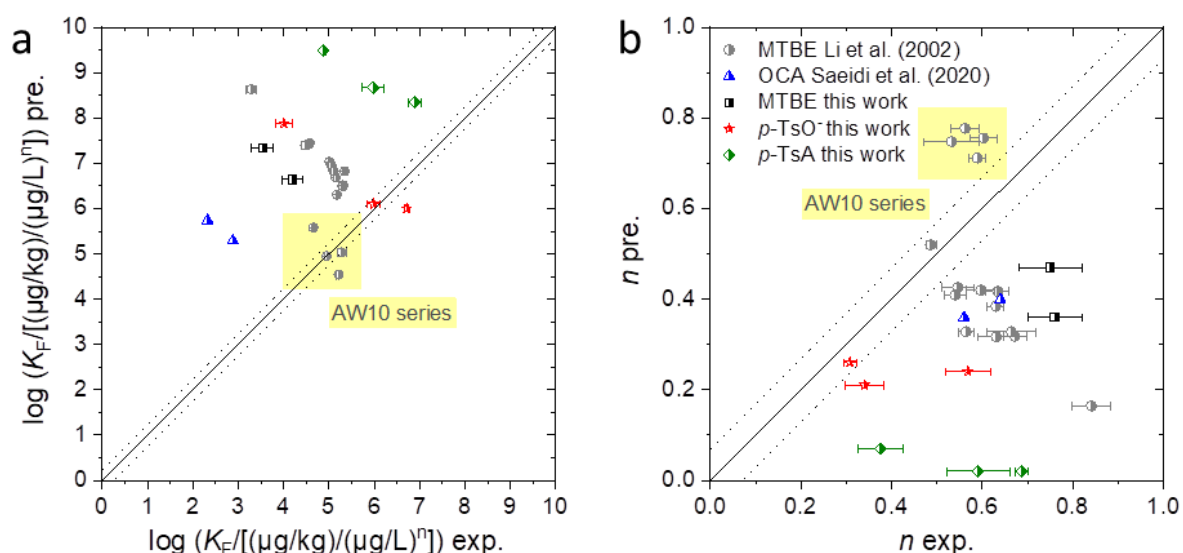


**Fig. 4:** Comparison of experimentally derived and predicted Freundlich isotherm parameters (a)  $\log K_F$  and (b)  $n$  by the model of Sigmund et al. (2020b).  $K_F$  are given in  $(\mu\text{g/kg})/(\mu\text{g/L})^n$  as used also by Sigmund et al. (2020b). Error bars are obtained from the regression analyses of experimentally derived Freundlich fittings. Functions  $y = x$  for both  $\log K_F$  and  $n$  are shown by the black solid lines. Typical expected deviation ranges for  $\log K_F$  and  $n$  are marked with dashed lines.

Generally, **Fig. 4** reveals higher predicted  $\log K_F$  coupled with lower predicted  $n$  than experimental-derived ones. In a few cases, for instance among the 17 sets of MTBE adsorption data compared, the most successful matches were found on AW10 carbon series (incl. oxidized OAW10,  $\text{H}_2$ -treated HAW10,  $\text{NH}_3$ -treated AAW10 and pristine AW10 reported in [33]) carrying  $S_{\text{BET}} < 850 \text{ m}^2/\text{g}$  (**Fig. 4**, SI S4 and SI Excel-file). In contrast, unreasonably high  $\log K_{F, \text{pre}} > \log K_{F, \text{exp}} + 1$  were observed on other AC-based sorbents carrying  $S_{\text{BET}} > 1100 \text{ m}^2/\text{g}$  (cf. SI S4). The observed mismatch may be explained by the fact that the model was trained heavily with biochar sorbents of relatively low  $S_{\text{BET}}$  (83% datasets with  $S_{\text{BET}} < 400 \text{ m}^2/\text{g}$ ) as datasets with well characterized AC carrying high  $S_{\text{BET}}$  are often hard to find in the literature. As  $S_{\text{BET}}$  was found to be the key property among all 12 input parameters to predict  $K_F$  and  $n$  for anionic and neutral PMOCs according to Sigmund et al. (2020) [24], results in **Fig. 4** suggest that further model training involving well-characterized AC materials of high  $S_{\text{BET}}$  is needed for successful prediction of PMOC in large-scale water treatment facilities.

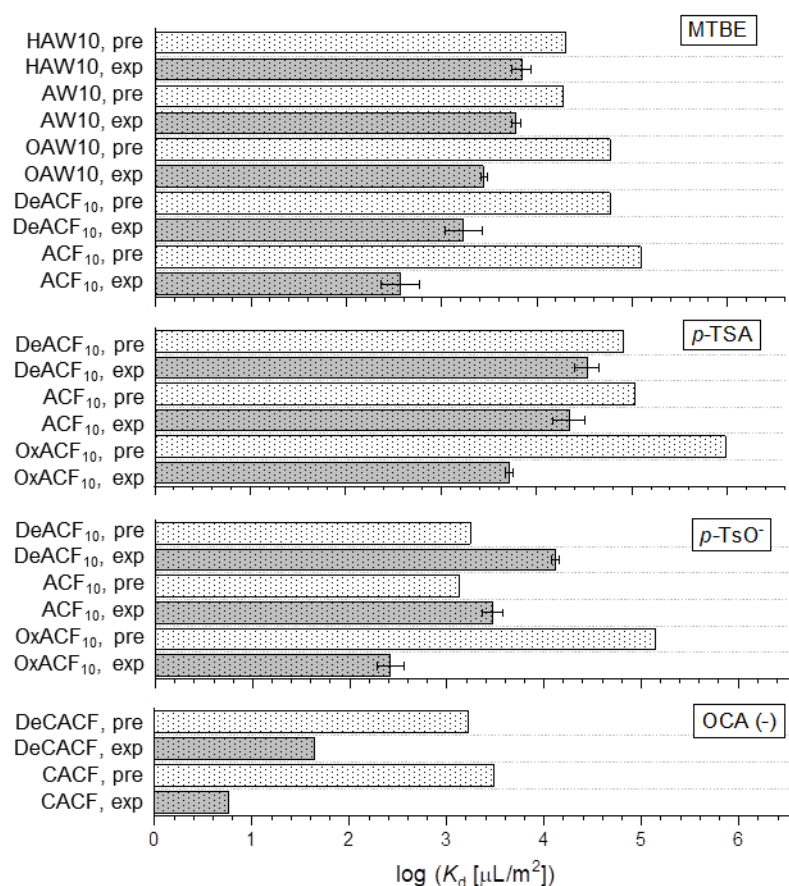


**Fig. 5:** Experimentally derived and predicted  $\log K_d$  of MTBE,  $p$ -TSA,  $p$ -TsO<sup>-</sup> and OCA (-) at  $c_e = 20 \mu\text{M}$  on various ACFs in 10 mM Na<sub>2</sub>SO<sub>4</sub> solution at pH 7.  $\log K_d$  and error bars were obtained as for **Fig. 1**. DeCACF contains a lower O-content and a more hydrophobic surface with a higher delocalized  $\pi$ -electron density than CACF [66].

Next, we tested if the model allows predicting the effect of changes of ACF's surface chemistry on PMOC adsorption. Although predicted and experimental  $\log K_d$  values for adsorption of  $p$ -TsO<sup>-</sup> to ACF<sub>10</sub> and  $p$ -TSA to ACF<sub>10</sub> and DeACF<sub>10</sub> were comparable (**Fig. 5**), the model generally failed to predict the poorer adsorption of PMOCs to ACFs with higher O-contents (i.e. ACFs of more elevated CEC and higher negative surface charge densities at neutral pH). This suggests that sorbent surface chemistry impacts may need to be better considered by the model. As proposed by Sigmund et al. (2020) [24], model improvements may implement EDA and electrostatic interactions between sorbents and sorbates and, hence, also consider parameters describing sorbent surface charge. Although ion exchange capacities more precisely quantify charges at a sorbent's surface at specified pH than commonly used O/C ratios, total acidity or  $\text{pH}_{\text{pzc}}$ , they are yet rare to find in literature. In addition, an inclusion of appropriate descriptors for ionic PMOCs may be required as the

current model applies Abraham parameters for uncharged compounds only [25-27]. Involvement of ionization degrees  $A^-$  % and  $B^+$  % solely might not fully solve the problem as implied by the distorted predicted trends. Finally, comprehensive characterization of the sorbents beyond ion exchange properties may be useful for updating prediction models. Nevertheless, a compromise between practical applicability (easily approachable AC characteristics which can be potentially offered by AC suppliers) and precision of prediction is certainly required.

#### 4. Conclusion

In the present study, surface chemistry of AC is identified as an important factor for adsorption performance especially towards ionic and ionizable PMOCs. Surface-defunctionalized ACF was found to promise the widest application potential to adsorb neutral, anionic and cationic PMOCs among three tested ACFs. The defunctionalization creates a rather hydrophobic carbon surface carrying positively charged sites which specifically improves the adsorption of anionic PMOCs, while benefiting the adsorption of all probed PMOCs including the studied quaternary amines. Therefore, surface defunctionalization can work as a universal strategy to facilitate the removal of a wide range of diverse PMOCs simultaneously meanwhile to extend fixed-bed adsorber operation times or reduce required dosage of powdered AC in WWTPs.

In contrast, surface oxidation of AC as a means to increase density of negative charges results in higher surface polarity which is clearly detrimental for adsorption of *p*-TSA, *p*-TsO<sup>-</sup> and TPA<sup>+</sup> due to enhanced competitive adsorption of water molecules to AC surface. However, it selectively enhanced the adsorption of BTMA<sup>+</sup>, i.e., the probed cationic PMOC with the smallest number of carbon atoms and the lowest log *D*. It is thus tentatively suggested that a threshold limit in the size of the hydrophobic part of cationic PMOCs exists, below which oxidized AC surfaces can benefit their adsorption due to intensified electrostatic attraction.

Our work further demonstrates that the challenges in prognosis of the complicated PMOC sorption behaviors on AC sorbents are not fully conquered by the state-of-the-art prediction tools, which evidently underestimates the impact of sorbent surface chemistry. Our findings alert that standardized quantitative parameters describing AC surface chemistry are needed

which should be commonly reported in scientific studies and finally also in product sheets by AC producers. Such parameters can be applied as input for the improvement of sorption prediction models for newly emerging PMOCs. In this respect, ion exchange capacity which quantifies sorbent surface charges at specified pH is recommended as a meaningful parameter.

### **Acknowledgement:**

We acknowledge the funding by Deutsche Forschungsgemeinschaft GE 3029/1-1 and the funding within the PhD-college STROMER of Thematic Area Environmental Engineering and Biotechnology of UFZ. We acknowledge Dr. Marcus Lange, Dr. Jens Möllmer, Dr. Hans Uhlig at Institut für Nichtklassische Chemie e.V. (INC), Leipzig, for CO<sub>2</sub> adsorption measurement; M.Sc. Andrea Prager at Leibniz Institute of Surface Engineering (IOM), Leipzig, for XPS determination; Dr. Ulf Roland and Dr. Frank Holzer for the ATR-FTIR measurement; Dr. Gabriel Sigmund at University of Vienna for fruitful discussions; and B.Sc. Ruonan Qin for assisting the work as an internship student on the adsorption of MTBE. We are thankful for the use of SEM at the Centre for Chemical Microscopy (ProVIS) at UFZ, which is supported by European Regional Development Funds (EFRE-Europe funds Saxony) and the Helmholtz Association.

### **References**

- [1] H.P.H. Arp, T.N. Brown, U. Berger, S.E. Hale, Ranking REACH registered neutral, ionizable and ionic organic chemicals based on their aquatic persistency and mobility, *Environ. Sci.: Process. Impacts*. 19 (2017) 939-955. <https://doi.org/10.1039/C7EM00158D>.
- [2] H.P.H. Arp, S.E. Hale, REACH: Improvement of guidance and methods for the identification and assessment of PMT/vPvM substances, Umweltbundesamt <https://www.umweltbundesamt.de/publikationen/reach-improvement-of-guidance-methods-for-the>, 2019 (accessed 1 June 2021).
- [3] T. Reemtsma, S. Weiss, J. Mueller, M. Petrovic, S. González, D. Barcelo, F. Ventura, T.P. Knepper, Polar pollutants entry into the water cycle by municipal wastewater: a european perspective, *Environ. Sci. Technol.* 40 (2006) 5451-5458. <https://doi.org/10.1021/es060908a>.
- [4] M.I. Farré, S. Pérez, L. Kantiani, D. Barceló, Fate and toxicity of emerging pollutants, their metabolites and transformation products in the aquatic environment, *TrAC Trends Anal. Chem.* 27 (2008) 991-1007. <https://doi.org/10.1016/j.trac.2008.09.010>.
- [5] R. Loos, R. Carvalho, D.C. António, S. Comero, G. Locoro, S. Tavazzi, B. Paracchini, M. Ghiani, T. Lettieri, L. Blaha, B. Jarosova, S. Voorspoels, K. Servaes, P. Haglund, J. Fick, R.H. Lindberg, D. Schwesig, B.M. Gawlik, EU-wide monitoring survey on emerging polar organic contaminants in wastewater treatment plant effluents, *Water Res.* 47 (2013) 6475-6487. <https://doi.org/10.1016/j.watres.2013.08.024>.



- [6] S. Schulze, D. Zahn, R. Montes, R. Rodil, J.B. Quintana, T.P. Knepper, T. Reemtsma, U. Berger, Occurrence of emerging persistent and mobile organic contaminants in European water samples, *Water Res.* 153 (2019) 80-90. <https://doi.org/10.1016/j.watres.2019.01.008>.
- [7] B. Teychene, F. Chi, J. Chokki, G. Darracq, J. Baron, M. Joyeux, H. Gallard, Investigation of polar mobile organic compounds (PMOC) removal by reverse osmosis and nanofiltration: rejection mechanism modelling using decision tree, *Water Supply* 20 (2020) 975-983. <http://doi.org/10.2166/ws.2020.020>.
- [8] C.J. Sinclair, A.B.A. Boxall, Assessing the ecotoxicity of pesticide transformation products, *Environ. Sci. Technol.* 37 (2003) 4617-4625. <http://doi.org/10.1021/es030038m>.
- [9] K. Fent, A.A. Weston, D. Caminada, Ecotoxicology of human pharmaceuticals, *Aquat. Toxicol.* 76 (2006) 122-159. <https://doi.org/10.1016/j.aquatox.2005.09.009>.
- [10] V.S. Thomaidi, A.S. Stasinakis, V.L. Borova, N.S. Thomaidis, Is there a risk for the aquatic environment due to the existence of emerging organic contaminants in treated domestic wastewater? Greece as a case-study, *J. Hazard. Mater.* 283 (2015) 740-747. <https://doi.org/10.1016/j.jhazmat.2014.10.023>.
- [11] B.t. Ferrari, N. Paxéus, R.L. Giudice, A. Pollio, J. Garric, Ecotoxicological impact of pharmaceuticals found in treated wastewaters: study of carbamazepine, clofibric acid, and diclofenac, *Ecotoxicol. Environ. Saf.* 55 (2003) 359-370. [https://doi.org/10.1016/S0147-6513\(02\)00082-9](https://doi.org/10.1016/S0147-6513(02)00082-9).
- [12] C. Sophia A, E.C. Lima, Removal of emerging contaminants from the environment by adsorption, *Ecotoxicol. Environ. Saf.* 150 (2018) 1-17. <https://doi.org/10.1016/j.ecoenv.2017.12.026>.
- [13] EPA, United States Environmental Protection Agency: drinking water treatment technology unit cost models and overview of technologies <https://www.epa.gov/sdwa/drinking-water-treatment-technology-unit-cost-models-and-overview-technologies> <https://www.epa.gov/sdwa/drinking-water-treatment-technology-unit-cost-models-and-overview-technologies>, 2020 (accessed 16 April 2021).
- [14] J. Watson, Separation methods for waste and environmental applications, Marcel Dekker, New York, 1999.
- [15] T. Reemtsma, U. Berger, H.P.H. Arp, H. Gallard, T.P. Knepper, M. Neumann, J.B. Quintana, P.d. Voogt, Mind the gap: persistent and mobile organic compounds—water contaminants that slip through, *Environ. Sci. Technol.* 50 (2016) 10308-10315. <https://doi.org/10.1021/acs.est.6b03338>.
- [16] L. Decrey, F. Bonvin, C. Bonvin, E. Bonvin, T. Kohn, Removal of trace organic contaminants from wastewater by superfine powdered activated carbon (SPAC) is neither affected by SPAC dispersal nor coagulation, *Water Res.* 185 (2020) 116302. <https://doi.org/10.1016/j.watres.2020.116302>.
- [17] M. Kah, G. Sigmund, F. Xiao, T. Hofmann, Sorption of ionizable and ionic organic compounds to biochar, activated carbon and other carbonaceous materials, *Water Res.* 124 (2017) 673-692. <https://doi.org/10.1016/j.watres.2017.07.070>.
- [18] K.-U. Goss, The pKa values of PFOA and other highly fluorinated carboxylic acids, *Environ. Sci. Technol.* 42 (2008) 456-458. <https://doi.org/10.1021/es702192c>.
- [19] D. Brooke, A. Footitt, T.A. Nwaogu, Environmental risk evaluation report: Perfluorooctanesulphonate (PFOS) [https://www.gov.uk/government/uploads/system/uploads/attachment\\_data/file/290857/scho1009brbl-e-e.pdf](https://www.gov.uk/government/uploads/system/uploads/attachment_data/file/290857/scho1009brbl-e-e.pdf), 2004 (accessed 1 June 2021).
- [20] B.A. Wellen, E.A. Lach, H.C. Allen, Surface pKa of octanoic, nonanoic, and decanoic fatty acids at the air–water interface: applications to atmospheric aerosol chemistry, *Phys. Chem. Chem. Phys.* 19 (2017) 26551-26558. <https://doi.org/10.1039/C7CP04527A>.
- [21] R. Mailler, J. Gasperi, Y. Coquet, C. Derome, A. Buleté, E. Vulliet, A. Bressy, G. Varrault, G. Chebbo, V. Rocher, Removal of emerging micropollutants from wastewater by activated carbon adsorption: experimental study of different activated carbons and factors influencing the adsorption of micropollutants in wastewater, *J. Environ. Chem. Eng.* 4 (2016) 1102-1109. <https://doi.org/10.1016/j.jece.2016.01.018>.
- [22] ECETOC, Environmental exposure assessment of ionizable organic compounds -technical report No. 123. European Centre for Ecotoxicology and Toxicology of Chemicals, Brussels.

- <https://www.ecetoc.org/publication/tr-123-environmental-risk-assessment-of-ionisable-compounds/>, 2013 (accessed 1 June 2021).
- [23] S. Endo, K.-U. Goss, Applications of polyparameter linear free energy relationships in environmental chemistry, *Environ. Sci. Technol.* 48 (2014) 12477-12491. [10.1021/es503369t](https://doi.org/10.1021/es503369t).
- [24] G. Sigmund, M. Gharasoo, T. Hüffer, T. Hofmann, Deep learning neural network approach for predicting the sorption of ionizable and polar organic pollutants to a wide range of carbonaceous materials, *Environ. Sci. Technol.* 54 (2020) 4583–4591. <http://doi.org/10.1021/acs.est.9b06287>.
- [25] Y. Zhao, S. Lin, J.-W. Choi, J.K. Bediako, M.-H. Song, J.-A. Kim, C.-W. Cho, Y.-S. Yun, Prediction of adsorption properties for ionic and neutral pharmaceuticals and pharmaceutical intermediates on activated charcoal from aqueous solution via LFER model, *Chem. Eng. J.* 362 (2019) 199-206. <https://doi.org/10.1016/j.cej.2019.01.031>.
- [26] K. Zhang, S. Zhong, H. Zhang, Predicting aqueous adsorption of organic compounds onto biochars, carbon nanotubes, granular activated carbons and resins with machine Learning, *Environ. Sci. Technol.* 54 (2020) 7008-7018. <https://doi.org/10.1021/acs.est.0c02526>.
- [27] M.H. Abraham, Y.H. Zhao, Determination of solvation descriptors for ionic species: hydrogen bond acidity and basicity, *J. Org. Chem.* 69 (2004) 4677-4685. <https://doi.org/10.1021/jo049766y>.
- [28] G. Sigmund, M. Gharasoo, T. Hüffer, T. Hofmann, Comment on predicting aqueous adsorption of organic compounds onto biochars, carbon nanotubes, granular activated carbons and resins with machine learning, *Environ. Sci. Technol.* 54 (2020) 11636-11637. <https://doi.org/10.1021/acs.est.0c03931>.
- [29] J.P. Guthrie, Hydrolysis of esters of oxy acids: pKa values for strong acids; Brønsted relationship for attack of water at methyl; free energies of hydrolysis of esters of oxy acids; and a linear relationship between free energy of hydrolysis and pKa holding over a range of 20 pK units, *Can. J. Chem.* 56 (1978) 2342-2354. <https://doi.org/10.1139/v78-385>.
- [30] E.P. Sergeant, B. Dempsey, Ionisation constants of organic acids in aqueous solution. IUPAC chemical data series No. 23, Pergamon Press, New York, 1979.
- [31] J.L. Atwood, J.W. Steed, *Encyclopedia of supramolecular chemistry* CRC Press, New York, 2004. <https://doi.org/10.1201/9780429075728>
- [32] S. Schulze, D. Sättler, M. Neumann, H.P.H. Arp, T. Reemtsma, U. Berger, Using REACH registration data to rank the environmental emission potential of persistent and mobile organic chemicals, *Sci. Total Environ.* 625 (2018) 1122-1128. <https://doi.org/10.1016/j.scitotenv.2017.12.305>.
- [33] L. Li, P.A. Quinlivan, D.R.U. Knappe, Effects of activated carbon surface chemistry and pore structure on the adsorption of organic contaminants from aqueous solution, *Carbon* 40 (2002) 2085-2100. [https://doi.org/10.1016/S0008-6223\(02\)00069-6](https://doi.org/10.1016/S0008-6223(02)00069-6).
- [34] T. Wu, X. Cai, S. Tan, H. Li, J. Liu, W. Yang, Adsorption characteristics of acrylonitrile, p-toluenesulfonic acid, 1-naphthalenesulfonic acid and methyl blue on graphene in aqueous solutions, *Chem. Eng. J.* 173 (2011) 144-149. <https://doi.org/10.1016/j.cej.2011.07.050>.
- [35] Y. Qi, X. Jin, C. Yu, Y. Wang, L. Yang, Y. Li, A novel chelating resin containing high levels of sulfamine group: Preparation and its adsorption characteristics towards p-toluenesulfonic acid and Hg(II), *Chem. Eng. J.* 233 (2013) 315-322. <https://doi.org/10.1016/j.cej.2013.08.016>.
- [36] M. Davarpanah, A. Ahmadpour, T. Rohani-Bastami, H. Dabir, Synthesis and application of diethanolamine-functionalized polystyrene as a new sorbent for the removal of p-toluenesulfonic acid from aqueous solution, *J. Ind. Eng. Chem.* 30 (2015) 281-288. <https://doi.org/10.1016/j.jiec.2015.05.034>.
- [37] H. Tamai, M. Kunihiro, H. Yasuda, Adsorption of tetraalkylammonium ions on microporous and mesoporous activated carbons prepared from vinylidene chloride copolymer, *J. Colloid Interface Sci.* 275 (2004) 44-47. <https://doi.org/10.1016/j.jcis.2003.12.039>.
- [38] O. Duman, E. Ayranci, Adsorptive removal of cationic surfactants from aqueous solutions onto high-area activated carbon cloth monitored by in situ UV spectroscopy, *J. Hazard. Mater.* 174 (2010) 359-367. <https://doi.org/10.1016/j.jhazmat.2009.09.058>.

- [39] B.M. Babić, S.K. Milonjić, M.J. Polovina, B.V. Kaludierović, Point of zero charge and intrinsic equilibrium constants of activated carbon cloth, *Carbon* 37 (1999) 477-481.  
[https://doi.org/10.1016/S0008-6223\(98\)00216-4](https://doi.org/10.1016/S0008-6223(98)00216-4).
- [40] N. Saeidi, F.-D. Kopinke, A. Georgi, Understanding the effect of carbon surface chemistry on adsorption of perfluorinated alkyl substances, *Chem. Eng. J.* 381 (2020) 122689.  
<https://doi.org/10.1016/j.cej.2019.122689>.
- [41] L.W. Zelazny, L. He, A. Vanwormhoudt, Charge analysis of soils and anion exchange, *Methods of soil analysis: Part 3 chemical methods*, 5.3, Soil Science Society of America, Inc., American Society of Agronomy, Inc., Madison, 1996, pp. 1231-1253. <https://doi.org/10.2136/sssabookser5.3.c41>.
- [42] L. Aljerf, High-efficiency extraction of bromocresol purple dye and heavy metals as chromium from industrial effluent by adsorption onto a modified surface of zeolite: Kinetics and equilibrium study, *J. Environ. Manage.* 225 (2018) 120-132. <https://doi.org/10.1016/j.jenvman.2018.07.048>.
- [43] S. Delpeux-Ouldriane, M. Gineys, N. Cohaut, F. Béguin, The role played by local pH and pore size distribution in the electrochemical regeneration of carbon fabrics loaded with bentazon, *Carbon* 94 (2015) 816-825. <https://doi.org/10.1016/j.carbon.2015.07.010>.
- [44] L. Messori, A. Casini, C. Gabbiani, L. Sorace, M. Muniz-Miranda, P. Zatta, Unravelling the chemical nature of copper cuprizone, *Dalton Trans.* (2007) 2112-2114.  
<https://doi.org/10.1039/B701896G>.
- [45] M. Vogel, F.-D. Kopinke, K. Mackenzie, Acceleration of microiron-based dechlorination in water by contact with fibrous activated carbon, *Sci. Total Environ.* 660 (2019) 1274-1282.  
<https://doi.org/10.1016/j.scitotenv.2019.01.070>.
- [46] J.-H. Zhou, Z.-J. Sui, J. Zhu, P. Li, D. Chen, Y.-C. Dai, W.-K. Yuan, Characterization of surface oxygen complexes on carbon nanofibers by TPD, XPS and FT-IR, *Carbon* 45 (2007) 785-796.  
<https://doi.org/10.1016/j.carbon.2006.11.019>.
- [47] W. Yang, Electrochemical Advanced Oxidation Processes for Emerging Organic Contaminants Removal with Graphene-based Modified Carbon Felt Electrode, PhD Dissertation, Université Paris-Est, Nankai University, 2019.
- [48] K.S.W. Sing, D.H. Everett, R.A.W. Haul, L. Moscou, R.A. Pierotti, J. Rouquerol, T. Siemieniowska, Reporting physisorption data for gas/solid systems with special reference to the determination of surface area and porosity (Recommendations 1984), *Pure Appl. Chem.* 57 (1985) 603-619.  
<https://doi.org/10.1351/pac198557040603>.
- [49] Z. Allothman, A review: fundamental aspects of silicate mesoporous materials, *Materials* 5 (2012) 2874-2902. <https://doi.org/10.3390/ma5122874>.
- [50] H. Zhao, L. Qian, X. Guan, D. Wu, G. Zhao, Continuous bulk FeCuC aerogel with ultradispersed metal nanoparticles: an efficient 3D heterogeneous electro-Fenton cathode over a wide range of pH 3–9, *Environ. Sci. Technol.* 50 (2016) 5225-5233. <https://doi.org/10.1021/acs.est.6b00265>.
- [51] K.J. Lee, J. Miyawaki, N. Shiratori, S.-H. Yoon, J. Jang, Toward an effective adsorbent for polar pollutants: Formaldehyde adsorption by activated carbon, *J. Hazard. Mater.* 260 (2013) 82-88.  
<https://doi.org/10.1016/j.jhazmat.2013.04.049>.
- [52] E. Bayram, E. Ayranci, A systematic study on the changes in properties of an activated carbon cloth upon polarization, *Electrochim. Acta* 56 (2011) 2184-2189.  
<https://doi.org/10.1016/j.electacta.2010.12.018>.
- [53] G. Hotová, V. Slovák, T. Zelenka, R. Maršálek, A. Parchaňská, The role of the oxygen functional groups in adsorption of copper (II) on carbon surface, *Sci. Total Environ.* 711 (2020) 135436.  
<https://doi.org/10.1016/j.scitotenv.2019.135436>.
- [54] X. Li, J.J. Pignatello, Y. Wang, B. Xing, New insight into adsorption mechanism of ionizable compounds on carbon nanotubes, *Environ. Sci. Technol.* 47 (2013) 8334-8341.  
<https://doi.org/10.1021/es4011042>.
- [55] M. Teixidó, J.J. Pignatello, J.L. Beltrán, M. Granados, J. Peccia, Speciation of the ionizable antibiotic sulfamethazine on black carbon (biochar), *Environ. Sci. Technol.* 45 (2011) 10020-10027.  
<http://doi.org/10.1021/es202487h>.

- [56] V. Strelko, D.J. Malik, M. Streat, Characterisation of the surface of oxidised carbon adsorbents, *Carbon* 40 (2002) 95-104. [https://doi.org/10.1016/S0008-6223\(01\)00082-3](https://doi.org/10.1016/S0008-6223(01)00082-3).
- [57] F. Xiao, J.J. Pignatello, Effects of post-pyrolysis air oxidation of biomass chars on adsorption of neutral and ionizable compounds, *Environ. Sci. Technol.* 50 (2016) 6276-6283. <http://doi.org/10.1021/acs.est.6b00362>.
- [58] R.P. Schwarzenbach, P.M. Gschwend, D.M. Imboden, *Environmental organic chemistry*, John Wiley & Sons, Inc., New York, 1993.
- [59] Y. Zhi, J. Liu, Surface modification of activated carbon for enhanced adsorption of perfluoroalkyl acids from aqueous solutions, *Chemosphere* 144 (2016) 1224-1232. <https://doi.org/10.1016/j.chemosphere.2015.09.097>.
- [60] Y. Liu, Is the free energy change of adsorption correctly calculated?, *J. Chem. Eng. Data* 54 (2009) 1981-1985. <https://doi.org/10.1021/je800661q>.
- [61] H.N. Tran, S.-J. You, A. Hosseini-Bandegharai, H.-P. Chao, Mistakes and inconsistencies regarding adsorption of contaminants from aqueous solutions: A critical review, *Water Res.* 120 (2017) 88-116. <https://doi.org/10.1016/j.watres.2017.04.014>.
- [62] M.A. Brown, A. Goel, Z. Abbas, Effect of electrolyte concentration on the Stern layer thickness at a charged interface, *Angew. Chem. Int. Ed.* 55 (2016) 3790-3794. <https://doi.org/10.1002/anie.201512025>.
- [63] J.-X. Xiao, Y. Zhang, C. Wang, J. Zhang, C.-M. Wang, Y.-X. Bao, Z.-G. Zhao, Adsorption of cationic–anionic surfactant mixtures on activated carbon, *Carbon* 43 (2005) 1032-1038. <https://doi.org/10.1016/j.carbon.2004.11.039>.
- [64] F. Xiao, J.J. Pignatello, Effect of adsorption nonlinearity on the pH–adsorption profile of ionizable organic compounds, *Langmuir* 30 (2014) 1994-2001. <http://doi.org/10.1021/la403859u>.
- [65] N. Ulrich, S. Endo, T.N. Brown, N. Watanabe, G. Bronner, M.H. Abraham, K.-U. Goss, *UFZ-LSER Database v 3.2* <http://www.ufz.de/lserd> 2017 (accessed 14 April 2021).
- [66] N. Saeidi, F.-D. Kopinke, A. Georgi, What is specific in adsorption of perfluoroalkyl acids on carbon materials?, *Chemosphere* (2020) 128520. <https://doi.org/10.1016/j.chemosphere.2020.128520>.

## Supporting information

### **S1. Experimental section**

#### ***Determination of $pH_{pzc}$***

The ACF samples (50 mg) were put into  $Na_2SO_4$  electrolyte solution (10 mM, 10 mL) at different initial pH values and stirred overnight in glass vessels. Initial pH values from 2 to 11 were adjusted by  $H_2SO_4$  and NaOH solutions while keeping the ionic strength of the electrolyte solution almost unaffected. The point at which the initial pH is equal to the final (equilibrium) pH was considered as the  $pH_{pzc}$ .

#### ***Determination of ion exchange capacity***

ACF (0.5 g) was first shaken in KCl solution (1 M, 10 mL) overnight, followed by washing five times with diluted KCl solutions (10 mM, 10 mL). The suspension was adjusted with KOH (1 M) and HCl (1 M) to  $pH = 7.0 \pm 0.5$  at each washing round. At the final washing step, the mixture was allowed to equilibrate overnight. The supernatant was taken for analysis of  $Cl^-$  and  $K^+$  using ion chromatography (Dionex) and ICP-OES (SPECTRO), respectively. It is expected that the concentrations of  $K^+$  and  $Cl^-$  in the entrained pore water were identical to that of the supernatant of the final washing step. The amount of adherent KCl solution (pore water + surface water) after discarding the supernatant was determined gravimetrically. Afterwards, the sample was washed with  $NaNO_3$  solution (0.5 M, 8 mL) four times to substitute the adsorbed  $K^+$  and  $Cl^-$ . The suspension was adjusted with NaOH (1 M) and  $HNO_3$  (1 M) to  $pH = 7.0 \pm 0.5$  at each exchange round. The exchanged solutions were decanted for  $K^+$  and  $Cl^-$  determination. The CEC and AEC were calculated based on the difference between the exchanged  $K^+$  and  $Cl^-$  and the previously determined dissolved  $K^+$  and  $Cl^-$ .

#### ***Headspace GC-MS for MTBE determination***

The concentration of the freely dissolved MTBE was determined by headspace-gas chromatography-mass spectrometry (SHIMADZU GCMS-2010) coupled with an autosampler (SHIMADZU, AOC-5000 Plus). Separation of the analytes was performed using a 60 m  $\times$  0.32 mm DB-1 column with a film thickness of 5  $\mu m$ . The following conditions were set:  $T_{GC\ oven} = 100\ ^\circ C$  isotherm,  $T_{injector} = 150\ ^\circ C$ , helium flow rate = 1.92 mL/min, electron impact ionization (70 eV), selected ion monitoring (SIM) mode with  $m/z = 73$  amu for quantification of MTBE,

$V_{\text{gas injection}} = 250 \mu\text{L}$ . The calibration curves were linear over the concentration range from 0.2 to 18.0 mg/L MTBE in water samples incubated at 90 °C (500 rpm, 10 min).

#### ***GC-MS for $p$ -TSA determination***

The filtered  $p$ -TSA-containing solutions were 1:1 (v/v) extracted with  $\text{CH}_2\text{Cl}_2$  containing 1 mg/L toluene as the internal standard. The two-phase mixture was shaken by hand for 1 min. Then, the bottom phase was withdrawn with a glass pipette, dried over  $\text{Na}_2\text{SO}_4$  and analysed using GC-MS (SHIMADZU GCMS-2010) in the SIM mode ( $m/z = 171$  amu). GC column 30 m  $\times$  0.32 mm HP-5ms,  $T_{\text{injector}} = 250$  °C,  $T_{\text{GC oven}} = 50$  °C for 1 min, then with 40 K/min up to 200 °C and held at 200 °C for 7 min.  $V_{\text{injection}} = 1 \mu\text{L}$ , 10:1 injection split ratio, Helium flow rate = 1.50 mL/min.

#### ***LC-PDA for $p$ -TsO<sup>-</sup> determination***

A liquid chromatography equipment coupled with photodiode array (PDA) detector (LC-SPD-M20A, SHIMADZU Corporation) was used to determine the concentration of  $p$ -TsO<sup>-</sup>. An autosampler was used. Aliquots of 20  $\mu\text{L}$  aqueous sample were injected onto a 100 mm  $\times$  2 mm Gemini C6-Phenyl column filled with fully porous organo-silica having 110 Å pore size and 3  $\mu\text{m}$  particle size (Phenomenex Company). The mobile phase was a combination of solvent A, consisting of 5 mM ammonium acetate dissolved in 90% deionized water and 10% methanol, and solvent B, consisting of 5 mM ammonium acetate dissolved in 90% methanol and 10% water. A combination of 90% of solvent A and 10% of solvent B was delivered at a flow rate of 0.27 mL/min. The oven temperature was kept at 40 °C. An acquisition time of 6 min was required for each measurement. The retention time of  $p$ -TsO<sup>-</sup> was around 2.8–3.5 min. The UV signal at 220 nm was recorded. Standard solutions containing 0.1, 1 and 10 ppm  $p$ -TsO<sup>-</sup> were used as reference for every measurement batch. The correlation coefficients ( $R^2$ ) of the linear calibration curves for  $p$ -TsO<sup>-</sup> were > 0.99 over the concentration range from 0.1 to 20.0 mg/L.

#### ***LC-MS for TPA<sup>+</sup> determination***

A liquid chromatography equipment coupled with mass spectrometer (LCMS-2020, SHIMADZU Corporation) was used to determine the concentration of TPA<sup>+</sup>. An autosampler was used. Aliquots of 3  $\mu\text{L}$  were injected onto the separation column as described above. The mobile phase was a combination of solvent A, consisting of 5 mM ammonium acetate

dissolved in 90% deionized water and 10% methanol, and solvent B, consisting of 5 mM ammonium acetate dissolved in 90% methanol and 10% water. A combination of 80% of solvent A and 20% of solvent B was delivered at a flow rate of 0.25 mL/min. The oven temperature was kept at 40 °C. Electrospray ionization mode was used. An acquisition time of 6 min was required for each measurement. The retention time of TPA<sup>+</sup> was around 3.0–4.0 min. SIM mode was selected for the analysis. TPA<sup>+</sup> was quantified using the  $m/z$  =186 amu signal. Standard solutions containing 0.01, 0.1, 1 mg/L TPA<sup>+</sup> were used as reference for every measurement batch. The correlation coefficients ( $R^2$ ) of the calibration curves for TPA<sup>+</sup> were >0.99 for sample concentrations from 0.001 to 4 mg/L.

## **S2. Material Characterization**

### ***ATR-FTIR***

The ATR-FTIR spectra of ACFs are shown in **Fig. S2**. The virgin ACF<sub>10</sub> shows broad bands around 1520 and 1060 cm<sup>-1</sup>. The 1520 cm<sup>-1</sup> band can be related to carbonyl C=O or C–H moieties [1] whereas the 1060 cm<sup>-1</sup> band is commonly assigned to C–O-related groups, O–H (bending) or –CH<sub>2</sub>– units on carbonaceous adsorbents [1, 2]. After surface oxidation, these two bands become more intensive. In addition, a band at 1710 cm<sup>-1</sup> emerged, which can be ascribed to carboxyl or carbonyl C=O, lactone and/or pyrone moieties [1, 2]. A stronger band at 3000–3600 cm<sup>-1</sup> due to O–H stretching [1, 3] is observed compared to the other two ACF types. These alterations in IR spectra evidently point to a higher oxidation degree of the OxACF<sub>10</sub>, and correlate well with our observation from TPD profiles and XPS spectra. On the other hand, no significant changes in IR spectra are noticed after surface defunctionalization. This is due to the fact that the band at 1710 cm<sup>-1</sup> which is most specific for O-containing groups is already of low intensity in the original ACF<sub>10</sub> so that any further reduction is hardly discernible. In addition, ATR-FTIR does not fully present the chemical properties throughout the bulk sample, but rather merely reflect the properties of the part close to the surface. CO<sub>2</sub>, H<sub>2</sub>O and carbon-containing impurities from the measurement atmosphere could adhere to the ACF surface and disturb the IR analysis, as also seen in the case of XPS.

Notice: the region of 1900–2600 cm<sup>-1</sup>, which is not specific for ACF samples, was omitted for clarity in all spectra. Bands in this region result from diamond crystal used in ATR-FTIR [4], and carbon dioxide in atmosphere also contribute to bands in range from 2100–2400 cm<sup>-1</sup> [5]. The noisy signals >3600 cm<sup>-1</sup> are attributed to H<sub>2</sub>O rotation.

## **XPS**

The XPS survey spectra (**Fig. S11**) indicate that all three ACF surfaces consisted mainly of carbon (C1s, 284–291 eV), oxygen (O1s, 531–534 eV) and trace amounts of nitrogen (N1s, ca. 400 eV). Although the exact atomic quantification is likely disturbed by surface-adhered carbonaceous contaminants as typically found for XPS samples [6], 2-fold higher O/C intensity ratio of OxACF<sub>10</sub> compared to the DeACF<sub>10</sub> or ACF<sub>10</sub> corresponds well to our elemental analysis and TPD results.

A closer look at the high resolution C1s spectra (**Fig. S3**) further gives hints for the distribution of the functional groups on ACF surfaces. Seven components assigned to  $\pi \rightarrow \pi^*$  shake-up (290.8 eV), O=C=O (288.9 eV), C=O (287.6 eV), C–O (286.5 eV), C–C/C–H (285.5 eV) and  $sp^2$  C (284.7 and 283.9 eV) were considered [3, 7, 8]. As nitrogen contents were found to be minor, only oxidized carbon moieties were considered for C1s peak deconvolution. Comparing the percentages of each C1s component of three ACF samples, we suggested that OxACF<sub>10</sub> carries the highest density of surface carboxylic groups while DeACF<sub>10</sub> presents the lowest hydroxyl/phenolic proportion. An increasing peak intensity relating to  $\pi \rightarrow \pi^*$  shake-up further implies higher contents of  $sp^2$  C and, accordingly, more hydrophobic surfaces in the order of OxACF<sub>10</sub> < ACF<sub>10</sub> < DeACF<sub>10</sub>.

## **SEM**

The SEM images of three ACFs are shown in **Fig. S6**. The fiber diameters are determined to be  $12 \pm 2$   $\mu\text{m}$  (ACF<sub>10</sub>),  $11 \pm 2$   $\mu\text{m}$  (DeACF<sub>10</sub>), and  $12 \pm 2$   $\mu\text{m}$  (OxACF<sub>10</sub>) by taking the mean value of the diameters of ca. 17 fibres for each sample and calculating the standard deviations of the single values. That is to say, no significant changes in fibre diameters occurred during the surface defunctionalization or oxidation.

## **S3. Adsorption study**

### ***Detailed experimental conditions for Fig. 2 and Fig. 3 in the main text***

Referring to **Fig. 2** in the main text, the ACF dosages for those adsorption experiments at different temperatures are set as follows: the dosages of all three ACFs for TPA<sup>+</sup> and BTMA<sup>+</sup> samples were set at 1 g/L. For *p*-TsO<sup>−</sup> samples, the dosages of ACF<sub>10</sub> and DeACF<sub>10</sub> were both set at 1 g/L, but 5 g/L for OxACF<sub>10</sub>. For *p*-TSA samples, the dosages of ACF<sub>10</sub> and DeACF<sub>10</sub> were kept both at 0.25 g/L, but 0.5 g/L for OxACF<sub>10</sub>.



Referring to **Fig. 3** in the main text, the detailed experimental conditions were set as follows:  $c_0 = 20$  mg/L for all compounds except for MTBE which is 14 mg/L; ACF dosage: in case of TPA<sup>+</sup> and BTMA<sup>+</sup> 1 g/L, of MTBE 4 g/L, of *p*-TsO<sup>-</sup>, for AFC<sub>10</sub> and DeACF<sub>10</sub> 1 g/L, and 5 g/L for OxACF<sub>10</sub>, of *p*-TSA, for AFC<sub>10</sub> and DeACF<sub>10</sub> 0.25 g/L, and 0.5 g/L for OxACF<sub>10</sub>.

### ***Adsorption of Cu<sup>2+</sup> on ACFs***

In **Fig. S4**, the adsorption isotherms of investigated cationic organic compounds as well as Cu<sup>2+</sup> on ACFs are shown. For Cu<sup>2+</sup>, the isotherms were collected at pH 5 to avoid the formation of precipitations, while for BTEA<sup>+</sup>, BTMA<sup>+</sup> and TPA<sup>+</sup> at pH 7. As shown in the figure, almost no adsorption capacity was observed for Cu<sup>2+</sup> on DeACF<sub>10</sub> with very little cation exchange sites at pH 5 (CEC of DeACF<sub>10</sub>  $\leq 0.010$   $\mu\text{mol}/\text{m}^2$  at pH 7). In contrast, the sorption capacity of Cu<sup>2+</sup> was found remarkably beyond the ACF<sub>10</sub>'s CEC (= 0.040  $\mu\text{mol}/\text{m}^2$ ). This is probably related to the complexation of Cu<sup>2+</sup> on the O/N-containing ACF<sub>10</sub> surface [9, 10], where the sulfate ions must be involved for surface charge-balancing, and should only partially result from different pH conditions applied in the CEC/AEC characterization (pH 7) and the sorption experiments (pH 5 [9]). The adsorption isotherms of Cu<sup>2+</sup> on OxACF<sub>10</sub> and ACF<sub>10</sub> are fitted with Freundlich and Langmuir equations with the corresponding parameters listed in **Table S2**.

### ***Calculation of the pore filling extents***

The pore size distributions of the studied ACFs in the range of  $\varnothing \leq 2$  nm are summarized in **Table 2** in the main text. The molar volumes of the sorbate molecules in **Table S3** are calculated based on Van der Waals molecular volumes freely accessed on chemicalize.com. According to total pore volume  $V_t$ ,  $S_{\text{BET}}$  and  $V_{\text{micro}, \varnothing < 1 \text{ nm}}$  presented in **Table 2**, and  $q_{\text{max}}$  listed in **Table 3**, the pore filling extent was calculated for the adsorption of individual sorbates in pores with  $\varnothing > 1$  nm of ACFs as follows and summarized in **Table S3**. Note, for the simplicity of calculation, we did not consider the contributions of micropores with  $\varnothing < 1$  nm here, which could however also be available for adsorption of some sorbates under investigation.

Pore filling extent (%)

$$= \frac{q_{\text{max}} \left( \frac{\mu\text{mol}}{\text{m}^2} \right) \cdot S_{\text{BET}} \left( \frac{\text{m}^2}{\text{g}} \right) \cdot \text{molar volume} \left( \frac{\text{cm}^3}{\text{mol}} \right) \cdot 10^{-6} \left( \frac{\text{mol}}{\mu\text{mol}} \right)}{(V_t - V_{\text{micro}, \varnothing < 1 \text{ nm}}) \left( \frac{\text{cm}^3}{\text{g}} \right)} \times 100 (\%)$$

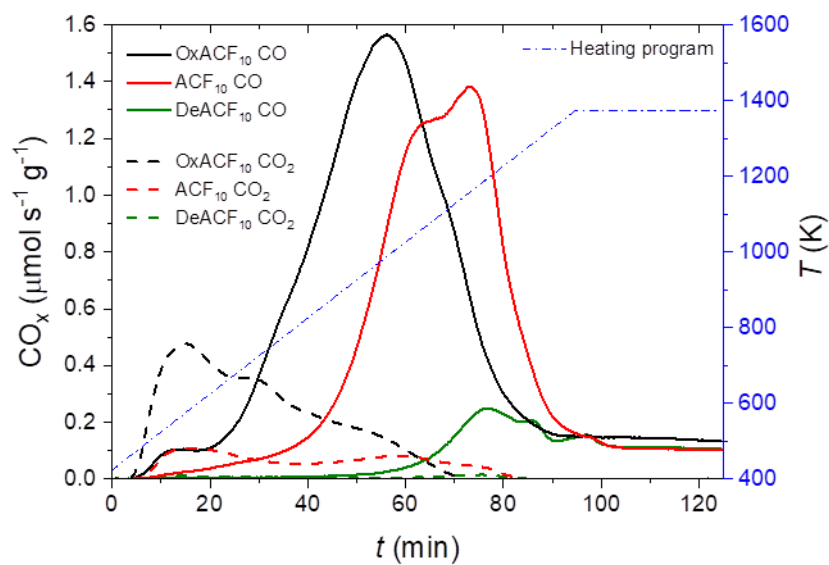
#### **S4. Comparison of experimental and predicted results**

In [11], 328 items from publications covering a range of sorbent compositions  $C\% \in [10, 98]$ ,  $H/C \in [0.001, 2.883]$ ,  $O/C \in [0.0002, 1.2002]$ ,  $S_{BET} \in [1, 1100]$ , experimental  $pH \in [3.3, 11.8]$ ,  $\log D \in [-9.64, 5.74]$ ,  $A^- \% \in [0.00, 100.00]$ ,  $E \in [0.39, 3.50]$ ,  $S \in [0.57, 3.60]$ ,  $A \in [0.00, 1.35]$ ,  $B \in [0.15, 3.29]$  and  $V \in [0.61, 3.10]$  were applied to train the model for prediction of sorption behaviors of polar and anionic organic compounds, leading to well-predictable  $\log$  ( $K_F / [(\mu g/kg)/(\mu g/L)^n]$ ) in the range of (0.80, 6.00) and  $n$  in ranges of (0.06, 0.85).

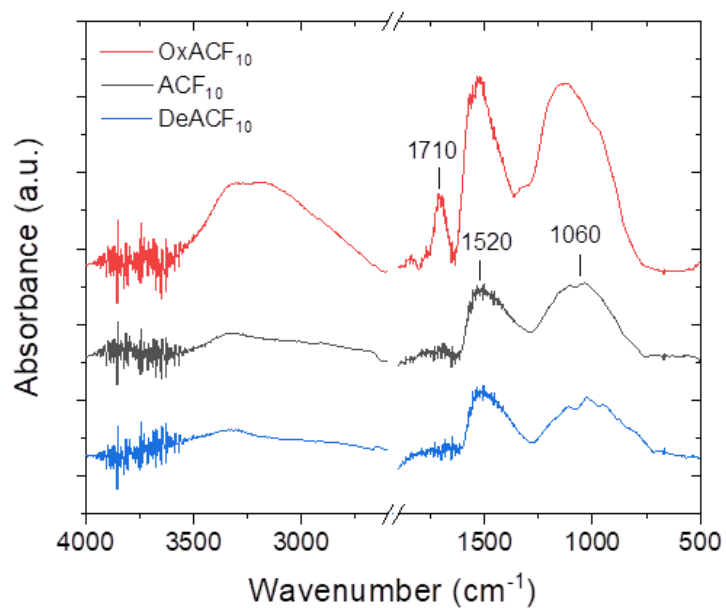
As shown in the **Table S4**, most of the sorbate parameters in this study are covered in the training ranges, except for  $E$  and  $S$  of MTBE (0.02 and 0.28, respectively). According to the sensitivity test performed in Sigmund et al. (2020) which revealed the contributions of the 12 input parameters to the prediction results,  $E$  only plays a very minor role while  $S$  is moderately important to the prediction of  $K_F$ . On the other hand,  $C\%$ ,  $H/C$  and  $O/C$  molar ratios of all studied ACFs fall in the training ranges. Note: the  $S_{BET}$  of the ACFs used in this work ( $\geq 1100 \text{ m}^2/\text{g}$ ) are beyond the range applied in the training set for Sigmund's model. As discussed in **Section 3.2.4** (main text), MTBE adsorption on AC materials with  $S_{BET} < 850 \text{ m}^2/\text{g}$  is apparently better predicted (see the four highlighted grey points in **Fig. 4a**), suggesting that the model works better for carbonaceous sorbents without exceedingly high  $S_{BET}$ .

Note to **Fig. 4** in the main text: according to our test results, the trends of the predicted  $K_F$  and  $n$  for a certain sorbate on sorbents bearing the same  $S_{BET}$  but different chemical compositions should not be affected by the exact value of  $S_{BET}$  in the range of 1100–1500  $\text{m}^2/\text{g}$ . Therefore, it seems that the model does not adequately reflect differences in adsorption behaviors of PMOCs on AC sorbents carrying different surface chemistry as discussed in **Section 3.2.4** (main text).

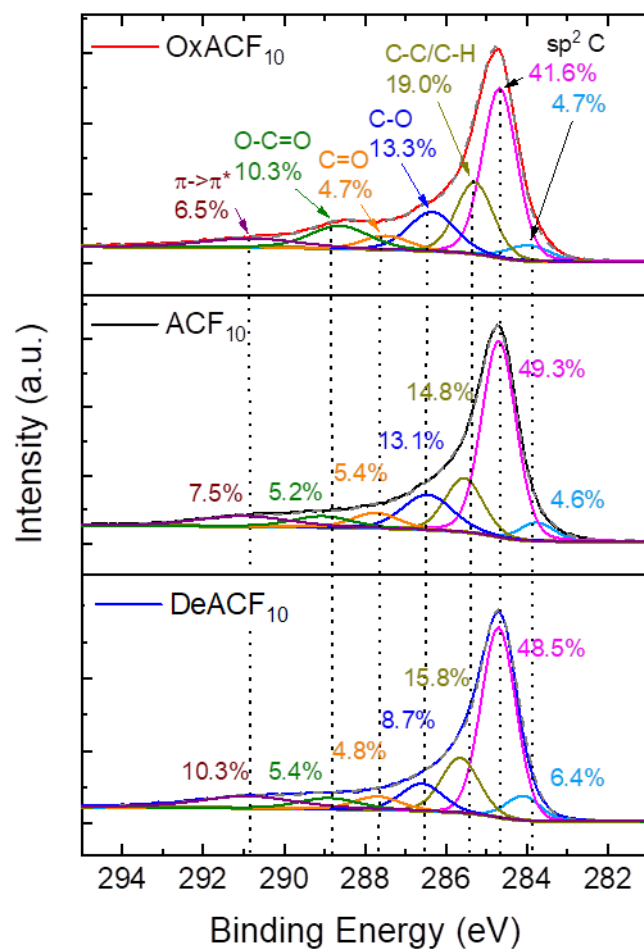
## Figures



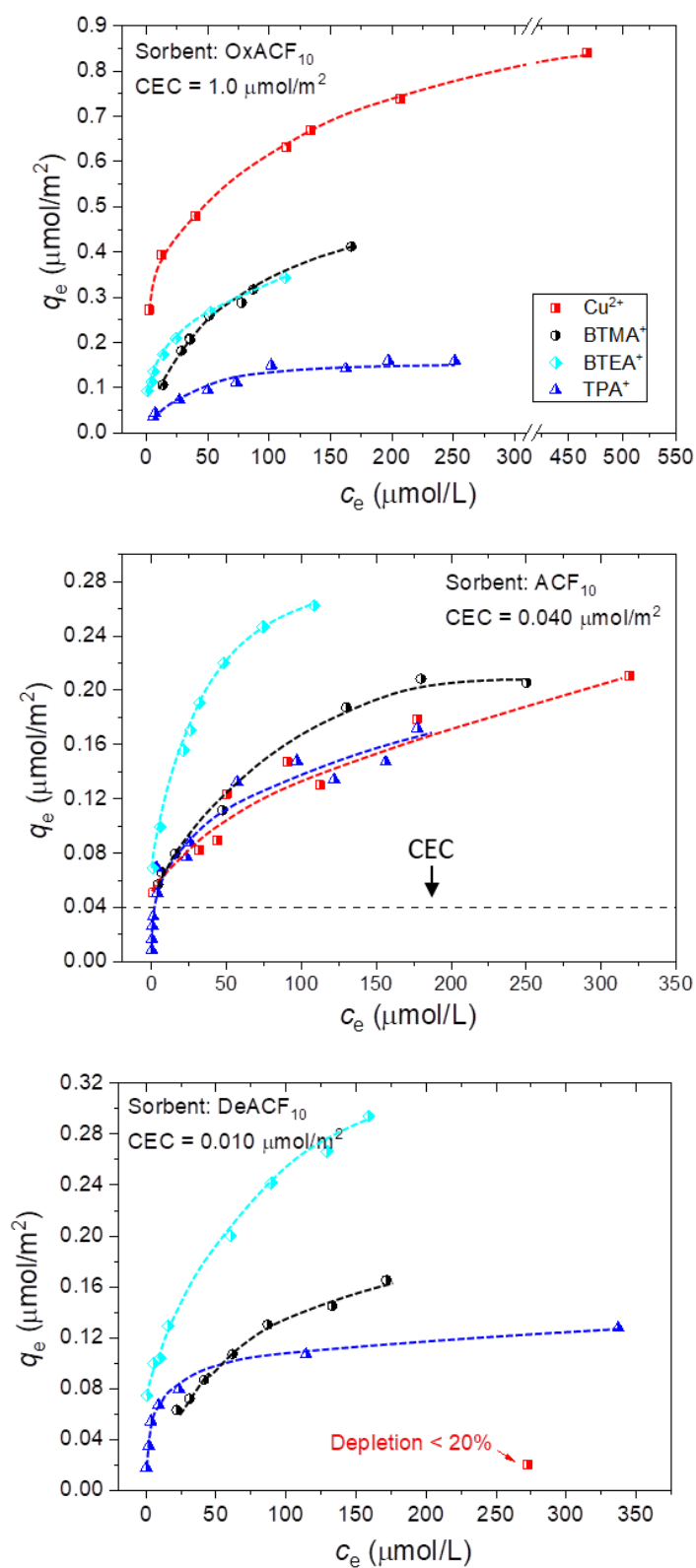
**Fig. S1:** TPD profiles of untreated ACF<sub>10</sub> and surface-modified OxACF<sub>10</sub> and DeACF<sub>10</sub>.



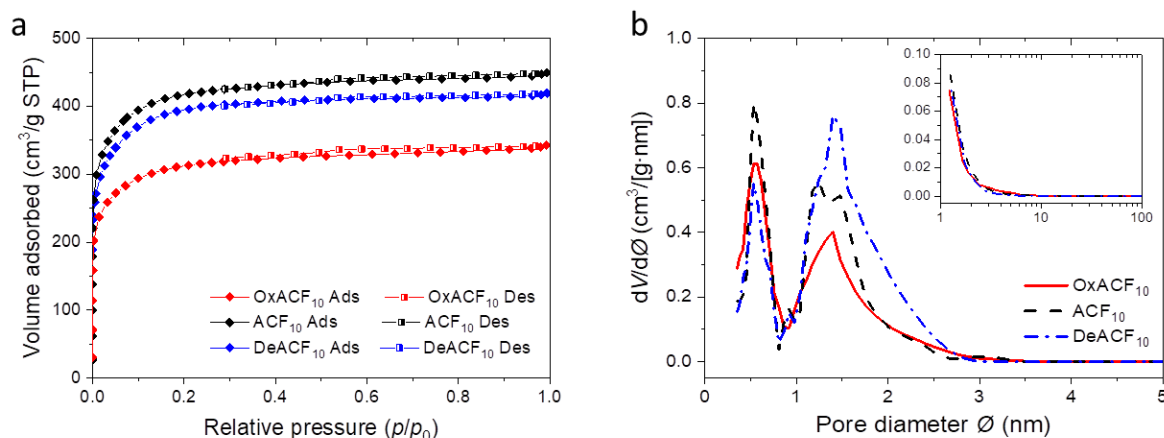
**Fig. S2:** ATR-FTIR spectra of untreated ACF<sub>10</sub> and surface-modified OxACF<sub>10</sub> and DeACF<sub>10</sub>.



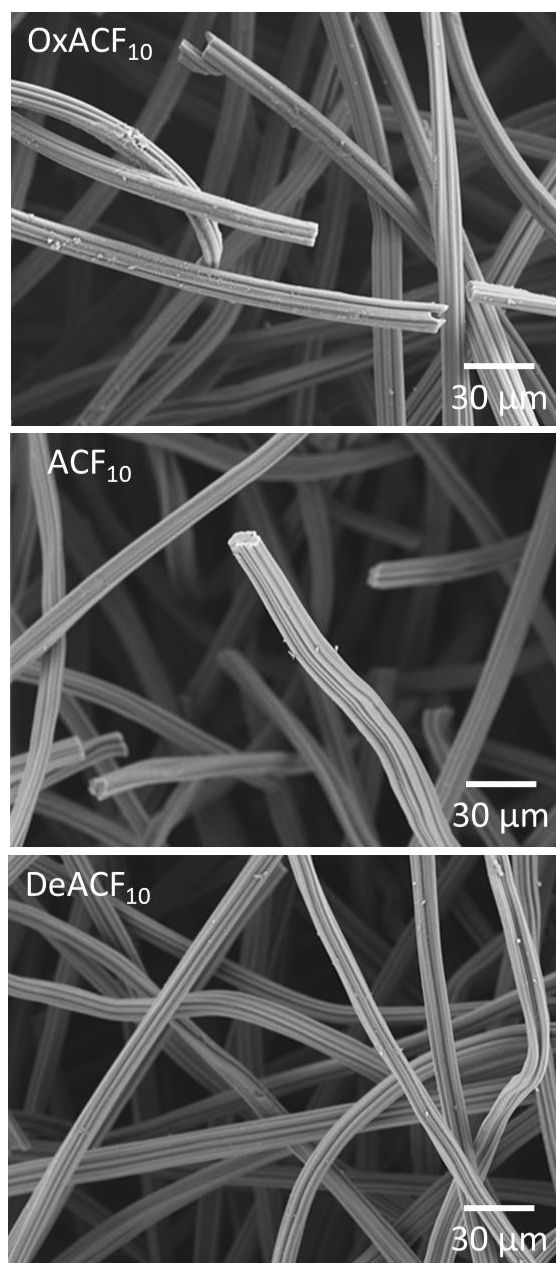
**Fig. S3:** XPS high resolution C1s spectra of ACF<sub>10</sub>, OxACF<sub>10</sub>, and DeACF<sub>10</sub> with peak deconvolutions. The percentages of carbon components in different chemical environments are given. Cumulative fits given in grey dashed lines.



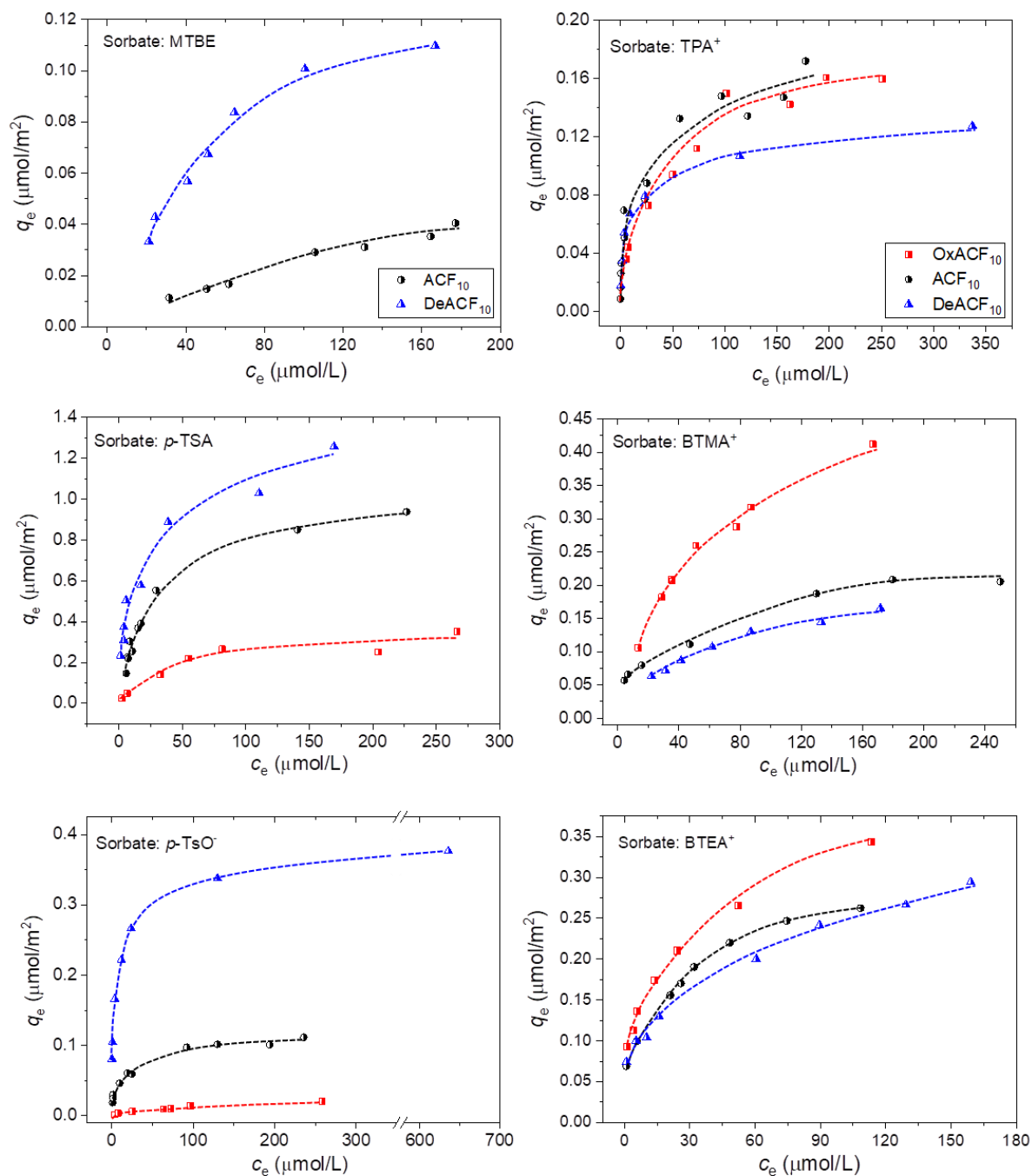
**Fig. S4:** Adsorption isotherm data of  $\text{Cu}^{2+}$ ,  $\text{BTEA}^+$ ,  $\text{BTMA}^+$  and  $\text{TPA}^+$  on ACFs in 10 mM  $\text{Na}_2\text{SO}_4$  solution. When depletion is <20%, the adsorption can no more be regarded as significant. Dashed lines serve as guides for the eye.



**Fig. S5:** (a)  $N_2$  adsorption (Ads) – desorption (Des) isotherms of ACF<sub>10</sub>, OxACF<sub>10</sub>, and DeACF<sub>10</sub> determined at 77 K. (b) Micropore size distribution analyzed by  $CO_2$  adsorption and NLDFT fitting. Insert: mesopore size distribution analyzed by  $N_2$  adsorption – desorption and BJH method.



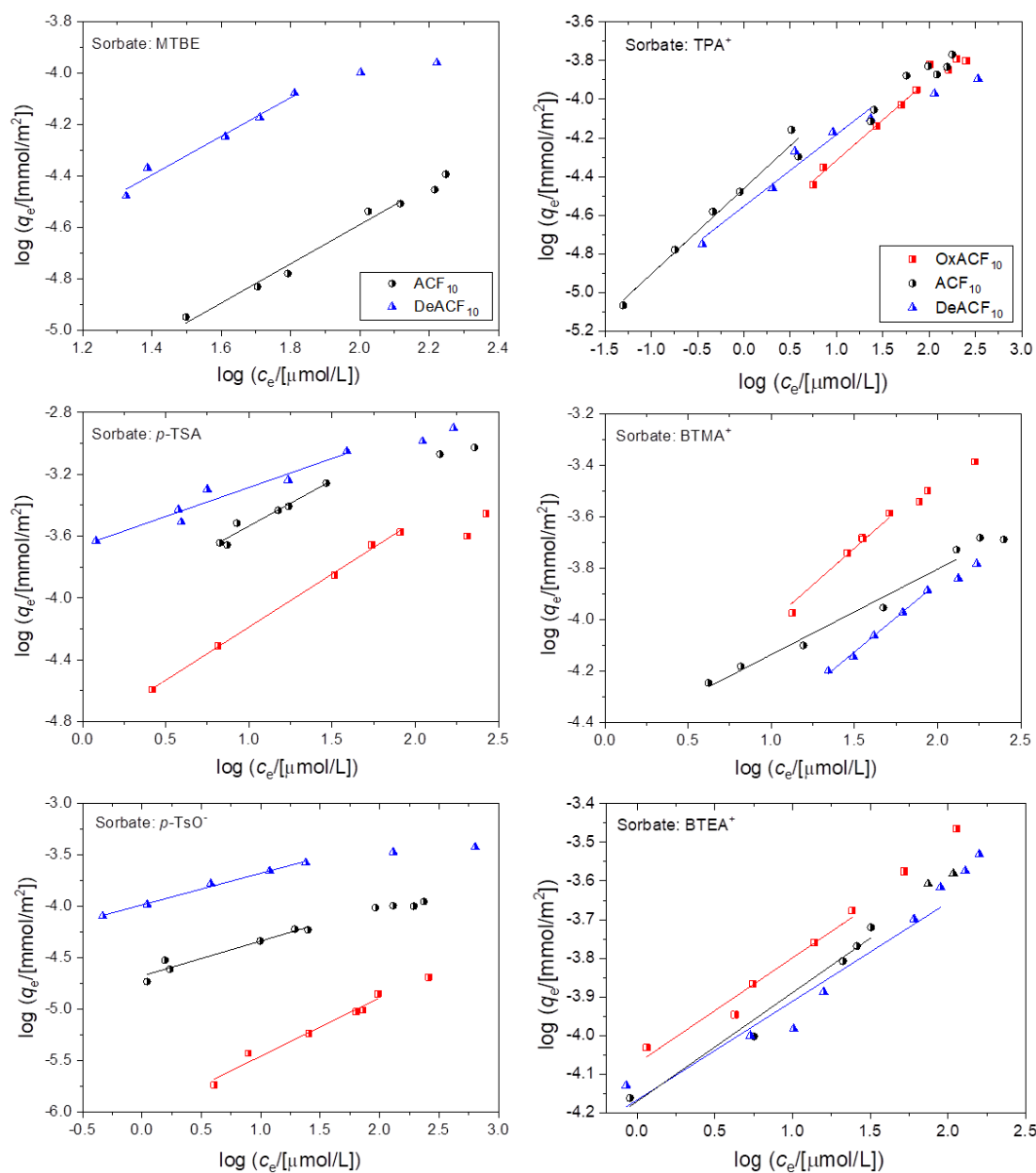
**Fig. S6:** SEM images of three ACFs.



**Fig. S7:** Adsorption isotherms obtained in 10 mM Na<sub>2</sub>SO<sub>4</sub> solution at pH 7, 20°C. Dashed lines serve as guides for the eye.

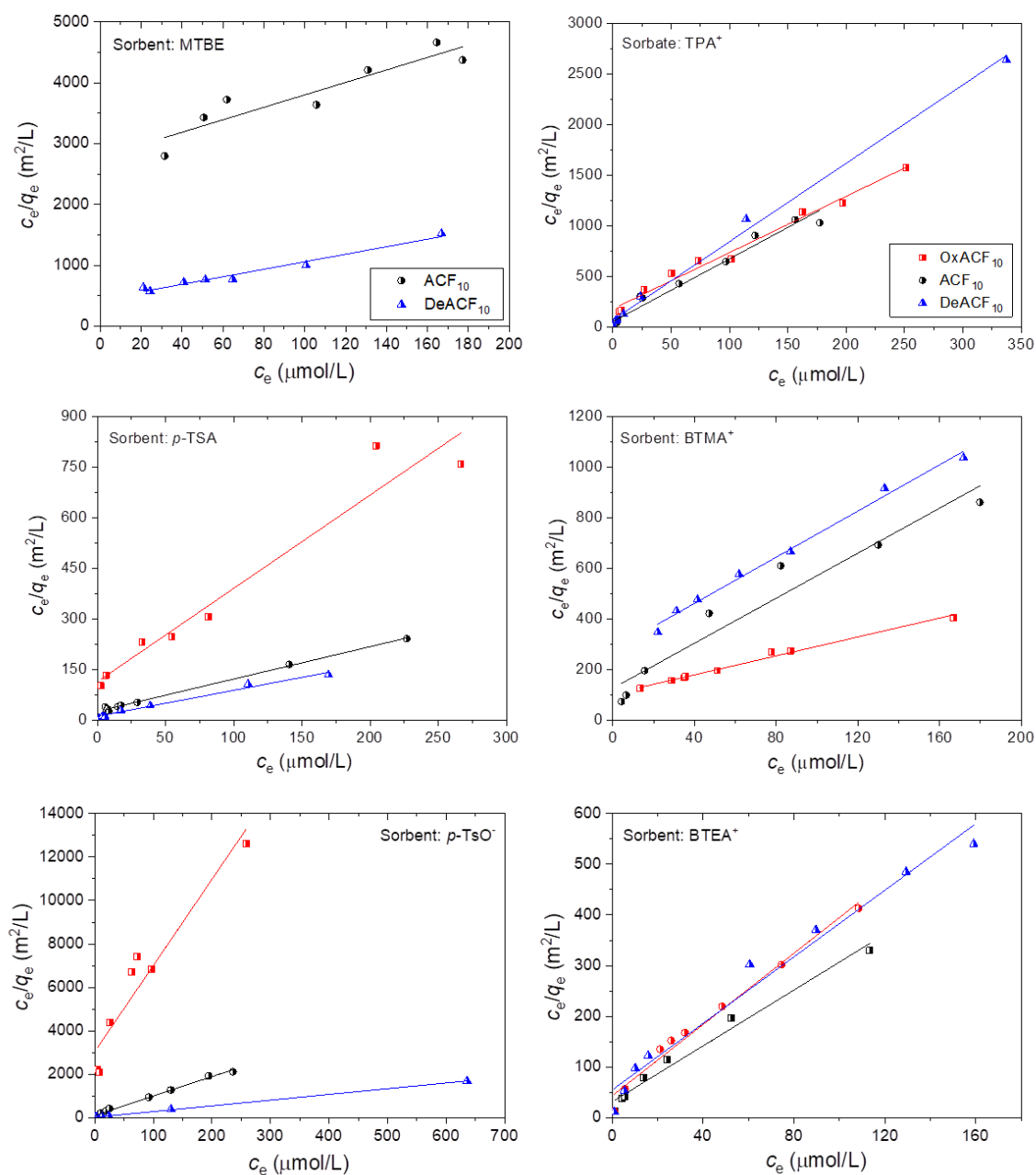


In **Fig. S8**, Freundlich linear fittings for the adsorption of selected PMOCs on ACFs are shown. Note: only data points significantly below the saturation loading were taken for these fittings.



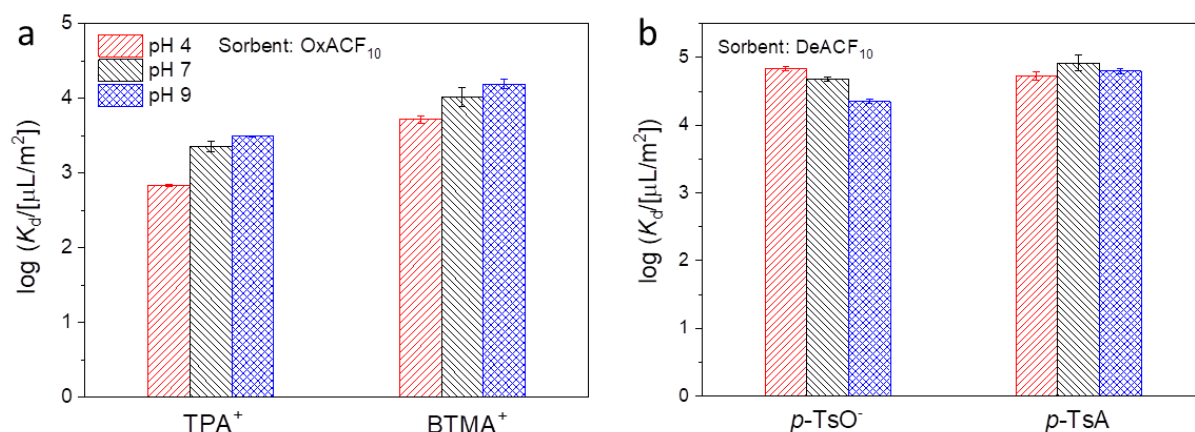
**Fig. S8:** Adsorption isotherm data in 10 mM Na<sub>2</sub>SO<sub>4</sub> solution at pH 7 fitted with Freundlich equation.

The isotherms are fitted with Langmuir equations as illustrated in **Fig. S9** for the entire  $c_e$  ranges.

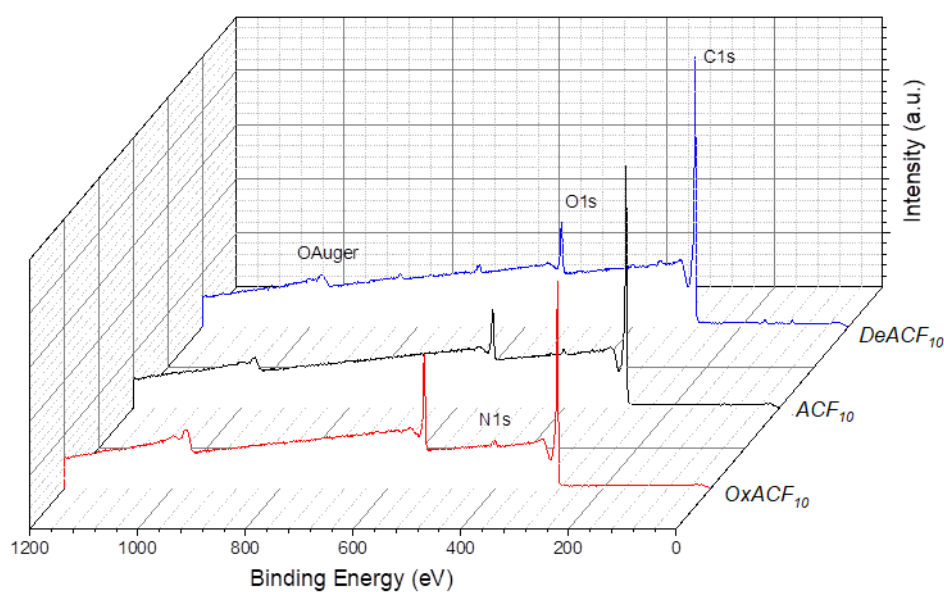


**Fig. S9:** Adsorption isotherm data obtained in 10 mM Na<sub>2</sub>SO<sub>4</sub> solution at pH 7 fitted with Langmuir equation.

The effect of pH on selected PMOC adsorption on chosen ACFs are demonstrated in **Fig. S10**.



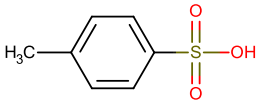
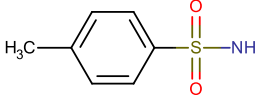
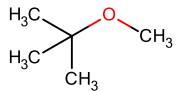
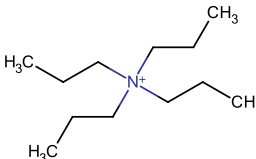
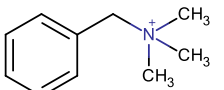
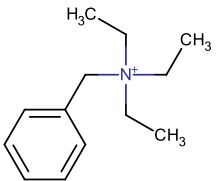
**Fig. S10:** Log  $K_d$  of (a) TPA<sup>+</sup> and BTMA<sup>+</sup> on OxACF<sub>10</sub> (b) *p*-TsO<sup>-</sup> and *p*-TsA on DeACF<sub>10</sub> in 10 mM Na<sub>2</sub>SO<sub>4</sub> solution at pH 4, 7 and 9. The experimental conditions were selected giving  $q < \frac{1}{2} q_{\max}$ . Details:  $c_0 = 20$  mg/L; ACF dosage: in cases of TPA<sup>+</sup> and BTMA<sup>+</sup> 1 g/L, of *p*-TsO<sup>-</sup> and *p*-TsA 0.25 g/L. The error bars from triplet measurements are presented.



**Fig. S11:** XPS survey spectra of studied ACFs.

## Tables

**Table S1:** Selected properties of sorbates.

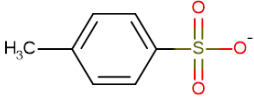
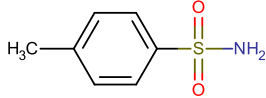
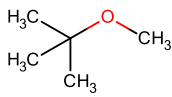
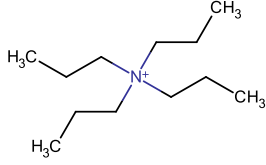
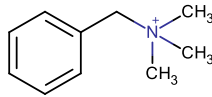
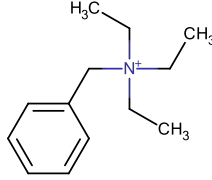
Sorbate type <sup>a</sup>	Name	Structure	Molecular weight (g/mol)	pK <sub>a</sub>	Log D <sup>b</sup>
anionic	<i>p</i> -TsOH		172.22	-1.3 [12]	-0.71
neutral	<i>p</i> -TSA		171.22	10.5 [13]	1.09
	MTBE		88.15	-	1.18 <sup>c</sup>
cationic	TPA <sup>+</sup>		186.36	-	-0.45
	BTMA <sup>+</sup>		150.24	-	-2.25
	BTEA <sup>+</sup>		192.32	-	-1.18

<sup>a</sup> Predominant form at circumneutral pH. <sup>b</sup> The octanol-water partition coefficient *D* was calculated at pH = 7 using ChemAxon (<https://www.chemaxon.com>). Note: log (*D*<sub>oc</sub>/(L/kg)) can be estimated by log *D*<sub>oc</sub> = log *D* – 0.21 [14]. <sup>c</sup> For non-ionizable MTBE, log *D* equals to the pH-independent octanol-water partition coefficient log *K*<sub>OW</sub>.

**Table S2:** Freundlich and Langmuir fitting parameters for Cu<sup>2+</sup> adsorption on OxACF<sub>10</sub> and ACF<sub>10</sub>.

Sorbate	ACF sorbent	Freundlich			Langmuir		
		$K_F$ (( $\mu\text{mol}/\text{m}^2$ )/( $\mu\text{mol}/\text{L}$ ) <sup><math>n</math></sup> )	$n$	$R^2$	$q_{\text{max}}$ ( $\mu\text{mol}/\text{m}^2$ )	$K_L$ ( $\text{L}/\mu\text{mol}$ )	$R^2$
Cu <sup>2+</sup>	OxACF <sub>10</sub>	0.23	0.21	0.993	0.87	0.038	0.992
	ACF <sub>10</sub>	0.043	0.24	0.872	0.21	0.027	0.987

**Table S3:** Molar volumes (calculated using Van der Waals molecular volumes accessible on chemicalize.com) and pore filling extents (for  $\varnothing \geq 1$  nm) of the selected polar organic molecules at  $q_{\max}$  on ACFs.

Name	Structure	Molar volume (cm <sup>3</sup> /mol)	Pore filling extent (%)	
<i>p</i> -TsO <sup>-</sup>		86.3 <sup>a</sup>	OxACF <sub>10</sub>	0.7
			ACF <sub>10</sub>	3.4
			DeACF <sub>10</sub>	7.0
<i>p</i> -TSA		88.1	OxACF <sub>10</sub>	10.0
			ACF <sub>10</sub>	32.0
			DeACF <sub>10</sub>	24.3
MTBE		63.6	ACF <sub>10</sub>	2.2
			DeACF <sub>10</sub>	2.2
TPA <sup>+</sup>		139.8	OxACF <sub>10</sub>	7.9
			ACF <sub>10</sub>	7.9
			DeACF <sub>10</sub>	3.9
BTMA <sup>+</sup>		100.4	OxACF <sub>10</sub>	16.8
			ACF <sub>10</sub>	7.9
			DeACF <sub>10</sub>	4.7
BTEA <sup>+</sup>		131.3	OxACF <sub>10</sub>	15.0
			ACF <sub>10</sub>	13.0
			DeACF <sub>10</sub>	8.6

<sup>a</sup> Calculated based on the protonated form.

**Table S4:**  $pK_a$ , percentage of the negatively charged species  $A^-$  (%) at pH 7 as well as Abraham parameters of selected polar organic compounds obtained from the UFZ LSER database [15].

	$pK_a$	$A^-$ (%)	E	S	A	B	V
<b>MTBE</b>	-	0.00	0.02	0.28	0.00	0.54	0.872
<b><i>p</i>-TSA</b>	10.5	0.03	1.13	1.54	0.56	0.87	1.238
<b><i>p</i>-TsOH</b>	-1.3	100.00	0.87	2.29	0.31	0.97	1.197
<b>OCA<sup>a</sup></b>	4.9	99.23	0.15	0.65	0.62	0.45	1.310

<sup>a</sup> OCA = octanoic acid

## References

- [1] X. Zhang, B. Gao, A.E. Creamer, C. Cao, Y. Li, Adsorption of VOCs onto engineered carbon materials: A review, *J. Hazard. Mater.* 338 (2017) 102-123. <https://doi.org/10.1016/j.jhazmat.2017.05.013>.
- [2] S. Shin, J. Jang, S.H. Yoon, I. Mochida, A study on the effect of heat treatment on functional groups of pitch based activated carbon fiber using FTIR, *Carbon* 35 (1997) 1739-1743. [https://doi.org/10.1016/S0008-6223\(97\)00132-2](https://doi.org/10.1016/S0008-6223(97)00132-2).
- [3] J. Zhou, C. Laube, W. Knolle, S. Naumov, A. Prager, F.-D. Kopinke, B. Abel, Efficient chlorine atom functionalization at nanodiamond surfaces by electron beam irradiation, *Diam. Relat. Mater.* 82 (2018) 150-159. <https://doi.org/10.1016/j.diamond.2018.01.012>.
- [4] PikeTechnologies, Design and performance features of ATR crystal plates for single reflection ATR accessories for FTIR, [http://www.piketech.com/skin/fashion\\_mosaic\\_blue/application-pdfs/AN\\_0601\\_CrystalPlates\\_MIRacle.pdf](http://www.piketech.com/skin/fashion_mosaic_blue/application-pdfs/AN_0601_CrystalPlates_MIRacle.pdf), (accessed 21 May 2021).
- [5] I.N. Sokolik, Lecture 6. Absorption by atmospheric gases in the IR, visible and UV spectral regions. [http://irina.eas.gatech.edu/EAS8803\\_Fall2009/Lec6.pdf](http://irina.eas.gatech.edu/EAS8803_Fall2009/Lec6.pdf), (accessed 21 May 2021).
- [6] J.F. Watts, J. Wolstenholme, *An Introduction to Surface Analysis by XPS and AES*, Wiley 2019. <https://doi.org/10.1002/9781119417651>
- [7] R. Flyunt, W. Knolle, A. Kahnt, C.E. Halbig, A. Lotnyk, T. Haupl, A. Prager, S. Eigler, B. Abel, High quality reduced graphene oxide flakes by fast kinetically controlled and clean indirect UV-induced radical reduction, *Nanoscale* 8 (2016) 7572-7579. <https://doi.org/10.1039/C6NR00156D>.
- [8] H. Zhao, L. Qian, Y. Chen, Q. Wang, G. Zhao, Selective catalytic two-electron O<sub>2</sub> reduction for onsite efficient oxidation reaction in heterogeneous electro-Fenton process, *Chem. Eng. J.* 332 (2018) 486-498. <https://doi.org/10.1016/j.cej.2017.09.093>.
- [9] G. Hotová, V. Slovák, T. Zelenka, R. Maršálek, A. Parchaňská, The role of the oxygen functional groups in adsorption of copper (II) on carbon surface, *Sci. Total Environ.* 711 (2020) 135436. <https://doi.org/10.1016/j.scitotenv.2019.135436>.
- [10] X. Yang, Y. Wan, Y. Zheng, F. He, Z. Yu, J. Huang, H. Wang, Y.S. Ok, Y. Jiang, B. Gao, Surface functional groups of carbon-based adsorbents and their roles in the removal of heavy metals from aqueous solutions: A critical review, *Chem. Eng. J.* 366 (2019) 608-621. <https://doi.org/10.1016/j.cej.2019.02.119>.

- [11] G. Sigmund, M. Gharasoo, T. Hüffer, T. Hofmann, Deep learning neural network approach for predicting the sorption of ionizable and polar organic pollutants to a wide range of carbonaceous materials, *Environ. Sci. Technol.* 54 (2020) 4583–4591. <http://doi.org/10.1021/acs.est.9b06287>.
- [12] E.P. Sergeant, B. Dempsey, Ionisation constants of organic acids in aqueous solution. IUPAC chemical data series No. 23, Pergamon Press, New York, 1979.
- [13] J.L. Atwood, J.W. Steed, *Encyclopedia of supramolecular chemistry* CRC Press, New York, 2004. <https://doi.org/10.1201/9780429075728>
- [14] H.P.H. Arp, T.N. Brown, U. Berger, S.E. Hale, Ranking REACH registered neutral, ionizable and ionic organic chemicals based on their aquatic persistency and mobility, *Environ. Sci.: Process. Impacts.* 19 (2017) 939-955. <https://doi.org/10.1039/C7EM00158D>.
- [15] N. Ulrich, S. Endo, T.N. Brown, N. Watanabe, G. Bronner, M.H. Abraham, K.-U. Goss, UFZ-LSER Database v 3.2 <http://www.ufz.de/lserd> 2017 (accessed 14 April 2021).



### 3.2 Electro-assisted removal of polar and ionic organic compounds from water using activated carbon felts

Jieying Zhou<sup>a</sup>, Yuan Zhang<sup>b,c</sup>, Maria Balda<sup>a</sup>, Volker Presser<sup>b,c</sup>, Frank-Dieter Kopinke<sup>a</sup>, Anett Georgi<sup>a\*</sup>

<sup>a</sup>*Helmholtz Centre for Environmental Research – UFZ, Department of Environmental Engineering, 04318 Leipzig, Germany*

<sup>b</sup>*INM - Leibniz Institute for New Materials, 66123 Saarbrücken, Germany*

<sup>c</sup>*Department of Materials Science and Engineering, Saarland University, 66123 Saarbrücken, Germany*

<sup>d</sup>*Saarene, Saarland Center for Energy Materials and Sustainability, Campus C4 2, 66123 Saarbrücken, Germany*

#### Abstract

Highly water-soluble, persistent, and mobile organic compounds (PMOCs) are more and more often detected in surface and groundwater, evoking potential threats to the environment and human health. Traditional water treatment strategies, including adsorption by activated carbon materials, fail to efficiently remove PMOCs due to their hydrophilic nature. Electro-assisted sorption processes offer a clean, facile, and promising solution to remove PMOCs on activated carbon-based electrodes and potentially allow an easy on-site sorbent regeneration (trap&release). In this work, the electrosorption of five selected PMOCs, that is, tetrapropylammonium (TPA<sup>+</sup>), benzyltrimethylammonium (BTMA<sup>+</sup>), *p*-tosylate (*p*-TsO<sup>-</sup>), *p*-toluenesulfonamide (*p*-TSA), and methyl-*tert*-butylether (MTBE), were investigated on two comprehensively characterized activated carbon felt (ACF) types carrying different surface functionalities. Significant enrichment factors in ranges of 10<sup>2</sup> to 10<sup>3</sup> for charged PMOCs were expected by our first estimation for electro-assisted trap&release on ACFs in flow systems applying potentials in the range of -0.1 V/+0.6 V vs. SHE for ad-/desorption, respectively. Defunctionalized ACF carrying larger density in surface  $\pi$ -systems and lower O-content promises a higher capability in electrosorption processes than the pristine material in terms of material stability (tested for 5 cycles over 500 h) and more than 3-times better removal efficiency of ionic PMOCs. In terms of improvement of ACFs adsorption performance for cationic and anionic PMOCs, permanent chemical surface modification and reversible electric polarization as alternative strategies are compared. Our

findings explore future electrode and process design of electrosorption for applications to treat water contaminated by emerging PMOCs.

**Keywords:** electrosorption; activated carbon; surface modification; polar organic micropollutant; ionic organic micropollutant

## 1. Introduction

Diverse organic compounds are contained in industrial and domestic wastes, which cause water pollution. While most persistent organic pollutants (POPs) regulated in the Stockholm Convention [1] are inherently not well water-soluble, a considerable proportion of emerging organic contaminants are identified to have highly polar, ionizable, or ionic structures [2, 3]. They form the group of persistent and mobile organic compounds (PMOCs) [2, 4]. Although modern wastewater treatment plants (WWTPs) can effectively remove many non-polar organic compounds, PMOCs may slip through the conventional technical barriers, exposing a treatment gap for drinking water [4] and potential threats to human health [5-8].

Existing typically in low concentrations (ng/L to mg/L) [9], PMOCs need to be pre-enriched before any degradation approaches for an energy-efficient and cost-effective treatment. Adsorption using activated carbon (AC) with a high specific surface area ( $\geq 10^3 \text{ m}^2/\text{g}$ ) is presently the prevailing technique to enrich organic micropollutants on adsorbents from wastewater in WWTPs [4, 10]. The less satisfying adsorption efficiency of AC-based materials to highly polar PMOCs can be enhanced by tailoring sorbent surface chemistry [11-14] or electrically polarizing conductive sorbent surfaces [15-17]. By tuning the electric field in the latter approach, desorption conditions can be met to regenerate exhausted adsorbents *in-situ* [15-19]. This may promote a green alternative for the state-of-the-art AC regeneration strategy: off-site high-temperature treatment associated with substantial carbon loss and CO<sub>2</sub> release, extra transportation burden, and considerable negative environmental impact [20]. On-site adsorbent regeneration using renewable electric energy is even more appealing for treating highly mobile PMOCs where early adsorber breakthroughs occur and short regeneration intervals are required accordingly.

The last decade has seen vast development in water desalination especially via capacitive deionization (CDI) where electrosorption processes on AC-based materials find their major application so far [21, 22]. With the increased awareness of PMOC pollution in water and the

call for on-site adsorbent regeneration, research interest gradually arises in the electrosorption of polar organic compounds. Ionizable/ionic organic compounds, partially highly environmentally relevant, were selected as target adsorbates in a few studies published during the past two decades [15-17, 23-35]. Still, compared to the achievements in the field of CDI, electrosorptive approaches for efficient removal of PMOCs remain to be established where an in-depth understanding of electrosorption behaviors of various PMOCs is essential. Nevertheless, very little work has covered PMOCs with nonionic, cationic, and/or anionic structures [29, 34, 36] as we present here.

Since the concept of electro-assisted ad/desorption, described here as trap&release approach, was first introduced in 1986 by Woodard et al. [36] to remove Rhodamine B using three-dimensional carbon fibers, it has been so far only explored by a few studies for limited polar, ionizable/ionic organic compounds [15, 17-19, 24, 29, 34, 37]. Our recent work [15] estimated achievable enrichment factors, that is, the ratio of water volume cleaned in the electro-adsorption step to the volume needed for electro-desorption, to be in the range of 40 to 100 for perfluoroalkyl acids (PFAAs) using AC carrying different surface functionalities. This suggests a great potential of electro-assisted trap&release in PMOC removal which shall be investigated for a broader selection of various candidates. In addition, AC adsorbents with modified surface chemistry were hardly involved in the previous research, leaving it rather unsolved how AC surface chemistry would improve or inhibit its electro-ad-/desorption efficiency. Moreover, except for a few cases [18, 19, 38], investigation of adsorbent stability during the electro-assisted trap&release process was generally missing to provide valuable insight into system long-term stability.

To identify the drivers for an effective, long-term stable electrosorptive removal of PMOCs from water, pristine and surface-defunctionalized activated carbon felts (ACFs) were polarized at different bias potentials to ad-/desorb five PMOCs, that are tetrapropylammonium (TPA<sup>+</sup>), benzyltrimethylammonium (BTMA<sup>+</sup>), *p*-toluenesulfonate (*p*-TsO<sup>-</sup>,  $pK_{a,p-TsOH} < -1$  [39, 40]), *p*-toluenesulfonamide (*p*-TSA,  $pK_{a,p-TSA} = 10.5$  [41]), and methyl-*tert*-butyl ether (MTBE). This selection covers two cationic, one anionic, and two nonionic (at neutral pH), highly environmentally relevant PMOCs detectable in various aquatic environments [2, 9, 42]. Their electrosorption behaviors on AC materials are investigated here for the first time.

In addition to charging AC adsorbents via an externally applied electric potential, chemical modification can alter the native charge state of an AC surface in a specific aqueous environment. The latter is related to protonation/deprotonation equilibria, which can also be decisive in the adsorption of ionic and polar PMOCs without any external electric potential [13]. Surface polarization via applied bias potential and surface chemical modification can both be employed to generate differently charged AC surfaces to influence PMOC adsorption; yet, most works in the past have explored them in individual studies and not in a much-needed comparative approach. Here, we applied both approaches in case studies of cationic TPA<sup>+</sup>, anionic *p*-TsO<sup>-</sup>, and nonionic *p*-TSA adsorption on ACFs and compared their effects. Adsorption isotherms determined in batch systems were fitted with Freundlich and Langmuir equations to quantify the adsorption capacity and affinity of differently surface-functionalized ACFs towards various PMOCs under selected polarization conditions.

We also evaluated the applicability of the electro-assisted trap&release approach using two ACFs. To this end, we analyzed 1) the impact of applied bias potential on single-point sorption coefficients  $K_d$  in batch systems for different PMOCs, and 2) the estimated achievable enrichment factors in a fixed-bed flow-through setup derived from Freundlich isotherm parameters collected under electro-ad-/desorption conditions in batch systems for the most promising PMOC candidates. The system stability was examined by ad-/desorption cycles of TPA<sup>+</sup> and *p*-TsO<sup>-</sup> on surface-defunctionalized ACF over 20 d, where potential changes in adsorbent properties were monitored via cyclic voltammetry (CV), temperature-programmed decomposition (TPD), and determination of the pore structure.

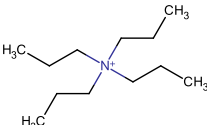
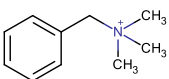
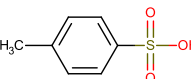
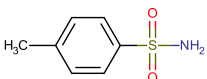
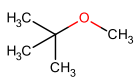
## 2. Experimental Section

### 2.1 Chemicals

BTMA-OH (20 mass% aq.) and *p*-TsOH·H<sub>2</sub>O (>98.5%) were purchased from Alfa Aesar. TPA-OH (1 M, aq.) and *p*-TSA (≥99%) were obtained from Sigma-Aldrich. MTBE (>99%) was purchased from Fluka Analytical. Selected sorbate properties are listed in **Table 1**. Na<sub>2</sub>SO<sub>4</sub> (99%), NaOH (99%), HCl (37%), NaNO<sub>3</sub> (>99%), KCl (>99%), H<sub>2</sub>SO<sub>4</sub> (0.5 M) and HNO<sub>3</sub> (65%) were purchased from Merck. Methanol (>99.95%) and 2-propanol (≥99.9%) were purchased

from Th. Geyer. Ammonium acetate ( $C_2H_7NO_2$ ,  $\geq 98.0\%$ ) was obtained from Bernd Kraft GmbH. All solutions were prepared using deionized water.

**Table 1:** Selected properties of studied PMOCs. References given in brackets.

	TPA <sup>+</sup>	BTMA <sup>+</sup>	<i>p</i> -TsOH	<i>p</i> -TSA	MTBE
Type <sup>a</sup>	Cationic	cationic	anionic	nonionic	nonionic
pK <sub>a</sub>	-	-	-1.3 [40]	10.5 [41]	-
log <i>D</i> <sup>b</sup>	-0.45	-2.25	-0.71	1.09	1.18
Mol. weight (g/mol)	186.4	150.2	172.2	171.22	88.15
Structure					

<sup>a</sup> Predominant form at pH = 7. <sup>b</sup> Log *D* is the pH-dependent octanol-water distribution coefficient, obtained from [43] at pH 7. For MTBE (not ionizable), log *D* = pH-independent log *K*<sub>OW</sub>.

## 2.2 Materials

Actitex-FC1001 (Jacobi CARBONS; referred to as ACF<sub>10</sub> in short in the following text) was pre-treated and further modified according to the procedures reported previously [13]. As a modification, we applied H<sub>2</sub>/N<sub>2</sub> instead of pure H<sub>2</sub> flow for surface defunctionalization. In short, the sample was washed once with 2-propanol and 5 times with H<sub>2</sub>O under shaking (each 30 min, 120 rpm) and then dried in air overnight (16 h) at 80°C before being ready for use. DeACF<sub>10</sub> was generated by heating ACF<sub>10</sub> in a tubular quartz oven (length: 40 cm, Ø: 2 cm) from room temperature to 900°C in a H<sub>2</sub>/N<sub>2</sub> 1:10 mixture (150°C/min, 40 mL/min gas flow) and kept at 900°C for 2 h. The oven with the sample inside was purged before heating with N<sub>2</sub> flow for 0.5 h, followed by adding H<sub>2</sub> gas and purging for another 10 min. After the heating procedure, the H<sub>2</sub> flow was kept until the oven had cooled below 500°C. The sample was continued to cool down in N<sub>2</sub> flow until *T* < 100°C before being taken out. It was then washed 5 times with water (30 min each, 120 rpm shaking) and dried overnight at 80°C before characterization. Note that the samples defunctionalized in the H<sub>2</sub>/N<sub>2</sub> mixture exhibited nearly identical characteristics compared to the sample prepared in the pure H<sub>2</sub> flow. OxACF<sub>10</sub> was accomplished by treating ACF<sub>10</sub> (1.0 g) in 5 M HNO<sub>3</sub> (120 mL) for 6 h at 95°C. After washing with H<sub>2</sub>O for 5 times (each 30 min, 120 rpm) until the solution pH approached 6, the sample was dried in air overnight at 50°C before further usage.

### 2.3 Material characterization

The pore size distributions and specific surface areas (SSA) were measured by applying an Autosorb iQ system under the N<sub>2</sub> atmosphere at -196°C. The quenched solid density functional theory (QSDFT) was applied for analysis by assuming a slit-shaped pore configuration. The electrode sample was first degassed at 100 Pa and 200°C for 1 h and then heated to 300°C for 20 h.

Raman spectroscopy was performed by a Renishaw inVia Raman spectrometer equipped with a 532 nm Nd-YAG laser (exposed power 0.5 mW on the sample, 2400 lines/mm grating, 50x objective with 0.75 numeric aperture). For each ACF sample, 10 points were selected to be measured. An acquisition with 5 accumulations was applied for each measurement point. Peak deconvolution was performed using a linear background and Voigt profiles for the fitting.

The point of zero net proton charge (pH<sub>pzc</sub>) of the ACFs was determined based on the procedures in [44]. In brief, a 10 mg sample was stirred overnight in 2 mL of aqueous 10 mM Na<sub>2</sub>SO<sub>4</sub> electrolyte solution at various initial pH values (2-11) adjusted using 0.1 M NaOH and 0.05 M H<sub>2</sub>SO<sub>4</sub> solutions. The pH values were recorded before and after. The pH<sub>pzc</sub> of the sample is the point where pH (initial) = pH (final).

Temperature-programmed decomposition (TPD) measurements were performed with a BELCAT-B chemisorption analyzer (BEL) connected to an IR detector (SAXON Junkalor). The samples were kept first in Ar at 150°C for 30 min before being heated up to 1100°C in a He flow (50 mL/min, 10°C/min), and evolving CO and CO<sub>2</sub> gases were detected. Elemental analysis was done with a CHN analyzer (LECO TruSpec CHN). The ash content was measured gravimetrically as residue after sample combustion at 750°C in O<sub>2</sub>. Anion and cation exchange capacities (AEC and CEC) were measured as described in the *Supporting Information*.

Cyclic voltammetry (CV) was carried out using a multi-channel potentiostat MSX-8 (ScioSpec). A three-electrode cell consisting of a Pt helix counter electrode, an Ag/AgCl sat. KCl reference electrode and a working electrode made of a piece of ACF (connected with a Pt wire) or a graphite rod, or a piece of boron-doped diamond (BDD) was used for the measurement. 1 M or 10 mM Na<sub>2</sub>SO<sub>4</sub> aqueous solution (initial pH 6.8-7.0) was used as the

electrolyte background solution. Before measurements, the solution was bubbled with N<sub>2</sub> under stirring (300 rpm) for 15 min to remove the dissolved O<sub>2</sub>. During the measurement, the upper gas phase of the cell was continuously purged with N<sub>2</sub>. All reported potential values were converted to potential vs. the standard hydrogen electrode (SHE) unless expressly stated ( $E$  ([V] vs. SHE) =  $E$  ([V] vs. Ag/AgCl sat. KCl) + 0.20 [V]).

Electrochemical impedance spectroscopy (EIS) measurements were performed using a specially designed cell carrying a poly(ether ether ketone) body (PEEK, outlined in Ref. [45]) and recorded by a BioLogic potentiostat (VMP-300). The PEEK cell is equipped with an Ag/AgCl sat. KCl reference electrode, an oversized YP-80F (Kuraray) activated carbon mixed with 10 mass% poly(tetrafluoroethylene) binder, and a working electrode made of ca. 10 mg ACF. The detailed structure of the cell is described in [45]. 1 M Na<sub>2</sub>SO<sub>4</sub> aqueous solution was used as the electrolyte background. Frequencies  $\omega$  in the range of 3 mHz to 1 kHz and potentials, where the studied ACF can be regarded as ideal polarizable electrodes, were applied. In this potential range, the areal capacitance  $C$  (F/m<sup>2</sup>) can be obtained from the impedance imaginary part  $Z_{\text{im}}$  at any electrode potential via  $C = -(\omega \cdot Z_{\text{im}})^{-1} / (m \cdot \text{SSA})$  [46, 47], where  $m$  (g) is the sample mass and SSA (m<sup>2</sup>/g) the specific surface area. To determine the potential of zero charge ( $E_{\text{pzc}}$ ) of ACFs, data collected at  $\omega = 96.2$  mHz were chosen, where  $Z_{\text{im}}$  showed a clear dependence on  $\omega$  in the nearby range. The potential where the areal capacitance reaches its minimum is assigned to be the ACF's  $E_{\text{pzc}}$ .

#### **2.4 Adsorption experiments without applying external bias potential**

Adsorption experiments without applying external potential on ACFs were performed according to the published protocols [13]. Briefly, the sorbent was pre-wetted in 10 mM Na<sub>2</sub>SO<sub>4</sub> background solution assisted by shaking (120 rpm) for 1-2 d with pH adjustment to 7 using 0.05 M H<sub>2</sub>SO<sub>4</sub> and/or 0.1 M NaOH solution. Then, aqueous stock solutions of sorbates, which were neutralized beforehand, were given to achieve various initial concentrations in the range of 2-100 mg/L. After 48 h of orbital shaking at 120 rpm with daily pH adjustment to 7, aliquots were taken through Whatman PTFE (0.45  $\mu\text{m}$ ) syringe filters for measurements. Examples of adsorption kinetics are given in *Supporting Information*, **Fig. S1**, indicating an approach to equilibrium within 48 h. The pH values of the background solutions were monitored to be within  $7.0 \pm 0.5$  after adsorption.

## 2.5 Electrosorption experiments

Electrosorption experiments were performed in a three-electrode batch cell consisting of an ACF working electrode (connected with a Pt wire), an Ag/AgCl sat. KCl reference electrode and a Pt helix counter electrode, connecting to a multi-channel potentiostat MSX-8 (ScioSpec). An aqueous 10 mM Na<sub>2</sub>SO<sub>4</sub> solution (initial pH 6.8-7.0) was used as background electrolyte solution with ACF dosage kept at 1 g/L. ACF was pre-wetted in stirred (300 rpm) solution overnight before adjusting pH using 0.1 M NaOH and 0.05 M H<sub>2</sub>SO<sub>4</sub> to 7.0 ± 0.3. Then, the open circuit potential (OCP) of ACF was measured by a multimeter. The system was purged with N<sub>2</sub> (water-saturated) for 15 min before charging the ACF at desired potentials. After 24 h polarization, the electrolyte solution was again adjusted to neutral pH before stock solutions containing target compounds were added to achieve initial concentrations in the range of 2-300 mg/L under N<sub>2</sub> purging. For cells containing MTBE, the purging step was skipped. A second pH adjustment step was carried out for cells containing TPA<sup>+</sup>, BTMA<sup>+</sup>, *p*-TsO<sup>-</sup> or *p*-TSA at 24 h after adding the stock solutions. Samples were taken 48 h after stock solution addition through Whatman PTFE (0.45 µm) syringe filters for measurement. Also, in cycle experiments, each ad-/desorption step lasted 48 h to ensure the approach to sorption equilibria. Adjustment of pH to 7.0 ± 0.3 was performed daily while N<sub>2</sub> purging was kept throughout the experiment (5 cycles for 20 d in total).

## 2.6 Analytical methods

The aqueous samples were analyzed with methods reported previously [13]. In short, analysis of samples containing *p*-TsO<sup>-</sup> was done by HPLC (LC-SPD-M20A, SHIMADZU) coupled with a UV/VIS detector at λ = 220 nm. Samples containing TPA<sup>+</sup> were analyzed with HPLC-MS (LCMS-2020, SHIMADZU) in SIM mode (m/z = 186 amu). BTMA<sup>+</sup> and *p*-TSA were analyzed by UV/VIS (UVmini-1240, SHIMADZU) at λ = 207 nm and 225 nm, respectively. MTBE was measured using Headspace-GC-MS (GCMS-2010, SHIMADZU).

## 2.7 Sorption calculations

The adsorption affinity of ACFs was indicated by the single point adsorption coefficient  $K_d$  (L/m<sup>2</sup>) at the adsorption equilibrium according to Eq. 1:

$$K_d = \frac{q_e}{c_e} \quad (1)$$



where the loading on the sorbent is given by  $q_e$  ( $\mu\text{mol}/\text{m}^2$ ), and the sorbate equilibrium concentration in the water phase is given by  $c_e$  ( $\mu\text{mol}/\text{L}$ ).

To analyze the adsorption isotherms, Freundlich (**Eq. 2**) and Langmuir fittings (**Eq. 3**) were employed:

$$\log q_e = n \cdot \log c_e + \log K_F \quad (2)$$

$$\frac{c_e}{q_e} = \frac{c_e}{q_m} + \frac{1}{q_m K_L} \quad (3)$$

The Freundlich parameters include  $n$  as the dimensionless Freundlich exponent and  $K_F$  in  $(\mu\text{mol}/\text{m}^2)/(\mu\text{mol}/\text{L})^n$  as the Freundlich constant. The Langmuir parameters include  $q_m$  ( $\mu\text{mol}/\text{m}^2$ ) as the maximal sorbent loading (only monolayer adsorption considered) and  $K_L$  ( $\text{L}/\mu\text{mol}$ ) as the so-called Langmuir constant. The adsorption affinity of the sorbent is indicated by  $K_F$  and  $K_L$  values, while the adsorption capacity is represented by  $q_m$ . Furthermore,  $n$  being close to 1 refers to relatively homogenous sorption sites and conditions far below maximum loading [14, 19].

In this work, we utilize the so-called trap&release strategy powered by switching the electro-assisted ad-/desorption steps to achieve I) enhanced removal of PMOCs and II) adsorbent regeneration. The trap&release performance can be estimated based on a fixed-bed flow-through model, which is closer to the reality than a batch design in wastewater treatment, using Freundlich  $n$  and  $K_F$  values derived from batch adsorption experiments [29]. Through an effective trap&release process, the water volume needed for desorbing the contaminants ( $V_{\text{des}}$ ) shall be significantly reduced compared to the volume of treated inflow water ( $V_{\text{ads}}$  with contaminant concentration  $c_{\text{in}}$ ). The concentrate obtained by electrodesorption can then be used for further degradation or treatment approaches. The extent of adsorbent unloading ( $X_{\text{des}}$ ) is defined by **Eq. 4**:

$$X_{\text{des}} = 1 - \frac{q_{\text{des,final}}}{q_{\text{ads}}} \quad (4)$$

with  $q_{\text{ads}}$  as loading achieved in the adsorption step and  $q_{\text{des,final}}$  as loading remaining after the desorption step. When using clean water for desorption, 100% adsorbent unloading is expected. The enrichment factor, i.e.,  $V_{\text{ads}}/V_{\text{des}}$  achieved by the trap&release strategy, can be estimated according to **Eq. (5)**; see *Supporting Information* for the derivation.

$$\frac{V_{ads}}{V_{des}} = c_{in}^{(n_{ads}/n_{des}-1)} \cdot \left( \frac{K_{F,ads}}{K_{F,des}} \right)^{1/n_{des}} \quad (5)$$

When using inflow water (i.e., the water to be treated by electrosorption) directly for desorption, the ratio of  $V_{ads}/V_{des}$  can be calculated according to **Eq. (6-7)** [15]:

$$\frac{V_{ads}}{V_{des}} = \frac{c_{in}^{(n_{ads}/n_{des}-1)} \cdot \left( \frac{K_{F,ads}}{K_{F,des}} \right)^{1/n_{des}} - 1}{X_{des}} \quad (6)$$

$$\text{with } X_{des} = 1 - \frac{K_{F,des}}{K_{F,ads}} \cdot c_{in}^{(n_{des}-n_{ads})} \quad (7)$$

### 3. Results and Discussion

#### 3.1 Characterization results of ACFs

The chemical properties of ACF<sub>10</sub> and DeACF<sub>10</sub> characterized using elemental analysis, pH<sub>PZC</sub>, ion exchange capacity measurement, TPD, and XPS were described in detail previously [13]. Selected results are summarized in *Supporting Information, Table S1*. Raman spectra are shown in **Fig. S2**. The textural properties of ACFs are shown in **Table S2**, and **Fig. S3**. As shown by the data, both ACFs are predominantly microporous with a volume-weighted, average pore diameter of ca. 1 nm. ACF<sub>10</sub> (O/C = 0.11 by mass) is richer in O-content than DeACF<sub>10</sub> (O/C = 0.05 by mass) according to the elemental analysis results. ACF<sub>10</sub> is negatively charged and more abundant in cation exchange sites at circum-neutral pH with a pH<sub>PZC</sub> ~ 6.0. In contrast, DeACF<sub>10</sub> (pH<sub>PZC</sub> ~ 10.0) carries a positively charged surface at circum-neutral pH via the adsorption of protons from the aqueous environment onto its delocalized  $\pi$ -electron systems [11]. The significant amount of sp<sup>2</sup>-hybridized carbon of DeACF<sub>10</sub> surface is confirmed by XPS analysis [13] and Raman results (**Fig. S2**), pointing to a higher surface hydrophobicity than ACF<sub>10</sub>.

Herein, the electrochemical properties of ACF<sub>10</sub> and DeACF<sub>10</sub>, being particularly important in terms of electro-assisted sorption processes, were characterized by CV and EIS, as shown in **Fig. 1-2**. Cyclic voltammograms were used to investigate the electrochemical processes at different potentials and to quantify the material's capacitance. For ACF<sub>10</sub>, the oxidation current slightly increased above +0.7 V. This can be assigned to the oxidation of the carbon surface as the standard potential for carbon oxidation is reported at +0.21 V (at 25 °C,  $c_{H^+} = 1 \text{ M}$ ,  $p_{CO_2} = 101.3 \text{ kPa}$ ) [48], equivalent to ca. +0.65 V at neutral pH. The reduction current

started to decline below +0.2 V, which might refer to the reduction of the remaining oxygen despite the N<sub>2</sub> purging (**Fig. S4**) or the reduction of the carbon surface (the respective standard potential so far not available) [48]. The electrochemically stable potential window of ACF<sub>10</sub> (in short as “potential window” in the following text), in which no Faradaic reactions of the electrode occurs, is between +0.2 V and +0.7 V. This range is well consistent with the reported potential map of redox processes of microporous activated carbon cloths in the aqueous phase [49]. The CV curve of DeACF<sub>10</sub> in **Fig. 1a** shows neither a significant rise of the oxidation current below +0.6 V nor a decline of the reduction current beyond -0.1 V. Thus, the potential window of DeACF<sub>10</sub> is estimated to be between -0.1 V and +0.6 V, reflecting its lower surface oxidation degree than ACF<sub>10</sub>. Information on the stability of ACFs at the edge of the potential windows can be found in **Section 3.4**. ACF<sub>10</sub> shows a capacitance of 0.059-0.082 F/m<sup>2</sup> in the range of +0.2 V to +0.7 V normalized to its SSA, which is 100-139 F/g (**Fig. 1a**). DeACF<sub>10</sub> presents an areal capacitance of 0.070-0.083 F/m<sup>2</sup> in the range of -0.1 V to +0.6 V, which is 98-116 F/g normalized to its mass.

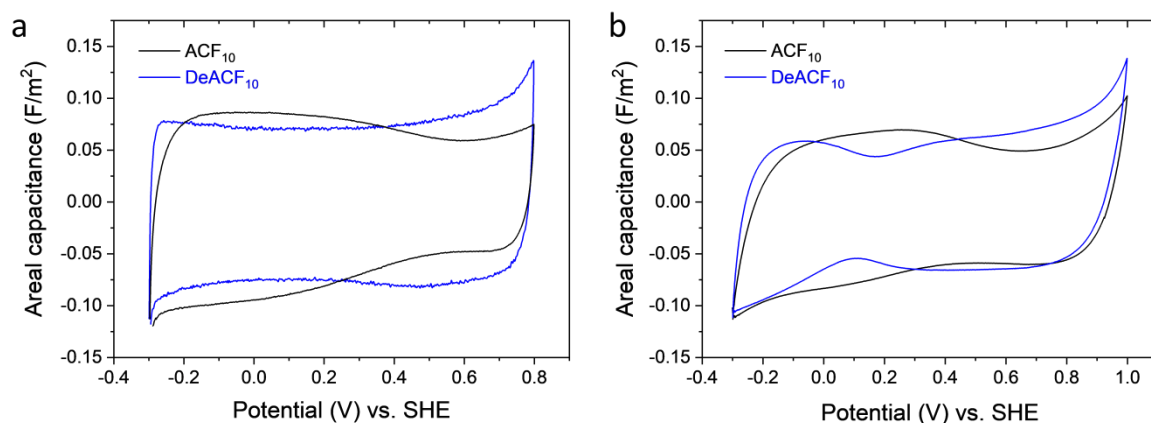


**Fig. 1:** Cyclic voltammograms of ACF<sub>10</sub> and DeACF<sub>10</sub> a) in 1 M Na<sub>2</sub>SO<sub>4</sub> at 1 mV/s and b) in 10 mM Na<sub>2</sub>SO<sub>4</sub> at 0.5 mV/s.

As seen for cyclic voltammograms obtained in 10 mM Na<sub>2</sub>SO<sub>4</sub> at a scan rate of 0.5 mV/s (**Fig. 1b**), the narrowing of the CV oxidation and reduction branches visualizes a more obvious V-shape region compared to those obtained in 1 M Na<sub>2</sub>SO<sub>4</sub> at a scan rate of 1 mV/s. Previous research suggested the electrode’s  $E_{pzc}$ , that is, the potential at which the electrode surface carries a zero net charge, is linked to the V-shaped region [50]. They related the appearance of V-shapes to electrochemical doping [45] or overlapping of the

electrochemical double-layer formation in microspores at low scan rates [51].  $E_{pzc}$  of ACF<sub>10</sub> is expected to fall within the region of +0.4 V to +0.7 V. The V-shape region is shifted to lower potential for DeACF<sub>10</sub>, that is, from 0 V to +0.2 V, confirming its reduced character [50].

The EIS measurements of ACFs provided a more accurate determination of the material's  $E_{pzc}$ . **Fig. 2a** shows the change in areal capacitance  $C$  of ACFs at different applied potentials measured in 1 M Na<sub>2</sub>SO<sub>4</sub> at pH = 7. The electrode's  $E_{pzc}$  is located at the potential showing a minimal  $C$ .  $E_{pzc}$  was proven to be adversely related to the material's pH<sub>pzc</sub> [50]. Electric charges are needed to compensate the material's native surface charges (and repulse counterions) prevalent at the pH conditions until a zero net charge state at  $E = E_{pzc}$  is reached. Thus, a significantly lower  $E_{pzc}$  is found for DeACF<sub>10</sub> compared to ACF<sub>10</sub> ((0.20 ± 0.05) V and (0.40 ± 0.05) V, respectively) following its higher pH<sub>pzc</sub> value (ca. 10.0 compared to 6.0 for ACF<sub>10</sub>). At  $E > E_{pzc}$ , the electrode surface becomes positively charged and accumulates SO<sub>4</sub><sup>2-</sup> from the background Na<sub>2</sub>SO<sub>4</sub> solution, whereas it is negatively charged at  $E < E_{pzc}$  and preferentially takes up Na<sup>+</sup>. The OCPs of ACF<sub>10</sub> and DeACF<sub>10</sub> are both measured to be (0.45 ± 0.05) V in Na<sub>2</sub>SO<sub>4</sub> solution at pH 7. This value indicates a nearly neutral surface of ACF<sub>10</sub> while a strongly positively charged DeACF<sub>10</sub> surface in the absence of external potential. Anion exchange capacities reported previously for ACF<sub>10</sub> (0.025 μmol/m<sup>2</sup>) and DeACF<sub>10</sub> (0.23 μmol/m<sup>2</sup>) measured at pH 7 [13] also confirm such charging status suggested by the material's  $E_{pzc}$ .

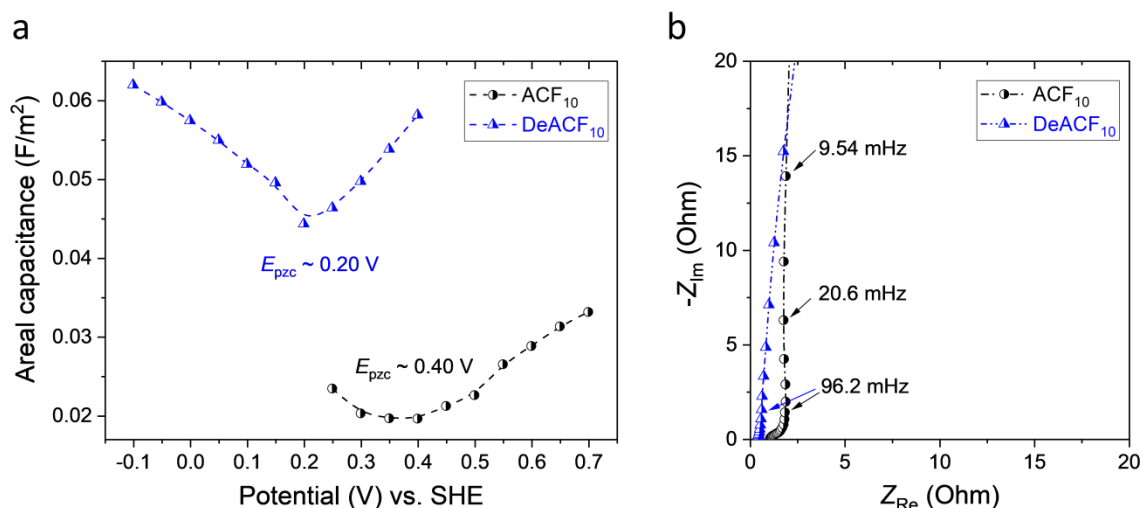


**Fig. 2:** (a) Areal capacitance of ACFs at various applied potentials measured at 96.2 mHz. (b) Nyquist plots of ACFs polarized at 0.4 V vs. SHE. Lines serve as guides for the eye.

The derived Nyquist plots (**Fig. 2b**) show a characteristic intercept with the  $Z_{\text{Re}}$ -axis, standing for the total resistance of the electrodes and electrolytes [52, 53], and linear lines with angles below  $45^\circ$  at low frequencies, typical for electrical double-layer capacitors [46]. For ACF<sub>10</sub>, there is a half semi-circle visible before the transition to the  $45^\circ$ -range; this half semi-circle is absent for DeACF<sub>10</sub>. Thereby, DeACF<sub>10</sub> behaves more like an ideal capacitor with less ion transportation limitation imposed by nanopores. DeACF<sub>10</sub> also shows a smaller charge transfer resistance, possibly owed to a better charge transfer at the electrode/current collector interface [54].

### 3.2 Effect of bias potential on the adsorption of selected PMOCs

The electrosorption of selected PMOCs was investigated on ACF<sub>10</sub> and DeACF<sub>10</sub> polarized at voltages within their potential windows. The selected PMOCs do not undergo electrochemical redox reactions under the probed conditions as indicated both experimentally in *Supporting Information, Fig. S4* and suggested in previous research [55, 56]. **Fig. 3** demonstrates the effect of electrode polarization on PMOC adsorption by showing the change in logarithmic single-point sorption coefficients  $K_d$  along with the applied potential.

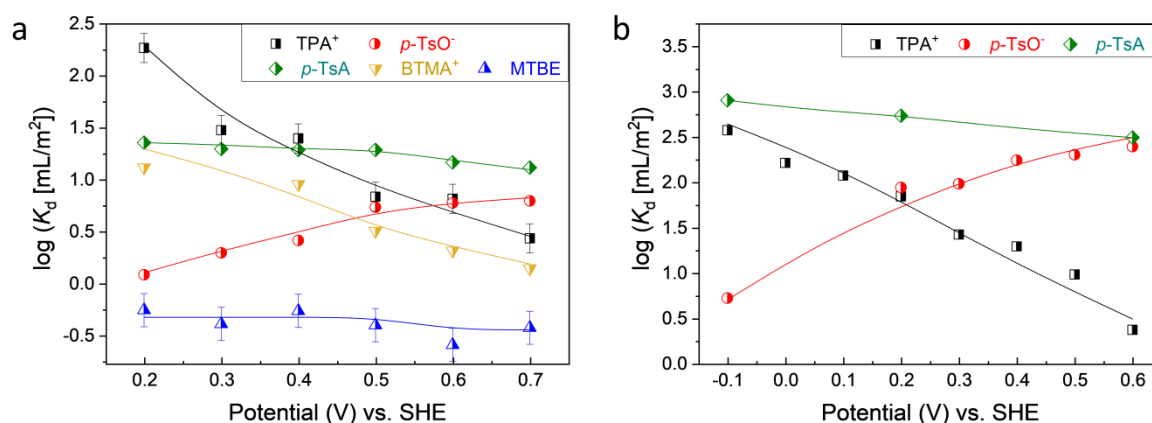


**Fig. 3:** Log  $K_d$  of selected PMOCs on polarized (a) ACF<sub>10</sub> and (b) DeACF<sub>10</sub>. Initial solute concentration: 20 mg/L; ACF dosage: 1 g/L. The error bars indicate the typical deviation of single values from the mean for duplicate experiments. Lines serve as guides for the eye.

As shown in **Fig. 3**, the nonionic adsorbates *p*-TSA and MTBE adsorption were only slightly affected by applying external potentials on ACFs. Only an insignificant increase in log  $K_d$  was observed at lower potentials. For the ionic PMOCs TPA<sup>+</sup>, BTMA<sup>+</sup>, and *p*-TsO<sup>-</sup>, log  $K_d$  generally

increased along with potential values in the opposite direction to the sorbate charge, indicating a promoted adsorption affinity caused by enhanced electrostatic attraction. In contrast, applying potentials in the same direction to the PMOCs' permanent charges led to a decrease in  $\log K_d$ , where desorption processes are facilitated due to stronger electrostatic repulsion.  $K_d$  values differed by a factor larger than 5 on both ACFs for all probed ionic PMOCs at adsorption vs. desorption conditions, that is, the boundary potentials allowed by the electrode potential windows. We see promising PMOC removal efficiency and significant capability for on-site adsorbent regeneration utilizing an electro-assisted trap&release strategy from these values. Similar approaches showed satisfactory results previously for the removal of perfluoroalkyl acids [15]. DeACF<sub>10</sub> allows a wider potential window than ACF<sub>10</sub> where the sorbent remained electrochemically stable. Higher ratios in  $K_{d,ads}/K_{d,des}$  on DeACF<sub>10</sub> for ad-/desorption processes (up to 159 for TPA<sup>+</sup> and 47 for *p*-TsO<sup>-</sup>) can be achieved compared with 67 and 5 on the original ACF<sub>10</sub>, respectively.

To further investigate the effect of electrode polarization on PMOC adsorption, we determined adsorption isotherms of TPA<sup>+</sup> and *p*-TsO<sup>-</sup> on the two ACF types (**Fig. 4**), both at OCP and selected ad-/desorption potentials. Derived from Freundlich parameters (**Table 2**, **Fig. S5**), we estimated achievable enrichment factors ( $V_{ads}/V_{des}$  ratios) in **Table 3** for the trap&release according to **Eq. 5-6** by assuming  $c_{in} = 100 \mu\text{g/L}$  for both TPA<sup>+</sup> and *p*-TsO<sup>-</sup> inflow water. The bias potential at which the highest  $K_d$  is delivered in **Fig. 3a-b** is set for the *trap* condition, while for the *release* steps the potential at which the lowest  $K_d$  is achieved. When using inflow water for desorption, around 90% adsorbent unloading is achievable in all trap&release cases. Using clean water for desorption (i.e., at 100% adsorbent unloading), an enrichment factor of 65 and 42 for TPA<sup>+</sup> and *p*-TsO<sup>-</sup>, respectively, can be achieved by electro-assisted trap&release on ACF<sub>10</sub>. These values increase to 780 and 158 on DeACF<sub>10</sub>, indicating a much stronger polarization-induced effect. The ionic PMOCs could be enriched by factors of  $10^2$  to  $10^3$  by manipulating the electrosorption conditions on defunctionalized AC surfaces. This is more than 10-times the enrichment factor achievable using a typical reverse osmosis setup for treating wastewater containing PMOCs [4, 57], underlining the promising efficiency of electro-assisted trap&release. However, its performance needs to be carefully evaluated further in real applications. If a flow system is smartly designed employing a suitable ACF dosage, a large volume of water can be cleaned by multiple runs of electro-assisted

trap&release procedures to pre-concentrate PMOCs ready for further treatment or degradation steps.

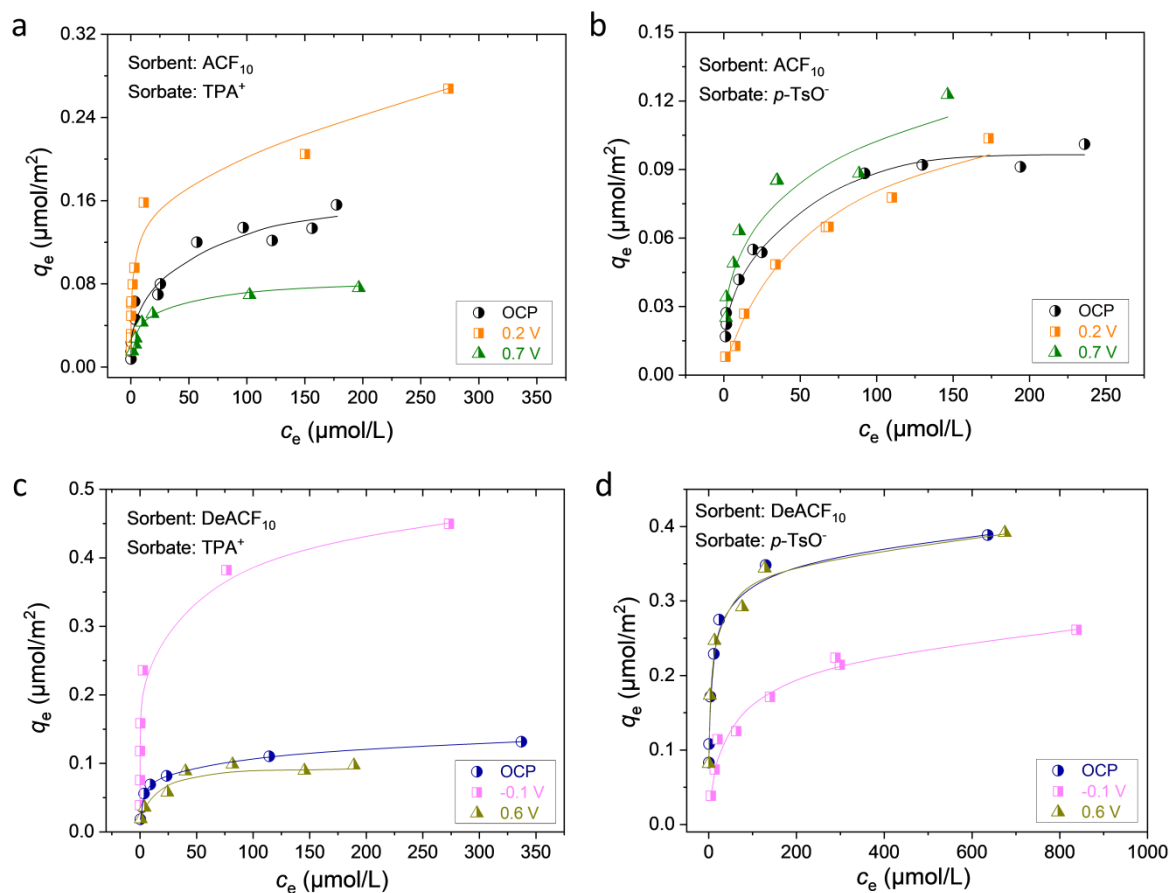


**Fig. 4:** Adsorption isotherms obtained at different potentials. OCPs of ACF<sub>10</sub> and DeACF<sub>10</sub> are around 0.45 V. All potential values are given vs. SHE. Lines serve as guides for the eye. Langmuir and Freundlich linear fittings are shown in *Supporting Information, Fig. S5-S6*.

The isotherms in **Fig. 4** also illustrate the influence of applied potentials on ACFs' adsorption capacities towards TPA<sup>+</sup> and *p*-TsO<sup>-</sup>. Langmuir fitting (**Eq. 3**) was applied to the isotherms as shown in **Fig. S6** to derive the adsorption capacities. Both adsorption affinities ( $K_d$ ) and capacities ( $q_m$ ) of the ACFs towards ionic PMOCs can be manipulated through electrode polarization. As shown in **Table 2**, compared to the  $q_m$  achieved under OCP conditions (+0.45 V),  $q_m$  of TPA<sup>+</sup> on ACF<sub>10</sub> increases by 1.7 times at +0.2 V whereas decreases about by half at +0.7 V. Applying a stronger adsorption potential such as -0.1 V to TPA<sup>+</sup> on DeACF<sub>10</sub> vs. its OCP (+0.45 V) resulted in a significant improvement of  $q_m$  by 3.8 fold. In contrast, a slight reduction by 23% occurred under mild desorption (+0.6 V) compared to OCP condition. Interestingly, comparing the potential effects on  $q_m$  (**Table 2**) and  $\log K_d$  (**Fig. 3**) for TPA<sup>+</sup> and

$p$ -TsO<sup>-</sup> where reversed potentials are needed to trigger ad- and desorption, the effect was lower for  $p$ -TsO<sup>-</sup> on both ACFs than for TPA<sup>+</sup>. Even in the heaviest loaded case, TPA<sup>+</sup> on DeACF<sub>10</sub> at -0.1 V, pores larger than 1 nm were only filled to 25% (*Supporting Information, Table S3*). Thus, ACFs' pore volume should not limit the uptake of ionic PMOCs. Also noting that TPA<sup>+</sup> and  $p$ -TsO<sup>-</sup> show a similar value for log  $D$  (-0.45 and -0.17) [43], which implies similar hydrophobicity.

**Table 2:** Freundlich and Langmuir isotherm fitting parameters for electrosorption of TPA<sup>+</sup> and  $p$ -TsO<sup>-</sup> on ACFs.

Sorbate	Sorbent	Conditions (V) vs. SHE	Freundlich			Langmuir		
			$K_F$ ([ $\mu\text{mol}/\text{m}^2$ ]/[ $\mu\text{mol}/\text{L}$ ] <sup><math>n</math></sup> )	$n$	$R^2$	$q_m$ ( $\mu\text{mol}/\text{m}^2$ )	$K_L$ (L/ $\mu\text{mol}$ )	$R^2$
TPA <sup>+</sup>	ACF <sub>10</sub>	0.45 (at OCP)	0.031	0.44	0.970	0.15	0.11	0.974
		0.20 (Ads.)	0.072	0.33	0.978	0.25	0.26	0.983
		0.70 (Des.)	0.014	0.47	0.962	0.08	0.12	0.999
	DeACF <sub>10</sub>	0.45 (at OCP)	0.029	0.43	0.977	0.13	0.11	0.996
		-0.10 (Ads.)	0.20	0.30	0.955	0.49	0.44	0.998
		0.60 (Des.)	0.020	0.37	0.978	0.10	0.13	0.992
$p$ -TsO <sup>-</sup>	ACF <sub>10</sub>	0.45 (at OCP)	0.017	0.38	0.988	0.10	0.084	0.993
		0.20 (Des.)	0.0037	0.69	0.956	0.09	0.04	0.964
		0.70 (Ads.)	0.024	0.38	0.976	0.12	0.10	0.962
	DeACF <sub>10</sub>	0.45 (at OCP)	0.11	0.31	0.994	0.39	0.14	1.000
		-0.10 (Des.)	0.021	0.44	0.980	0.27	0.02	0.993
		0.60 (Ads.)	0.12	0.23	0.950	0.41	0.07	0.999



**Table 3:** Electro-assisted trap&release parameters and performances for TPA<sup>+</sup> and *p*-TsO<sup>-</sup> adsorption on ACFs under fixed-bed flow-through conditions.

Sorbate	Sorbent	Bias potential (V) vs. SHE		Enrichment factors	
		Trap step	Release step	$V_{ads}/V_{des}^a$	$V_{ads}/V_{des}^b$
TPA <sup>+</sup>	ACF <sub>10</sub>	0.2	0.7	74.2 (0.86)	64.7
	DeACF <sub>10</sub>	-0.1	0.6	851 (0.91)	780
<i>p</i> -TsO <sup>-</sup>	ACF <sub>10</sub>	0.7	0.2	44.7 (0.92)	42.3
	DeACF <sub>10</sub>	0.6	-0.1	176 (0.89)	158

<sup>a</sup> Using inflow water (water to be treated) for desorption.  $X_{des}$  given in brackets. <sup>b</sup> Using clean water for desorption, that is,  $X_{des} = 1$ .

A recent study on electrosorption of the anionic form of aliphatic perfluorooctanoic acid (PFOA,  $pK_a < 1$  [58],  $\log D = 1.58$  [43], carrying a strongly hydrophobic moiety) demonstrated a strong effect of AC charging on its sorption capacity ( $q_m$  differed by a factor of 9 over a 600 mV potential range) [15]. Thus, the as-observed much less sensitive potential effects on  $q_m$  of *p*-TsO<sup>-</sup> compared to TPA<sup>+</sup> could tentatively be related to a predominant, strong  $\pi$ - $\pi$  electron donor-acceptor ( $\pi$ - $\pi$  EDA) interaction between *p*-TsO<sup>-</sup> and ACF surfaces [59, 60] which maintain adsorption even under unfavorable electrostatic conditions.

### **3.3 Charging at bias potential vs. chemical modification of AC surface: Which has a stronger effect on PMOC adsorption?**

The contribution of ACF surface modification on its electrosorption affinity to selected PMOCs can be visualized by referring  $E$  to  $E_{pzc}$  as shown in **Fig. 5**. When  $E = E_{pzc}$ , both DeACF<sub>10</sub> and ACF<sub>10</sub> surfaces carry zero net charge. The difference in  $\log K_d$  at  $E$  (vs.  $E_{pzc}$ ) = 0 indicates their different adsorption affinities towards a certain PMOC resulting from the intrinsically distinct sorbent surface chemistries. DeACF<sub>10</sub> generally showed higher adsorption affinities towards all three tested PMOCs at  $E$  (vs.  $E_{pzc}$ ) = 0 due to its enhanced surface hydrophobicity, which strongly favors adsorption of PMOCs over water molecules and inorganic ions. As seen in **Fig. 5**, the difference in adsorption affinities of the two ACFs is not overcompensated by applying a potential bias in the studied potential ranges. However, strong modulating effects of potential on  $K_d$  were observed for the ionic PMOCs. For TPA<sup>+</sup> (**Fig. 5a**), cathodic charging of ACF<sub>10</sub> is much more effective for increasing sorption affinity than surface chemical modifications where Freundlich parameters remained nearly unaffected by defunctionalization nor oxidation of the carbon surface [13] (**Fig. S7-8, Table S4**). Although

surface defunctionalization improves the adsorbent hydrophobicity, it creates positively charged sites (by proton adsorption onto its delocalized  $\pi$ -electron systems) which repulse  $\text{TPA}^+$  [13]. For  $p\text{-TsO}^-$  (**Fig. 5b**), comparable or stronger enhancement of ACF adsorption affinity can be caused by surface defunctionalization vs. anodic charging. A strong synergetic promotion effect on  $p\text{-TsO}^-$  adsorption was achieved on  $\text{DeACF}_{10}$  surface carrying higher hydrophobicity and positive charges [13]. This suggests that an intrinsic alteration of sorbent surface chemistry is required to achieve a remarkable interference in the adsorption behavior of  $p\text{-TsO}^-$  on ACFs predominated by  $\pi$ - $\pi$  EDA interactions. AC surface charging can hardly manipulate its sorption affinity to nonionic  $p\text{-TSA}$  (**Fig. 5c**), whereas surface defunctionalization significantly improves it.

Even though AC's chemical or thermal surface modification can be applied to improve adsorption performance, it is not applicable for initiating desorption in on-site regeneration as being practically irreversible. In contrast, surface charging via applying bias potential is switchable and can facilitate trap&release in continuous water treatment for PMOC removal.

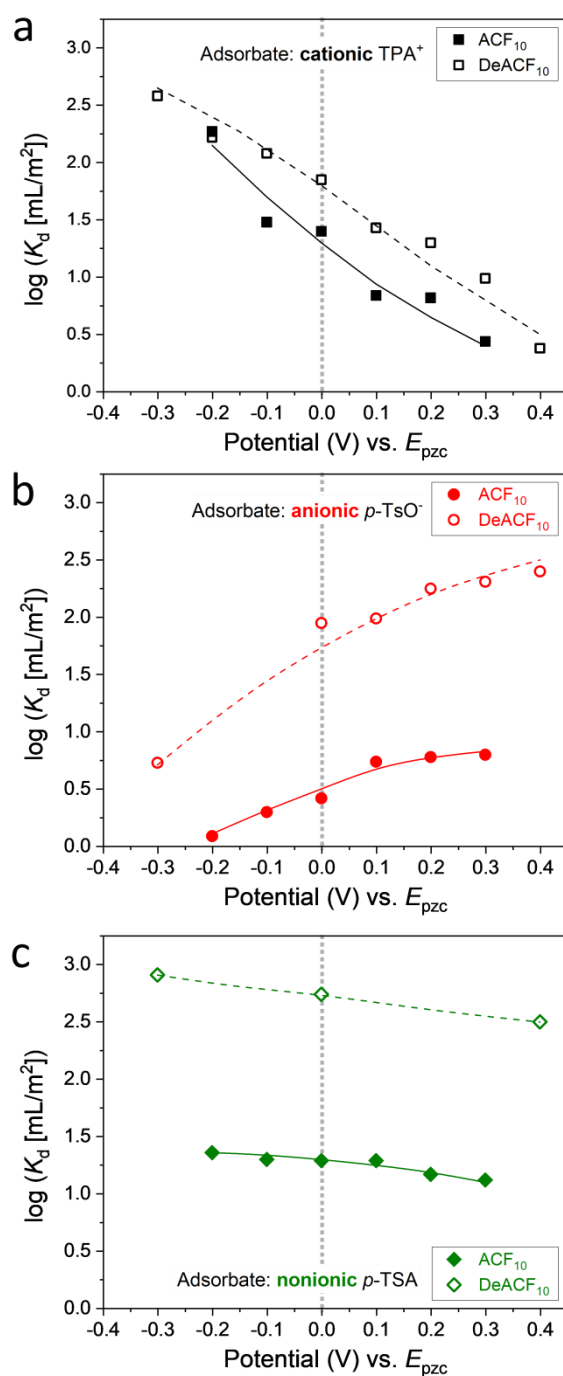


**Fig. 5:** Log  $K_d$  of selected PMOCs on polarized ACF<sub>10</sub> (filled symbols) and DeACF<sub>10</sub> (hollow symbols). The applied potential is referred to  $E_{pzc}$  in the x-axis. The  $E_{pzc}$  of ACF<sub>10</sub> and DeACF<sub>10</sub> are ca. 0.4 V and 0.2 V vs. SHE, respectively. Initial solute concentration: 20 mg/L; ACF dosage: 1 g/L. Lines serve as guides for the eye.

### 3.4 System stability study

Experiments up to 5 adsorption-desorption cycles (48 h for each adsorption or desorption step) were performed to assess the system stability. As DeACF<sub>10</sub> delivers better electro-assisted trap&release performance than ACF<sub>10</sub> (**Table 3**), we focused on the stability testing of electrosorption on DeACF<sub>10</sub>. We chose a potential of +0.6 V for the desorption and the adsorption conditions for TPA<sup>+</sup> and *p*-TsO<sup>-</sup>, respectively, to obtain the optimal effects (**Table 3**). Unlike -0.1 V chosen as the adsorption condition for TPA<sup>+</sup>, desorption of *p*-TsO<sup>-</sup> was probed under OCP as it shows almost the identical sorption isotherm with the one obtained at -0.1 V (**Fig. 4d**).

As shown in **Fig. 6**, DeACF<sub>10</sub> maintained a stable performance for electro-assisted trap&release of both TPA<sup>+</sup> and *p*-TsO<sup>-</sup> over at least 5 cycles. There were only minor deviations of log  $K_d$  within its typical error range ( $\pm 0.15$  units).

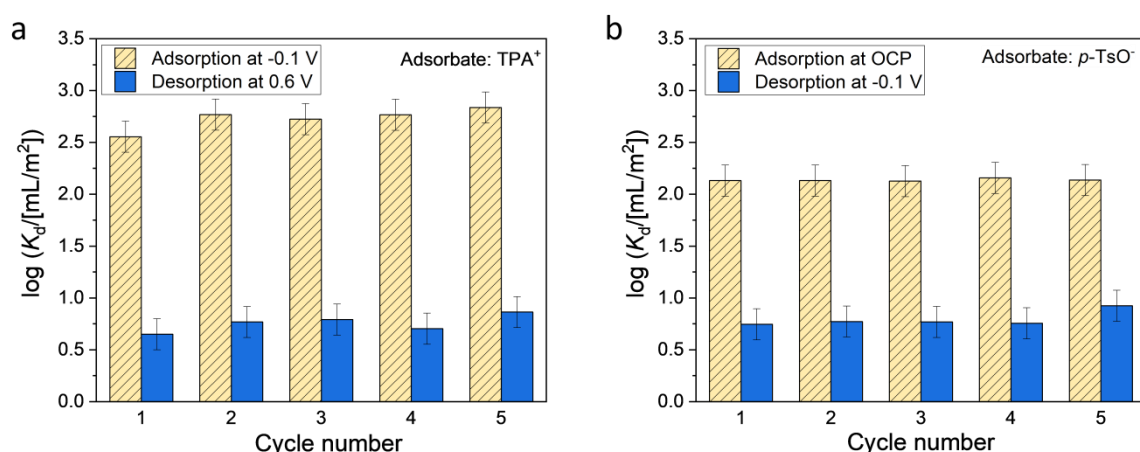


**Fig. 6:** Log  $K_d$  of (a) TPA<sup>+</sup> and (b) *p*-TsO<sup>-</sup> on DeACF<sub>10</sub> over 5 electro-assisted adsorption and desorption cycles. Initial solute concentration: 20 mg/L; ACF dosage: 1 g/L. All potential values are given vs. SHE. The error bars indicate the typical deviation of single values from the mean for duplicate experiments. Lines serve as guides for the eye.

We further recorded cyclic voltammograms and carried out TPD measurements (**Fig. 7**) to track the changes of the ACF electrodes after treatment under different electrosorption conditions. Since the cycled ACF samples were all washed and dried before characterization, a sample only washed and dried just like the cycled ACFs was characterized to serve as a reference (i.e., the sample “washed and dried”). Despite the relatively insignificant changes

in adsorption properties detected for most of the cycled DeACF<sub>10</sub> samples, a considerable alteration was found after using DeACF<sub>10</sub> for five cycles (at -0.1/+0.6 V) with the V-shape position shifted by +245 mV and the content of oxygen increased by 50% (**Table S5**). TPD shows CO<sub>2</sub> release with almost double the intensity compared to the “washed and dried” DeACF<sub>10</sub> sample. This indicates the formation of more carboxylic, anhydride and/or lactone groups on the carbon surface [61, 62], while the corresponding pore size distribution and SSA remained mostly unaffected (**Fig. S9**). However, a ca. 20% sacrifice in total pore volume and SSA was caused when more harsh conditions (~-1 V vs. SHE) were applied to regenerate bentazone pre-loaded AC cloth over 6 cycles [18]. The minor alteration of DeACF<sub>10</sub> has not harmed the performance of DeACF<sub>10</sub> in electro-assisted trap&release of TPA<sup>+</sup> during the 5-cycle experiments, which is not surprising as TPA<sup>+</sup> adsorption was found adequate even on OxACF<sub>10</sub> surface of higher oxidation degree (**Fig. S7**, **Table S4**). The CV and TPD results reveal a more sensitive surface of ACF<sub>10</sub> upon charging, especially at a negative electric potential (**Fig. S10**). This seemingly implies a narrower range of applicable polarization conditions as suggested by cyclic voltammograms (**Section 3.1**, **Fig. 1**).

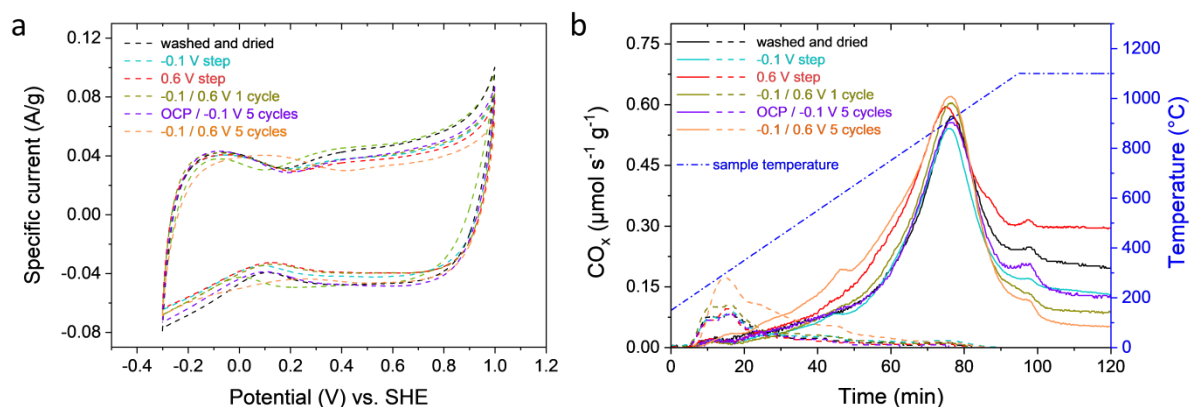


**Fig. 7:** (a) Cyclic voltammograms and (b) TPD measurements of DeACF<sub>10</sub> after treating under different conditions. CV was performed in 10 mM Na<sub>2</sub>SO<sub>4</sub> at 0.5 mV/s. In (b), solid and dashed lines represent the CO and CO<sub>2</sub> release profiles, respectively. All potential values are given vs. SHE.

For simultaneous removal of anionic and cationic PMOCs from contaminated water in a trap&release electrosorption system, symmetric AC electrodes can be applied as anode and cathode covered with an anion- or cation-selective membrane, respectively, as also done in

membrane CDI applications [21]. This setup should prevent re-adsorption of PMOCs released from one electrode to the other upon the potential switch in the desorption step.

#### 4. Conclusions

In this work, electro-assisted polarization of ACF is demonstrated to remarkably manipulate the ad- and desorption processes of charged PMOCs in aqueous media but has only a minor effect on nonionic PMOCs. Great potential is especially shown for  $\text{TPA}^+$  where differences in adsorption affinities ( $\log K_d$ ) and capacities ( $q_m$ ) in factors  $> 5$  were provided by charging ACF at ad-/desorption potentials. A much milder manipulating effect of applied potential on  $p\text{-TsO}^-$  adsorption was proposed to be related to its strong  $\pi\text{-}\pi$  EDA interaction with ACF surfaces. Electrosorption can be applied for I) enhancing adsorption performance towards ionic PMOCs and thus extending operation life of AC adsorbers and/or II) utilizing charge-dependent ad-/desorption performance for on-site regeneration of AC (trap&release).

In terms of improvement of *adsorption* performance for cationic PMOCs, electro-enhanced adsorption by cathodic polarization of AC is more favourable than surface chemical modification of AC. This is because surface oxidation typically sacrifices sorbent surface hydrophobicity when introducing cation exchange sites. In contrast, for anionic and nonionic PMOCs, surface defunctionalization reduces overall surface polarity while creating positively charged sites, which is, more effective in enhancing adsorption efficiency than the anodic polarization of ACs bearing intrinsic negative charges at neutral pH.

Surface-defunctionalized  $\text{DeACF}_{10}$  remains stable over a wider potential window than  $\text{ACF}_{10}$  and thus fosters the trap&release performance even further. Batch systems based on  $\text{DeACF}_{10}$  maintained high trap&release efficiency for both  $\text{TPA}^+$  and  $p\text{-TsO}^-$  in a 5-cycle stability test over 20 days. A first estimation resulted in achievable enrichment factors of  $10^2$ – $10^3$  derived from Freundlich fitting parameters for a flow-through trap&release unit. This suggests a facile, green on-site regeneration alternative for exhausted ACFs through electro-assisted polarization in contrast to common off-site thermal regeneration requiring extra transportation cost and AC losses. Further research should employ flow-through systems to evaluate the potential of electro-assisted trap&release in treating real wastewater containing complex media. Nonetheless, our findings provide valuable guidance in AC-based materials modification and process design for electro-assisted removal of emerging PMOCs

from contaminated water. The electrosorption techniques shall effectively enrich PMOCs in a small water volume, which can considerably lower the energy consumption of any further treatment technique such as electrochemical degradation [63, 64] to achieve the complete mineralization of PMOCs.

## Acknowledgement

We are grateful for the funding offered by Deutsche Forschungsgemeinschaft GE 3029/1-1 and the PhD-college STROMER within the Thematic Area: Environmental Engineering and Biotechnology at UFZ. We thank Ruonan Qin for assisting the electrosorption experiments of MTBE in her internship and Navid Saeidi for fruitful discussions. The INM authors thank Eduard Arzt (INM) for his continuing support.

## References

- [1] All POPs listed in the Stockholm Convention, <http://chm.pops.int/TheConvention/ThePOPs/AllPOPs/tabid/2509/Default.aspx>, (accessed 31 May 2021).
- [2] H.P.H. Arp, T.N. Brown, U. Berger, S.E. Hale, Ranking REACH registered neutral, ionizable and ionic organic chemicals based on their aquatic persistency and mobility, *Environ. Sci.: Process. Impacts*. 19 (2017) 939-955. <https://doi.org/10.1039/C7EM00158D>.
- [3] R. Loos, R. Carvalho, D.C. António, S. Comero, G. Locoro, S. Tavazzi, B. Paracchini, M. Ghiani, T. Lettieri, L. Blaha, B. Jarosova, S. Voorspoels, K. Servaes, P. Haglund, J. Fick, R.H. Lindberg, D. Schwesig, B.M. Gawlik, EU-wide monitoring survey on emerging polar organic contaminants in wastewater treatment plant effluents, *Water Res.* 47 (2013) 6475-6487. <https://doi.org/10.1016/j.watres.2013.08.024>.
- [4] T. Reemtsma, U. Berger, H.P.H. Arp, H. Gallard, T.P. Knepper, M. Neumann, J.B. Quintana, P.d. Voogt, Mind the gap: persistent and mobile organic compounds—water contaminants that slip through, *Environ. Sci. Technol.* 50 (2016) 10308-10315. <https://doi.org/10.1021/acs.est.6b03338>.
- [5] S.E. Hale, H.P.H. Arp, I. Schliebner, M. Neumann, Persistent, mobile and toxic (PMT) and very persistent and very mobile (vPvM) substances pose an equivalent level of concern to persistent, bioaccumulative and toxic (PBT) and very persistent and very bioaccumulative (vPvB) substances under REACH, *Environ. Sci. Eur.* 32 (2020) 155. <https://doi.org/10.1186/s12302-020-00440-4>.
- [6] C. Sophia A, E.C. Lima, Removal of emerging contaminants from the environment by adsorption, *Ecotoxicol. Environ. Saf.* 150 (2018) 1-17. <https://doi.org/10.1016/j.ecoenv.2017.12.026>.
- [7] M. Bonato, F. Corrà, M. Bellio, L. Guidolin, L. Tallandini, P. Irato, G. Santovito, PFAS environmental pollution and antioxidant responses: An overview of the impact on human field, *Int. J. Environ. Res. Public Health* 17 (2020). <https://doi.org/10.3390/ijerph17218020>.
- [8] P. Roslev, T. Lentz, M. Hesselsoe, Microbial toxicity of methyl tert-butyl ether (MTBE) determined with fluorescent and luminescent bioassays, *Chemosphere* 120 (2015) 284-291. <https://doi.org/10.1016/j.chemosphere.2014.07.003>.
- [9] S. Schulze, D. Zahn, R. Montes, R. Rodil, J.B. Quintana, T.P. Knepper, T. Reemtsma, U. Berger, Occurrence of emerging persistent and mobile organic contaminants in European water samples, *Water Res.* 153 (2019) 80-90. <https://doi.org/10.1016/j.watres.2019.01.008>.

- [10] L. Decrey, F. Bonvin, C. Bonvin, E. Bonvin, T. Kohn, Removal of trace organic contaminants from wastewater by superfine powdered activated carbon (SPAC) is neither affected by SPAC dispersal nor coagulation, *Water Res.* 185 (2020) 116302. <https://doi.org/10.1016/j.watres.2020.116302>.
- [11] N. Saeidi, F.-D. Kopinke, A. Georgi, Understanding the effect of carbon surface chemistry on adsorption of perfluorinated alkyl substances, *Chem. Eng. J.* 381 (2020) 122689. <https://doi.org/10.1016/j.cej.2019.122689>.
- [12] N. Saeidi, F.-D. Kopinke, A. Georgi, What is specific in adsorption of perfluoroalkyl acids on carbon materials?, *Chemosphere* (2020) 128520. <https://doi.org/10.1016/j.chemosphere.2020.128520>.
- [13] J. Zhou, N. Saeidi, L.Y. Wick, F.-D. Kopinke, A. Georgi, Adsorption of polar and ionic organic compounds on activated carbon: surface chemistry matters, *Sci. Total Environ.* (2021) 148508. <https://doi.org/10.1016/j.scitotenv.2021.148508>.
- [14] L. Li, P.A. Quinlivan, D.R.U. Knappe, Effects of activated carbon surface chemistry and pore structure on the adsorption of organic contaminants from aqueous solution, *Carbon* 40 (2002) 2085-2100. [https://doi.org/10.1016/S0008-6223\(02\)00069-6](https://doi.org/10.1016/S0008-6223(02)00069-6).
- [15] N. Saeidi, F.-D. Kopinke, A. Georgi, Controlling adsorption of perfluoroalkyl acids on activated carbon felt by means of electrical potentials, *Chem. Eng. J.* 416 (2021) 129070. <https://doi.org/10.1016/j.cej.2021.129070>.
- [16] E. Bayram, E. Ayranci, Electrochemically enhanced removal of polycyclic aromatic basic dyes from dilute aqueous solutions by activated carbon cloth electrodes, *Environ. Sci. Technol.* 44 (2010) 6331-6336. <https://doi.org/10.1021/es101177k>.
- [17] E. Bayram, E. Ayranci, Structural effects on electrosorptive behavior of aromatic organic acids from aqueous solutions onto activated carbon cloth electrode of a flow-through electrolytic cell, *J. Electroanal. Chem.* 683 (2012) 14-20. <https://doi.org/10.1016/j.jelechem.2012.07.028>.
- [18] C.O. Ania, F. Béguin, Electrochemical regeneration of activated carbon cloth exhausted with bentazone, *Environ. Sci. Technol.* 42 (2008) 4500-4506. <https://doi.org/10.1021/es703192x>.
- [19] S. Delpoux-Ouldiane, M. Gineys, N. Cohaut, F. Béguin, The role played by local pH and pore size distribution in the electrochemical regeneration of carbon fabrics loaded with bentazon, *Carbon* 94 (2015) 816-825. <https://doi.org/10.1016/j.carbon.2015.07.010>.
- [20] E. Gagliano, M. Sgroi, P.P. Falciglia, F.G.A. Vagliasindi, P. Roccaro, Removal of poly- and perfluoroalkyl substances (PFAS) from water by adsorption: Role of PFAS chain length, effect of organic matter and challenges in adsorbent regeneration, *Water Res.* 171 (2020) 115381. <https://doi.org/10.1016/j.watres.2019.115381>.
- [21] M.E. Suss, S. Porada, X. Sun, P.M. Biesheuvel, J. Yoon, V. Presser, Water desalination via capacitive deionization: what is it and what can we expect from it?, *Energy Environ. Sci.* 8 (2015) 2296-2319. <https://doi.org/10.1039/C5EE00519A>.
- [22] L. Wang, Y. Zhang, K. Moh, V. Presser, From capacitive deionization to desalination batteries and desalination fuel cells, *Curr. Opin. Electrochem.* (2021) 100758. <https://doi.org/10.1016/j.coelec.2021.100758>.
- [23] Y. Han, X. Quan, H. Zhao, S. Chen, Y. Zhao, Kinetics of enhanced adsorption by polarization for organic pollutants on activated carbon fiber, *Front. Environ. Sci. Eng. China* 1 (2007) 83-88. <https://doi.org/10.1007/s11783-007-0016-2>.
- [24] C.O. Ania, F. Béguin, Mechanism of adsorption and electrosorption of bentazone on activated carbon cloth in aqueous solutions, *Water Res.* 41 (2007) 3372-3380. <https://doi.org/10.1016/j.watres.2007.03.031>.
- [25] O. Kitous, A. Cheikh, H. Lounici, H. Grib, A. Pauss, N. Mammeri, Application of the electrosorption technique to remove Metribuzin pesticide, *J. Hazard. Mater.* 161 (2009) 1035-1039. <https://doi.org/10.1016/j.jhazmat.2008.04.091>.
- [26] W. Yang, H. Han, M. Zhou, J. Yang, Simultaneous electricity generation and tetracycline removal in continuous flow electrosorption driven by microbial fuel cells, *RSC Adv.* 5 (2015) 49513-49520. <https://doi.org/10.1039/C5RA05545H>.



- [27] S. López-Bernabeu, R. Ruiz-Rosas, C. Quijada, F. Montilla, E. Morallón, Enhanced removal of 8-quinolinecarboxylic acid in an activated carbon cloth by electroadsorption in aqueous solution, *Chemosphere* 144 (2016) 982-988. <https://doi.org/10.1016/j.chemosphere.2015.09.071>.
- [28] E. Bayram, Ç. Kızıl, E. Ayrancı, Flow-through electrosorption process for removal of 2,4-D pesticide from aqueous solutions onto activated carbon cloth fixed-bed electrodes, *Water Sci. Technol.* 77 (2018) 848-854. <https://doi.org/10.2166/wst.2017.598>.
- [29] S. Wang, X. Li, H. Zhao, X. Quan, S. Chen, H. Yu, Enhanced adsorption of ionizable antibiotics on activated carbon fiber under electrochemical assistance in continuous-flow modes, *Water Res.* 134 (2018) 162-169. <https://doi.org/10.1016/j.watres.2018.01.068>.
- [30] X. Li, Y. Hu, D. She, W.-B. Shen, Modified activated carbon fiber felt for the electrosorption of norfloxacin in aqueous solution, *Sustainability* 12 (2020). <https://doi.org/10.3390/su12103986>.
- [31] Y. Lester, E. Shaulsky, R. Epsztein, I. Zucker, Capacitive deionization for simultaneous removal of salt and uncharged organic contaminants from water, *Sep. Purif. Technol.* 237 (2020) 116388. <https://doi.org/10.1016/j.seppur.2019.116388>.
- [32] J. Niu, B.E. Conway, Adsorptive and electrosorptive removal of aniline and bipyridyls from waste-waters, *J. Electroanal. Chem.* 536 (2002) 83-92. [https://doi.org/10.1016/S0022-0728\(02\)01206-8](https://doi.org/10.1016/S0022-0728(02)01206-8).
- [33] J. Niu, B.E. Conway, Molecular structure factors in adsorptive removal of pyridinium cations, 1,4-pyrazine and 1-quinoline at high-area C-cloth electrodes for waste-water remediation, *J. Electroanal. Chem.* 529 (2002) 84-96. [https://doi.org/10.1016/S0022-0728\(02\)00910-5](https://doi.org/10.1016/S0022-0728(02)00910-5).
- [34] J.M. Serrano, A.U. Khan, T. Liu, Z. Xu, A.R. Esker, G. Liu, Capacitive organic dye removal by block copolymer based porous carbon fibers, *Adv. Mater. Interfaces* 7 (2020) 2000507. <https://doi.org/10.1002/admi.202000507>.
- [35] E. Ayrancı, B.E. Conway, Adsorption and electrosorption of ethyl xanthate and thiocyanate anions at high-area carbon-cloth electrodes studied by in situ UV spectroscopy: Development of procedures for wastewater purification, *Anal. Chem.* 73 (2001) 1181-1189. <https://doi.org/10.1021/ac000736e>.
- [36] F.E. Woodard, D.E. McMackins, R.E.W. Jansson, Electrosorption of organics on three dimensional carbon fiber electrodes, *J. Electroanal. Chem. Interf. Electrochem.* 214 (1986) 303-330. [https://doi.org/10.1016/0022-0728\(86\)80105-X](https://doi.org/10.1016/0022-0728(86)80105-X).
- [37] A. Ban, A. Schafer, H. Wendt, Fundamentals of electrosorption on activated carbon for wastewater treatment of industrial effluents, *J. Appl. Electrochem.* 28 (1998) 227-236. <https://doi.org/10.1023/A:1003247229049>.
- [38] E. Bayram, E. Ayrancı, Investigation of changes in properties of activated carbon cloth upon polarization and of electrosorption of the dye basic blue-7, *Carbon* 48 (2010) 1718-1730. <https://doi.org/10.1016/j.carbon.2010.01.013>.
- [39] J.P. Guthrie, Hydrolysis of esters of oxy acids: pKa values for strong acids; Brønsted relationship for attack of water at methyl; free energies of hydrolysis of esters of oxy acids; and a linear relationship between free energy of hydrolysis and pKa holding over a range of 20 pK units, *Can. J. Chem.* 56 (1978) 2342-2354. <https://doi.org/10.1139/v78-385>.
- [40] E.P. Sergeant, B. Dempsey, Ionisation constants of organic acids in aqueous solution. IUPAC chemical data series No. 23, Pergamon Press, New York, 1979.
- [41] J.L. Atwood, J.W. Steed, *Encyclopedia of supramolecular chemistry* CRC Press, New York, 2004. <https://doi.org/10.1201/9780429075728>
- [42] S. Schulze, D. Sättler, M. Neumann, H.P.H. Arp, T. Reemtsma, U. Berger, Using REACH registration data to rank the environmental emission potential of persistent and mobile organic chemicals, *Sci. Total Environ.* 625 (2018) 1122-1128. <https://doi.org/10.1016/j.scitotenv.2017.12.305>.
- [43] ChemAxon online platform, <https://chemicalize.com>, (accessed 11 June 2021).
- [44] B.M. Babić, S.K. Milonjić, M.J. Polovina, B.V. Kaludierović, Point of zero charge and intrinsic equilibrium constants of activated carbon cloth, *Carbon* 37 (1999) 477-481. [https://doi.org/10.1016/S0008-6223\(98\)00216-4](https://doi.org/10.1016/S0008-6223(98)00216-4).

- [45] D. Weingarth, M. Zeiger, N. Jäckel, M. Aslan, G. Feng, V. Presser, Graphitization as a universal tool to tailor the potential-dependent capacitance of carbon supercapacitors, *Adv. Energy Mater.* 4 (2014) 1400316. <https://doi.org/10.1002/aenm.201400316>.
- [46] L.-H. Shao, J. Biener, D. Kramer, R.N. Viswanath, T.F. Baumann, A.V. Hamza, J. Weissmüller, Electrocapillary maximum and potential of zero charge of carbon aerogel, *Phys. Chem. Chem. Phys.* 12 (2010) 7580-7587. <https://doi.org/10.1039/B916331J>.
- [47] V. Lockett, R. Sedev, J. Ralston, M. Horne, T. Rodopoulos, Differential Capacitance of the Electrical Double Layer in Imidazolium-Based Ionic Liquids: Influence of Potential, Cation Size, and Temperature, *J. Phys. Chem. C* 112 (2008) 7486-7495. <https://doi.org/10.1021/jp7100732>.
- [48] C. Zhang, D. He, J. Ma, W. Tang, T.D. Waite, Faradaic reactions in capacitive deionization (CDI) - problems and possibilities: A review, *Water Res.* 128 (2018) 314-330. <https://doi.org/10.1016/j.watres.2017.10.024>.
- [49] N. Holubowitch, A. Omosebi, X. Gao, J. Landon, K. Liu, Quasi-steady-state polarization reveals the interplay of capacitive and Faradaic processes in capacitive deionization, *ChemElectroChem* 4 (2017) 2404-2413. <https://doi.org/10.1002/celec.201700082>.
- [50] X. Gao, A. Omosebi, J. Landon, K. Liu, Surface charge enhanced carbon electrodes for stable and efficient capacitive deionization using inverted adsorption-desorption behavior, *Energy Environ. Sci.* 8 (2015) 897-909. <https://doi.org/10.1039/C4EE03172E>.
- [51] C.-H. Hou, C. Liang, S. Yiaccoumi, S. Dai, C. Tsouris, Electrosorption capacitance of nanostructured carbon-based materials, *J. Colloid Interface Sci.* 302 (2006) 54-61. <https://doi.org/10.1016/j.jcis.2006.06.009>.
- [52] A. Lasia, Electrochemical impedance spectroscopy and its applications. In: Conway B.E., Bockris J.O., White R.E. (eds) *Modern aspects of electrochemistry. Modern aspects of electrochemistry*, Springer, Boston, MA, 2002. [https://doi.org/10.1007/0-306-46916-2\\_2](https://doi.org/10.1007/0-306-46916-2_2).
- [53] T. Bordjiba, M. Mohamedi, L.H. Dao, Synthesis and electrochemical capacitance of binderless nanocomposite electrodes formed by dispersion of carbon nanotubes and carbon aerogels, *J. Power Sources* 172 (2007) 991-998. <https://doi.org/10.1016/j.jpowsour.2007.05.011>.
- [54] D.D. Macdonald, Reflections on the history of electrochemical impedance spectroscopy, *Electrochim. Acta* 51 (2006) 1376-1388. <https://doi.org/10.1016/j.electacta.2005.02.107>.
- [55] J. Lybaert, B.U.W. Maes, K. Abbaspour Tehrani, K. De Wael, The electrochemistry of tetrapropylammonium perruthenate, its role in the oxidation of primary alcohols and its potential for electrochemical recycling, *Electrochim. Acta* 182 (2015) 693-698. <https://doi.org/10.1016/j.electacta.2015.09.107>.
- [56] C.K. Mann, P.T. Cottrell, Electrochemical reduction of arylsulfonamides, *J. Am. Chem. Soc.* 93 (1971) 3579-3583. <http://doi.org/10.1021/ja00744a006>.
- [57] T.D. Appleman, C.P. Higgins, O. Quiñones, B.J. Vanderford, C. Kolstad, J.C. Zeigler-Holady, E.R.V. Dickenson, Treatment of poly- and perfluoroalkyl substances in U.S. full-scale water treatment systems, *Water Res.* 51 (2014) 246-255. <https://doi.org/10.1016/j.watres.2013.10.067>.
- [58] K.-U. Goss, The pKa values of PFOA and other highly fluorinated carboxylic acids, *Environ. Sci. Technol.* 42 (2008) 456-458. <https://doi.org/10.1021/es702192c>.
- [59] X.-F. Sun, B.-B. Guo, L. He, P.-F. Xia, S.-G. Wang, Electrically accelerated removal of organic pollutants by a three-dimensional graphene aerogel, *AIChE Journal* 62 (2016) 2154-2162. <https://doi.org/10.1002/aic.15185>.
- [60] D. Zhu, J.J. Pignatello, Characterization of aromatic compound sorptive interactions with black carbon (charcoal) assisted by graphite as a model, *Environ. Sci. Technol.* 39 (2005) 2033-2041. <http://doi.org/10.1021/es0491376>.
- [61] M. Vogel, F.-D. Kopinke, K. Mackenzie, Acceleration of microiron-based dechlorination in water by contact with fibrous activated carbon, *Sci. Total Environ.* 660 (2019) 1274-1282. <https://doi.org/10.1016/j.scitotenv.2019.01.070>.
- [62] J.-H. Zhou, Z.-J. Sui, J. Zhu, P. Li, D. Chen, Y.-C. Dai, W.-K. Yuan, Characterization of surface oxygen complexes on carbon nanofibers by TPD, XPS and FT-IR, *Carbon* 45 (2007) 785-796. <https://doi.org/10.1016/j.carbon.2006.11.019>.

- [63] Y. Chen, Y. Tu, Y. Bai, J. Li, J. Lu, Electrosorption enhanced electrooxidation of a model organic pollutant at 3D SnO<sub>2</sub>-Sb electrode in superimposed pulse current mode, *Chemosphere* 195 (2018) 63-69. <https://doi.org/10.1016/j.chemosphere.2017.12.074>.
- [64] K. Kim, P. Baldaguez Medina, J. Elbert, E. Kaya, R.D. Cusick, Y. Men, X. Su, Molecular tuning of redox-copolymers for selective electrochemical remediation, *Adv. Funct. Mater.* 30 (2020) 2004635. <https://doi.org/10.1002/adfm.202004635>.

## Supporting information

### Supporting experimental information

According to the reports, anion and cation exchange capacities (AEC and CEC) were measured [1, 2]. In brief, 0.5 g ACF was shaken overnight in 10 mL of aqueous 1 M KCl solution and then washed 5 times with 10 mL of aqueous 10 mM KCl solution. In each washing step, the pH of the suspension was adjusted using 1 M KOH and 1 M HCl to  $7.0 \pm 0.5$ . After shaking overnight in the final washing round, an aliquot from the supernatant was taken for  $K^+$  and  $Cl^-$  analysis performed by ICP-OES (SPECTRO) and ion chromatography (Dionex), respectively. The  $K^+$  and  $Cl^-$  concentrations of this bulk sample were expected to be the same as that of the entrained solution. The mass of the adherent KCl solution after removing the supernatant was weighted. Next, the ACF was washed 4 times with 8 mL 0.5 M  $NaNO_3$  solution to exchange the adsorbed ions. In each exchange step, the pH of the suspension was adjusted using 1 M NaOH and 1 M  $HNO_3$  to  $7.0 \pm 0.5$ . The  $K^+$  and  $Cl^-$  concentrations of the exchanged solutions were measured. Based on the amount difference between the  $K^+$  and  $Cl^-$  exchanged out and previously entrained, values of CEC and AEC were calculated.

Examples of adsorption kinetics study are shown in **Fig. S1**. Extended adsorption after 10 h only resulted in a change of  $K_{d,t} = q_t/c_t \leq 5\%$  for the two cases shown. 48 h adsorption hence guaranteed an approach to equilibrium.

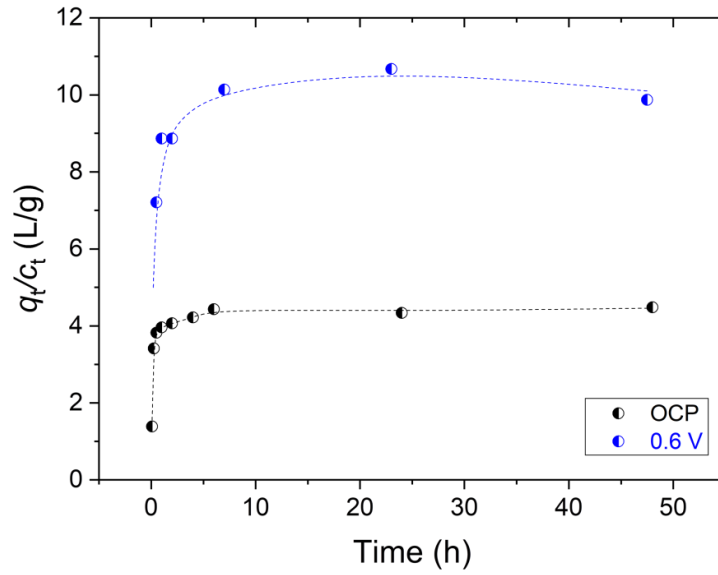


**Fig. S1:** Single point adsorption coefficients  $K_{d,t} = q_t/c_t$  of  $p\text{-TsO}^-$  on  $\text{ACF}_{10}$  along the adsorption time. Initial solute concentration: 20 mg/L; ACF dosage: 1 g/L, pH = 6.4-7.2. All potentials are given in values vs. SHE. Lines serve as guides for the eye.

#### **Estimation of trap&release performance (desorption using clean water)**

The trap&release performance can be estimated based on a fixed-bed flow-through model as described in [3]. This simplified model considers a step-function breakthrough curve. Band-broadening effects due to incomplete establishment of adsorption equilibria or dispersion effects are neglected. While in [3] only the case of desorption by flushing the bed with inflow water (water to be treated by electrosorption) was considered, we here also calculate the concentration factor for the case of using clean water (free of the pollutant) for desorption. The main difference between the two approaches is that there is a low residual loading remaining, that is, the degree of unloading  $X_{\text{des}} \leq 1$  for desorption with inflow water, while using clean water for desorption results in 100% adsorbent unloading if adsorption is fully reversible via  $q_{\text{des,final}} = 0$  and  $X_{\text{des}} = 1 - \frac{q_{\text{des,final}}}{q_{\text{ads}}} = 1$ .

In this case, the following mass balance exists

$$c_{\text{in}} \cdot V_{\text{ads}} = c_{\text{des}} \cdot V_{\text{des}} \quad (\text{S1})$$

$$m_{\text{ACF}} \cdot q_{\text{ads}} = m_{\text{ACF}} \cdot q_{\text{des,initial}}, \text{ i.e., } q_{\text{ads}} = q_{\text{des,initial}} \quad (\text{S2})$$

with  $q_{\text{des,initial}}$  as adsorbent loading at the end of adsorption and start of the desorption process. According to the Freundlich equation ( $\log q_e = n \cdot \log c_e + \log K_F$ ) it holds during the adsorption:

$$q_{\text{ads}} = c_{\text{in}}^{n_{\text{ads}}} \cdot K_{F,\text{ads}} \quad (\text{S3})$$

and during the desorption:

$$q_{\text{des,initial}} = c_{\text{des}}^{n_{\text{des}}} \cdot K_{F,\text{des}} \quad (\text{S4})$$

with  $c_{\text{des}}$  as concentration of adsorbate in the water leaving the fixed bed in the desorption step. Due to Eq. (S2,S4), it follows:

$$c_{\text{des}} = \left( \frac{q_{\text{ads}}}{K_{F,\text{des}}} \right)^{1/n_{\text{des}}} \quad (\text{S5})$$

When considering Eq. (S3), we obtain:

$$c_{\text{des}} = \left( \frac{q_{\text{ads}}}{K_{F,\text{des}}} \right)^{1/n_{\text{des}}} = \left( \frac{K_{F,\text{ads}}}{K_{F,\text{des}}} \right)^{1/n_{\text{des}}} \cdot c_{\text{in}}^{n_{\text{ads}}/n_{\text{des}}} \quad (\text{S6})$$

Therefore, according to Eq. (S1), we obtain:

$$\frac{V_{\text{ads}}}{V_{\text{des}}} = \frac{c_{\text{des}}}{c_{\text{in}}} = c_{\text{in}}^{(n_{\text{ads}}/n_{\text{des}}-1)} \cdot \left( \frac{K_{F,\text{ads}}}{K_{F,\text{des}}} \right)^{1/n_{\text{des}}} \quad (\text{S7})$$

### **Material characterization**

Previously, we investigated the adsorption behavior of selected polar PMOCs, including  $\text{TPA}^+$  and  $p\text{-TsO}^-$  on differently surface-modified ACFs [4]. In addition to defunctionalization (DeACF<sub>10</sub>), a wet-oxidation in  $\text{HNO}_3$  was applied on pristine ACF<sub>10</sub> to generate OxACF<sub>10</sub>.

The Raman spectra of all three ACFs (**Fig. S2a**) resemble amorphous activated carbon materials with typical broad D-bands ( $1345 \text{ cm}^{-1}$ ) relating to defects in carbon structures and G-bands (ca.  $1600 \text{ cm}^{-1}$ ) attributing to planar graphite moieties [5-8]. The band's appearance at  $1160 \text{ cm}^{-1}$  in the Raman spectrum of DeACF<sub>10</sub> aligns with trans-polyacetylene moieties [9] and, hence, implies the formation of C=C bonds after annealing in  $\text{H}_2$  atmosphere. In addition, a slight increase in the intensity ratio of the G-band and D-band, that is,  $I_G/I_D$ , from 0.89 (OxACF<sub>10</sub>) to 0.97 (ACF<sub>10</sub>) and 0.98 (DeACF<sub>10</sub>) as well as area ratio  $A_G/A_D$ , from 0.27

(OxACF<sub>10</sub>) to 0.34 (ACF<sub>10</sub>) and 0.46 (DeACF<sub>10</sub>) was observed after peak deconvolution by applying Voigt functions, suggesting the highest level of sp<sup>2</sup>-hybridized carbon of DeACF<sub>10</sub>.

For the peak deconvolution in the range of 800-2000 cm<sup>-1</sup> (**Fig. S2b**), one I-mode and one D'-mode, assigned to the impurities embedding in the graphitic carbon lattice and the stacking defects existing in the graphene layers, respectively, are considered. These peaks were fitted in addition to the D-band, G-band and the band referred to trans-polyacetylene. The minor blue shift of the D-band and the 2D-band of OxACF<sub>10</sub> are related to heteroatoms like O and/or N [7], and more charged defects [5], respectively. This is not unexpected for this type of surface oxidized ACF.

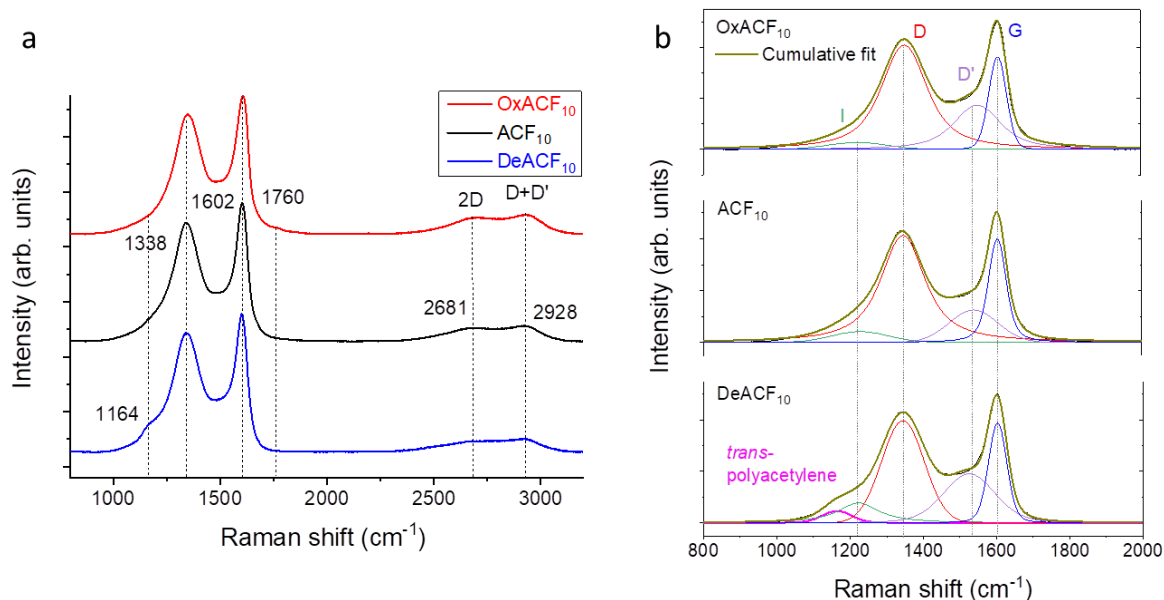


**Fig. S2:** (a) Raman spectra of ACFs and (b) deconvolution of peaks in the range of 800–2000 cm<sup>-1</sup>.

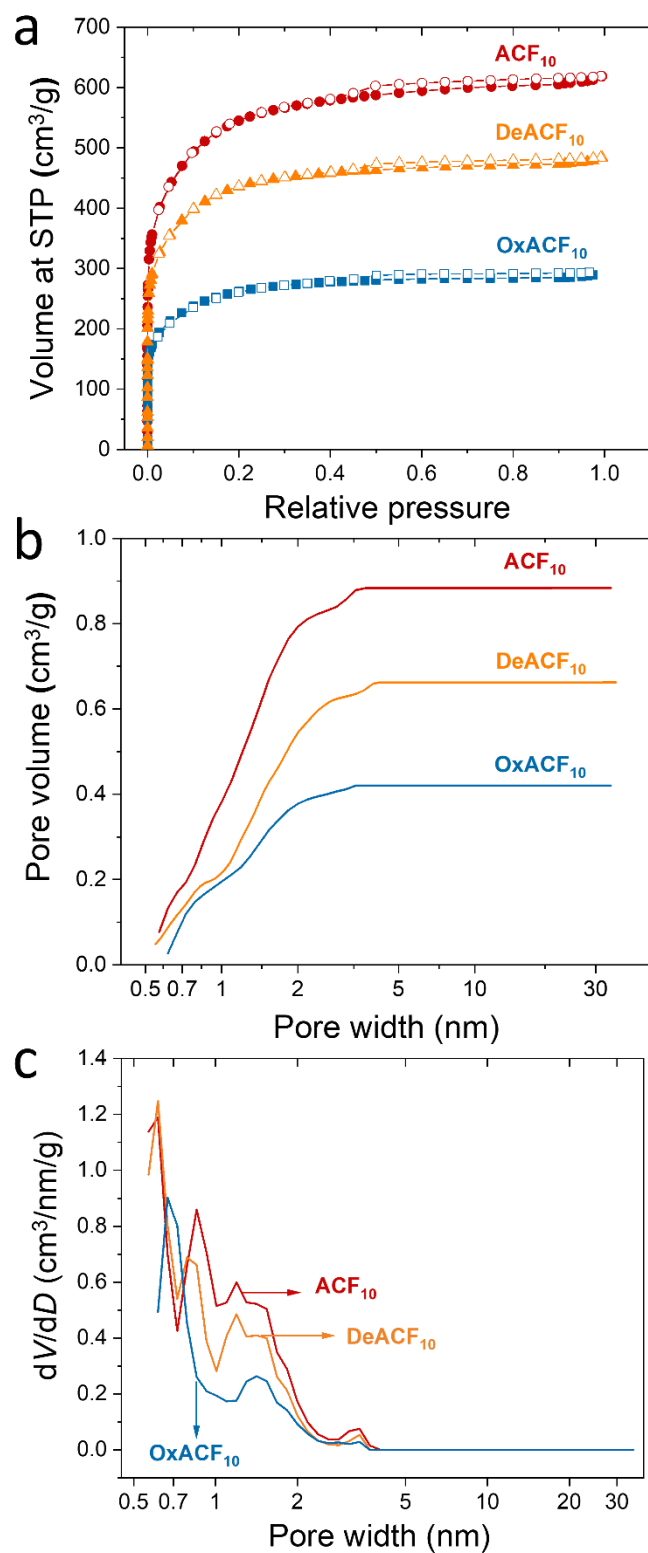


**Fig. S3:** (a) N<sub>2</sub> adsorption (filled points) – desorption (hollow points) isotherms, (b) cumulative and (c) differential pore size distribution fitted by QSDFT method for different ACFs. STP: standard temperature and pressure.



**Table S1:** Chemical properties of different ACFs.

Sample	C (mass%)	H (mass%)	O <sup>a</sup> (mass%) <sup>a</sup>	N (mass%)	CEC (μmol/m <sup>2</sup> )	AEC (μmol/m <sup>2</sup> )	pH <sub>PZC</sub>
ACF <sub>10</sub>	87.7	0.3	9.9	1.8	0.040	0.025	5.7 ± 0.2
DeACF <sub>10</sub>	93.4	0.4	4.3	0.9	≤0.010	0.23	10.2 ± 0.2
OxACF <sub>10</sub>	78.5	0.3	18.1	2.7	1.0	0.0087	2.4 ± 0.1

<sup>a</sup> Calculated according to O mass% = 100% – N mass% – H mass% – C mass% – ash mass%.

Ash contents were weighed as residues after combusting ACFs in O<sub>2</sub> at 750 °C.

**Table S2:** Pore structure of ACFs via nitrogen gas sorption at -196°C.  $V_{\text{micro}, \varnothing = 1-2 \text{ nm}}$  and  $V_{\text{micro}, \varnothing < 1 \text{ nm}}$ : volume of micropores with  $\varnothing = 1-2 \text{ nm}$  and  $\varnothing < 1 \text{ nm}$ ;  $V_{\text{meso}}$ : mesopore volume;  $V_t$ : total pore volume. SSA: specific surface area. QSDFT was applied for analysis.

Sample	SSA (m <sup>2</sup> /g)	$V_t$ (cm <sup>3</sup> /g)	$V_{\text{micro}, \varnothing < 1 \text{ nm}}$ (cm <sup>3</sup> /g)	$V_{\text{micro}, \varnothing = 1-2 \text{ nm}}$ (cm <sup>3</sup> /g)	$V_{\text{meso}}$ (cm <sup>3</sup> /g)
ACF <sub>10</sub>	1700	0.88	0.33	0.44	0.09
DeACF <sub>10</sub>	1400	0.69	0.29	0.33	0.06
OxACF <sub>10</sub>	800	0.42	0.18	0.19	0.05

### **Supporting discussion to Section 3.2 of the main text**

The pore filling extent ( $\varnothing \geq 1 \text{ nm}$ ) in ionic PMOC adsorption on ACFs are calculated as follows. To simplify the calculation, only the pores with  $\varnothing \geq 1 \text{ nm}$  are considered.

Pore filling extent (%)

$$= \frac{q_m \left( \frac{\mu\text{mol}}{\text{m}^2} \right) \cdot \text{SSA} \left( \frac{\text{m}^2}{\text{g}} \right) \cdot \text{molar volume} \left( \frac{\text{cm}^3}{\text{mol}} \right) \cdot 10^{-6} \left( \frac{\text{mol}}{\mu\text{mol}} \right)}{(V_{\text{micro}, \varnothing = 1-2 \text{ nm}} + V_{\text{meso}}) \left( \frac{\text{cm}^3}{\text{g}} \right)} \times 100 (\%)$$

In **Table S3**, the pore filling extents are reported according to the pore volumes and SSAs given in **Table S2**, and  $q_m$  listed in **Table 2** and **Table S4**.

**Table S3:** Molar volumes of selected compounds and their pore filling extents (for  $\varnothing \geq 1$  nm) at  $q_m$  on ACFs. Applied electric potentials are given vs. SHE. References given in brackets.

Compounds	Molar volume (cm <sup>3</sup> /mol)	Pore filling extent (%)	
<i>p</i> -TsOH	130.8 [10]	ACF <sub>10</sub> at 0.2 V	3.8
		ACF <sub>10</sub> at OCP	4.2
		ACF <sub>10</sub> at 0.7 V	5.0
		DeACF <sub>10</sub> at -0.1 V	23.0
		DeACF <sub>10</sub> at OCP	6.1
		DeACF <sub>10</sub> at 0.6 V	4.7
		OxACF <sub>10</sub> at OCP	1.6
TPA <sup>+</sup>	139.8 [11]	ACF <sub>10</sub> at 0.2 V	11.2
		ACF <sub>10</sub> at OCP	6.7
		ACF <sub>10</sub> at 0.7 V	3.6
		DeACF <sub>10</sub> at -0.1 V	24.6
		DeACF <sub>10</sub> at OCP	6.5
		DeACF <sub>10</sub> at 0.6 V	5.0
		OxACF <sub>10</sub> at OCP	12.1

**Fig. S4** shows the electrochemical stability of investigated PMOCs in 10 mM Na<sub>2</sub>SO<sub>4</sub> at pH 7. Since ACFs typically exhibit large capacitive currents as indicated in their CV curves (Fig. 1), any electrochemical redox reaction of PMOCs is much less obvious when using ACF as the working electrode. Therefore, a graphite rod and a piece of boron-doped diamond (BDD) were employed as working electrodes in **Fig. S4a-b**, respectively, to expose any redox reaction of the investigated PMOCs, which could have occurred when the potential was externally applied.

Typically, graphitic carbon contains similar surface chemical properties ( $\pi$  system + O-containing functional groups) to those of DeACF<sub>10</sub> and ACF<sub>10</sub>. As shown in **Fig. S4a**, the redox peak of reversible  $[\text{Fe}(\text{H}_2\text{O})_6]^{2+} \rightleftharpoons [\text{Fe}(\text{H}_2\text{O})_6]^{3+} + e^-$  in the system containing (NH<sub>4</sub>)<sub>2</sub>Fe(SO<sub>4</sub>)<sub>2</sub>·6H<sub>2</sub>O was observed around 0.65 V vs. SHE, close to what was previously reported on a glassy carbon working electrode [12]. In the presence of TPA<sup>+</sup>, *p*-TsO<sup>-</sup>, BTMA<sup>+</sup>,

or *p*-TSA, the electrochemical measurement cell was protected by N<sub>2</sub> flow above the electrolyte surface. No signals indicating redox reactions of PMOCs were observed. When probing CV for the MTBE-containing system, the N<sub>2</sub> purging was abandoned to avoid MTBE loss during the measurement. Comparing the cyclic voltammograms in the presence of MTBE to the one obtained from the pure background solution without N<sub>2</sub> purging, the signal that appeared below 0.1 V vs. SHE may relate to O<sub>2</sub> reduction rather than any redox reaction related to MTBE.

BDD electrode is well-known for its exceptionally low background current and superior O<sub>2</sub> overpotential [13], thus suitable for the study of the electrochemical stability of selected PMOCs at high positive bias potentials. As shown in **Fig. S4b**, *p*-TSA is the most vulnerable candidate among the probed PMOCs upon electrochemical oxidation. Still, a very high external potential bias at 2.1 V vs. SHE is required to trigger its oxidation on BDD.

The CV results in **Fig. S4** deliver an overall message: all selected sorbate molecules in this study are robust against electrochemical redox reactions and can serve as reliable targets for investigating electro-assisted manipulation of PMOC adsorption.

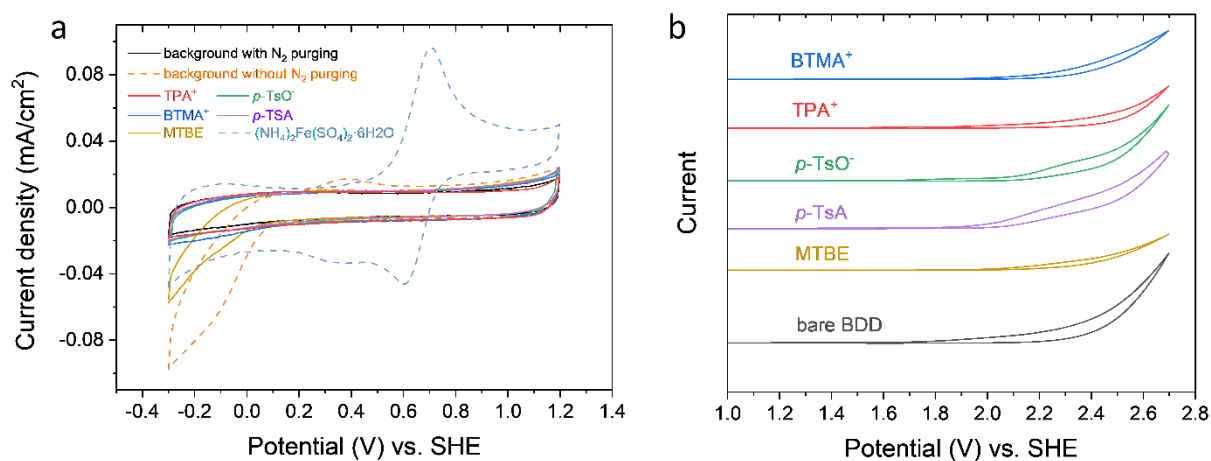


**Fig. S4:** Cyclic voltammograms obtained in aqueous 10 mM Na<sub>2</sub>SO<sub>4</sub> at pH 7 using (a) a graphite rod and (b) a piece of BDD electrode as the working electrode. Scan rate: 5 mV/s. For systems containing PMOCs or (NH<sub>4</sub>)<sub>2</sub>Fe(SO<sub>4</sub>)<sub>2</sub>·6H<sub>2</sub>O, at least 2 mM solute (final concentration) was given before the measurement. N<sub>2</sub> purging above the electrolyte solution was applied during CV measurements except for MTBE-containing systems.

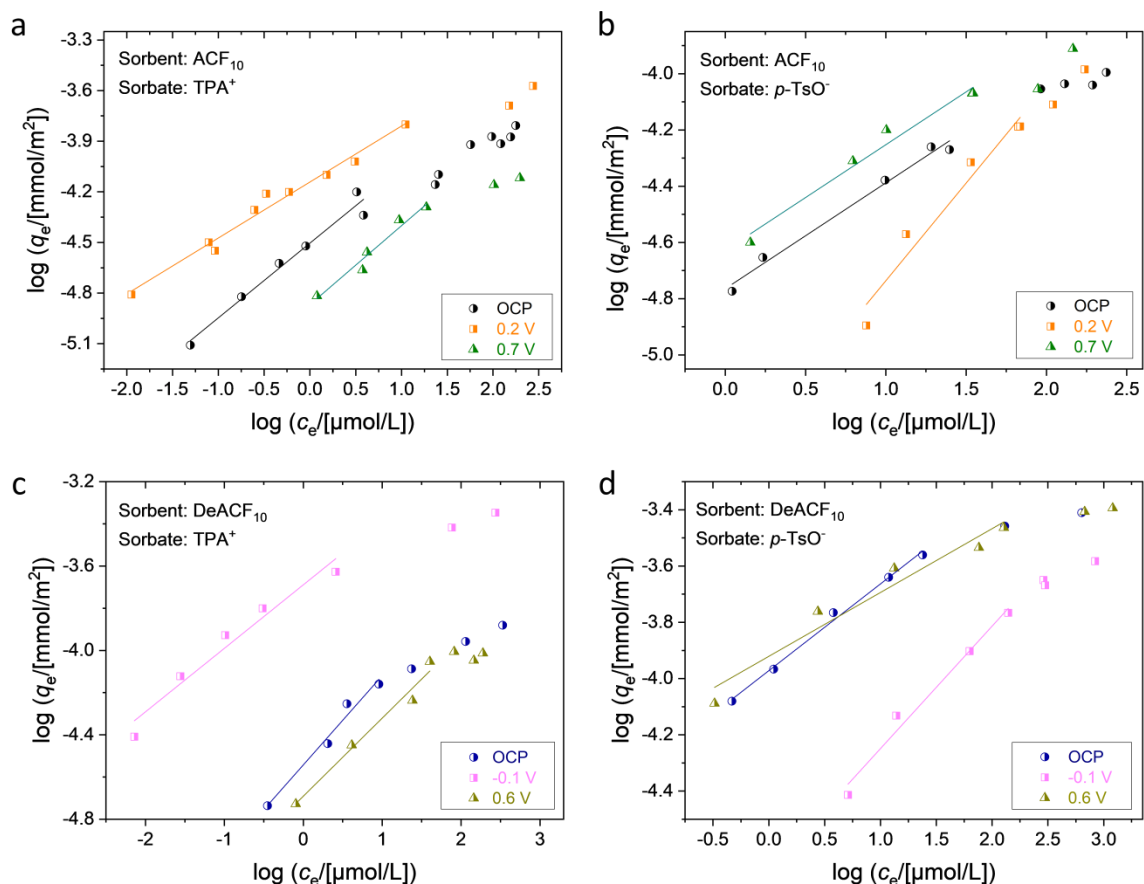


**Fig. S5:** Freundlich isotherm fitting of electrosorption data at pH 7 in aqueous 10 mM Na<sub>2</sub>SO<sub>4</sub> solution. Only data points away from the maximal loadings were applied for the linear fittings. Potentials are given vs. SHE.

Fitting according to the Freundlich equation was only applied for the low concentration range, as this empirical model generally cannot adequately describe the region approaching the maximum loading of an adsorbent. Nevertheless, as PMOCs frequently need to be treated at trace level concentrations, the Freundlich isotherm model is still valuable and a commonly applied approach. To determine maximum loadings of the adsorbates we applied the Langmuir isotherm model (**Fig. S6**).

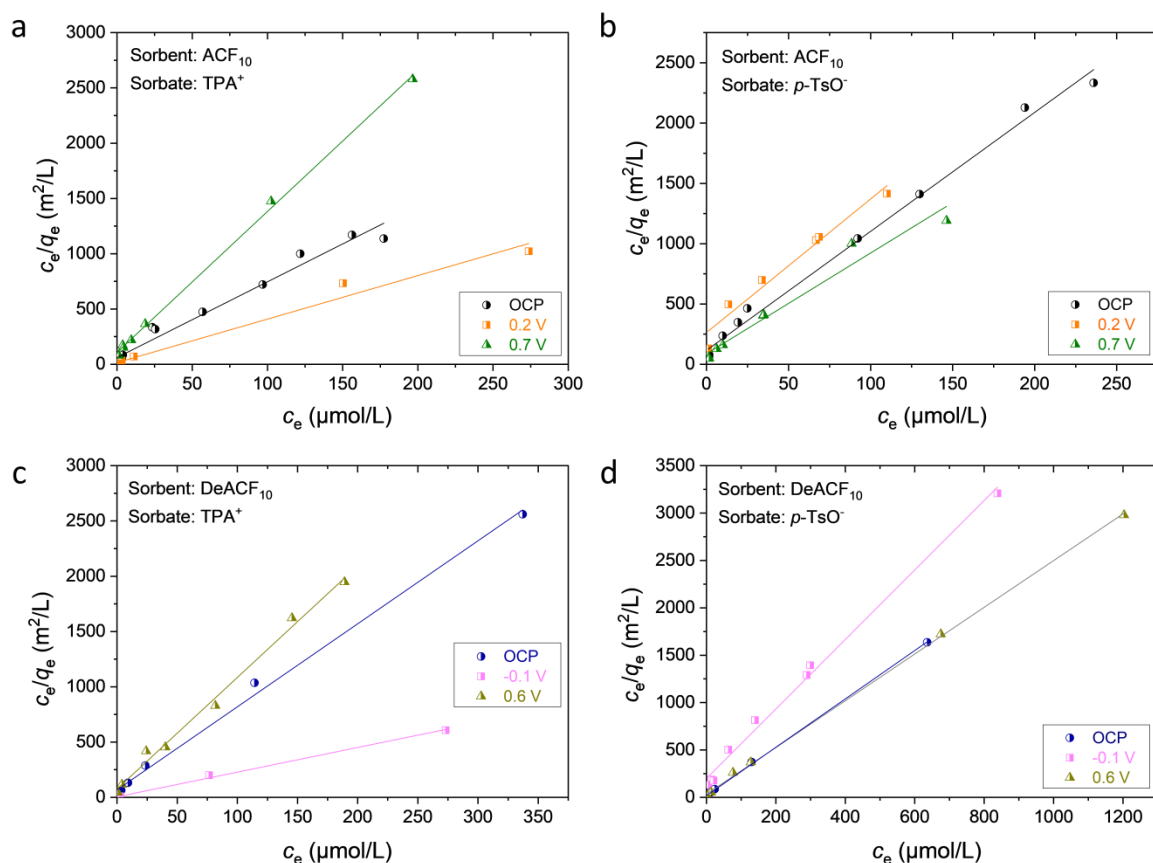


**Fig. S6:** Langmuir isotherm fittings of electrosorption data at pH 7 in 10 mM Na<sub>2</sub>SO<sub>4</sub> solution. Potentials are given vs. SHE.

### Supporting discussion to Section 3.3 of the main text

We investigated in our previous study [4] the adsorption behavior of selected polar PMOCs on ACFs carrying different surface chemistries. Wet oxidation in HNO<sub>3</sub> was used to generate OxACF<sub>10</sub> from pristine ACF<sub>10</sub> (chemical properties shown in **Table S1**). The adsorption isotherms for TPA<sup>+</sup> and *p*-TsO<sup>-</sup> and their Freundlich and Langmuir fittings on three ACFs at OCP are shown in **Fig. S7-S8** with fitting parameters summarized in **Table S4**. Wet oxidation, a common strategy to introduce negatively charged sites on the adsorbent surface for attracting cationic adsorbates electrostatically, causes a decline in surface hydrophobicity and thus sacrifices the preferable non-Coulombic interactions between TPA<sup>+</sup> and ACF compared to water. Overall, sorbent surface chemical modification is less effective than applying cathodic potentials in improving ACF's sorption affinity towards TPA<sup>+</sup>. For anionic *p*-TsO<sup>-</sup>, surface oxidation led to electrostatic repulsion between *p*-TsO<sup>-</sup> and ACF while diminishing the hydrophobic effect and/or  $\pi$ - $\pi$  interactions. On the contrary, a

defunctionalized AC surface promotes both the hydrophobic effect and the electrostatic attraction and thereby leads to a significantly improved sorption affinity to  $p$ -TsO $^-$ . Overall, sorbent surface chemical modification affects more intensively ACF's sorption affinity towards  $p$ -TsO $^-$  compared to applying anodic potentials in the studied range.

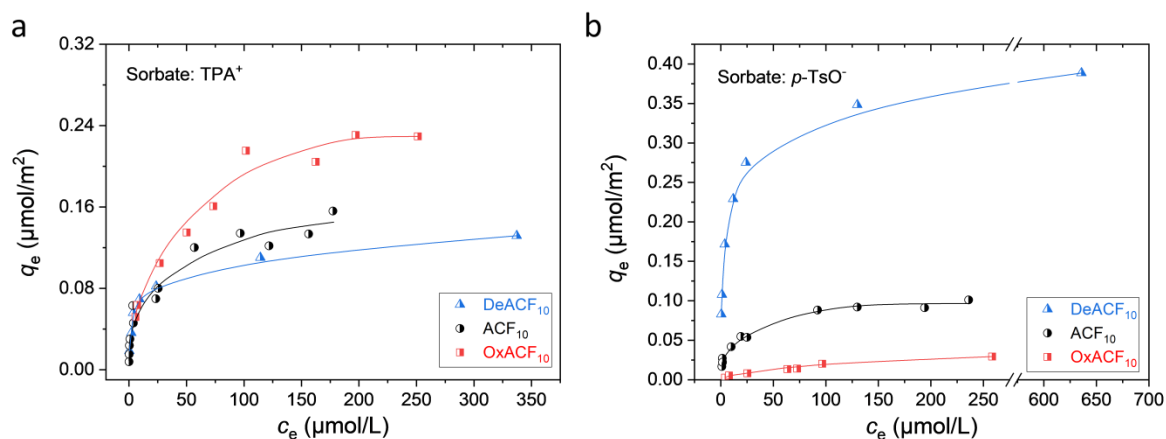


**Fig. S7:** Adsorption isotherms obtained at OCP (i.e., without external potential) for ACFs. Lines serve as guides for the eye.

**Table S4:** Freundlich and Langmuir isotherm parameters for adsorption of TPA $^+$  and  $p$ -TsO $^-$  on ACFs at pH 7 in 10 mM Na $_2$ SO $_4$ .

Sorbate	ACF sorbent	Freundlich			Langmuir		
		$K_F$ [( $\mu\text{mol}/\text{m}^2$ )/( $\mu\text{mol}/\text{L}$ ) $^n$ ]	$n$	$R^2$	$q_m$ [ $\mu\text{mol}/\text{m}^2$ ]	$K_L$ [L/ $\mu\text{mol}$ ]	$R^2$
TPA $^+$	DeACF $_{10}$	0.029	0.43	0.977	0.13	0.11	0.996
	ACF $_{10}$	0.031	0.44	0.970	0.15	0.11	0.974
	OxACF $_{10}$	0.026	0.42	0.995	0.26	0.031	0.986
$p$ -TsO $^-$	DeACF $_{10}$	0.11	0.31	0.994	0.39	0.14	1.000
	ACF $_{10}$	0.017	0.38	0.988	0.10	0.084	0.993
	OxACF $_{10}$	0.0014	0.57	0.970	0.036	0.013	0.916

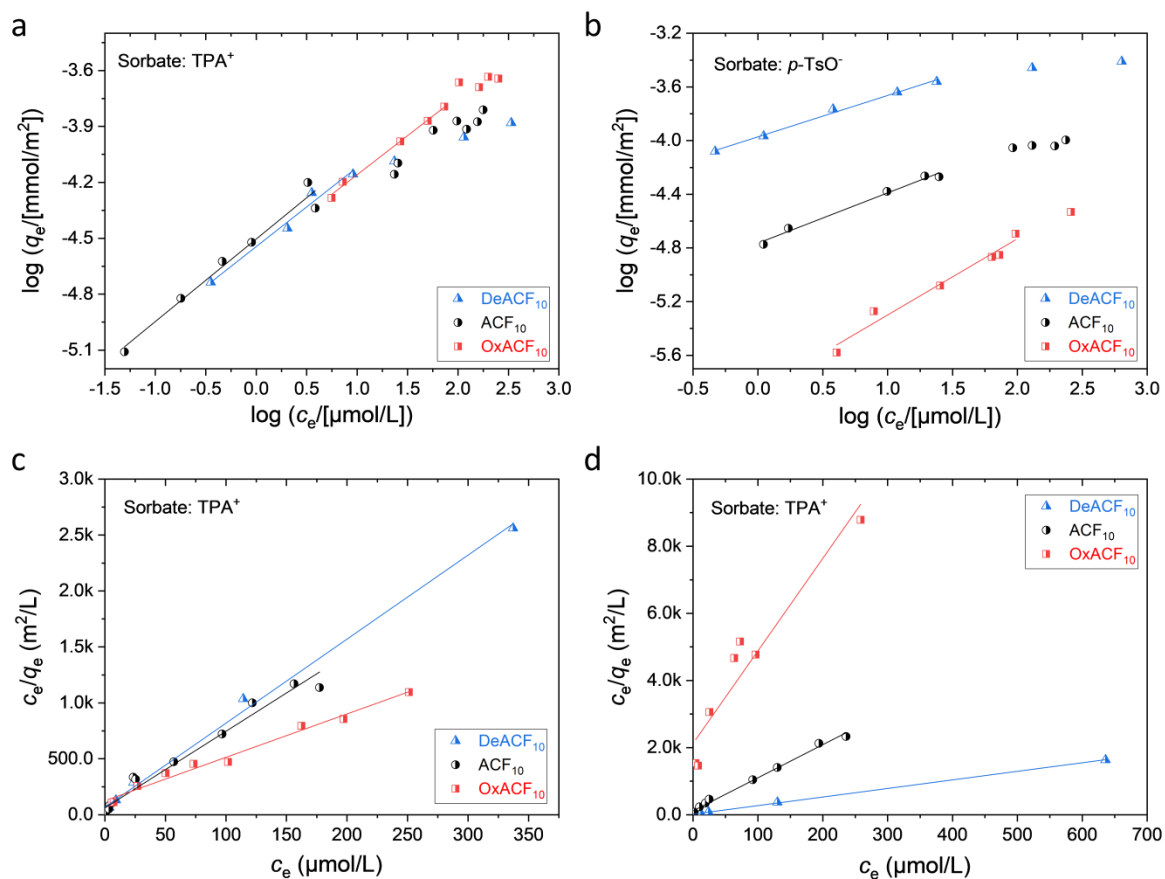


**Fig. S8:** Freundlich isotherm fittings of (a) TPA<sup>+</sup> and (b) *p*-TsO<sup>-</sup> adsorption on different ACFs; Langmuir isotherm fittings of (c) TPA<sup>+</sup> and (d) *p*-TsO<sup>-</sup> adsorption on different ACFs. Isotherms were determined at pH 7 in 10 mM Na<sub>2</sub>SO<sub>4</sub> solution. Only data points away from the maximal loadings were applied for the Freundlich linear fittings.

### Supporting information to Section 3.4 of the main text

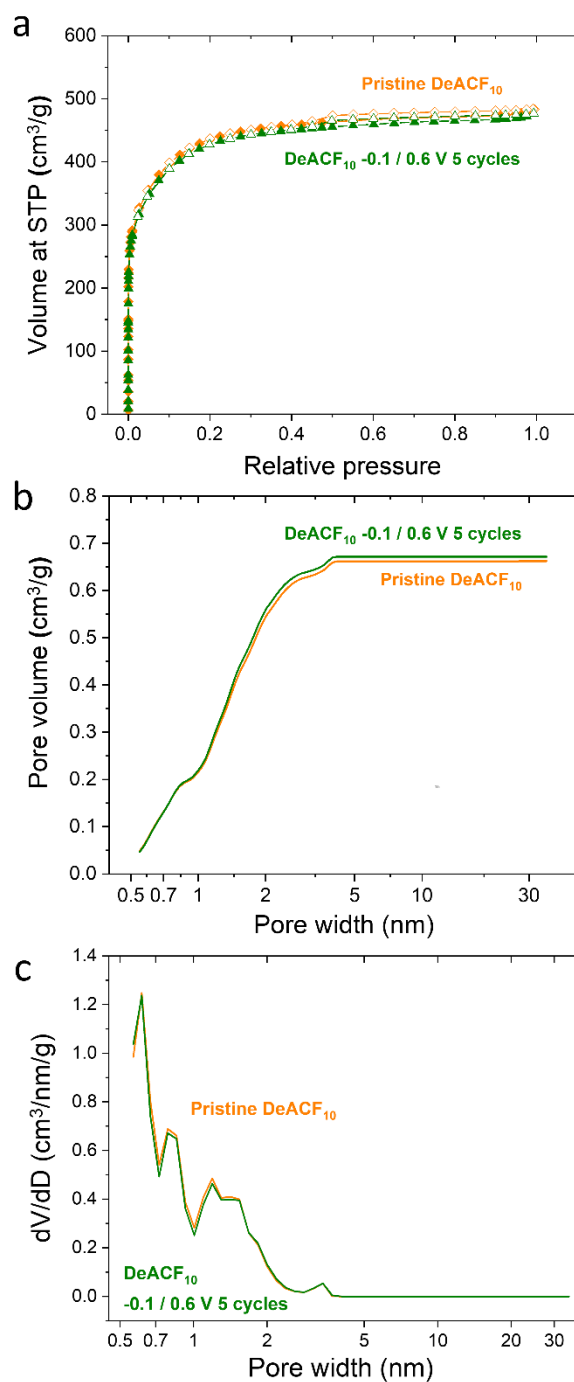


**Fig. S9:** (a) N<sub>2</sub> adsorption (filled points) – desorption (hollow points) isotherms measured at -196 °C, (b) cumulative and (c) differential pore size distribution fitted by QSDFT and assuming slip-shaped pore for pristine DeACF<sub>10</sub> and DeACF<sub>10</sub> after charging at -0.1 / 0.6 V vs. SHE for 5 cycles.



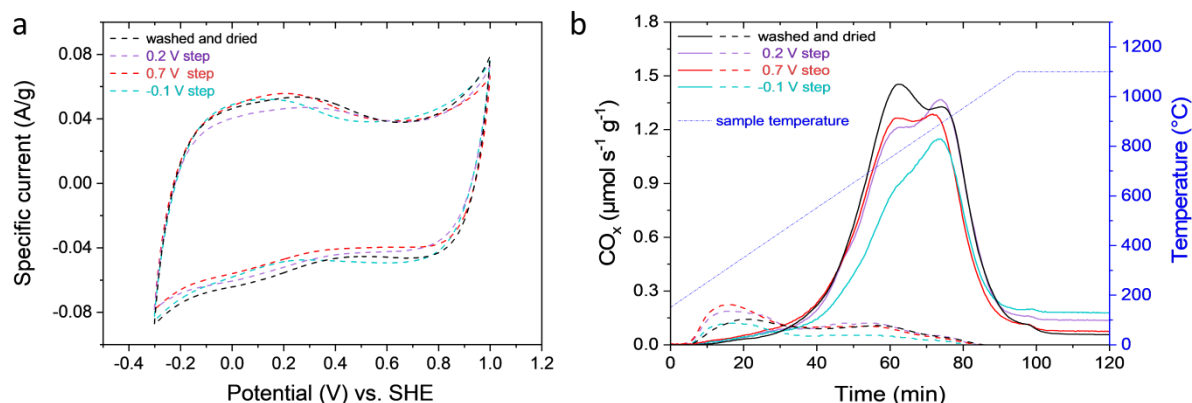


**Fig. S10:** (a) Cyclic voltammograms and (b) TPD measurements of ACF<sub>10</sub> after treating under different conditions. CV was performed in 10 mM Na<sub>2</sub>SO<sub>4</sub> at 0.5 mV/s. A typical deviation of the V-shape region from triplet measurements is  $\pm 25$  mV. In (b), solid and dashed lines represent the CO and CO<sub>2</sub> desorption profiles, respectively. Potentials are given vs. SHE.

The characteristic CO and CO<sub>2</sub> release during the TPD measurement happens at  $T \leq 1100$  °C. A cut-off at  $t = 85$  min was applied for the quantitative comparison of O mass% of ACF samples given in **Table S5** to minimize the influence of long tailings (**Fig. S11**). Such tailings might arise from reactions of AC with oxygen traces in the carrier gas flow. Insignificant changes in the cyclic voltammograms and TPD profiles (as well as O mass%) were observed for ACF<sub>10</sub> samples polarized at 0.2 V and 0.7 V vs. SHE for 72 h compared to the washed-and-dried-only sample. This indicates sufficient stability of ACF<sub>10</sub> in its potential window, that is, from 0.2 V to 0.7 V vs. SHE, defined by its cyclic voltammogram curve in **Fig. 1**. However, after polarizing at -0.1 V vs. SHE for 72 h, the V-shape region of ACF<sub>10</sub> shifted by -120 mV, and the O mass% was decreased by 30% compared to the washed-and-dried only sample.

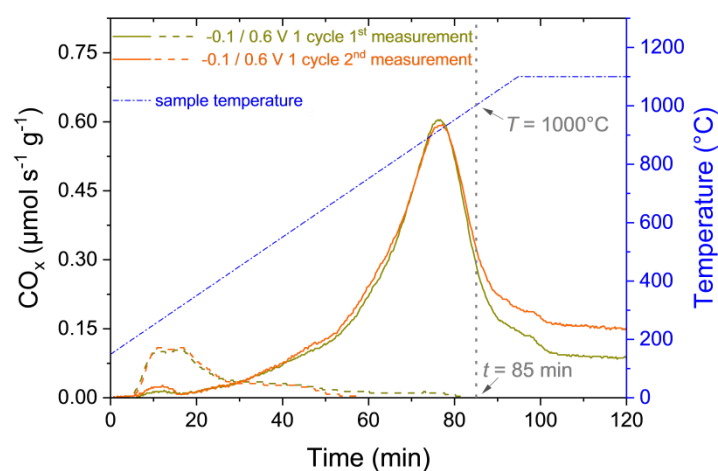


**Fig. S11:** Example of two TPD measurements of the same DeACF<sub>10</sub> sample. Solid and dashed lines represent the CO and CO<sub>2</sub> desorption profiles, respectively. The most noticeable difference lies in the tailing at  $t \geq 85$  min. The difference of the rest TPD profiles is within the typical error range as given in **Table S5**. Potentials are given vs. SHE.

**Table S5:** O mass% of ACFs in terms of released CO and CO<sub>2</sub> derived from TPD profiles. A cut-off at  $t = 85$  min was applied when calculating the O mass% from CO.

ACF type	Conditions (vs. SHE)	O mass% from CO	O mass% from CO <sub>2</sub>	Total O mass%
DeACF <sub>10</sub>	washed and dried	1.31 ± 0.03	0.41 ± 0.04	1.71 ± 0.07
	-0.1 V step	1.23 ± 0.02	0.47 ± 0.05	1.70 ± 0.07
	0.6 V step	1.56 ± 0.03	0.35 ± 0.04	1.91 ± 0.07
	-0.1 / 0.6 V 1 cycle	1.39 ± 0.03	0.51 ± 0.05	1.90 ± 0.08
	-0.1 / 0.6 V 5 cycles	1.72 ± 0.03	0.84 ± 0.08	2.56 ± 0.11
	OCP / -0.1 V 5 cycles	1.30 ± 0.03	0.35 ± 0.04	1.65 ± 0.07
ACF <sub>10</sub>	washed and dried	4.47 ± 0.09	1.30 ± 0.13	5.77 ± 0.22
	0.2 V step	4.16 ± 0.08	1.57 ± 0.16	5.73 ± 0.24
	0.7 V step	4.06 ± 0.08	1.57 ± 0.16	5.64 ± 0.24
	-0.1 V step	3.18 ± 0.06	0.85 ± 0.09	4.03 ± 0.15

## References

- [1] N. Saeidi, F.-D. Kopinke, A. Georgi, Understanding the effect of carbon surface chemistry on adsorption of perfluorinated alkyl substances, *Chem. Eng. J.* 381 (2020) 122689. <https://doi.org/10.1016/j.cej.2019.122689>.
- [2] L.W. Zelazny, L. He, A. Vanwormhoudt, Charge analysis of soils and anion exchange, *Methods of soil analysis: Part 3 chemical methods*, 5.3, Soil Science Society of America, Inc., American Society of Agronomy, Inc., Madison, 1996, pp. 1231-1253. <https://doi.org/10.2136/sssabookser5.3.c41>.
- [3] N. Saeidi, F.-D. Kopinke, A. Georgi, Controlling adsorption of perfluoroalkyl acids on activated carbon felt by means of electrical potentials, *Chem. Eng. J.* 416 (2021) 129070. <https://doi.org/10.1016/j.cej.2021.129070>.
- [4] J. Zhou, N. Saeidi, L.Y. Wick, F.-D. Kopinke, A. Georgi, Adsorption of polar and ionic organic compounds on activated carbon: surface chemistry matters, *Sci. Total Environ.* (2021) 148508. <https://doi.org/10.1016/j.scitotenv.2021.148508>.
- [5] T. Milenov, I. Avramova, Deposition of graphene by sublimation of pyrolytic carbon, *Opt. Quant. Electron* 47 (2015) 851-863. <http://doi.org/10.1007/s11082-014-0015-z>.
- [6] A.K. dos Santos Poli, R.B. Hilário, A.M. Gama, M.R. Baldan, E.S. Gonçalves, Influence of heat treatment temperature of carbon fiber felt substrate on polyaniline electrosynthesis and its properties, *J. Solid State Electrochem.* 23 (2019) 33-52. <http://doi.org/10.1007/s10008-018-4107-8>.
- [7] W. Chen, X. Zhou, S. Shi, N. Thiphuong, M. Chen, Synergistical enhancement of the electrochemical properties of lignin-based activated carbon using NH<sub>3</sub>-H<sub>2</sub>O dielectric barrier discharge plasma, *RSC Adv.* 7 (2017) 7392-7400. <http://doi.org/10.1039/C6RA26010A>.
- [8] H. Zhao, L. Qian, Y. Chen, Q. Wang, G. Zhao, Selective catalytic two-electron O<sub>2</sub> reduction for onsite efficient oxidation reaction in heterogeneous electro-Fenton process, *Chem. Eng. J.* 332 (2018) 486-498. <https://doi.org/10.1016/j.cej.2017.09.093>.
- [9] T. Oshiro, M. Yamazato, A. Higa, M. Toguchi, Raman Analysis of trans-Polyacetylene Chains in Hydrogenated Amorphous Carbon Films, *Jpn. J. Appl. Phys* 46 (2007) 756-760. <http://doi.org/10.1143/jjap.46.756>.
- [10] S.K. Arora, M. Sundaralingam, The crystal and molecular structure of 4-methyl sulfonic acid (p-toluenesulfonic acid) monohydrate, C<sub>7</sub>H<sub>8</sub>SO<sub>3</sub>·H<sub>3</sub>O<sup>+</sup>, an oxonium salt, *Acta Crystallogr., Sect. B* 27 (1971) 1293-1298. <https://doi.org/10.1107/S0567740871003893>.
- [11] ChemAxon online platform, <https://chemicalize.com>, (accessed 11 June 2021).
- [12] K. Hawthorne, J. Wainright, R. Savinell, Studies of Iron-Ligand Complexes for an All-Iron Flow Battery Application, *J. Electrochem. Soc.* 161 (2014) A1662-A1671. <http://doi.org/10.1149/2.0761410jes>.
- [13] N. Bensalah, S. Dbira, A. Bedoui, M.I. Ahmad, Electrolytic Oxidation as a Sustainable Method to Transform Urine into Nutrients, *Processes* 8 (2020). <https://doi.org/10.3390/pr8040460>.

### 3.3 Efficient removal of trifluoroacetic acid from water using surface-modified activated carbon and electro-assisted desorption

Jieying Zhou<sup>a</sup>, Navid Saeidi<sup>a</sup>, Lukas Y. Wick<sup>b</sup>, Yanlin Xie<sup>a</sup>, Frank-Dieter Kopinke<sup>a</sup>, Anett Georgi<sup>a\*</sup>

<sup>a</sup>*Helmholtz Centre for Environmental Research – UFZ, Department of Environmental Engineering, 04318 Leipzig, Germany*

<sup>b</sup>*Helmholtz Centre for Environmental Research – UFZ, Department of Environmental Microbiology, D-04318 Leipzig, Germany*

#### Abstract

Trifluoroacetic acid (TFA) is defined as a very persistent, very mobile substance (vPvM) with potential toxicity, which causes increasing environmental concerns worldwide. Conventional wastewater treatment strategies are inefficient for selective TFA removal in the presence of co-existing inorganic anions. Herein, surface defunctionalized activated carbon felt (DeACF) carrying anion exchange sites exhibits an outstanding adsorption efficiency towards TFA ( $q_{\max} = 30 \text{ mg/g}$ ,  $K_d = (840 \pm 80) \text{ L/kg}$  at  $c_{\text{TFA}} = 3.4 \text{ mg/L}$ ) in tap water thanks to introduced electrostatic attraction and enhanced interactions between  $\text{CF}_3$  moieties and hydrophobic carbon surface. A time-lapse flow unit test demonstrated a clearly favored TFA uptake by DeACF from tap water over  $\text{Cl}^-$  and  $\text{SO}_4^{2-}$  but a remarkable co-adsorption of inorganic water contaminant  $\text{NO}_3^-$ . Electro-assisted TFA desorption using 10 mM  $\text{Na}_2\text{SO}_4$  as electrolyte and oxidized ACF as anode showed high recoveries of  $\geq 87\%$  at low cell voltages ( $< 1.1 \text{ V}$ ). Despite an initial decrease in TFA adsorption capacity (by 33%) after the 1<sup>st</sup> ad-/desorption cycle caused by the surface oxidation of DeACF, the system stability was fully maintained over the next 4 cycles. The electro-assisted trap&release approach for TFA removal using DeACF can inspire future treatment strategies for water containing emerging, charged organic micropollutants.

**Keywords:** trifluoroacetic acid; electrosorption; activated carbon; surface modification

## 1. Introduction

Trifluoroacetic acid (TFA) belongs to the family of perfluoroalkyl acids (PFAA), which are causing increasing attention in recent years due to their global detection in various aquatic systems and potential threat to environmental and human health [1]. Being a strong organic acid with  $pK_a = 0.23$  [2], TFA predominantly exists in the anionic form in water. It is the shortest-chain (also called ultra-short-chain) and most mobile PFAA in water with an estimated organic carbon-water partition coefficient  $\log D$  in the range of -0.6 to -3.4 at neutral pH [3, 4]. TFA has been detected worldwide in rain and snow samples up to the  $\mu\text{g/L}$  range [4], and in Swiss and German rivers between 0.01 – 0.63  $\mu\text{g/L}$  [5-7]. A risk in TFA accumulation exists particularly in terminal water bodies with elevated evaporation degrees [8, 9].

In the recent guidelines text 127/2019 from German Federal Environment Agency, TFA is classified in the category of very persistent, very mobile substances (vPvM) with potential toxicity [3]. Taking into account additionally its high emission likelihood according to REACH registration (100-1000 t per year to the European Economic Area alone) [10], TFA can be especially hazardous to drinking water sources. A large-scale incident in 2016 in Germany reported the detection of TFA concentrations higher than 20  $\mu\text{g/L}$  in the tap water obtained by bank filtration from river Neckar (Germany) containing >100  $\mu\text{g/L}$  TFA caused by an industrial discharge located 300 km away [4]. This case shows how mobile TFA can be in surface water and how it readily slips through the state-of-the-art water treatment barriers. As one of the “substances from multiple sources (SMS)” [11], TFA is also found in natural marine sources [12], and the transformation products of various chemical products including many pesticides and pharmaceuticals bearing  $\text{CF}_3$  groups in their structure. It can also be produced by atmospheric degradation of refrigerant emissions [13] and released from fluoropolymers upon heating [14, 15]. It can even be generated in wastewater treatment plants during ozonation due to degradation of polyfluoroalkyl substances [11].

Most of the conventional water treatment techniques are inefficient for TFA removal and/or need to be upgraded. Among them, ion exchange favors the removal of co-existing inorganic ions including  $\text{Cl}^-$ ,  $\text{SO}_4^{2-}$  and  $\text{NO}_3^-$  while achieving merely a partial removal of TFA [4]. Reverse osmosis is proven to be effective to remove TFA from wastewater. Nevertheless, the selectivity for TFA versus divalent ions was found to be less satisfying [4]. Although Scheurer

et al. [4] observed a rapid breakthrough of TFA on a small-scale fixed bed of granular activated carbon (GAC), Sun et al. [16, 17] lately developed two types of surface modified AC, quaternary nitrogen-grafted and polypyrrole-grafted, showing encouraging TFA adsorption performance with maximal loadings of about 30 mg/g in the absence of inorganic ions. Regarding degradation methods, TFA is reluctant to biodegradation [2, 3, 18], ozonation and chlorination [4, 19] due to its strong C-F bonds. It was found, however, to be effectively degraded by sulfate radicals [20], via electrochemical oxidation on boron-doped diamond (BDD) electrodes [21], and homogeneous photocatalytic degradation involving specially designed photocatalysts under very acidic conditions [22] .

Recent research has demonstrated the potential of electro-assisted ad-/desorption using AC adsorbents (electro-assisted trap&release approach) for removal of ionic organic compounds [23, 24]. By utilizing the distinct adsorption efficiencies of AC towards charged organic compounds achievable at different external bias potential, the targeted compounds can be effectively pre-enriched for the next-step treatment in a controllable manner while the AC adsorbent is simultaneously *in-situ* regenerated. Our previous study [23] estimated high enrichment factors of  $\geq 40$  for perfluorooctanoic acid (PFOA) in fixed-bed setups derived from the Freundlich parameters obtained in batch electrosorption experiments. It is thus highly interesting to test the concept in real continuous flow mode as well as for shorter-chain PFAAs.

In this work, we modified commercially available activated carbon felts (ACFs) to form a largely defunctionalized surface for an effective, specific adsorption of TFA. As poor selectivity against co-existing inorganic anions was previously reported in ion-exchange and reverse osmosis of TFA, it is crucial to check whether it remains an obstacle for AC adsorption as well. We thus applied various salt solutions containing  $\text{Cl}^-$ ,  $\text{SO}_4^{2-}$  and  $\text{NO}_3^-$  as well as tap water to measure the effect of co-existing anions and ionic strength on TFA adsorption. In addition, a rapid small scale test using a continuous flow unit was performed to study (i) the efficiency of dynamic TFA uptake on AC from tap water and (ii) the resulting ion selectivity.

Electro-assisted desorption of TFA for adsorbent regeneration was tested for the first time using a 10 mM  $\text{Na}_2\text{SO}_4$  eluent *in-situ*, that is, in the same flow unit employed in the previous adsorption step. The applied three-electrode flow cell has a one-channel design, where

surface-defunctionalized ACF (DeACF) was employed as the cathode (and adsorbent). For use as anode material an oxidized ACF (OxACF) with high density of surface O-containing groups was prepared. By this means, TFA uptake on the anode is effectively prevented even at elevated potentials (e.g. +0.8 V vs. Ag/AgCl). This is an important prerequisite for a complete TFA recovery in the electro-desorption step, which eliminates the need for additional ion-exchange membranes in the flow unit. Meanwhile, using OxACF with high specific surface area (800 m<sup>2</sup>/g) as the anode allowed low cell voltages (<1.1 V) below the water splitting potential [25] in this membrane-free system under the tested desorption conditions. Our cell design is conceptionally similar to the inverted capacitive deionization (i-CDI) used in water desalination, where less performance decline is expected upon electrode charging during the desorption step [26, 27]. The effects of bias potentials and flow rates on recovery and enrichment factors in the desorption steps are investigated. Five successive ad-/desorption cycles were performed to verify the system stability while the changes in the chemical and electrochemical properties of DeACF were examined.

## **2. Experimental Section**

### **2.1 Chemicals**

TFA (≥99.0%) was purchased from Fluka. Na<sub>2</sub>SO<sub>4</sub> (99%), NaNO<sub>3</sub> (>99%), KCl (>99%), HNO<sub>3</sub> (65%), NaOH (99%), H<sub>2</sub>SO<sub>4</sub> (0.5 M) and HCl (37%) were obtained from Merck. NaF (≥99%) was purchased from Sigma Aldrich. Methanol (MeOH, >99.95%) and 2-propanol (i-PrOH, ≥99.9%) were purchased from Th. Geyer.

### **2.2 Materials**

Actitex-FC1001 (Jacobi CARBONS) was pre-treated and further modified according to the procedures reported previously [28]. Briefly, the pristine ACF (0.8 g) was washed first with *i*-PrOH (300 mL) and then 5 times with H<sub>2</sub>O (300 mL) under shaking (each 30 min, 120 rpm), then air-dried at 80°C overnight before further treatments. To form surface defunctionalized ACF (labeled as DeACF), ACF (0.4 g) was placed in a tubular quartz oven (length: 40 cm, Ø: 2 cm) and heated from room temperature to 900°C (150 °C/min) in a H<sub>2</sub>/N<sub>2</sub> flow (1:10 volume ratio, 40 mL/min). The sample was kept at 900°C for 2 h. After that, the oven was cooled down below 500°C with H<sub>2</sub>/N<sub>2</sub> provided, and then to  $T < 100^{\circ}\text{C}$  in the pure N<sub>2</sub> flow. To prepare surface oxidized ACF (labeled as OxACF), ACF (1.0 g) was heated at 95°C for 6 h in

5 M HNO<sub>3</sub> (120 mL). After that, the sample was washed with H<sub>2</sub>O (300 mL) at 60°C for 5 times under shaking (each 30 min, 120 rpm). In the final washing step, the solution pH was close to 6. The sample was then air-dried at 50°C overnight before use.

### **2.3 Material characterization**

The specific surface area (SSA) of ACFs was determined by using BELSORP MINI (BEL Japan Ltd.) under N<sub>2</sub> at -196°C with samples pretreated at 100°C. A CHN analyzer (LECO TruSpec CHN) was applied for elemental analysis.

Temperature-programmed decomposition (TPD) measurements were accomplished using a BELCAT-B chemisorption analyzer (BEL) coupled with an IR detector (SAXON Junkalor). ACF samples were first pretreated in Ar at 150°C for 30 min, then heated up to 1100°C (50 mL/min N<sub>2</sub>, 10°C/min). The CO and CO<sub>2</sub> released from thermally unstable surface groups upon heating were detected by IR.

X-ray photoelectron spectroscopy (XPS) measurements were done using an Axis Ultra photoelectron spectrometer (Kratos Analytical Ltd.) equipped with a monochromatized Al K $\alpha$  radiation ( $h\nu = 1486.6$  eV). The binding energy was determined by referring all signals to the main C1s component at 284.8 eV.

Procedures reported in [29] were used to measure anion and cation exchange capacities (AEC and CEC). More details are described in the *Supporting Information*. Our previous work [24, 28] additionally reported the characterization results of ACFs by means of Raman spectroscopy and X-ray photoelectron spectroscopy.

Cyclic voltammetry (CV) was performed with a multi-channel potentiostat MSX-8 (ScioSpec) in 300 mL flask equipped with a working electrode, an reference Ag/AgCl sat. KCl electrode and a helix Pt counter electrode in 10 mM or 1 M Na<sub>2</sub>SO<sub>4</sub> electrolyte solution. The working electrode was either an ACF piece connected to a Pt wire or a graphite stick, or a piece of boron-doped diamond electrode (Condias). The solution was pre-purged with N<sub>2</sub> under stirring (300 rpm) for 15 min, and the system was kept under N<sub>2</sub> atmosphere throughout the measurement. Potential values are given always converted vs. the Ag/AgCl sat. KCl electrode in the following text unless specified.



## 2.4 Batch adsorption experiments

Batch adsorption experiments without external potentials applied were performed in 20 mL vials, whereas electrosorption experiments (including the ones at open circuit potential, OCP) employed three-electrode cells as described for CV. In both cases, ACFs were pre-wetted in different electrolyte solutions, shaking at 120 rpm overnight. The solution pH was adjusted to  $7.0 \pm 0.3$  using 0.1 M NaOH and acid which produces the same anion as the electrolyte solution does, or HCl for deionized (DI) water and tap water background (containing 0.021 mM  $\text{NO}_3^-$ , 1.1 mM  $\text{SO}_4^{2-}$  and 2.7 mM  $\text{Cl}^-$  after pH adjustment). The OCP of DeACF was measured to be  $(290 \pm 10)$  mV in 1 mM and 10 mM  $\text{Na}_2\text{SO}_4$  at pH 7. Then, TFA stock solution, neutralized beforehand, was added to form initial concentrations in the range of 5-200 mg/L. For electrosorption experiments, the ACF was first charged at desired potentials for 24 h under  $\text{N}_2$  (water-saturated) purging of the cell and the water phase was neutralized to pH =  $7.0 \pm 0.3$  before the addition of TFA stock solutions. After 48 h adsorption with daily pH control, aliquots were taken with syringe filters (Labsolute, 0.22  $\mu\text{m}$ , cellulose acetate) for measurement of aqueous phase TFA concentrations performed by ion chromatography (IC, Dionex). Adsorption kinetics study given in *Supporting Information, Fig. S1* confirmed the approach to adsorption equilibrium within 48 h. To determine the single point adsorption coefficients  $K_d$  (definition see **Section 2.7**) of TFA on DeACF in 10 mM  $\text{Na}_2\text{SO}_4$  at bias potentials of -0.1 and -0.3 V vs. Ag/AgCl where adsorption efficiency was very low, adsorbed TFA was determined directly by extraction of the adsorbent. The loaded samples after 48 h adsorption were extracted by a mixture of MeOH : 10 mM NaOH = 1:1 (v:v) at room temperature overnight with shaking (120 rpm). 1 mL supernatant after centrifugation (Hettich Universal, 3500 rpm) was then taken and evaporated in air. 2 mL DI water were added to dissolve the precipitate, and then 1 mL aliquot was taken for IC measurement.

## 2.5 Batch desorption experiments at external bias potentials

For the study of electro-assisted desorption kinetics, desorption experiments with external bias potentials were performed in batch cells as described for CV measurements. First, 1 g/L DeACF was preloaded using a solution with an initial TFA concentration of 100 mg/L for 48 h in tap water. An aliquot sample was measured by IC. After that, the DeACF sample was transferred to clean 10 mM  $\text{Na}_2\text{SO}_4$  solution where desorption at -0.3 V, -0.1 V, +0.1 V took place. A strong stirring at 650 rpm was applied while desorption. Aliquots of 0.1 mL were

taken in selected time intervals for IC measurements. The weights of the wet DeACF pieces after preloading were measured in order to determine the solution transferred together with DeACF, and correct the total TFA amount existing in the desorption cell.

## **2.6 Flow experiments**

A three-electrode single-channel flow cell (ElectroCell) as illustrated in **Fig. 1** was applied for the flow experiments. DeACF (0.1 g) was used as the working electrode, OxACF (0.06 g) as counter electrode, and a pseudo Ag/AgCl electrode as the reference electrode. The pseudo Ag/AgCl electrode presents a potential  $+(270 \pm 25)$  mV vs. Ag/AgCl sat. KCl. Pt/Ti plates were applied as current collectors. Teflon<sup>TM</sup> band and Whatman ashless filter paper (1440-110) were used as separators between the electrodes. The bias potential was applied by a single-channel potentiostat (Orignalys, OGS100). A microprocessor-controlled pump (Ismatec) was used for driving the inflow solution. The dead volume (tubings, pump) was determined to be 5 mL. Tap water containing 3.4 mg/L TFA was fed as the inflow while 10 mM Na<sub>2</sub>SO<sub>4</sub> solution was applied for TFA desorption. A higher TFA concentration than reported in real water systems were set here due to the detection limit of IC  $\geq 0.1$  mg/L.

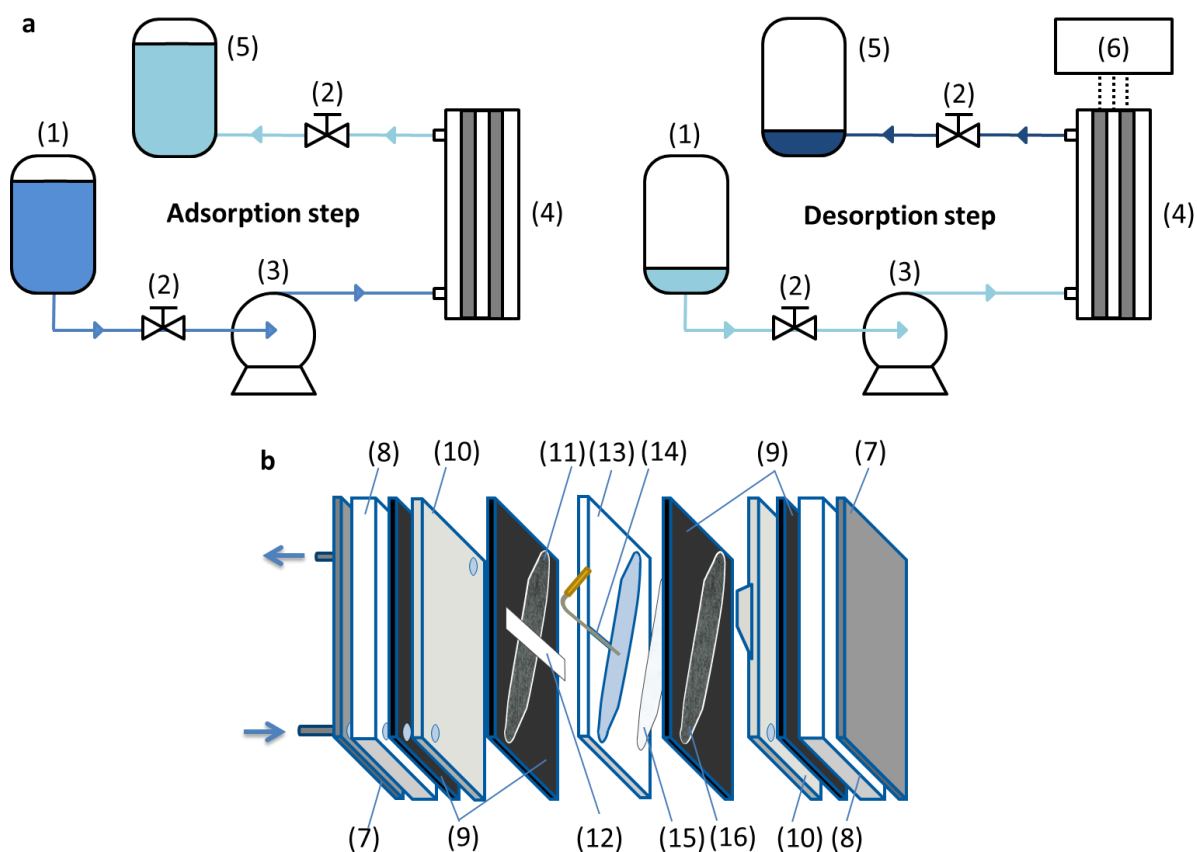


**Fig. 1:** (a) The schematic illustration of the flow system at adsorption step and electrodesorption step. (b) The configuration of the three-electrode, single-channel flow cell. (1) Inflow reservoir, (2) liquid valve, (3) pump, (4) flow cell, (5) outflow container, (6) potentiostat, (7) stainless steel endplate, (8) Teflon™ end frame, (9) ethylene propylene diene monomer rubber sealing set, (10) Pt/Ti current collector, (11) DeACF as working electrode, (12) Teflon™ band as separator, (13) Teflon™ holder for electrode materials, (14) pseudo Ag/AgCl reference electrode, (15) filter paper as separator, (16) OxACF as counter electrode. Solid lines: inflow and outflow solutions, dashed lines: cables.

## 2.7 Sorption calculations

Single point adsorption coefficients  $K_d$  (L/kg) at the adsorption equilibrium were used to identify ACFs' adsorption affinity towards TFA according to **Eq. 1** with the sorbent loading  $q_e$  (mg/kg) and the equilibrium concentration of sorbate in water  $c_e$  (mg/L).

$$K_d = \frac{q_e}{c_e} \quad (1)$$

To evaluate the adsorption isotherms, Freundlich (**Eq. 2**) and Langmuir equations (**Eq. 3**) were applied:

$$\log q_e = n \cdot \log c_e + \log K_F \quad (2)$$

$$\frac{c_e}{q_e} = \frac{c_e}{q_m} + \frac{1}{q_m K_L} \quad (3)$$

Dimensionless Freundlich exponent  $n$  and the Freundlich constant  $K_F$  in (mg/kg)/(mg/L) <sup>$n$</sup>  can be derived from **Eq. 2**. An  $n$  close to 1 indicates rather homogeneous sorption sites and conditions far enough from sorbent saturation [30, 31]. The maximal loading  $q_m$  (mg/kg) on sorbent and the Langmuir constant  $K_L$  (L/mg) can be derived from **Eq. 3**.  $K_F$  and  $K_L$  values indicate the sorbent adsorption affinity, and  $q_m$  the adsorption capacity.

### 3. Results and Discussion

#### 3.1 Characteristics of ACFs

The chemical and textural properties of the pristine ACF, DeACF and OxACF are reported in detail previously [24, 28] and summarized in **Tables S1 and S2**.

Elemental analysis reveals the largest O/C mass ratio of 0.23 for OxACF, followed by 0.11 for pristine ACF and 0.05 for DeACF, indicating accordingly the introduction and removal of O-containing surface functional groups on oxidized and defunctionalized carbon surface. Raman spectra and XPS results reported previously [24, 28] revealed the increased sp<sup>2</sup> C moieties on DeACF surface compared to pristine ACF. The ion exchange capacities were determined to quantify the charged surface sites of each ACF type. The CEC of ACFs at pH 7 was found in the order of OxACF (1 μmol/m<sup>2</sup>) > pristine ACF (0.04 μmol/m<sup>2</sup>) > DeACF (≤0.01 μmol/m<sup>2</sup>) whereas the AEC in the adverse order of OxACF (0.0087 μmol/m<sup>2</sup>) < pristine ACF (0.025 μmol/m<sup>2</sup>) < DeACF (0.23 μmol/m<sup>2</sup>). That is, at pH 7, OxACF surface carries the highest density of negative net charges among the three ACFs while DeACF's surface is positively charged due to proton adsorption on its delocalized π-electron regions [32, 33]. Overall, DeACF surface is expected to benefit the specific adsorption of TFA via 1) attractive electrostatic interactions and 2) possible interactions between hydrophobic sorbent surface and the CF<sub>3</sub> moiety of TFA.

Regarding the textural properties, high SSAs of 1700, 1400 and 800 m<sup>2</sup>/g were determined for pristine ACF, DeACF and OxACF with a total pore volume of 0.88, 0.69 and 0.42 cm<sup>3</sup>/g, respectively. Approx. 90% of the pores are assigned to micropores for all three materials. The shrinkage of SSA and pore volume of OxACF is likely due to the formation of O-containing functional groups at its pore surfaces [34, 35].

According to cyclic voltammograms (**Fig. S2**), pristine ACF and DeACF show significant capacitive currents in the range of -0.5 to +0.6 V. The potential windows in which the ACFs remain electrochemically stable are found for DeACF between -0.3 and +0.4 V, pristine ACF between 0 and +0.5 V, and OxACF between +0.5 and +0.9 V. That is, DeACF shows the widest potential window among all three ACFs. A significant decline of the reduction current is particularly seen at potential  $E < +0.5$  V for OxACF, which is earlier compared to other two ACFs and thus seem to associate with the reduction of surface oxidized carbon species [27]. On the other hand, the oxidation current of OxACF rises only at  $E > +0.8$  V, suggesting a surface more resistant to further oxidation. The specific capacitance values of DeACF, pristine ACF and OxACF are approx. 107 F/g, 120 F/g and 20 F/g considering their individual potential windows. OxACF shows a significantly smaller specific capacitance likely related to the formation of water clusters at its hydrophilic pore surfaces which blocked some pores for access of electrolyte ions [34]. The butterfly shape in cyclic voltammogram suggests the position of ACF's potential zero charge  $E_{pzc}$  [27], which is found to locate for DeACF at  $(-0.13 \pm 0.05)$  V, for pristine ACF at  $(0.38 \pm 0.03)$  V and for OxACF at  $(0.68 \pm 0.06)$  V indicating increasing oxidation degree of the carbon surface.

### **3.2 Effect of co-existing inorganic ions and ionic strength on TFA adsorption**

Pristine ACF and DeACF were tested for TFA adsorption. To reach a 20% depletion (i.e., 20% of the total adsorbate is adsorbed) in 10 mM Na<sub>2</sub>SO<sub>4</sub> (pH 7) with an initial concentration of 20 mg/L TFA, only 0.5 g/L DeACF ( $K_d = 500$  L/kg) whereas as much as 10 g/L pristine ACF ( $K_d = 25$  L/kg) were required. That is, strongly increased adsorption affinity (a 20-fold higher adsorption coefficient) to TFA was enabled after sorbent surface defunctionalization. A superposition of the introduced surface anion exchange sites for additional electrostatic attraction and the enhanced sorbent hydrophobicity for stronger interactions towards TFA's CF<sub>3</sub> moiety is likely the reason for the significantly improved adsorption efficiency of DeACF to TFA, as previously observed for longer-chain PFAAs [36] and *p*-toluenesulfonic acid [28].

DeACF presents a high TFA adsorption capacity of 43 mg/g in 1 mM Na<sub>2</sub>SO<sub>4</sub> at pH 7 (**Table S3**), which is beyond the 32.9 mg/g and 29.0 mg/g achieved by quaternary nitrogen-doped [16] and polypyrrole-grafted ACs [17], respectively, without co-existing inorganic anions in the water phase. DeACF hence shows one of the best adsorption capacities towards TFA among the presently reported AC-based materials in literature.

Being highly polar in structure (calculated Log  $D_{ow}$  reported from -0.6 to -3.4 [3, 4]), TFA adsorption cannot benefit much from hydrophobic effects known for longer-chain PFAA anions [32, 36]. Thus, it is likely to be interfered by competition adsorption of co-existing inorganic anions in the aqueous phase. **Fig. 2** demonstrates the influence of SO<sub>4</sub><sup>2-</sup>, NO<sub>3</sub><sup>-</sup>, Cl<sup>-</sup> and F<sup>-</sup> (each 10 mM) on the adsorption affinity of DeACF towards TFA indicated by the change in single point adsorption coefficients  $K_d$ . All co-existing anions diminished the adsorption of TFA on DeACF. The bulky, divalent hydrated SO<sub>4</sub><sup>2-</sup> has the largest size [37, 38] and can theoretically occupy two nearby anion exchange sites per adsorption, thus is expected to suppress the access of TFA and to be more favorably adsorbed than monovalent anions [39]. However, NO<sub>3</sub><sup>-</sup> shows the most significant hindrance effect on TFA adsorption, even stronger than SO<sub>4</sub><sup>2-</sup>. The surprisingly high hindrance effect of NO<sub>3</sub><sup>-</sup> may be owing to a size-selective adsorption of planar NO<sub>3</sub><sup>-</sup> into micropores as it possesses rather a disk-like hydration shell compared to the 3D hydration shells forming around the other anions [37]. The  $\delta^+$ -charged N centre is thereby less shielded and could better interact with the delocalized  $\pi$  systems on DeACF surface [40] and lead to enhanced specific adsorption. The  $K_d$  of TFA in NaF solution was higher than in NaCl, suggesting a weaker competing effect of F<sup>-</sup> than Cl<sup>-</sup> on TFA adsorption to DeACF. This reflects the preferred uptake of Cl<sup>-</sup> carrying a smaller hydration radius than F<sup>-</sup> in micropore electric double layers [38, 39] and stronger anion- $\pi$  electron acceptor-donor interactions between Cl<sup>-</sup> and DeACF surface [41].

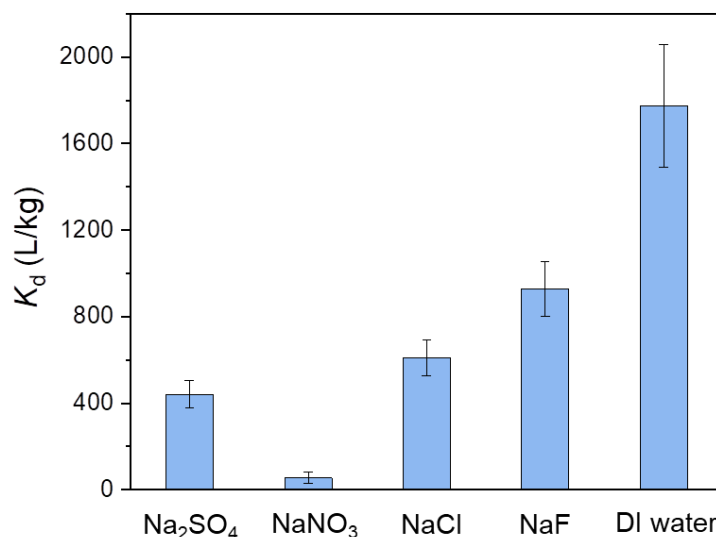


**Fig. 2:** Single point adsorption coefficients of DeACF to TFA in various water matrices. The concentration of  $\text{Na}_2\text{SO}_4$ ,  $\text{NaNO}_3$ ,  $\text{NaCl}$  and  $\text{NaF}$  was 10 mM individually added to deionized (DI) water. DeACF dosage: 2 g/L. TFA initial concentration: 20 mg/L (0.175 mM). DI water: contains 0.25 mM  $\text{Cl}^-$  after pH adjustment using HCl. The errors are estimated based on standard deviations of the single values from the mean in triplicate measurements considering a 95% probability.

**Fig. 3a** shows an enhanced decline of  $K_d$  in background solution containing higher concentration of  $\text{Na}_2\text{SO}_4$ . As salting-out effects are expected to be minor [42] especially for highly polar TFA, an intensified adsorption competition of  $\text{SO}_4^{2-}$  of increasing concentration [32, 43] and/or a stronger shielding of anion exchange sites on DeACF caused by a denser electric double layer [44] should serve as the main reasons for the weakened adsorption affinity of DeACF to TFA. A milder ionic strength effect was found for PFOA ( $\text{p}K_a < 1$  [45], calculated  $\log D = 1.58$  [46]) at pH 7 on a similar activated carbon felt type which underwent surface defunctionalization [36]. This implies that the increase of ionic strength can lead to a more intensive adsorption competition for highly polar ionic compounds compared to those carrying rather hydrophobic moieties. Such effect should be further tested by including other short-chain PFAAs utilizing the same DeACF in solution of different ionic strengths.

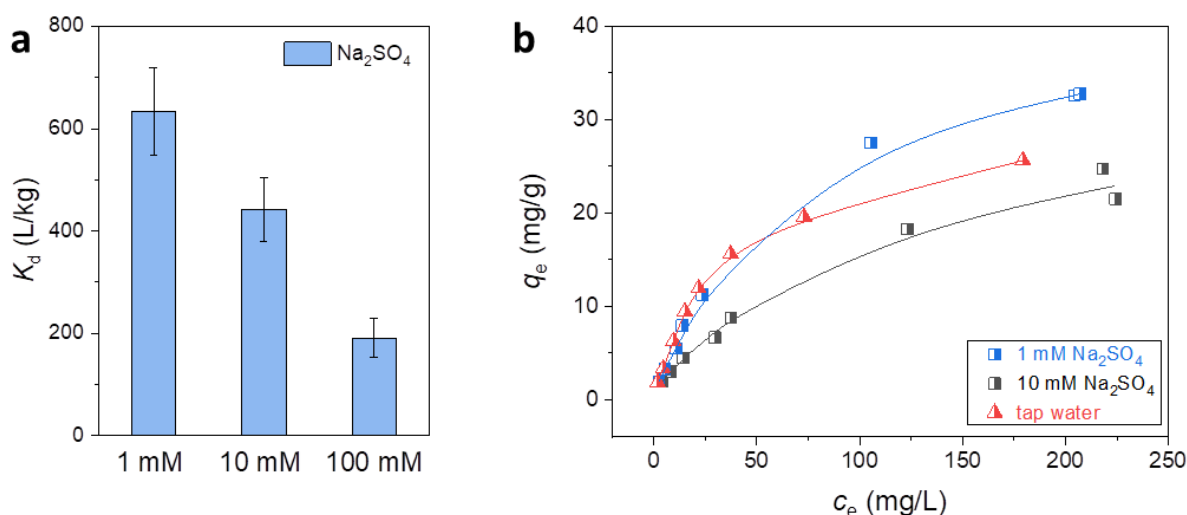


**Fig. 3:** (a) Single point adsorption coefficient of DeACF to TFA at pH 7 in 1 mM, 10 mM and 100 mM  $\text{Na}_2\text{SO}_4$ . DeACF dosage: 2 g/L. TFA initial concentration: 20 mg/L (0.175 mM). (b) Adsorption isotherms of TFA on DeACF at pH 7 in 1 mM  $\text{Na}_2\text{SO}_4$ , 10 mM  $\text{Na}_2\text{SO}_4$  and tap water. Lines serve as guides for the eye. Langmuir and Freundlich linear fittings are shown in **Fig. S2** with parameters given in **Table S3**. The errors are estimated based on standard deviations of the single values from the mean in triplicate measurements considering a 95% probability.

Adsorption of TFA was also investigated in tap water containing 0.021 mM  $\text{NO}_3^-$ , 1.1 mM  $\text{SO}_4^{2-}$  and 2.7 mM  $\text{Cl}^-$  after adjusting pH to 7 using HCl. The adsorption isotherms of TFA on DeACF in tap water, 1 mM  $\text{Na}_2\text{SO}_4$  and 10 mM  $\text{Na}_2\text{SO}_4$  are shown in **Fig. 3b**. The Freundlich and Langmuir fittings (**Eq. 2 & 3**) were illustrated in **Fig. S3**, and the fitting parameters summarized in **Table S3**. The adsorption affinity of DeACF to TFA in the low concentration range can be indicated by the slopes of the isotherms (**Eq. 1:**  $K_d = q_e/c_e$ , or **Eq. 2:**  $K_d = c_e^{n-1} \cdot K_F$ ), and are similar in tap water and in 1 mM  $\text{Na}_2\text{SO}_4$ . The co-existing anions in tap water seem to have a larger hindrance effect on the adsorption capacity of DeACF to TFA as the maximal loading  $q_m$  in tap water was closer to  $q_m$  in 10 mM  $\text{Na}_2\text{SO}_4$  and lower than the value in 1 mM  $\text{Na}_2\text{SO}_4$ . Even though, the maximal loading of TFA reached 30.2 mg/g on DeACF in tap water, which is comparable to the highest reported TFA adsorption capacity of AC materials without co-existence of background inorganic ions [16, 17]. A trace amount of  $\text{NO}_2^-$  was detectable after TFA adsorption on DeACF in tap water, indicating a trivial oxidation of defunctionalized carbon surface upon contact with  $\text{NO}_3^-$ . A further test in which 2 g/L DeACF was immersed in 1 mM  $\text{NaNO}_3$  aqueous solution for 3 days led to a detection of only



0.001 mM  $\text{NO}_2^-$  in the final solution. Cycle experiments in **Section 3.6** provide further insights into the stability of DeACF in tap water.

### 3.3 Effect of bias potential on TFA adsorption affinity

The effects of bias potentials on TFA adsorption in  $\text{Na}_2\text{SO}_4$  solutions (pH 7) were investigated on DeACF as shown in **Fig. 4**. Similar to longer-chain PFAAs, TFA is highly reluctant to be electrochemically oxidized or reduced [47-49] and thereby remained stable at applied bias potentials as indicated by the cyclic voltammogram in **Fig. S4**.

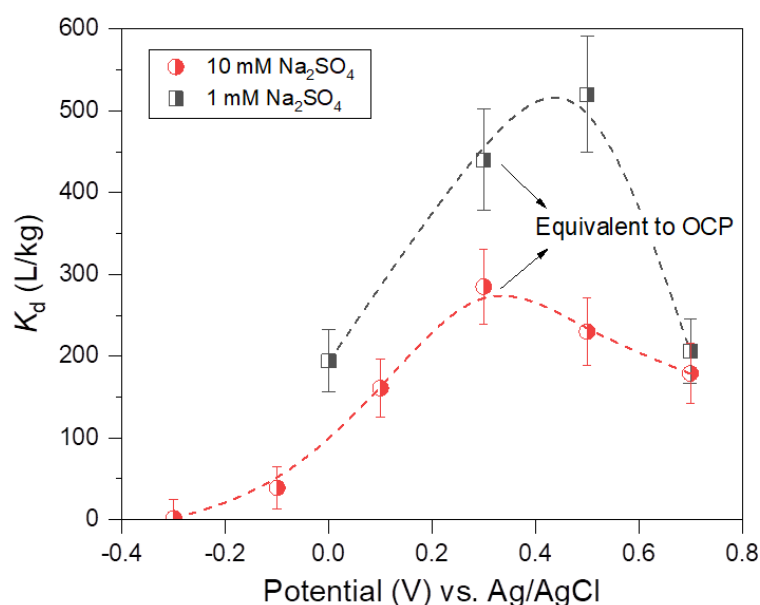


**Fig. 4:** Single point adsorption coefficients of DeACF to TFA in 1 mM and 10 mM  $\text{Na}_2\text{SO}_4$  (pH 7). DeACF dosage: 2 g/L. TFA initial concentration: 20 mg/L. The  $K_d$  values at OCP ( $E \approx 0.3$  V vs. Ag/AgCl) were given together with the points obtained when applying different external bias potentials. The same electrochemical cell setup was used. The errors are estimated based on standard deviations of the single values from the mean in triplicate measurements considering a 95% probability.

Declining  $K_d$  values along decreasing  $E < +0.3$  V in both 1 mM and 10 mM  $\text{Na}_2\text{SO}_4$  indicated the reduced TFA adsorption when polarizing DeACF at bias potentials below its OCP ( $\approx 0.3$  V vs. Ag/AgCl). The ratios between the  $K_d$  at OCP and  $K_d$  at +0.1, -0.1 and -0.3 V in 10 mM  $\text{Na}_2\text{SO}_4$  are approx. 2, 7 and 170, respectively. At  $E = -0.1$  V  $\approx E_{\text{pzc, DeACF}}$ , DeACF surface is nearly charge neutral. A lower  $K_d$  was thus observed than at  $E = +0.1$  V or OCP where electrostatic attraction between negatively charged TFA and positively charged DeACF

surface resulted in stronger adsorption affinities. At  $E < -0.1$  V, DeACF surface carries net negative charges which repulsed TFA anions and led to a drastically reduced  $K_d$ .

At  $E = +0.5$  V,  $K_d$  in 1 mM  $\text{Na}_2\text{SO}_4$  slightly increased compared to the value at OCP despite that DeACF might get oxidized to a minor extent at this potential according to its cyclic voltammogram (**Fig. S2**). On the contrary, no significant increase in  $K_d$  was observed in 10 mM  $\text{Na}_2\text{SO}_4$ . In the bias potential range from 0 to +0.5 V, higher  $K_d$  values reflect generally a stronger adsorption affinity of DeACF to TFA in 1 mM  $\text{Na}_2\text{SO}_4$  than in 10 mM  $\text{Na}_2\text{SO}_4$ . At  $E = +0.7$  V, a reduction in  $K_d$  to nearly the same value was found in 1 mM  $\text{Na}_2\text{SO}_4$  and 10 mM  $\text{Na}_2\text{SO}_4$ . Anodic polarization at +0.7 V could lead to 1) a sorbent surface carrying a higher density of positive charges, and/or 2) a partially oxidized carbon surface carrying less positive net charge due to the formation of acidic O-containing functional groups [25]. In both scenarios, the sorbent surface becomes more hydrophilic, thus favouring the adsorption of water and inorganic electrolyte ions instead of TFA. Compared to longer-chain PFAAs, the electrosorption behavior of TFA is closer to that of perfluorobutanoic acid (PFBA) than PFOA in terms of the effect of anodic polarization. As observed for PFBA, hardly any improvement was seen for TFA adsorption when applying  $E > \text{OCP}$  whereas anodic polarization was reported to enhance the adsorption affinity of AC towards PFOA [23, 47].

In summary, bias potentials can arouse a significant effect on TFA adsorption on DeACF. Especially, TFA desorption into clean electrolyte solutions can be effectively facilitated by applying cathodic polarization on DeACF to allow on-site sorbent regeneration and to enrich TFA in a small outflow volume as elucidated in the next sections in a flow setup. Moreover, stronger desorption efficiency can be achieved by applying a higher electrolyte concentration, which can meanwhile reduce the electric energy costs thanks to a better system conductivity.

### **3.4 TFA adsorption in flow mode**

The dynamic uptake of TFA and co-existing anions from the tap water by DeACF without external bias potential is shown in forms of breakthrough curves in **Fig. 5**. Sorption isotherms in tap water fall in between those in 1 mM and 10 mM  $\text{Na}_2\text{SO}_4$  according to **Fig. 3b**. Furthermore, **Fig. 4** suggests a rather limited improvement in adsorption efficiency by applying anodic charging for TFA in both 1 mM and 10 mM  $\text{Na}_2\text{SO}_4$ . Thus, open circuit

condition was applied for the TFA adsorption step in the flow-through experiments with tap water.

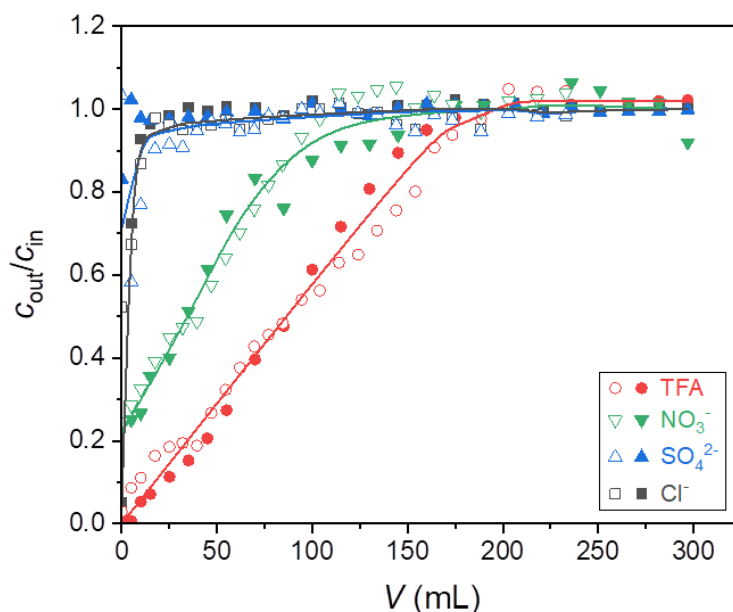


**Fig. 5:** Breakthrough curves of TFA,  $\text{NO}_3^-$ ,  $\text{SO}_4^{2-}$  and  $\text{Cl}^-$  in the flow cell experiment using 0.1 g DeACF pre-wetted in deionized water. Inflow: tap water containing 3.4 mg/L TFA and 1.3 mg/L  $\text{NO}_3^-$ . Hollow dots: at  $5.0 \text{ mL}\cdot\text{g}^{-1}\cdot\text{min}^{-1}$  mass-related flow rate, filled dots: at  $10 \text{ mL}\cdot\text{g}^{-1}\cdot\text{min}^{-1}$  mass-related flow rate. Lines serve as guides for the eye.

No significant difference was recognizable for the adsorption processes when applying two different mass-related flow rates ( $10 \text{ mL}\cdot\text{g}^{-1}\cdot\text{min}^{-1}$  and  $5 \text{ mL}\cdot\text{g}^{-1}\cdot\text{min}^{-1}$ ). Around 87 mL could be fed to DeACF in the flow cell until 50% breakthrough of TFA ( $C_{\text{out}}/C_{\text{in}} = 0.5 \pm 0.03$ ) was reached. At the full breakthrough, the loading of TFA on DeACF was calculated to be ( $3.0 \pm 0.2$ ) mg/g by integrating the area below the curve  $C_{\text{in}} - C_{\text{out}}$  vs. in-flow volume then normalized by the DeACF mass. This value corresponds well to the loading (2.8 mg/g) predicted by the adsorption isotherm of TFA on DeACF in tap water (pH 7, **Fig. 3b**) at  $C_{\text{out}} = C_{\text{in}} = C_e = 3.4 \text{ mg/L}$ , and reached around 10% of the maximal loading estimated by the Langmuir fitting (Table S3). Nearly instantaneous breakthrough was observed for  $\text{Cl}^-$  and  $\text{SO}_4^{2-}$  on DeACF which spoke for very minor uptake, unlike reported for N-doped materials on which the adsorption of TFA was strongly interfered by the co-existence of  $\text{SO}_4^{2-}$  [16, 17]. We observe a significant uptake of  $\text{NO}_3^-$  from tap water by DeACF with a loading of ( $0.52 \pm 0.08$ ) mg/g at the full breakthrough, while a 50% breakthrough was reached after approx. 35 mL in-flow water was fed. Similar strong specific  $\text{NO}_3^-$  adsorption was reported before on defunctionalized AC [33].

Notably, the  $\text{NO}_3^-$  adsorbed from tap water (0.021  $\mu\text{M}$ ) can be fully recovered in the desorption step as elucidated in **Section 3.5**, suggesting an insignificant redox reaction at the surface of DeACF when contacting  $\text{NO}_3^-$ . Moreover, as shown in **Fig. S5**, the dynamic uptake performance of TFA and  $\text{NO}_3^-$  from tap water by DeACF was largely unaffected by a pre-treatment in  $\text{NaNO}_3$  solution of much higher concentration (1 mM) overnight.

Separation performance of DeACF under open circuit conditions for TFA versus anion adsorption from tap water in the flow mode can be quantified by applying **Eq. 4** as defined in ref. [50].

$$\text{Separation factor } S_{\text{TFA}/\text{X}} = \frac{q_{\text{TFA}}/q_{\text{X}}}{c_{0,\text{TFA}}/c_{0,\text{X}}} \text{ with } \text{X} = \text{Cl}^-, \text{SO}_4^{2-} \text{ or } \text{NO}_3^- \quad (4)$$

where  $c_{0,\text{TFA}}$  and  $c_{0,\text{X}}$  (mg/L) are the initial concentrations in the in-flow water and  $q_{\text{TFA}}$  and  $q_{\text{X}}$  (mg/g) are the loadings at full breakthrough. The separation factor equals to the ratio of the single point adsorption coefficients of the considered compounds at the respective inflow concentrations as well as approximately to the ratio of 50%-breakthrough volumes ( $V_{50\% \text{ ads}}$ ):

$$S_{\text{TFA}/\text{X}} = \frac{K_{\text{d,TFA}}}{K_{\text{d,X}}} \approx \frac{V_{50\% \text{ ads,TFA}}}{V_{50\% \text{ ads,X}}} \quad (5)$$

For rapid small-scale tests, breakthrough curves are typically not ideal step-functions, but rather of S-shape curves due to dispersion effects and rate-limited sorption/desorption [16]. Thus, in a simplified approach we use the 50%-breakthrough volume ( $V_{50\% \text{ ads}}$ ) to calculate selectivity factors.  $\text{SO}_4^{2-}$  and  $\text{Cl}^-$  are considered as not significantly retarded ions with  $V_{100\% \text{ ads}} \approx 5$  mL. This is the void and pore water volume of the adsorbent unit which needs to be replaced.

According to **Fig. 5**, separation factors of TFA were calculated to be about 35 versus  $\text{Cl}^-$  and  $\text{SO}_4^{2-}$  and 2.5 versus  $\text{NO}_3^-$ . This indicates a significant separation power of DeACF-based flow-mode adsorption for TFA versus  $\text{Cl}^-$  and  $\text{SO}_4^{2-}$ , but considerable co-adsorption for TFA and  $\text{NO}_3^-$ . Longer-chain PFAAs were reported to show much higher separation factors versus inorganic anions due to the stronger interaction between carbon sorbent surfaces and the longer C-F containing chains [50].

### 3.5 Electro-assisted desorption of TFA in flow mode

Flow-mode trap&release allows a flexible selection of eluent for the desorption step. Here, we applied 10 mM  $\text{Na}_2\text{SO}_4$  for the electro-assisted TFA desorption from DeACF after its adsorption from tap water ( $c_{\text{in}} = 3.4 \text{ mg/L}$ ) at +0.1 V, -0.1 V, -0.3 V where a detachment of TFA is triggered according to **Fig. 4**.

For the choice of background electrolyte,  $\text{Na}_2\text{SO}_4$  is favored as it is cheap and electrochemically inert within the applied potential range in this work [51]. Sulfate radicals  $\text{SO}_4^{\cdot-}$  are reported to be generated from  $\text{Na}_2\text{SO}_4$  at extended high bias potential (e.g. at >1.25 V vs. Ag/AgCl on boron-doped diamond electrode [52]) which can be of use to degrade TFA [20] in the regeneration concentrate applying a subsequent electrooxidation step. A  $\text{Na}_2\text{SO}_4$  concentration of 10 mM is preferred over 1 mM to improve the desorption efficiency for TFA. Other options of electrolytes might lead to undesired byproducts upon redox processes in electrooxidation, such as chlorate, perchlorate or chlorinated organic compounds in NaCl [53, 54]. While combination of electro-assisted trap&release with electrooxidation is clearly beyond the scope of this work, optimized integration of both processes deserves detailed studies in future.

In the flow mode, OxACF with high surface oxidization degree and minor anion exchange (**Table S1**) capacity was applied as the counter electrode. OxACF does not take up TFA even under anodic potential due to the strong electrostatic repulsion and weak sorbent-sorbate interactions in general, so that the electro-assisted ad-/desorption of TFA on DeACF is not interfered by OxACF. Moreover, the high specific surface area of OxACF (**Table S2**) can efficiently balance the electrons/counterions at the cathode [55] and strongly reduced the cell voltages during the electro-assisted desorption (up to 1.1 V at a bias potential of -0.3 V on DeACF) compared to the case using bare Pt/Ti plate as the anode.

**Fig. 6a** shows the effect of applied bias potential on the TFA desorption profiles at the mass-related flow rate of  $10 \text{ mL}\cdot\text{g}^{-1}\cdot\text{min}^{-1}$ . The TFA out-flow concentration  $c_{\text{out,TFA}}$  close to the TFA in-flow concentration  $c_{\text{in,TFA}}$  was observed in the adsorption step before potential applied. Once the charging started,  $c_{\text{out,TFA}}$  drastically increased, and distinct desorption peaks were observed in cases at +0.1 V, -0.1 V and -0.3 V. Achievable recoveries (Re%), that is, the percentage of the adsorbed TFA which could be desorbed within the first 120 min after

switching to desorption conditions at a mass-related flow rate of 10 mL·g<sup>-1</sup>·min<sup>-1</sup> (**Table 1**), rised from (72 ± 4)% for OC condition (≈ +0.3 V) to approx. (97 ± 6)% for -0.1 V and -0.3 V. This indicates a more complete TFA desorption from DeACF into a smaller volume of 10 mM Na<sub>2</sub>SO<sub>4</sub> at a more negative bias potential. A full recovery of TFA at OCP was expected to take considerably longer desorption time (and water volume) as a low TFA out-flow concentration around 0.1 mg/L which almost met the detection limit of the IC device was still detectable after 200 min. To reach 95% of the respective recovery, the volume of the Na<sub>2</sub>SO<sub>4</sub> eluent needed to be fed to the system ( $V_{95\% \text{ des}}$ ) decreased from 93 mL to 24 mL from OCP to -0.3 V conditions. An enrichment factor can be defined using **Eq. 5** to evaluate the electro-assisted trap&release performance:

$$\text{Enrichment factor} = \frac{V_{50\% \text{ ads}}}{V_{95\% \text{ des}}} \cdot \text{achievable total recovery (Re\%)} / 100 \quad (5)$$

where  $V_{50\% \text{ ads}}$  is the volume of the in-flow tap water fed until a 50% breakthrough was reached (i.e. 92.5 mL), and  $V_{95\% \text{ des}}$  is the volume of 10 mM Na<sub>2</sub>SO<sub>4</sub> needed to reach 95% of the respective recovery achieved with 120 mL eluent. The highest enrichment factor was estimated as 3.5 ± 0.2 at -0.3 V, which is 5-times higher compared to the lowest of 0.67 ± 0.07 at OCP. This indicates a better electro-assisted trap&release performance by applying more negative bias potential for TFA desorption from DeACF in a 10 mM Na<sub>2</sub>SO<sub>4</sub> flow.

Both desorption kinetics and thermodynamics can contribute to the distinct TFA desorption profiles observed at the chosen bias potentials. We examined the desorption kinetics of TFA in 10 mM Na<sub>2</sub>SO<sub>4</sub> from DeACF in batch systems as shown in **Fig. S6**. Very fast desorption (≥90% within 10 min) with similar kinetics was observed at all applied bias potentials. Thus, the significant effect on TFA desorption behavior by applying different bias potentials on DeACF has to be explained by thermodynamics, that is, by the different adsorption affinities under the chosen desorption conditions. DeACF shows a  $K_d = 660$  L/kg for TFA uptake in tap water at OCP (**Fig. S1**). With  $K_d = 1.7$  L/kg (**Table 1**), cathodic charging at -0.3 V in 10 mM Na<sub>2</sub>SO<sub>4</sub> has led to a significant enrichment effect after the ad-/desorption cycle.

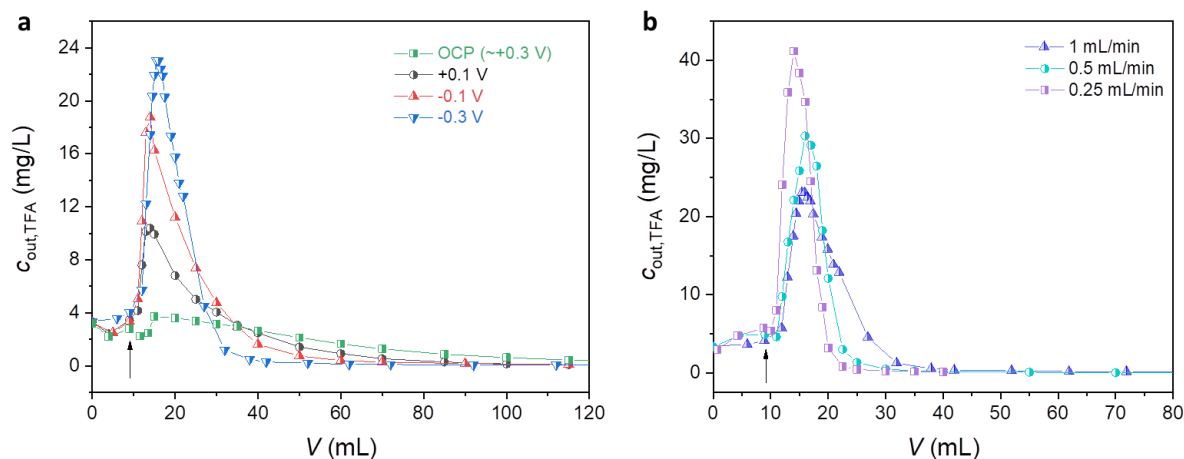


**Fig. 6:** Desorption profiles of TFA in the flow-cell experiment (a) at +0.1, -0.1, -0.3 V vs. Ag/AgCl at  $10 \text{ mL} \cdot \text{g}^{-1} \text{min}^{-1}$  mass-related flow rate and (b) at -0.3 V vs. Ag/AgCl at  $10 \text{ mL} \cdot \text{g}^{-1} \text{min}^{-1}$ ,  $5.0 \text{ mL} \cdot \text{g}^{-1} \text{min}^{-1}$  and  $2.5 \text{ mL} \cdot \text{g}^{-1} \text{min}^{-1}$  after adsorption at full breakthrough from tap water on 0.1 g DeACF at OCP. Bias potential was added after 9 mL flowed out as indicated by the black arrows. Lines serve as guides for the eye.

During the desorption, detached TFA molecules diffuse first through the pores of the ACF fibers (intraparticle diffusion) before diffusing through the stagnant water layer at the outer surface (film diffusion) [56], and finally reach the bulk phase by convective mixing. While the flow rate of the eluent for desorption can affect the film diffusion (and the convection in the bulk electrolyte phase), it does not play a role on the rate-limiting intraparticle diffusion process. Hence, the flow rate for the eluent at the desorption step needs to be optimized for a desired electro-assisted trap&release performance. On the one hand, a too high flow rate will result in a waste of eluent volume (= out flow volume) where the desorption equilibria are by far not reached, and hence lead to a reduced enrichment factor. A too slow flow, on the other hand, could limit the overall mass transfer (higher contribution of film diffusion, less steep concentration gradients) and thereby hinder the desorption process.

**Fig. 6b** shows the TFA desorption profiles in 10 mM  $\text{Na}_2\text{SO}_4$  at -0.3 V at the mass-related flow rates of  $10 \text{ mL} \cdot \text{g}^{-1} \text{min}^{-1}$ ,  $5 \text{ mL} \cdot \text{g}^{-1} \text{min}^{-1}$  and  $2.5 \text{ mL} \cdot \text{g}^{-1} \text{min}^{-1}$ .  $(90 \pm 6)\%$  and  $(95 \pm 6)\%$  recovery were achieved at the  $5 \text{ mL} \cdot \text{g}^{-1} \text{min}^{-1}$  and  $2.5 \text{ mL} \cdot \text{g}^{-1} \text{min}^{-1}$  flow rates, respectively, which are very close to  $(97 \pm 6)\%$  as obtained at  $10 \text{ mL} \cdot \text{g}^{-1} \text{min}^{-1}$  (**Table 1**). The TFA desorption peaks are evidently sharper at lower flow rates. Desorption with a mass-related flow rate  $2.5 \text{ mL} \cdot \text{g}^{-1} \text{min}^{-1}$  and  $5 \text{ mL} \cdot \text{g}^{-1} \text{min}^{-1}$  led to a 2.1-fold and 1.5-fold larger enrichment factor than

achievable at 10 mL·g<sup>-1</sup>min<sup>-1</sup>, respectively. The overall relatively small enrichment factors obtained in the time-lapse lab-scale due to geometric constraints can be increased in larger scale units up to about  $K_{d,desorption}/K_{d,adsorption} = 285/1.7 = 168$  (see **Table 1**), which is technically much more attractive.

**Table 1:** Single point adsorption coefficient ( $K_d$ ) of TFA on DeACF in 10 mM Na<sub>2</sub>SO<sub>4</sub> under selected conditions. TFA recovery (Re%) achievable using 120 mL eluent, the Na<sub>2</sub>SO<sub>4</sub> eluent volume needed to reach 95% of the respective recovery ( $V_{95\% \text{ des}}$ ) and enrichment factor in 10 mM Na<sub>2</sub>SO<sub>4</sub> after adsorbed from tap water onto 0.1 g DeACF. Potentials are given vs. Ag/AgCl. The OCP of DeACF in Na<sub>2</sub>SO<sub>4</sub> is around 0.3 V vs. Ag/AgCl.

	Adsorption parameter	Desorption parameters			
	$K_d$ (L/kg)	Mass-related flow rate (mL·g <sup>-1</sup> min <sup>-1</sup> )	Re% <sup>a</sup>	$V_{95\% \text{ des}}$ (mL) <sup>b</sup>	Enrichment factor
<b>OCP</b>	285	10	72%	93	0.67
<b>+0.1 V</b>	160	10	81%	61	1.2
<b>-0.1 V</b>	38	10	97%	46	1.8
<b>-0.3 V</b>	1.7	10	97%	24	3.5
<b>-0.3 V</b>	1.7	5.0	90%	15	5.2
<b>-0.3 V</b>	1.7	2.5	95%	11	7.5

<sup>a</sup> Mean relative error of ±6% for recovery. <sup>b</sup> Calculated for eluent volumes after charging started for +0.1 V, -0.1 V and -0.3 V.

Similar to TFA, ≥83% recovery for NO<sub>3</sub><sup>-</sup> was achieved when applying +0.1 V, -0.1 V and -0.3 V for desorption (**Fig. S8, Table S2**). However, a full recovery and the best enrichment factor was observed at -0.1 V instead of -0.3 V (87% recovery). This implies that NO<sub>3</sub><sup>-</sup> could undergo redox processes and be converted to different reduced species including NO<sub>2</sub><sup>-</sup> and N<sub>2</sub>, upon contact with a cathode at -0.3 V [57]. One evidence is a trace amount of NO<sub>2</sub><sup>-</sup> (≤0.15 mg/L) detected in the out-flow water in the desorption steps at -0.1 V and -0.3 V. Corresponding to the very minor adsorption in the trap steps, no desorption peaks for Cl<sup>-</sup> and SO<sub>4</sub><sup>2-</sup> were observed.



### 3.6 System stability throughout TFA ad-/desorption cycles

Five successive TFA ad-/desorption cycles on DeACF were run to evaluate the system stability as shown in **Fig. 7**. A tap water eluent spiked with 3.4 mg/L TFA (**Fig. 5**) was used for adsorption while 10 mM Na<sub>2</sub>SO<sub>4</sub> was applied for desorption, in which DeACF was charged at a bias potential of -0.3 V to reach the highest enrichment factor (**Table 1**). The TFA loading at the full breakthrough in each adsorption step is recorded in **Table 2** together with the recovery parameters for each cycle. The adsorption capacity dropped by 1/3 after the first cycle which showed a loading of 2.9 mg/g. It then maintained around 2.0 mg/g throughout the 2<sup>nd</sup>-5<sup>th</sup> cycles. High achievable recovery degree of 88-107% was observed for all five cycles, indicating a largely reversible ad-/desorption of TFA from DeACF.

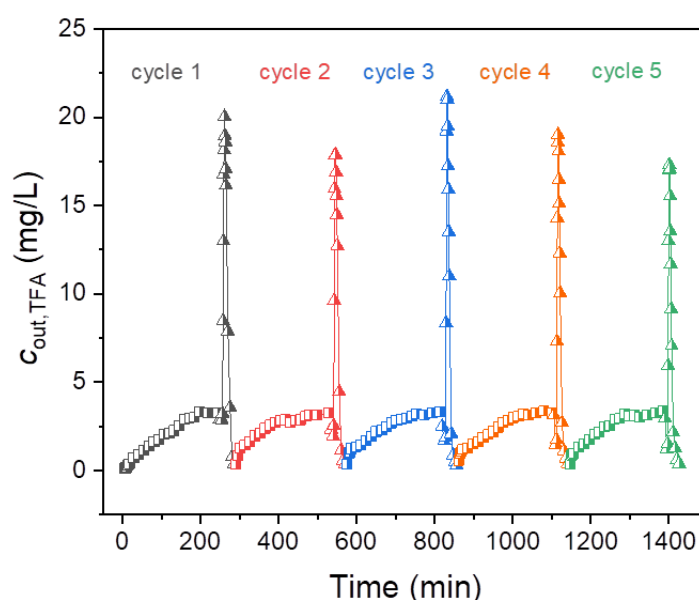


**Fig. 7:** Out-flow concentration of TFA over five successive ad-/desorption cycles on DeACF in the flow-cell experiment. Square symbols: adsorption steps; Triangle symbols: desorption steps. Adsorption conditions: tap water spiked with 3.4 mg/L TFA at OCP, 10 mL·g<sup>-1</sup>min<sup>-1</sup> for 234 min; Desorption conditions: 10 mM Na<sub>2</sub>SO<sub>4</sub> at -0.3 V vs. Ag/AgCl for 30 min, 10 mL·g<sup>-1</sup>min<sup>-1</sup>. Lines serve as guides for the eye.

Temperature-programmed decomposition and cyclic voltammetry (**Fig. 8**) were performed to track the changes in surface chemistry of exhausted DeACFs over ad-/desorption cycles. As all cycled DeACF were washed using deionized water and dried in air before being characterized, we measured a DeACF sample only “washed and dried” for comparison.

As shown in **Fig. 8a**, the butterfly shape of the cyclic voltammogram shifted by +40 mV for DeACF after being washed and dried compared to the original sample. A remarkable further up-shift by +75 mV was observed for DeACF after the 1<sup>st</sup> ad-/desorption cycle compared to the “washed and dried” DeACF, suggesting that the adsorbent surface was significantly oxidized already during the 1<sup>st</sup> cycle [24, 27]. It seems that the next 4 ad-/desorption cycles only caused minor change in the surface chemistry of DeACF, as the butterfly shape was found almost in the same location for DeACF after the 1<sup>st</sup> and 5<sup>th</sup> cycle. Temperature-programmed desorption (TPD) measurements (**Fig. 8b**) also showed quite similar release profiles of CO and CO<sub>2</sub> from DeACFs cycled once and five times. This is in accordance with the quick decline in DeACF adsorption capacity towards TFA after the 1<sup>st</sup> cycle and the stable adsorption performance over the subsequent four cycles. More detailed discussion on the TPD results and the NO<sub>3</sub><sup>-</sup> ad-/desorption cycles are given in the *Supporting Information*.

**Table 2:** Loading of TFA on DeACF after full breakthrough in the adsorption steps and achievable TFA recovery (Re%) in the desorption steps of the cycle experiments. Adsorption conditions: OCP in tap water containing 3.4 mg/L TFA. Desorption conditions: at -0.3 V vs. Ag/AgCl in 10 mM Na<sub>2</sub>SO<sub>4</sub>. Mass-related flow rate: 10 mL·g<sup>-1</sup>min<sup>-1</sup> for both ad- and desorption steps.

	Cycle 1	Cycle 2	Cycle 3	Cycle 4	Cycle 5
<b>Loading (mg/g)<sup>a</sup></b>	2.9	2.0	2.1	2.1	2.0
<b>Recovery (Re%)<sup>b</sup></b>	91%	107%	100%	93%	88%

<sup>a</sup> At full breakthrough. <sup>b</sup>Mean relative error of ±8% for recovery.

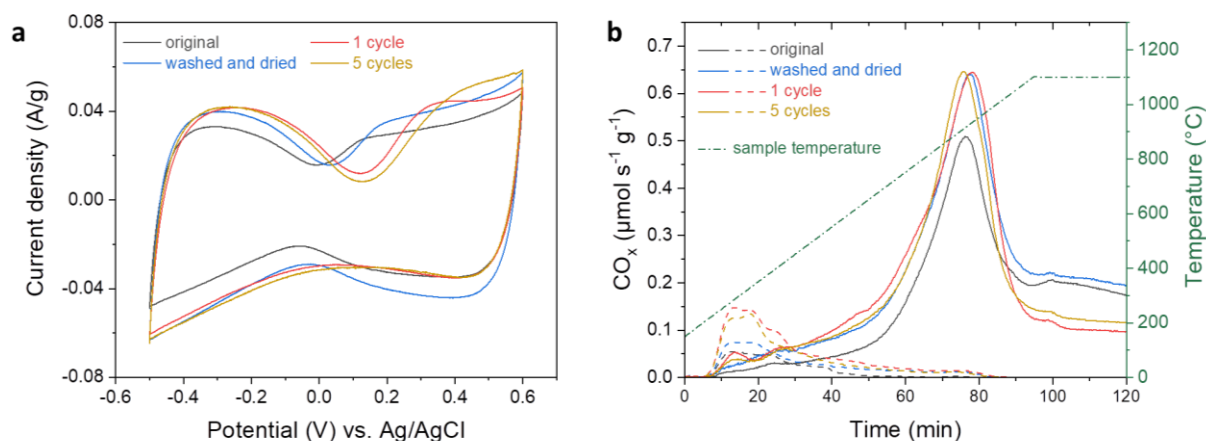


**Fig. 8:** (a) Cyclic voltammograms and (b) TPD curves of the original DeACF, the “washed and dried” DeACF, DeACF after 1<sup>st</sup> cycle and after five ad-/desorption cycles (shown in Fig. 7). Scan rate: 0.5 mV/s. Background solution: 10 mM Na<sub>2</sub>SO<sub>4</sub>. In (b), the release profiles of CO and CO<sub>2</sub> are indicated by the solid and dashed lines, respectively.

#### 4. Conclusions

In this work, we present an efficient approach to enrich the highly mobile TFA from various water matrices containing inorganic ions into a smaller volume of electrolyte solution utilizing 1) the adsorption power of surface-defunctionalized ACF and 2) a following *in-situ* electro-assisted desorption step.

A 20-fold higher adsorption coefficient for anionic TFA was achieved on AC after surface defunctionalization. The positively charged, hydrophobic DeACF surface allows an electrostatic attraction to TFA and a favored adsorption of TFA over inorganic anions. An outstanding maximal adsorption capacity of 30 mg/g comparable to the best reported values for AC-based materials [16, 17] was shown by DeACF towards TFA despite the co-existence of inorganic anions including Cl<sup>-</sup>, SO<sub>4</sub><sup>2-</sup> and NO<sub>3</sub><sup>-</sup> in tap water. The flow experiments carried out in a rapid small-scale test demonstrated a remarkable separation performance of DeACF for TFA versus Cl<sup>-</sup> and SO<sub>4</sub><sup>2-</sup> while a co-adsorption for environmentally undesired NO<sub>3</sub><sup>-</sup> [33].

Applying negative bias potentials on DeACF can effectively desorb TFA with a recovery rate higher than 90%. Improved enrichment effect was observed using a more negative bias potential (-0.3 V vs. Ag/AgCl) and a lower mass-related flow rate (2.5 mL/(g min)). The TFA

enrichment factors up to 7.5 achieved in the lab-scale flow cell can be increased up to >150 when the approach is used in larger scale.

Although the adsorption capacity of DeACF towards TFA was reduced to 67% after the first ad-/desorption cycle due to partial surface oxidation, very stable adsorption efficiencies and adequate enrichment effects were observed for the next 2<sup>nd</sup>-5<sup>th</sup> cycles. Our findings in the cycle experiments revealed a challenge to treat real water containing  $\text{NO}_3^-$  using electro-assisted approaches on porous carbon materials as environmentally hazardous  $\text{NO}_2^-$  could be produced via reduction at the cathode. As in the presented approach, electric potential is applied only for AC regeneration, meaning the regeneration concentrate but not the cleaned water would be affected by this issue while any oxidative post-treatment of the concentrate will re-oxidize the potentially formed  $\text{NO}_2^-$ . Nevertheless, in further studies, a deeper understanding of the fate of  $\text{NO}_3^-$  upon electrode charging should be gained and conditions could be optimized to yield  $\text{N}_2$  rather than  $\text{NO}_2^-$  [58].

The as-established electro-assisted trap&release for TFA removal on DeACF can inspire promising treatment strategies for wastewater containing emerging polar organic micropollutants, especially the anionic ones. The smart, membrane-free, one-channel flow cell design permits low cell voltages by using an OxACF anode. The setup can be applied in the future work for removal of longer-chain PFAAs as well since the oxidized AC surface should merely weakly adsorb the more hydrophobic anionic compounds [32]. The two-step trap&release approach enables a flexible selection of eluent in the electro-assisted desorption step. This can avoid undesired by-products in subsequent electrooxidation processes (as caused e.g. by  $\text{Cl}^-$  oxidation [33, 34]). It also opens up possibilities for enhanced degradation of concentrated target contaminants in the next treatment steps, e.g. by sulfate radicals ( $\text{SO}_4^{\cdot-}$ ) generated via electrooxidation of  $\text{SO}_4^{2-}$  used in the eluent [20, 52].

## **Acknowledgement**

We thank Evelyn Becker and Birgit Forkert for IC measurements, and Maria Balda for her kind assistance in TPD measurements.

## References

- [1] K. Sznajder-Katarzyńska, M. Surma, I. Cieślík, A review of perfluoroalkyl acids (PFAAs) in terms of sources, applications, human exposure, dietary intake, toxicity, legal regulation, and methods of determination, *J. Chem.* 2019 (2019) 2717528. <https://doi.org/10.1155/2019/2717528>.
- [2] J.C. Boutonnet, P. Bingham, D. Calamari, C.d. Rooij, J. Franklin, T. Kawano, J.-M. Libre, A. McCulloch, G. Malinverno, J.M. Odom, G.M. Rusch, K. Smythe, I. Sobolev, R. Thompson, J.M. Tiedje, Environmental risk assessment of trifluoroacetic acid, *Hum. Ecol. Risk Assess.* 5 (1999) 59-124. <http://doi.org/10.1080/10807039991289644>.
- [3] H.P.H. Arp, S.E. Hale, REACH: Improvement of guidance and methods for the identification and assessment of PMT/vPvM substances, Umweltbundesamt <https://www.umweltbundesamt.de/publikationen/reach-improvement-of-guidance-methods-for-the>, 2019 (accessed 1 June 2021).
- [4] M. Scheurer, K. Nödler, F. Freeling, J. Janda, O. Happel, M. Riegel, U. Müller, F.R. Storck, M. Fleig, F.T. Lange, A. Brunsch, H.-J. Brauch, Small, mobile, persistent: trifluoroacetate in the water cycle – overlooked sources, pathways, and consequences for drinking water supply, *Water Res.* 126 (2017) 460-471. <https://doi.org/10.1016/j.watres.2017.09.045>.
- [5] M. Berg, S.R. Müller, J. Mühlemann, A. Wiedmer, R.P. Schwarzenbach, Concentrations and mass fluxes of chloroacetic acids and trifluoroacetic acid in rain and natural waters in Switzerland, *Environ. Sci. Technol.* 34 (2000) 2675-2683. <https://doi.org/10.1021/es990855f>.
- [6] H. Frank, A. Klein, D. Renschen, Environmental trifluoroacetate, *Nature* 382 (1996) 34-34. <https://doi.org/10.1038/382034a0>.
- [7] A. Jordan, H. Frank, Trifluoroacetate in the environment. Evidence for sources other than HFC/HCFCs, *Environ. Sci. Technol.* 33 (1999) 522-527. <https://doi.org/10.1021/es980674y>.
- [8] T.M. Cahill, C.M. Thomas, S.E. Schwarzbach, J.N. Seiber, Accumulation of trifluoroacetate in seasonal wetlands in California, *Environ. Sci. Technol.* 35 (2001) 820-825. <https://doi.org/10.1021/es0013982>.
- [9] M.H. Russell, G. Hoogeweg, E.M. Webster, D.A. Ellis, R.L. Waterland, R.A. Hoke, TFA from HFO-1234yf: accumulation and aquatic risk in terminal water bodies, *Environ. Toxicol. Chem.* 31 (2012) 1957-1965. <https://doi.org/10.1002/etc.1925>.
- [10] ECHA (2021) <https://echa.europa.eu/de/brief-profile/-/briefprofile/100.000.846>, (accessed 17 July 2021).
- [11] K. Nödler, M. Scheurer, Substances from Multiple Sources (SMS): the presence of multiple primary and secondary sources of persistent and mobile organic contaminants is an upcoming challenge for the drinking water sector and regulatory frameworks, *Environ. Sci. Technol.* 53 (2019) 11061-11062. <https://doi.org/10.1021/acs.est.9b05168>.
- [12] H. Frank, E.H. Christoph, O. Holm-Hansen, J.L. Bullister, Trifluoroacetate in ocean waters, *Environ. Sci. Technol.* 36 (2002) 12-15. <https://doi.org/10.1021/es0101532>.
- [13] H. Rüdél, W. Körner, T. Letzel, M. Neumann, K. Nödler, T. Reemtsma, Persistent, mobile and toxic substances in the environment: a spotlight on current research and regulatory activities, *Environ. Sci. Eur.* 32 (2020) 5. <https://doi.org/10.1186/s12302-019-0286-x>.
- [14] D.A. Ellis, S.A. Mabury, J.W. Martin, D.C. Muir, Thermolysis of fluoropolymers as a potential source of halogenated organic acids in the environment, *Nature* 412 (2001) 321-324. <https://doi.org/10.1038/35085548>.
- [15] J.n. Cui, J. Guo, Z. Zhai, J. Zhang, The contribution of fluoropolymer thermolysis to trifluoroacetic acid (TFA) in environmental media, *Chemosphere* 222 (2019) 637-644. <https://doi.org/10.1016/j.chemosphere.2019.01.174>.
- [16] H. Sun, F.S. Cannon, X. He, Enhanced trifluoroacetate removal from groundwater by quaternary nitrogen-grafted granular activated carbon, *Sci. Total Environ.* 660 (2019) 577-585. <https://doi.org/10.1016/j.scitotenv.2019.01.057>.
- [17] H. Sun, F.S. Cannon, X. He, Polypyrrole-tailored activated carbon for trifluoroacetate removal from groundwater, *Environ. Eng. Sci.* 36 (2019) 1379-1387. <https://doi.org/10.1089/ees.2018.0453>.

- [18] B.R. Kim, M.T. Suidan, T.J. Wallington, X. Du, Biodegradability of trifluoroacetic acid, *Environ. Eng. Sci.* 17 (2000) 337-342. <https://doi.org/10.1089/ees.2000.17.337>.
- [19] G.A. Zoumpouli, M. Scheurer, H.-J. Brauch, B. Kasprzyk-Hordern, J. Wenk, O. Happel, COMBI, continuous ozonation merged with biofiltration to study oxidative and microbial transformation of trace organic contaminants, *Environ. Sci.: Water Res. Technol.* 5 (2019) 552-563. <https://doi.org/10.1039/C8EW00855H>.
- [20] H.V. Lutze, J. Brekenfeld, S. Naumov, C. von Sonntag, T.C. Schmidt, Degradation of perfluorinated compounds by sulfate radicals – new mechanistic aspects and economical considerations, *Water Res.* 129 (2018) 509-519. <https://doi.org/10.1016/j.watres.2017.10.067>.
- [21] T. Ochiai, Y. Iizuka, K. Nakata, T. Murakami, D.A. Tryk, A. Fujishima, Y. Koide, Y. Morito, Efficient electrochemical decomposition of perfluorocarboxylic acids by the use of a boron-doped diamond electrode, *Diam. Relat. Mater.* 20 (2011) 64-67. <https://doi.org/10.1016/j.diamond.2010.12.008>.
- [22] H. Hori, Y. Takano, K. Koike, K. Takeuchi, H. Einaga, Decomposition of environmentally persistent trifluoroacetic acid to fluoride ions by a homogeneous photocatalyst in water, *Environ. Sci. Technol.* 37 (2003) 418-422. <https://doi.org/10.1021/es025783y>.
- [23] N. Saeidi, F.-D. Kopinke, A. Georgi, Controlling adsorption of perfluoroalkyl acids on activated carbon felt by means of electrical potentials, *Chem. Eng. J.* 416 (2021) 129070. <https://doi.org/10.1016/j.cej.2021.129070>.
- [24] J. Zhou, Y. Zhang, M. Balda, V. Presser, F.-D. Kopinke, A. Georgi, Electro-assisted removal of polar and ionic organic compounds from water using activated carbon felts, *Chem. Eng. J.* (2021) submitted.
- [25] N. Holubowitch, A. Omosebi, X. Gao, J. Landon, K. Liu, Quasi-steady-state polarization reveals the interplay of capacitive and Faradaic processes in capacitive deionization, *ChemElectroChem* 4 (2017) 2404-2413. <https://doi.org/10.1002/celc.201700082>.
- [26] X. Gao, A. Omosebi, J. Landon, K. Liu, Enhanced salt removal in an inverted capacitive deionization cell using amine modified microporous carbon cathodes, *Environ. Sci. Technol.* 49 (2015) 10920-10926. <https://doi.org/10.1021/acs.est.5b02320>.
- [27] X. Gao, A. Omosebi, J. Landon, K. Liu, Surface charge enhanced carbon electrodes for stable and efficient capacitive deionization using inverted adsorption–desorption behavior, *Energy Environ. Sci.* 8 (2015) 897-909. <https://doi.org/10.1039/C4EE03172E>.
- [28] J. Zhou, N. Saeidi, L.Y. Wick, F.-D. Kopinke, A. Georgi, Adsorption of polar and ionic organic compounds on activated carbon: surface chemistry matters, *Sci. Total Environ.* (2021) 148508. <https://doi.org/10.1016/j.scitotenv.2021.148508>.
- [29] L.W. Zelazny, L. He, A. Vanwormhoudt, Charge analysis of soils and anion exchange, *Methods of soil analysis: Part 3 chemical methods*, 5.3, Soil Science Society of America, Inc., American Society of Agronomy, Inc., Madison, 1996, pp. 1231-1253. <https://doi.org/10.2136/sssabookser5.3.c41>.
- [30] S. Delpeux-Ouldriane, M. Gineys, N. Cohaut, F. Béguin, The role played by local pH and pore size distribution in the electrochemical regeneration of carbon fabrics loaded with bentazon, *Carbon* 94 (2015) 816-825. <https://doi.org/10.1016/j.carbon.2015.07.010>.
- [31] L. Li, P.A. Quinlivan, D.R.U. Knappe, Effects of activated carbon surface chemistry and pore structure on the adsorption of organic contaminants from aqueous solution, *Carbon* 40 (2002) 2085-2100. [https://doi.org/10.1016/S0008-6223\(02\)00069-6](https://doi.org/10.1016/S0008-6223(02)00069-6).
- [32] N. Saeidi, F.-D. Kopinke, A. Georgi, Understanding the effect of carbon surface chemistry on adsorption of perfluorinated alkyl substances, *Chem. Eng. J.* 381 (2020) 122689. <https://doi.org/10.1016/j.cej.2019.122689>.
- [33] G.V. Nunell, M.E. Fernandez, P.R. Bonelli, A.L. Cukierman, Nitrate uptake improvement by modified activated carbons developed from two species of pine cones, *J. Colloid Interface Sci.* 440 (2015) 102-108. <https://doi.org/10.1016/j.jcis.2014.10.058>.
- [34] E. Bayram, E. Ayranci, A systematic study on the changes in properties of an activated carbon cloth upon polarization, *Electrochim. Acta* 56 (2011) 2184-2189. <https://doi.org/10.1016/j.electacta.2010.12.018>.

- [35] G. Hotová, V. Slovák, T. Zelenka, R. Maršálek, A. Parchaňská, The role of the oxygen functional groups in adsorption of copper (II) on carbon surface, *Sci. Total Environ.* 711 (2020) 135436. <https://doi.org/10.1016/j.scitotenv.2019.135436>.
- [36] N. Saeidi, F.-D. Kopinke, A. Georgi, What is specific in adsorption of perfluoroalkyl acids on carbon materials?, *Chemosphere* (2020) 128520. <https://doi.org/10.1016/j.chemosphere.2020.128520>.
- [37] S.A. Hawks, M.R. Cerón, D.I. Oyarzun, T.A. Pham, C. Zhan, C.K. Loeb, D. Mew, A. Deinhart, B.C. Wood, J.G. Santiago, M. Stadermann, P.G. Campbell, Using ultramicroporous carbon for the selective removal of nitrate with capacitive deionization, *Environ. Sci. Technol.* 53 (2019) 10863-10870. <https://doi.org/10.1021/acs.est.9b01374>.
- [38] E.R. Nightingale, Phenomenological theory of ion solvation. Effective radii of hydrated ions, *The Journal of Physical Chemistry* 63 (1959) 1381-1387. <https://doi.org/10.1021/j150579a011>.
- [39] M.E. Suss, Size-based ion selectivity of micropore electric double layers in capacitive deionization electrodes, *J. Electrochem. Soc.* 164 (2017) E270-E275. <https://doi.org/10.1149/2.1201709jes>.
- [40] A. Bauzá, A. Frontera, T.J. Mooibroek, NO<sub>3</sub><sup>-</sup> anions can act as Lewis acid in the solid state, *Nat. Commun.* 8 (2017) 14522. <https://doi.org/10.1038/ncomms14522>.
- [41] J. Pitarch-Jarque, R.J. Zaragoza, R. Ballesteros, B. Abarca, E. Garcia-España, B. Verdejo, R. Ballesteros-Garrido, About the relevance of anion- $\pi$  interactions in water, *Dalton Trans.* 50 (2021) 6834-6839. <https://doi.org/10.1039/D1DT00771H>.
- [42] R.P. Schwarzenbach, P.M. Gschwend, D.M. Imboden, *Environmental organic chemistry*, John Wiley & Sons, Inc., New York, 1993.
- [43] M. Kah, G. Sigmund, F. Xiao, T. Hofmann, Sorption of ionizable and ionic organic compounds to biochar, activated carbon and other carbonaceous materials, *Water Res.* 124 (2017) 673-692. <https://doi.org/10.1016/j.watres.2017.07.070>.
- [44] M.A. Brown, A. Goel, Z. Abbas, Effect of electrolyte concentration on the Stern layer thickness at a charged interface, *Angew. Chem. Int. Ed.* 55 (2016) 3790-3794. <https://doi.org/10.1002/anie.201512025>.
- [45] K.-U. Goss, The pK<sub>a</sub> values of PFOA and other highly fluorinated carboxylic acids, *Environ. Sci. Technol.* 42 (2008) 456-458. <https://doi.org/10.1021/es702192c>.
- [46] ChemAxon online platform, <https://chemicalize.com>, (accessed 11 June 2021).
- [47] X. Li, S. Chen, X. Quan, Y. Zhang, Enhanced adsorption of PFOA and PFOS on multiwalled carbon nanotubes under electrochemical assistance, *Environ. Sci. Technol.* 45 (2011) 8498-8505. <https://doi.org/10.1021/es202026v>.
- [48] Z. Niu, Y. Wang, H. Lin, F. Jin, Y. Li, J. Niu, Electrochemically enhanced removal of perfluorinated compounds (PFCs) from aqueous solution by CNTs-graphene composite electrode, *Chem. Eng. J.* 328 (2017) 228-235. <https://doi.org/10.1016/j.cej.2017.07.033>.
- [49] J.N. Uwayezu, I. Carabante, T. Lejon, P. van Hees, P. Karlsson, P. Hollman, J. Kumpiene, Electrochemical degradation of per- and poly-fluoroalkyl substances using boron-doped diamond electrodes, *J. Environ. Manage.* 290 (2021) 112573. <https://doi.org/10.1016/j.jenvman.2021.112573>.
- [50] K. Kim, P. Baldaque Medina, J. Elbert, E. Kayiwa, R.D. Cusick, Y. Men, X. Su, Molecular tuning of redox-copolymers for selective electrochemical remediation, *Adv. Funct. Mater.* 30 (2020) 2004635. <https://doi.org/10.1002/adfm.202004635>.
- [51] R.P. Rastogi, Chapter 13 - COMPLEX PATTERN FORMATION, in: R.P. Rastogi (Ed.) *Introduction to Non-equilibrium Physical Chemistry*, Elsevier, Amsterdam, 2008, pp. 235-269. <https://doi.org/10.1016/B978-044452188-0.50015-X>.
- [52] F. Zhang, Z. Sun, J. Cui, Research on the mechanism and reaction conditions of electrochemical preparation of persulfate in a split-cell reactor using BDD anode, *RSC Adv.* 10 (2020) 33928-33936. <https://doi.org/10.1039/D0RA04669H>.
- [53] H. Li, Y. Long, X. Zhu, Y. Tian, J. Ye, Influencing factors and chlorinated byproducts in electrochemical oxidation of bisphenol A with boron-doped diamond anodes, *Electrochim. Acta* 246 (2017) 1121-1130. <https://doi.org/10.1016/j.electacta.2017.06.163>.

- [54] T. Muddemann, A. Bulan, M. Sievers, U. Kunz, Avoidance of chlorine formation during electrolysis at boron-doped diamond anodes in highly sodium chloride containing and organic-polluted wastewater, *J. Electrochem. Soc.* 165 (2018) J3281-J3287. <https://doi.org/10.1149/2.0371815jes>.
- [55] C. Lefrou, R.P. Nogueira, F. Huet, H. Takenouti, 1.02 - Electrochemistry, in: B. Cottis, M. Graham, R. Lindsay, S. Lyon, T. Richardson, D. Scantlebury, H. Stott (Eds.) *Shreir's Corrosion*, Elsevier, Oxford, 2010, pp. 13-51. <https://doi.org/10.1016/B978-044452787-5.00003-2>.
- [56] I. Medved', R. Černý, Surface diffusion in porous media: A critical review, *Microporous and Mesoporous Materials* 142 (2011) 405-422. <https://doi.org/10.1016/j.micromeso.2011.01.015>.
- [57] D. Reyter, Electrochemical Reduction of Nitrate, in: G. Kreysa, K.-i. Ota, R.F. Savinell (Eds.) *Encyclopedia of Applied Electrochemistry*, Springer New York, New York, NY, 2014, pp. 585-593. [https://doi.org/10.1007/978-1-4419-6996-5\\_135](https://doi.org/10.1007/978-1-4419-6996-5_135).
- [58] V. Georgeaud, A. Diamand, D. Borrut, D. Grange, M. Coste, Electrochemical treatment of wastewater polluted by nitrate: selective reduction to N<sub>2</sub> on boron-doped diamond cathode, *Water Sci. Technol.* 63 (2011) 206-212. <https://doi.org/10.2166/wst.2011.034>.



## Supporting information

### Supporting experimental information

**BET analysis** for specific surface area (SSA) measurement: the size distribution of mesopores ( $\varnothing = 2\text{-}50\text{ nm}$ ) was analyzed by applying the BJH method. The micropore size distribution ( $\varnothing < 2\text{ nm}$ ) was determined via  $\text{CO}_2$  adsorption at  $0^\circ\text{C}$  applying a magnetic suspension balance (Rubotherm GmbH). The results were analyzed with a NLDFT fitting.

**Anion and cation exchange capacities** (AEC and CEC) were measured as follows: ACF (0.5 g) was first shaken in 1 M KCl aq. solution (10 mL) overnight then washed with 10 mM KCl aq. solution (10 mL, 5 times). At each washing step, 1 M HCl and 1 M KOH were used to adjust the suspension pH to  $7.0 \pm 0.5$ . After the final washing round, the supernatant was analyzed using ion chromatography (Dionex) and ICP-OES (SPECTRO) for  $\text{Cl}^-$  and  $\text{K}^+$  concentrations, respectively. The entrained solution was expected to have the identical ion concentrations as for the bulk phase. The entrained KCl solution after discarding the supernatant was carefully weighted. Then, the ACF was washed with 0.5 M  $\text{NaNO}_3$  aq. solution (8 mL, 4 times) to exchange the  $\text{Cl}^-$  and  $\text{K}^+$  adsorbed. At each exchange step, 1 M NaOH and 1 M  $\text{HNO}_3$  were used to adjust the suspension pH to  $7.0 \pm 0.5$ . The exchanged out  $\text{Cl}^-$  and  $\text{K}^+$  concentrations in the solutions were determined. ACFs' AEC and CEC were finally calculated according to the difference in amounts between the  $\text{Cl}^-$  and  $\text{K}^+$  which are substituted out and entrained before.

**Fig. S1** demonstrates the adsorption kinetics of TFA on DeACF in tap water (pH 7) with no external bias potential added. A change  $<5\%$  was observed for  $K_{d,t} = q_t/c_t$  after 30 min adsorption, indicating a rather fast approach to TFA adsorption equilibrium on DeACF.

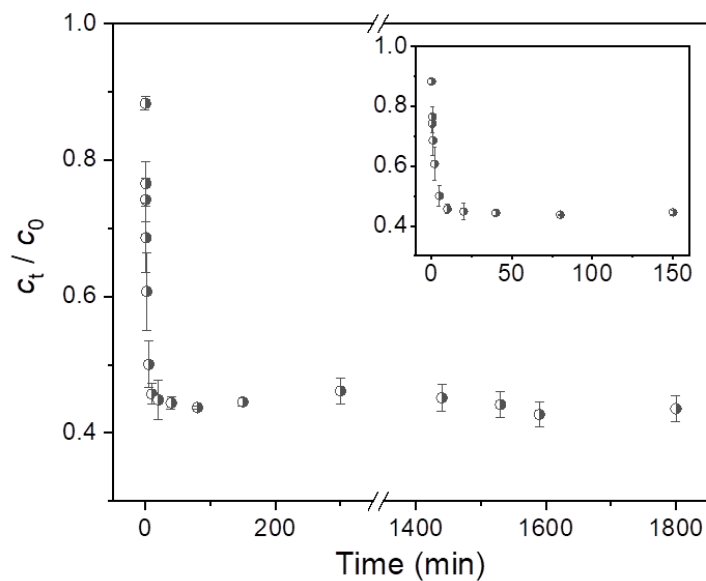


**Fig. S1:** TFA concentration in the aqueous phase normalized to its initial concentration (20 mg/L) along the time in contact with DeACF (2 g/L) in tap water (pH 7) without external bias potential.  $K_d$  under adsorption equilibrium was around 660 L/kg. Error bars are the deviation from the mean values of duplicate experiments.

### SI to Section 3.1

**Fig. S2** shows the cyclic voltammograms of three ACFs. The butterfly shape suggests the position of  $E_{pzc}$ . In Fig. S1, the upper and lower limit of each  $E_{pzc}$  range is shown.

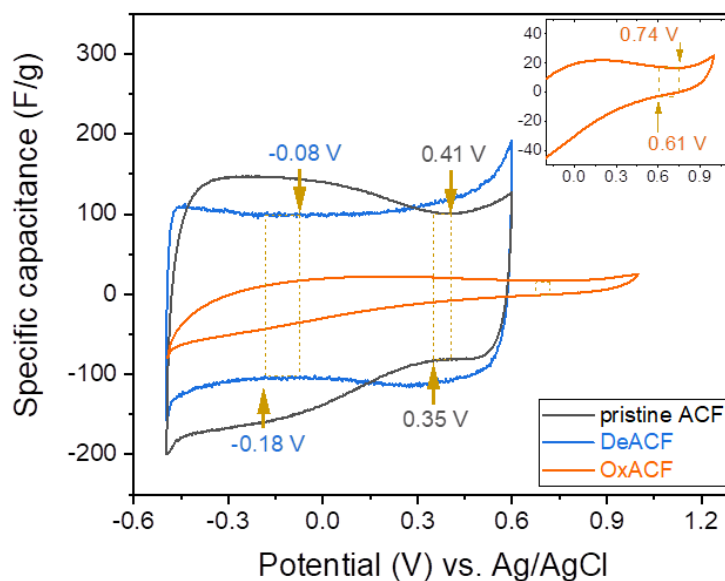


**Fig. S2:** Cyclic voltammograms of pristine ACF, DeACF and OxACF in 1 M  $\text{Na}_2\text{SO}_4$  at 1 mV/s.

**Tables S1 and S2** present respectively the chemical and textural properties of the applied ACFs. Readers are referred to our previous work for comprehensive interpretation of the sample characteristics as well as the details of measurement procedures [1, 2].

**Table S1:** Chemical properties of different ACFs.

Sample	C (wt%)	H (wt%)	O <sup>a</sup> (wt%) <sup>a</sup>	N (wt%)	CEC (μmol/m <sup>2</sup> )	AEC (μmol/m <sup>2</sup> )	I <sub>G</sub> /I <sub>D</sub> <sup>b</sup>
Pristine ACF	87.7	0.3	9.9	1.8	0.040	0.025	0.97
DeACF	93.4	0.4	4.3	0.9	≤0.010	0.23	0.98
OxACF	78.5	0.3	18.1	2.7	1.0	0.0087	0.89

<sup>a</sup> Calculated according to O wt% = 100% – N wt% – H wt% – C wt% – ash wt%. Ash contents were determined by weighing the residues after combusting ACFs in O<sub>2</sub> at 750 °C. <sup>b</sup> The intensity ratio of the G- and D-band derived from Raman spectra. A band at 1160 cm<sup>-1</sup> related to trans-polyacetylene moieties [9] was observed only for DeACF, further indicating the higher content of C=C bonds on its surface.

**Table S2:** Pore structure of ACFs determined via nitrogen gas sorption at -196°C.  $V_{\text{micro}, \varnothing = 1-2 \text{ nm}}$  and  $V_{\text{micro}, \varnothing < 1 \text{ nm}}$ : volume of micropores with  $\varnothing = 1-2 \text{ nm}$  and  $\varnothing < 1 \text{ nm}$ , respectively;  $V_{\text{meso}}$ : mesopore volume with  $\varnothing = 2-50 \text{ nm}$ ;  $V_t$ : total pore volume. SSA: specific surface area. QSDFT was applied for analysis.

Sample	SSA (m <sup>2</sup> /g)	$V_t$ (cm <sup>3</sup> /g)	$V_{\text{micro}, \varnothing < 1 \text{ nm}}$ (cm <sup>3</sup> /g)	$V_{\text{micro}, \varnothing = 1-2 \text{ nm}}$ (cm <sup>3</sup> /g)	$V_{\text{meso}, \varnothing = 2-50 \text{ nm}}$ (cm <sup>3</sup> /g)
Pristine ACF	1700	0.88	0.33	0.44	0.09
DeACF	1400	0.69	0.29	0.33	0.06
OxACF	800	0.42	0.18	0.19	0.05

### SI to Section 3.2

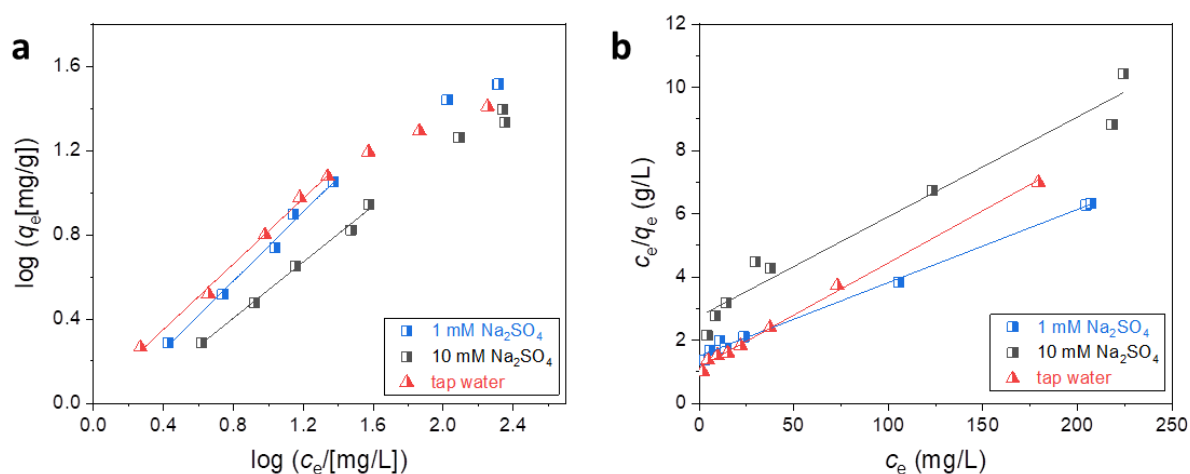


**Fig. S3:** (a) Freundlich and (b) Langmuir isotherm fittings of TFA adsorption on DeACF at pH 7 in 1 mM  $\text{Na}_2\text{SO}_4$ , 10 mM  $\text{Na}_2\text{SO}_4$  and tap water. Only data points away from the maximal loadings were applied for the Freundlich linear fittings.

**Table S3:** Freundlich and Langmuir isotherm parameters for TFA adsorption on DeACF at pH 7 in various background solutions. Deviations are given based on regression analyses.

Background solution	Freundlich			Langmuir		
	$K_F [(\text{mg/g})/(\text{mg/L})^n]$	$n$	$R^2$	$q_m [\text{mg/g}]$	$K_L [\text{L/mg}]$	$R^2$
1 mM $\text{Na}_2\text{SO}_4$	$0.84 \pm 0.09$	$0.82 \pm 0.05$	0.991	$43.1 \pm 1.2$	$0.015 \pm 0.002$	0.996
10 mM $\text{Na}_2\text{SO}_4$	$0.74 \pm 0.07$	$0.67 \pm 0.03$	0.994	$31.7 \pm 2.8$	$0.011 \pm 0.003$	0.963
Tap water	$1.09 \pm 0.07$	$0.78 \pm 0.03$	0.996	$30.2 \pm 0.7$	$0.029 \pm 0.002$	0.997

### SI to Section 3.3

The electrochemical stability of TFA between -0.5 to 1.3 V vs. Ag/AgCl was examined by cyclic voltammetry as shown in **Fig S4**. A graphite rod carrying similar surface functionalities ( $\pi$  system and O-containing groups) and carbon backbones to ACFs was used as the working electrode in order to reduce the large background capacitive current in case of using ACF working electrodes, and expose electrochemical redox reactions which took place (**Fig. S4a**).

The oxidation of graphite rod was indicated by the rising anodic current at  $E > 0.6$  V vs. Ag/AgCl followed by the co-oxidation of water [3]. The reversible redox peaks around -0.1 V vs. Ag/AgCl might relate to system impurities. No additional redox signals were visible in the cyclic voltammogram of the system containing TFA compared to the system without TFA, indicating that TFA is resistant to electrochemical redox reactions in the wide potential window probed. In addition, the cyclic voltammogram in **Fig. S4b** obtained using boron-doped diamond (BDD) working electrode shows a weak redox signal in the presence of TFA only at elevated potentials  $>1.9$  V vs. Ag/AgCl, which was not reached under the electrosorption conditions applied in this study.

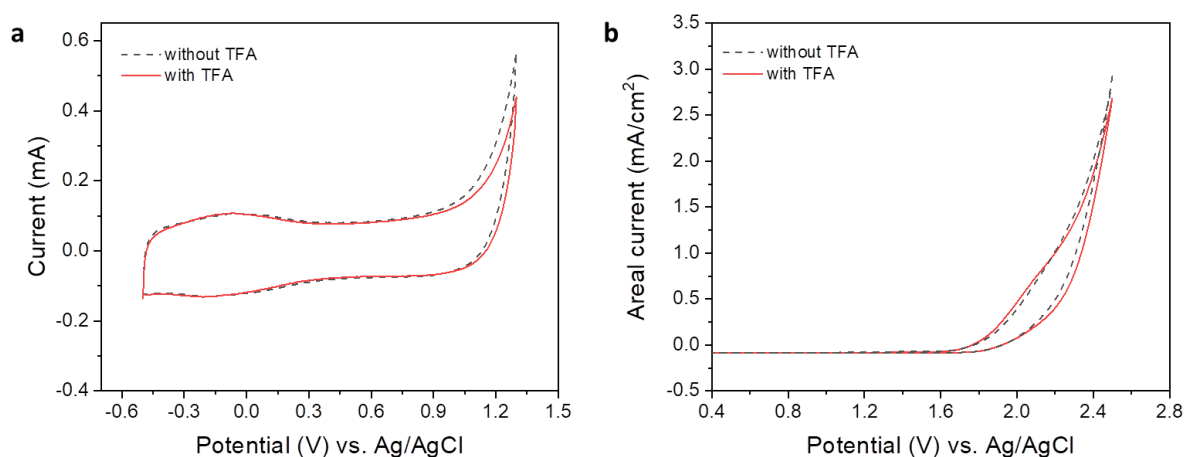


**Fig. S4:** Cyclic voltammograms measured in aqueous 10 mM  $\text{Na}_2\text{SO}_4$  (pH 7) with (a) a graphite rod or (b) BDD being the working electrode. Scan rate: 5 mV/s. 2 mM TFA was present in the system containing TFA.

### SI to Section 3.4

To examine whether a contact to  $\text{NO}_3^-$  containing water does harm to the adsorption efficiency of DeACF towards TFA, one breakthrough curves were collected using DeACF pre-wetted in 1 mM  $\text{NaNO}_3$  and in deionized water (**Fig. S5**). The DeACF pre-wetted in 1 mM  $\text{NaNO}_3$  was prepared as follows: 0.1 g DeACF was first shaken (120 rpm) in 20 mL 1 mM  $\text{NaNO}_3$  overnight. Then, the DeACF was washed in 20 mL 10 mM KCl (30 min x 6 times, 120 rpm) until  $<0.2$  mg/L  $\text{NO}_3^-$  was detected by the UV/VIS signal (SHIMADZU UVmini-1240) at  $\lambda = 204$  nm [4]. After that, the DeACF was washed in 80 mL deionized water (30 min x 5 times, 120 rpm) and was ready for usage.

According to **Fig. S5**, 50% breakthrough was reached at identical volumes for both TFA and  $\text{NO}_3^-$  on DeACF pre-wetted in DI and 1 mM  $\text{NaNO}_3$  solution. This suggests only a minor change on adsorption performance of DeACF upon contact with  $\text{NaNO}_3$  solution, and  $\text{NO}_3^-$  was indeed consumed via adsorption (also see recovery in Sections 3.5 and 3.6). A slightly less sharp breakthrough curve of TFA on DeACF pre-wetted in 1 mM  $\text{NaNO}_3$  implies a consumption of some high-affinity sorption sites due to oxidation by  $\text{NO}_3^-$ .

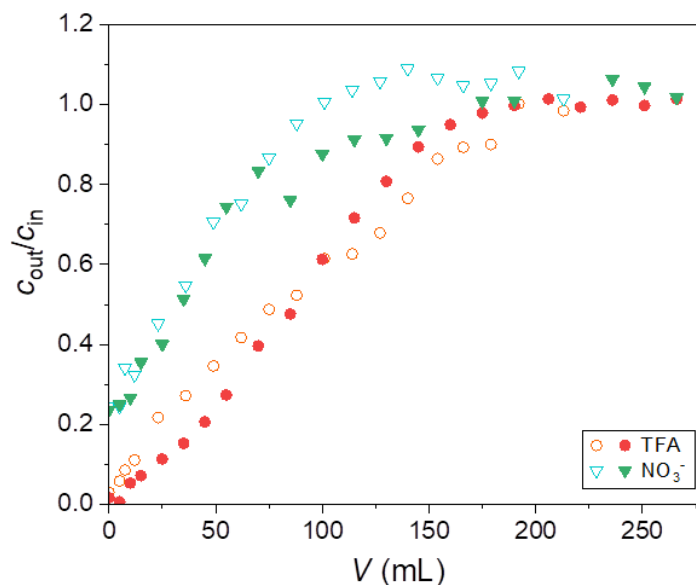


**Fig. S5:** Breakthrough curves of TFA and  $\text{NO}_3^-$  through 0.1 g DeACF adsorbers. Inflow: tap water containing 3.4 mg/L TFA and 1.3 mg/L  $\text{NO}_3^-$ . Mass-related flow rate:  $10 \text{ mL} \cdot \text{g}^{-1} \cdot \text{min}^{-1}$ . Mean relative error of  $\pm 8\%$  and  $\pm 13\%$  can be expected for each  $c_{\text{out}}/c_{\text{in}}$  point for TFA and  $\text{NO}_3^-$ . Hollow dots: DeACF pre-wetted in 1 mM  $\text{NaNO}_3$  (= 62 mg/L  $\text{NO}_3^-$ ), filled dots: DeACF pre-wetted in deionized water.

### SI to Section 3.5

The desorption kinetics of TFA in 10 mM  $\text{Na}_2\text{SO}_4$  from DeACF in batch systems is shown in **Fig. S6**. At all selected bias potentials, a 64-69% decrease in loading due to establishment of new adsorption equilibria were achieved after about 20 min of desorption. A fast desorption was achieved at a stirring rate of 650 rpm with only changes of  $<10\%$  in  $K_{d,t} = q_t/c_t$  after the first 10 min desorption under all three conditions.

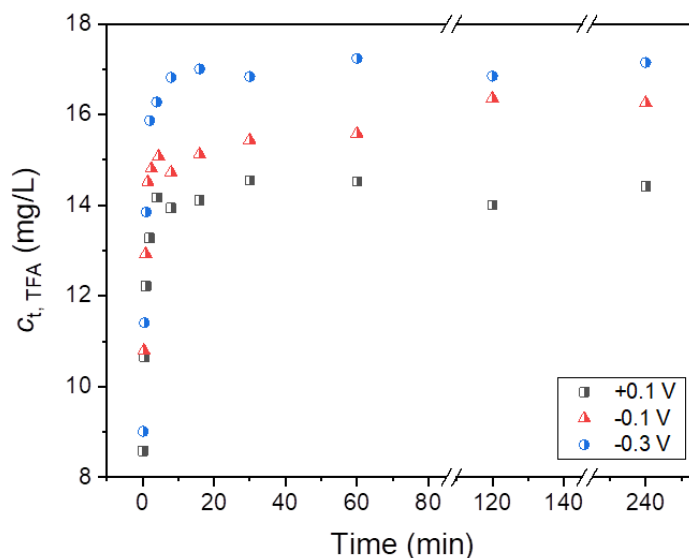


**Fig. S6:** TFA desorption kinetics from DeACF in 10 mM Na<sub>2</sub>SO<sub>4</sub> (pre-loaded with TFA by adsorption from spiked tap water at OCP) at +0.1 V, -0.1 V, -0.3 V vs. Ag/AgCl in a stirred batch adsorber.

According to **Fig. 5** in the main text, around 35 mL in-flow tap water ( $c_{\text{in,nitrate}} = 1.3 \text{ mg/L}$ ) needed to be fed to the cell to reach a 50% breakthrough of NO<sub>3</sub><sup>-</sup>. The NO<sub>3</sub><sup>-</sup> desorption profiles in 10 mM Na<sub>2</sub>SO<sub>4</sub> under selected conditions are shown in **Fig. S8**. The recovery parameters are summarized in **Table S4**. Note that the 10 mM Na<sub>2</sub>SO<sub>4</sub> eluent contained approx. 0.2 mg/L NO<sub>3</sub><sup>-</sup>, which is also approaching the detection limit.

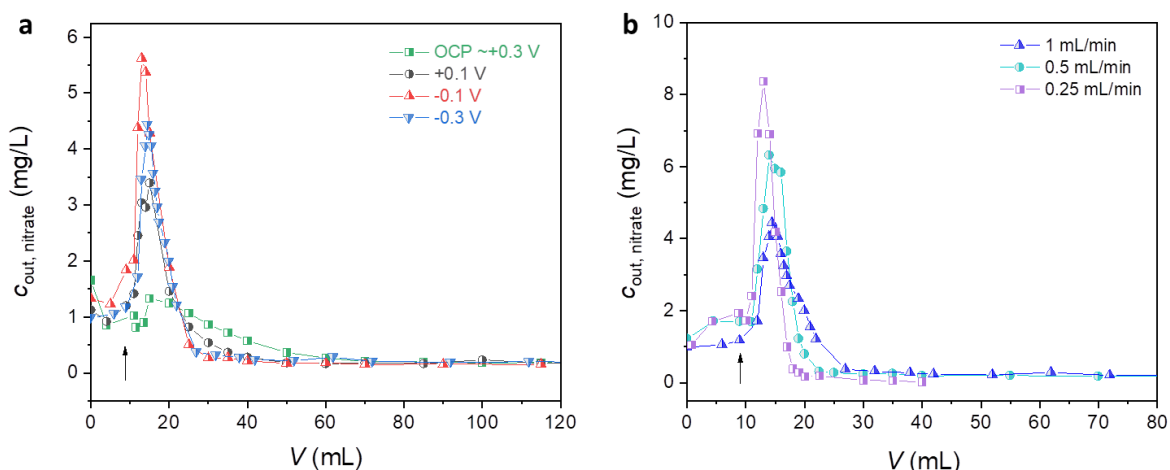


**Fig. S8:** Desorption profiles of  $\text{NO}_3^-$  at (a) +0.1 V, -0.1 V, -0.3 V vs. Ag/AgCl at  $10 \text{ mL} \cdot \text{g}^{-1} \text{min}^{-1}$  mass-related flow rate, and at (b) -0.3 V vs. Ag/AgCl at  $10 \text{ mL} \cdot \text{g}^{-1} \text{min}^{-1}$ ,  $5.0 \text{ mL} \cdot \text{g}^{-1} \text{min}^{-1}$  and  $2.5 \text{ mL} \cdot \text{g}^{-1} \text{min}^{-1}$  after adsorption at full breakthrough from tap water on 0.1 g DeACF at OCP. Bias potentials were added after 9 mL flowed out as indicated by the black arrows. Lines serve as guides for the eye. Notice: the 10 mM  $\text{Na}_2\text{SO}_4$  eluent contained approx. 0.2 mg/L  $\text{NO}_3^-$ .

**Table S4:**  $\text{NO}_3^-$  recovery (Re%) achievable using 120 mL eluent, the  $\text{Na}_2\text{SO}_4$  eluent volume needed to reach 95% respective recovery ( $V_{95\% \text{ des}}$ ) and enrichment factors in 10 mM  $\text{Na}_2\text{SO}_4$  after adsorbed from tap water onto DeACF. Potentials are given vs. Ag/AgCl. The OCP of DeACF is around 0.3 V vs. Ag/AgCl.

	Desorption parameters			
	Mass-related flow rate ( $\text{mL} \cdot \text{g}^{-1} \text{min}^{-1}$ )	Re% <sup>a</sup>	$V_{\text{des}, 95\%}$ (mL) <sup>b</sup>	Enrichment factor
OCP	10	77%	59	0.46
+0.1 V	10	83%	30	0.97
-0.1 V	10	106%	20	1.9
-0.3 V	10	87%	23	1.3
-0.3 V	5.0	100%	11	3.2
-0.3 V	2.5	97%	9	3.8

<sup>a</sup> Mean relative error of  $\pm 13\%$  for recovery. <sup>b</sup> Calculated for eluent volumes after charging started for +0.1 V, -0.1 V, and -0.3 V.



### SI to Section 3.6

The adsorption capacity of DeACF towards  $\text{NO}_3^-$  (contained in tap water at 1.3 mg/L) was found to be stable over five ad-/desorption cycles within the range of  $(0.50 \pm 0.07)$  mg/L (**Fig. S9, Table S5**). The surface oxidation of the DeACF during the cycles seems, therefore, harmless to its adsorption capacity towards  $\text{NO}_3^-$ . However, the achievable recovery, decreased first significantly from 84% to 65% from the 1<sup>st</sup> to the 2<sup>nd</sup> cycle, than slightly further to 55% in the final cycle. It might be associated with a facilitated approach of  $\text{NO}_3^-$  ions towards the oxidized, thereby more hydrophilic carbon surface after cycles [5] where  $\text{NO}_3^-$  was reduced. The resulting reduction products were not detectable by the IC device [6], e.g.  $\text{N}_2$ . Binding of nitrogen species on the carbon surface is indicated by XPS results, which showed a slight increase in the N/C atomic ratio for DeACF cycled five times compared to the “washed and dried” sample (**Fig. S10**), although insignificant redox reactions took place when DeACF contacts  $\text{NO}_3^-$  at OCP (see **Section 3.4**).

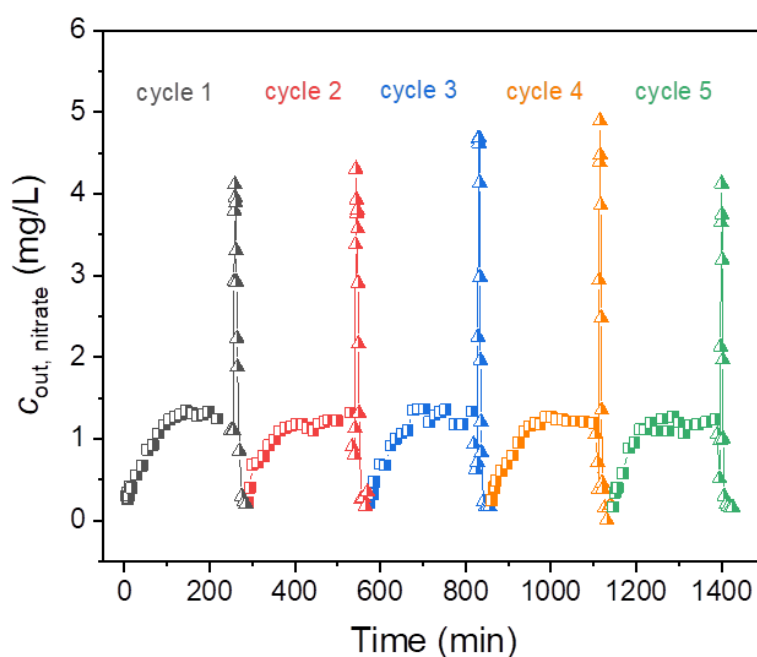


**Fig. S9:** Out-flow concentration of  $\text{NO}_3^-$  over five successive ad-/desorption cycles on 0.1 g DeACF. Square symbols: adsorption steps; Triangle symbols: desorption steps. Adsorption conditions: tap water at OCP,  $10 \text{ mL} \cdot \text{g}^{-1} \cdot \text{min}^{-1}$  for 234 min; Desorption conditions: 10 mM  $\text{Na}_2\text{SO}_4$  at -0.3 V vs. Ag/AgCl for 30 min,  $10 \text{ mL} \cdot \text{g}^{-1} \cdot \text{min}^{-1}$ , start of charging after first 10 min at OCP. Lines serve as guides for the eye.

**Table S5:** NO<sub>3</sub><sup>-</sup> recovery parameters in 10 mM Na<sub>2</sub>SO<sub>4</sub> at -0.3 V vs. Ag/AgCl after adsorbed from tap water onto 0.1 g DeACF over five successive cycles. Mass-related flow rate: 10 mL·g<sup>-1</sup>min<sup>-1</sup> for both ad-/desorption steps. For more detailed conditions see the caption of Fig. 7 in the main text.

	Cycle 1	Cycle 2	Cycle 3	Cycle 4	Cycle 5
<b>NO<sub>3</sub><sup>-</sup> loading (mg/g)<sup>a</sup></b>	0.49	0.55	0.48	0.47	0.45
<b>Achievable total recovery<sup>b</sup></b>	84%	65%	69%	63%	55%

<sup>a</sup> At full breakthrough. <sup>b</sup> Mean relative error of ±13% for recovery.

The release of CO and CO<sub>2</sub> of DeACF samples takes place at  $T \leq 1100$  °C in the temperature-programmed desorption (TPD) measurement. The quantitative comparison of O wt% derived from CO and CO<sub>2</sub> of different samples is given in **Table S6**. As the extended CO tailings were related to reactions of DeACF surfaces with traces of oxygen in the inert carrier gas [2] and not relevant to the respective samples *per se*, a cut-off at  $t = 85$  min was applied for the calculation. According to the **Fig. 8b** in the main text, the washing and drying steps had caused increase of both CO and CO<sub>2</sub> releasing moieties [7] on DeACF surface. In comparison, the ad-/desorption cycles have mainly introduced further lactone, anhydride, and/or carboxylic groups [7, 8] on DeACF surface as indicated by the significantly higher intensities of the CO<sub>2</sub> profiles.

The XPS survey spectra of “washed and dried” DeACF and 5-times cycled DeACF are shown in **Fig. S10**. The N/C atomic ratio has increased slightly from 0.013 for the “washed and dried” sample to 0.018 for DeACF after five ad-/desorption cycles. The N1s signal was found around 400.1 eV indicating organic N species [9].

**Table S6:** O wt% derived from released CO and CO<sub>2</sub> on DeACF surfaces calculated from TPD profiles.

Sample	O wt% from CO	O wt% from CO <sub>2</sub>	Total O wt%
Original	1.07 ± 0.02	0.25 ± 0.03	1.33 ± 0.05
washed and dried	1.48 ± 0.03	0.41 ± 0.04	1.89 ± 0.08
1 cycle	1.61 ± 0.03	0.73 ± 0.07	2.34 ± 0.09
5 cycles	1.50 ± 0.03	0.61 ± 0.06	2.11 ± 0.08

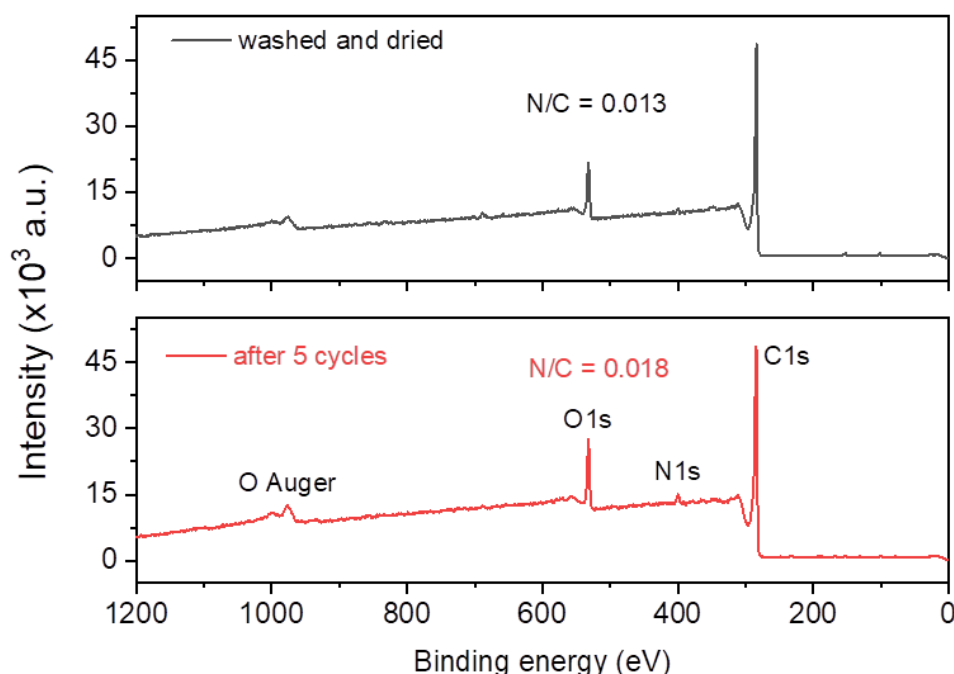


**Fig. S10:** XPS survey spectra of DeACF only “washed and dried” and after 5 ad-/desorption cycles. The N/C atomic ratios are given in the diagrams.

## References

- [1] J. Zhou, N. Saeidi, L.Y. Wick, F.-D. Kopinke, A. Georgi, Adsorption of polar and ionic organic compounds on activated carbon: surface chemistry matters, *Sci. Total Environ.* (2021) 148508. <https://doi.org/10.1016/j.scitotenv.2021.148508>.
- [2] J. Zhou, Y. Zhang, M. Balda, V. Presser, F.-D. Kopinke, A. Georgi, Electro-assisted removal of polar and ionic organic compounds from water using activated carbon felts, *Chem. Eng. J.* (2021) submitted.
- [3] N. Holubowitch, A. Omosebi, X. Gao, J. Landon, K. Liu, Quasi-steady-state polarization reveals the interplay of capacitive and Faradaic processes in capacitive deionization, *ChemElectroChem* 4 (2017) 2404-2413. <https://doi.org/10.1002/celec.201700082>.

- [4] M.-N. Pons, A. Assaad, C. Oucacha, S. Pontvianne, B. Pollier, P. Wagner, A. Legout, F. Guérol, Nitrates monitoring by UV–vis spectral analysis, *Ecohydrol. Hydrobiol.* 17 (2017) 46-52.  
<https://doi.org/10.1016/j.ecohyd.2016.12.001>.
- [5] K. Jo, Y. Baek, C. Lee, J. Yoon, Effect of hydrophilicity of activated carbon electrodes on desalination performance in membrane capacitive deionization, *Appl. Sci.* 9 (2019).  
<https://doi.org/10.3390/app9235055>.
- [6] D. Reyter, Electrochemical Reduction of Nitrate, in: G. Kreysa, K.-i. Ota, R.F. Savinell (Eds.) *Encyclopedia of Applied Electrochemistry*, Springer New York, New York, NY, 2014, pp. 585-593.  
[https://doi.org/10.1007/978-1-4419-6996-5\\_135](https://doi.org/10.1007/978-1-4419-6996-5_135).
- [7] M. Vogel, F.-D. Kopinke, K. Mackenzie, Acceleration of microiron-based dechlorination in water by contact with fibrous activated carbon, *Sci. Total Environ.* 660 (2019) 1274-1282.  
<https://doi.org/10.1016/j.scitotenv.2019.01.070>.
- [8] J.-H. Zhou, Z.-J. Sui, J. Zhu, P. Li, D. Chen, Y.-C. Dai, W.-K. Yuan, Characterization of surface oxygen complexes on carbon nanofibers by TPD, XPS and FT-IR, *Carbon* 45 (2007) 785-796.  
<https://doi.org/10.1016/j.carbon.2006.11.019>.
- [9] NIST X-ray Photoelectron Spectroscopy Database, NIST Standard Reference Database Number 20, National Institute of Standards and Technology, Gaithersburg MD, 20899 (2000).  
<http://dx.doi.org/10.18434/T4T88K>.

## 4. Summary

In this dissertation, we investigated the AC-based sorptive and electrosorptive approaches for removal of neutral, anionic and cationic PM substances from water. The findings of three presented manuscripts provided deepened insights to 1) the desired AC chemical properties in use of adsorption and electrosorption (trap&release) of various PM substances, 2) the sensitivity of various PM kinds to electro-assisted ad-/desorption using AC, and 3) the design of electro-sorption cell for selective removal of PM substances from water in the presence of co-existing inorganic ions.

The study “Adsorption of polar and ionic organic compounds on activated carbon: Surface chemistry matters” contributed to the fundamental understanding of the effect of AC surface chemistry on the adsorption behaviors of various PM types. The main outcomes of this work are:

- Surface chemistry is recognized as an important factor in AC adsorption especially towards ionic and ionizable PM compounds. Sophisticated drivers dependent on the adsorbent/adsorbate properties, such as hydrophobic effects,  $\pi$ - $\pi$  interaction, EDA interactions and electrostatic interactions, etc., can have joint effects on the adsorption of PM contaminants by AC materials.
- Surface defunctionalization can function as a universal strategy to facilitate the removal of diverse PM substances carrying neutral, anionic and cationic structures. Surface defunctionalized AC can be applied in WWTPs to extend fixed-bed adsorber operation times or reduce required adsorbent dosage.
- The state-of-the-art prediction tools underestimate the essential role of AC surface chemistry on the adsorption behaviors of various PM compounds. To update the prediction models, ion exchange capacity giving quantitative information on adsorbent surface charges at specified pH is recommended as an adsorbent-relevant input parameter for model training. It is a clear indicator for strong hydrophobic effects in the uptake of ionic PM substances when the maximal loadings exceed the ion exchange capacity of the applied adsorbent.

The effectiveness of the AC-based electrosorption on removal of various PM contaminants was explored in the study “Electro-assisted removal of polar and ionic organic compounds from water using activated carbon felts”. The main outcomes of this work are:

- The ad- and desorption processes of charged PM substances in water can be significantly regulated via electro-assisted polarization of AC felts, whereas it has only a minor effect on nonionic PM substances.
- Particularly great potential of electro-assisted trap&release approach was shown for the cationic probe compound tetrapropylammonium (TPA<sup>+</sup>). A stronger enhancing effect on AC adsorption to TPA<sup>+</sup> was achievable by means of cathodic polarization compared to surface chemical oxidation. The latter is a common means to introduce net negative charges on AC for additional electrostatic attraction with cationic adsorbates, but meanwhile makes the adsorbent surface less hydrophobic and thereby sacrifices the hydrophobic effects.
- On the contrary, a milder manipulating effect on sorption behavior was found for *p*-toluenesulfonate (*p*-TsO<sup>-</sup>) via electrode polarization. This suggests that strong  $\pi$ - $\pi$  interactions between adsorbate and adsorbent could mitigate charging-induced effects.
- Due to a wider potential window than the pristine AC felt, defunctionalized AC felt (DeACF) allows better electro-assisted trap&release performances with higher estimated enrichment factors of 10<sup>2</sup>–10<sup>3</sup> derived from Freundlich fitting parameters for flow-through units. The batch systems equipped with DeACF demonstrated an adequately stable electro-ad-/desorption performance for TPA<sup>+</sup> and *p*-TsO<sup>-</sup> over at least 5 cycles and 20 days.
- Electrosorption cannot only be applied for enhancing adsorption performance towards ionic PMOCs and extending operation life of AC adsorbers, but also for facilitating a facile, green on-site AC regeneration in contrast to the common off-site thermal regeneration costing extra transportation and AC losses. Ionic PM substances can be effectively concentrated in small water volumes before next degradation steps, thereby significantly lower the energy consumption.

In the study “Efficient removal of trifluoroacetic acid from water using surface defunctionalized activated carbon and electro-assisted desorption”, we established an efficient approach to enrich the highly mobile trifluoroacetic acid (TFA) from water

containing common inorganic ions into a small volume of electrolyte solution using 1) the adsorption power of DeACF and 2) a subsequent *in-situ* electro-assisted desorption step. The main outcomes of this work are:

- Surface defunctionalization can significantly improve AC adsorption towards TFA, i.e. a 20-fold higher adsorption coefficient achieved using DeACF instead of the pristine material. DeACF shows one of the best reported adsorption efficiency to TFA (adsorption capacity of 30.2 mg/g) despite the co-existence of  $\text{Cl}^-$ ,  $\text{SO}_4^{2-}$  and  $\text{NO}_3^-$ . The positively charged, hydrophobic DeACF surface allows an intensive electrostatic attraction to negatively charged TFA at neutral pH and a favored adsorption of TFA over inorganic anions.
- The rapid small-scale flow test showed a remarkable separation performance of DeACF for TFA versus  $\text{Cl}^-$  and  $\text{SO}_4^{2-}$  in tap water while an effective adsorptive co-removal of the undesired water contaminant  $\text{NO}_3^-$ .
- TFA can be effectively desorbed in the flow unit upon the feed of inflow  $\text{Na}_2\text{SO}_4$  solution when applying cathodic polarization on DeACF, showing a recovery rate higher than 90%.
- Despite an initial decline in adsorption capacity of DeACF (by 33%) towards TFA due to partial surface oxidation after the first ad-/desorption cycle, stable adsorption efficiencies and recovery rates were maintained for the next 4 cycles, indicating adequate long-term enrichment effects.
- The as-established electro-assisted removal approach of TFA is conceptually similar to an inverted-CDI cell, where the electrode was pre-treated to enhance the trap of the target compounds driven by the specific, strong adsorbent/adsorbate interactions and the desorption was triggered by applying adverse polarization conditions to repulse the charged targets. The membrane-free flow cell in a simple, one-channel design enables low cell voltages (<1.1 V) by using oxidized AC felt of high specific surface area (800  $\text{m}^2/\text{g}$ ) but no significant adsorption capability to anionic TFA as the anode during the electro-assisted TFA desorption. The setup can be applied for removal of longer-chain perfluoroalkyl acids (PFAAs) in the future work as the oxidized AC surface can only weakly adsorb these compounds, too ([20] in the reference list of the **Section 2**). The two-step trap&release approach allows a flexible choice of eluent in the electro-desorption step, which can avoid undesired byproducts in subsequent oxidative

degradation processes, or open up possibilities for improved performance in the next-step treatment of the concentrated target pollutants.

We hope the findings of this dissertation can provide valuable guidance in AC-based materials modification and process design in adsorptive and electro-adsorptive removal of PM substances from water, as well inspire the next breakthroughs of water treatment techniques aiming at newly emerging micropollutants.



## **Declaration of authorship contribution**

The authorship contribution of the three involved manuscripts is stated as follows:

In manuscript 3.1 “Adsorption of polar and ionic organic compounds on activated carbon: Surface chemistry matters” published in Science of The Total Environment (2021):

**Jieying Zhou:** Conceptualization, Methodology, Investigation, Discussion, Writing - original draft, review& editing. Navid Saeidi: Conceptualization, Methodology, Discussion, Writing - review & editing. Lukas Y. Wick: Supervision, Discussion, Writing - review & editing. Frank-Dieter Kopinke: Supervision, Conceptualization, Discussion, Writing - review & editing. Anett Georgi: Supervision, Conceptualization, Methodology, Discussion, Writing - review & editing.

In the manuscript 3.2 “Electro-assisted removal of polar and ionic organic compounds from water using activated carbon felts” submitted to Chemical Engineering Journal (2021):

**Jieying Zhou:** Conceptualization, Methodology, Investigation, Discussion, Writing - original draft, review& editing. Yuan Zhang: Methodology, Investigation, Discussion, Writing - review & editing. Maria Balda: Methodology, Investigation, Discussion, Writing - review & editing. Volker Presser: Supervision, Methodology, Discussion, Writing - review & editing. Frank-Dieter Kopinke: Supervision, Conceptualization, Discussion, Writing - review & editing. Anett Georgi: Supervision, Conceptualization, Methodology, Discussion, Writing - review & editing.

In the manuscript 3.3 “Efficient removal of trifluoroacetic acid from water using surface-modified activated carbon and electro-assisted desorption” ready to submit to Journal of Hazardous Materials (2021):

**Jieying Zhou:** Conceptualization, Methodology, Investigation, Discussion, Writing - original draft, review& editing. Navid Saeidi: Conceptualization, Methodology, Investigation, Discussion, Writing - review & editing. Lukas Y. Wick: Supervision, Discussion, Writing - review & editing. Yanlin Xie: Methodology, Investigation, Discussion, Writing - review & editing. Frank-Dieter Kopinke: Supervision, Conceptualization, Discussion, Writing - review & editing. Anett Georgi: Supervision, Conceptualization, Methodology, Discussion, Writing - review & editing. Acknowledgements

## Acknowledgement

In the first place, I would like to express my gratitude to my supervisor Prof. Dr. Frank-Dieter Kopinke for offering me the opportunity to work on this interesting research topic in his group. It was my pleasure to learn from him who is so experienced, yet still so enthusiastic and curious about science. I thank him for always inspiring us with interesting findings in the scientific community, and providing us highly useful suggestions whenever needed.

I own the most sincere thanks to my “daily supervisor” Dr. Anett Georgi for her professional advices on my research work and caring support in other aspects of my life throughout the 3.5-year PhD journey. I am so lucky to be guided by her as being easily approachable, highly experienced and reliable. I am grateful to have learned the knowledge of adsorption and other water treatment approaches from her.

I wish to express my thanks to Dr. Lukas Y. Wick for supervising me and sharing his valuable scientific insights with me. Heartfelt thanks go to Prof. Volker Presser for providing me the chance for the short research visit in his group in Saarbrücken. I am very happy to have the opportunity to learn from them and work on our manuscripts together.

I would like to thank my dear colleagues Dr. Navid Saeidi, Yuan Zhang and Maria Balda for having contributing to our joint manuscripts. I thank them for giving me helping hands on the measurements, and brainstorming with me whenever questions in lab first arise. I also wish to express my appreciation to my students Ruonan Qin and Yanlin Xin for having enthusiastically worked with me on this project.

Many thanks to my colleagues Silke Woszidlo, Evelyn Becker, Birgit Forkert-Keller and Dr. Frank Holzer who assisted me in different measurements. I enjoyed a lot having my lovely colleagues Lisa-Marie Frenzel, Ali Shee and Sarah Sühnholz around with encouraging vibes which always motivated me. Special thanks go to Lin Qian, who has not only supported me in science with many inspiring discussions, but in many other aspects as well.

Last but not least, let me thank my dear family and friends for their unconditional love and support, which keeps me strong in finishing my PhD work. I thank Dr. Kaipu Jin especially for her warm-hearted attention to my mom when she suffered from heart diseases and I was not around.

## Curriculum vitae

Name	Jieying Zhou
Address	Schmidt-Rühl-Str. 22, 04347 Leipzig
Tel	+49 176 61 35 84 65
E-Mail	jieying.zhou@web.de
Date and place of birth	Jan 5 <sup>th</sup> 1991, Shanghai

## Education

May 2018 – present	<b>Doctoral candidate in Chemistry</b> <ul style="list-style-type: none"><li>• Faculty of Chemistry and Mineralogy, University Leipzig.</li><li>• PhD dissertation: “Improved Sorptive Removal of Polar Organic Micropollutants from Water Using Surface Modified and Polarized Activated Carbons”</li><li>• Thesis conducted at Department of Environmental Engineering, Helmholtz Centre for Environmental Research - UFZ, Leipzig</li></ul>
Oct 2014 – Feb 2017	<b>Master of Science - Chemistry</b> <ul style="list-style-type: none"><li>• Leipzig University, Leipzig</li><li>• Master’s thesis focused on surface functionalization of nanodiamond using radiation chemistry approaches</li><li>• Thesis conducted at Leibniz Institute of Surface Engineering IOM, Leipzig</li></ul>
Oct 2011 – Sep 2014	<b>Bachelor of Science - Chemistry</b> <ul style="list-style-type: none"><li>• Friedrich Schiller University, Jena</li><li>• Bachelor’s thesis focused on synthesis and characterization of organometallic compounds</li></ul>
Sep 2009 – Jul 2011	<b>Bachelor of Science – Chemistry (not finished)</b> <ul style="list-style-type: none"><li>• Fudan University, Shanghai</li></ul>

## **Scientific activities during PhD study**

### **Publications**

**J. Zhou**, N. Saeidi, L.Y. Wick, F.-D. Kopinke, A. Georgi, Adsorption of polar and ionic organic compounds on activated carbon: surface chemistry matters, Sci. Total Environ. (2021) 148508.

**J. Zhou**, Y. Zhang, M. Balda, V. Presser, F.-D. Kopinke, A. Georgi, Electro-assisted removal of polar and ionic organic compounds from water using activated carbon felts, Chem. Eng. J. (2021), in revision.

**J. Zhou**, N. Saeidi, L.Y. Wick, Y. Xie, F.-D. Kopinke, A. Georgi, Efficient removal of trifluoroacetic acid from water using surface-modified activated carbon and electro-assisted desorption, J. Hazard. Mater. (2021), ready to submit.

### **Conference contributions**

- Oral presentation, Characterization and Remediation of Per- and Polyfluoroalkyl Substances and Other Emerging Contaminants (PFAS) International Conference 2021, Online
- Poster presentation, Wasser 2021, Online
- Science Slammer, N2 conference 2019, Berlin, Germany
- Oral presentation, UFZ Energy Days 2019, Leipzig, Germany
- Oral presentation, Kick-off Symposium STROMERs 2018, Leipzig, Germany

ISSN 1860-0387

Helmholtz Centre for  
Environmental Research – UFZ  
Permoserstraße 15  
04318 Leipzig | Germany  
[www.ufz.de](http://www.ufz.de)

NOT FOR SALE.